

5-2-2014

Experimental Investigations of the Combination of a Heat Pipe with Metal Foam or Foils for Enhancing Heat Transfer during the Melting and Solidification of a Phase Change Material (PCM) for Latent Heat Thermal Energy Storage Applications

Michael J. Allen

University of Connecticut - Storrs, michael.allen@engineer.uconn.edu

Recommended Citation

Allen, Michael J., "Experimental Investigations of the Combination of a Heat Pipe with Metal Foam or Foils for Enhancing Heat Transfer during the Melting and Solidification of a Phase Change Material (PCM) for Latent Heat Thermal Energy Storage Applications" (2014). *Master's Theses*. 570.
https://opencommons.uconn.edu/gs_theses/570

This work is brought to you for free and open access by the University of Connecticut Graduate School at OpenCommons@UConn. It has been accepted for inclusion in Master's Theses by an authorized administrator of OpenCommons@UConn. For more information, please contact opencommons@uconn.edu.

**Experimental Investigations of the Combination of a Heat Pipe with Metal Foam or Foils for
Enhancing Heat Transfer during the Melting and Solidification of a Phase Change Material (PCM)
for Latent Heat Thermal Energy Storage Applications**

Michael J. Allen

B.S., University of Connecticut, 2012

A Thesis

Submitted in Partial Fulfillment of the

Requirements for the Degree of

Masters of Science

At the

University of Connecticut

2014

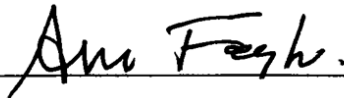
Approval Page

Master of Science Thesis

**Experimental Investigations of the Combination of a Heat Pipe with Metal Foam or Foils for
Enhancing Heat Transfer during the Melting and Solidification of a Phase Change Material (PCM)
for Latent Heat Thermal Energy Storage Applications**

Presented by:

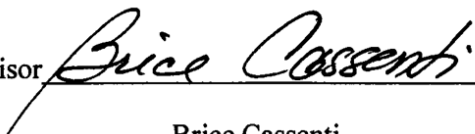
Michael John Allen

Major Advisor 

Amir Faghri

Associate Advisor 

Tianfeng Lu

Associate Advisor 

Brice Cassenti

University of Connecticut

2014

Acknowledgements

I would like to personally thank those who have aided me during my master's thesis research. The obtained knowledge over the past two years regarding science, experimentation and engineering would have not been achievable without the encouragement of my peers.

I would like to express my gratitude to my major advisor Dr. Faghri, for offering me the opportunity to perform research in the field of latent heat thermal energy storage as well as heat pipe technology and implementation. The years of Dr. Faghri mentorship as my Senior Design project advisor during my B.S., graduate school professor, and my major advisor throughout my stay at the University of Connecticut has helped me improve as a student, critical reviewer, technical writer, researcher, and leader.

During both my undergraduate and graduate education, I have had the pleasure of taking classes with both Dr. Lu and Dr. Cassenti which have made a lasting impact on my education. I would like to thank them for their contributions as associate advisors for my thesis.

I would also like to acknowledge Dr. Bergman who has greatly contributed to my experimental success and has spent many hours thoroughly editing my journal publications. His influence on my research experience is greatly appreciated.

The excellent support and advice I have received from my lab mates on a day to day basis will be missed in the future. They have always guided my endeavors such as classwork, experiments and analyzing data, and have become close friends in the process and I could not thank them enough. Additionally, I could not have been blessed with a greater network of family and friends who have reinforced the pursuit of my goals all throughout my life, particularly my mother and father. I would like to thank God for all of the many gifts and talents he has blessed me with. I have been very fortunate to have had the opportunity to work with the above mentioned people. Thank you all for your great influence on my life.

Finally, I would like to thank Boeing and the U.S. Department of Energy for their financial support on the projects in which I was involved.

Table of Contents

List of Tables	vii
List of Figures	viii
Abstract	xi
Chapter 1. Review and Advances in Energy Storage Systems with an Emphasis on Thermal Energy	
Systems	1
1.1 Introduction.....	1
1.1.1. Energy storage types	4
1.2. TES properties	16
1.2.1. Thermal/physical.....	16
1.2.2. Kinetic.....	17
1.2.3. Chemical	17
1.2.4. Economic	17
1.3. SHTES systems.....	17
1.3.1. Types of SHTES	18
1.4. Latent heat thermal energy storage systems.....	21
1.4.1. Phase change materials (PCMs).....	21
1.4.2. Enhancement techniques.....	25
1.5. Applications of TES.....	27
1.5.1. Thermal energy storage.....	27
1.6. Conclusions.....	29
Chapter 2. Challenges and Applications of Latent Heat Thermal Energy Storage Systems Including	
Enhancement Techniques: Approach and Methodology	56
2.1. Introduction.....	56
2.2. Numerical modeling of PCMs	58
2.3. Enhancement techniques.....	61

2.3.1. Extended surfaces	62
2.3.2. Nanoparticles	67
2.3.3. High thermal conductivity structures	69
2.3.4. Heat pipes, thermosyphons and reflux systems	72
2.3.5. Encapsulation.....	74
2.3.6. Cascaded	77
2.4. Combined enhancement.....	79
2.5. Comparison of various techniques.....	81
2.6. Conclusions.....	83
Chapter 3. Robust Heat Transfer Enhancement during Melting and Solidification of a PCM using a Combined Heat Pipe-Metal Foam or Foil Configuration	
128	
3.1. Introduction.....	128
3.2 Experimental Apparatus.....	131
3.3. Experimental Procedure	133
3.4. Results and discussion	134
3.4.1. Temperature distribution within the PCM	135
3.4.2. Temperature drops along the HP / Rod.....	136
3.4.3. Effect of foil number and thickness on the HP-Foil-PCM configuration performance	137
3.4.4. Effect of pore density and porosity for HP-Foam-PCM performance	138
3.4.5. Comparison between the HP-Foam-PCM and HP-Foil-PCM configuration performance.....	138
3.5. Conclusions.....	140
Chapter 4. Effect of Inclination Angle during Melting and Solidification of a Phase Change Material using a Combined Heat Pipe-Metal Foam or Foil Configuration	
158	
4.1. Introduction.....	159
4.2. Experimental apparatus.....	162
4.3. Experimental procedure	164

4.4. Results and discussion	165
4.4.1 Temperature distribution in the PCM	167
4.4.2 Photographic observations	169
4.4.3 Liquid fraction histories	171
4.4.4 Performance comparison for each heat transfer enhancement technique	174
4.4.5 Average melting rates	175
4.4.6 Effectiveness at 95 % complete phase change	176
4.4.7 Time ratio for complete phase change	177
4.5. Conclusions.....	177

List of Tables

Table 1.1. Summary of recent studies on energy storage techniques.	40
Table 1.2. Desired characteristics of a thermal energy storage system.	41
Table 1.3. Common materials used in SHTES systems.	42
Table 1.4. Comparison of common SHTES and LHTES materials with $\Delta T = 50\text{ }^{\circ}\text{C}$ [46].	43
Table 1.5. Typical PCM melting temperature and enthalpy ranges [72].	44
Table 1.6. Common PCM materials.	45
Table 2.1. Experimental investigations involving fin enhanced PCM systems.	96
Table 2.2. Numerical investigations involving fin enhanced PCM systems.	97
Table 2.3. Recent investigations involving foil enhanced PCM systems.	98
Table 2.4. Studies involving nano-particle enhanced PCMs.	99
Table 2.5. LHTES systems involving high thermal conductivity structures.	101
Table 2.6. Experimental investigations involving heat pipes and reflux systems integrated with PCMs.	104
Table 2.7. Numerical studies on LHTES systems utilizing heat pipes and reflux systems.	105
Table 2.8. Studies involving encapsulation of PCMs.	107
Table 2.9. Numerical studies investigating the encapsulation of PCMs.	109
Table 2.10. Recent studies involving cascaded PCM systems.	112
Table 2.11. LHTES systems utilizing combined enhancement techniques.	113
Table 2.12. Advantages, disadvantages, challenges and unresolved issues for each enhancement technique.	117
Table 3.1. Summary of studies on PCMs enhanced with metal foams.	145
Table 3.2. Thermophysical properties of n-octadecane [19].	147
Table 3.3. Location of thermocouples.	148
Table 3.4. Phase change time (t_m, t_s), average effectiveness ($\varepsilon_m, \varepsilon_s$), average melting rate ($r_{m,avg}$) and solidification rate ($r_{s,avg}$) for 95 % completion of phase change.	149
Table 4.1. Thermophysical properties of n-octadecane at $T = 301.5\text{ K}$ [10].	183
Table 4.2. Time, effectiveness and melting rates for 95 % complete phase change (min).	184

List of Figures

Fig. 1.1. Energy storage types.	47
Fig. 1.2. Schematic of a typical flow battery.	48
Fig. 1.3. Schematic of hydrogen regenerative fuel cell.	49
Fig. 1.4. Schematic of a pumped hydro storage system.	50
Fig. 1.5. Schematic of a flywheel energy storage system.	51
Fig. 1.6. Schematic of a packed bed SHTES.	52
Fig. 1.7. Schematic of a solar pond.	53
Fig. 1.8. Classification of PCMs.	54
Fig. 1.9. Applications of TES.	55
Fig. 2.1. Various heat transfer enhancement techniques implemented in PCM systems.	121
Fig. 2.2. Effect of nanoparticle concentration on the melting and solidification of a PCM (adopted from [54]).	122
Fig. 2.3. Effectiveness histories for isothermal, HP and tube cases (adopted from [37]).	123
Fig. 2.4. Effect of the HTF inlet temperature on charging time (adopted form [65]).	124
Fig. 2.5. Energy storage and recovery during charging–discharging cycles with charging periods of 8 and 12 h (adopted from [72]).	125
Fig. 2.6. Comparison between enhancement techniques for a vertical cylindrical PCM system ($d = 41$ mm, $h = 60$ mm) with heat transfer through the base using a HP (copper- water, $d = 6$ mm), rod (solid-copper, $d = 6$ mm) and aluminum foam ($\phi = 0.95$, $\omega =$ 20 PPI) during (a) melting and (b) solidification (adopted from [76]).	126
Fig. 2.7. Comparison of enhancement techniques in a vertical cylindrical PCM system ($d =$ 41 mm, $h = 60$ mm) with heat transfer through the base using a HP (copper-water, $d =$ 6 mm) alone or combined with aluminum foils ($\phi = 0.95$, $t = 24$ μ m) or foam ($\phi =$ 0.95, $\omega = 20$ PPI) during (a) melting and (b) solidification (adopted from [76]).	127
Fig. 3.1. Schematic of the experimental apparatus.	150
Fig. 3.2. Temperature distribution histories during melting for the (a) HP-Foil-PCM ($\phi =$ 0.957, $N = 162$, $t_2 = 0.024$) (b) HP-Foam-PCM ($\phi = 0.949$, $\omega = 20$ PPI), (c) HP-	151

PCM and (d) Rod-PCM configurations.	
Fig. 3.3. Temperature distribution histories during solidification for the (a) HP-Foil-PCM ($\varphi = 0.957$, $N = 162$, $t_2 = 0.024$) (b) HP-Foam-PCM ($\varphi = 0.949$, $\omega = 20$ PPI), (c) HP-PCM and (d) Rod-PCM configurations.	152
Fig. 3.4. Temperature drop along the HP (or rod) in the Rod-PCM, HP-PCM and HP-Foam-PCM ($\varphi = 0.912$, $\omega = 20$ PPI) configurations during (a) melting and (b) solidification.	153
Fig. 3.5. Volumetric liquid fraction (left) and effectiveness (right) for the HP-Foil-PCM cases for various porosities, foil numbers and foil thicknesses during (a) melting and (b) solidification.	154
Fig. 3.6. Volumetric liquid fraction (left) and effectiveness (right) for HP-Foam-PCM cases with a similar porosity ($0.943 < \varphi < 0.957$) during (a) melting and (b) solidification.	155
Fig. 3.7. Volumetric liquid fraction (left) and effectiveness (right) for HP-Foam-PCM cases for various porosities with $\omega = 20$ PPI during (a) melting and (b) solidification.	156
Fig. 3.8. Comparison of volumetric liquid fraction (left) and effectiveness (right) for the HP-Foil-PCM and HP-Foam-PCM configurations during (a) melting and (b) solidification.	157
Fig. 4.1. Schematic of the experimental apparatus (a) central cross section parallel to the right side view (plane of symmetry) and (b) top view.	185
Fig. 4.2. Temperature distribution during solidification with $\alpha = 0^\circ$ and $\Delta T = 17^\circ\text{C}$ ($r_1 = 9$ mm, $r_2 = 15$ mm, $z_1 = 15$ mm, $z_2 = 30$ mm, $z_3 = 45$ mm) for the (a) Foam-PCM, (b) HP-PCM and (c) HP-Foam-PCM configurations.	186
Fig. 4.3. Temperature distribution during melting with $\alpha = 0^\circ$ and $\Delta T = 17^\circ\text{C}$ ($r_1 = 9$ mm, $r_2 = 15$ mm, $z_1 = 15$ mm, $z_2 = 30$ mm, $z_3 = 45$ mm) for the (a) Foam-PCM, (b) HP-PCM and (c) HP-Foam-PCM configurations.	187
Fig. 4.4. Temperature distribution during melting for the HP-Foil-PCM (left) and HP-Foam-PCM (right) configurations with $\Delta T = 17^\circ\text{C}$ and $\alpha = 90^\circ$ ($r_1 = 9$ mm, $r_2 = 15$ mm, $\theta_1 = 0^\circ$, $\theta_2 = 90^\circ$, $\theta_3 = 180^\circ$) for (a) $z_1 = 15$ mm (b) $z_2 = 30$ mm and (c) $z_3 = 45$ mm.	188

- Fig. 4.5. Photographs during solidification with $\alpha = 0^\circ$ and $\Delta T = 17^\circ\text{C}$ for the (a) HP-PCM, (b) Rod-PCM, and (c) non-enhanced PCM configurations at $t = 15$ min (left) and $t = 30$ min (right). 189
- Fig. 4.6. Photographs during melting at $t = 60$ min with $\alpha = 0^\circ$ (left), $\alpha = 90^\circ$ (right) and $\Delta T = 17^\circ\text{C}$ for the (a) HP-PCM, (b) Rod-PCM and (c) non-enhanced PCM configurations. 190
- Fig. 4.7. Photographs progression during melting with $\alpha = 0^\circ$ (left), $\alpha = 0^\circ$ (left-middle), $\alpha = 0^\circ$ (right-middle), $\alpha = 90^\circ$ (right) and $\Delta T = 17^\circ\text{C}$ for the HP-PCM configuration at (a) $t = 30$ min (b) $t = 60$ min and (c) $t = 90$ min. 191
- Fig. 4.8. Liquid fraction histories for the HP-PCM cases with $\Delta T = 17^\circ\text{C}$ using a copper disc (open symbols) and an acrylic disc (solid symbols) during (a) solidification and (b) melting. 192
- Fig. 4.9. Liquid fraction histories during solidification with varying ΔT and orientation for the (a) HP-Foil-PCM, (b) HP-Foam-PCM, (c) HP-PCM, (d) Rod-PCM, (e) Foam-PCM and (f) non-enhanced PCM configurations. 193
- Fig. 4.10. Liquid fraction histories during melting with varying ΔT and orientation for the (a) HP-Foil-PCM, (b) HP-Foam-PCM, (c) HP-PCM, (d) Rod-PCM, (e) Foam-PCM and (f) non-enhanced PCM configurations. 194
- Fig. 4.11. Liquid fraction histories for each configuration with $\Delta T = 17^\circ\text{C}$ (a) solidification, $\alpha = 0^\circ$, (b) melting, $\alpha = 0^\circ$, (c) solidification, $\alpha = 90^\circ$ and (d) melting, $\alpha = 90^\circ$. 195
- Fig. 4.12. Time ratio and effectiveness for each configuration at 95 % complete phase change with respect to the non-enhanced PCM case with $\Delta T = 17^\circ\text{C}$ (a) solidification, $\alpha = 0^\circ$, (b) melting, $\alpha = 0^\circ$, (c) solidification, $\alpha = 90^\circ$ and (d) melting, $\alpha = 90^\circ$. 196

Abstract

Various thermal energy storage (TES) systems including latent heat TES (LHTES), sensible heat TES and chemical TES are reviewed and analyzed with an emphasis on LHTES. LHTES is considered here due its high energy density which results in a significant reduction in the overall system size (volume and mass). However, LHTES systems have been limited in the past by the low thermal conductivity of most phase change materials (PCMs). A detailed experimental investigation is conducted to investigate the innovative combination of a heat pipe (HP) with either metal foam or foils. A cylindrical experimental apparatus is constructed to obtain the liquid fraction and temperature distribution histories, as well as obtain photographic observations during the melting and solidification processes. A relative effectiveness, calculated as the ratio of the liquid fraction for a distinct case to that of a base case, as well as the complete melting and solidification times quantify the relative performance for each configuration. A total of six configurations: HP-Foil-PCM, HP-Foam-PCM, HP-PCM, Rod-PCM, Foam-PCM and Pure PCM, are investigated for a cylindrical PCM enclosure that contains a concentrically-located HP or rod. In a vertical orientation (vertically oriented cylinder) without base heat transfer, improved melting and solidification rates are achieved for the HP-Foil-PCM case with approximately one-third of the foil volume fraction relative to that of the foam in the HP-Foam-PCM case. The HP-Foil-PCM case with a 4.3% foil volume fraction was capable of improving the melting and solidification rates by a factor of 15 and 8, respectively, relative to a Rod-PCM system. When base heat transfer was present, the effect of system orientation (ranging from vertical to horizontal) was shown to be negligible for the HP-Foil-PCM and HP-Foam-PCM configurations when compared to the overall performance of the other configurations. The total melting and solidification times for the HP-Foil-PCM configuration were reduced to 12 % and 3%, respectively, of that for a non-enhanced (only base heat transfer) Pure-PCM configuration when the system was oriented both vertically and horizontally.

Chapter 1. Review and Advances in Energy Storage Systems with an Emphasis on Thermal Energy Systems

Energy storage technologies will play a key role in utilizing alternative energy solutions. Its implementation may provide the necessary link between the supply and demand of energy leading to higher efficiencies. Installation of an energy storage system may also improve the quality of the delivered energy, which is of particular interest for intermittent systems. The four main classifications of energy storage include chemical, electrical, mechanical and thermal, which are discussed in this work. When electricity is both present and is the desired final form of energy, chemical and electrical energy may be most applicable for smaller systems. However, other methods such as pumped hydro storage (PHS) and compressed air energy storage (CAES), as mechanical energy storage mechanisms, may also be implemented. Globally, PHS and CAES consist of the most utilized energy storage systems, but are strictly limited to select geographical locations and large scale applications. In other systems involving either hot or cold thermal energy, thermal energy storage (TES) is the method of choice. TES can be used to capture waste heat or to improve thermal management of a system. Sensible heat TES (SHTES) is more mature than latent heat TES (LHTES), however, it is typically limited to stationary and larger scale applications. Since LHTES systems utilize a phase change material (PCM), they can achieve high energy storage densities which allow their integration into small scale as well as portable systems, but most common PCMs have low thermal conductivities requiring a heat transfer enhancement. Intuitively, there is no single energy storage method that is ideal for all situations which establishes the need for a variety of approaches. Overall, further research on nearly all energy storage techniques is required to continuously improve the state of the art and lead to more wide-spread usage of energy storage applications.

1.1 Introduction

The demand for alternative energy solutions in recent years has increased as a means for reducing pollution, carbon dioxide production and consumption of petroleum products [1]. One method to attain these goals is to implement energy storage systems at locations where excess energy is present. Energy

storage techniques may be applied directly at power plants or at the location of end use, as well as intermediate points. The process of energy storage is achieved by three main steps (i) *charging*, where one form of energy (chemical, electrical, mechanical and thermal) is converted into another form, (ii) *storage*, where no intentional change in energy occurs (note that undesired self-discharge may occur during storage, such as heat loss) and finally (iii) *discharging*, where the stored energy is utilized at the time of need. Note that the storage phase is not necessary, hence charging may proceed directly into a simultaneous charging-discharging phase or discharging phase in some cases. Regardless of its operation scheme, a system must be cyclic in nature to facilitate both charging and discharging and may occur over a period of a few seconds to several months or even years [2,3]. While energy storage is essential to alleviate current power demands and better utilize intermittent power supplies, only approximately 2.5 % of the electric power delivered in the United States uses energy storage (mainly pumped hydro systems) compared to about 10 % and 15 % for Europe and Japan, respectively [4]. This is mainly due to the economic and political atmosphere which significantly limits the implementation of alternative energy systems, as well as energy storage, in the United States of America.

Intermittent power generation systems, such as wind and solar, require energy storage techniques to better integrate these systems into the electric grid [5,6]. The input energy in both systems is stochastic in nature with a variable supplied power due to factors such as time of day, cloud cover and seasons. Therefore, electrical conditioning needed to meet the grid requirements or an energy storage mechanism that is capable of handling a variable charging rate and able to achieve a stable discharging rate. The daily fluctuations in demand for electricity require generation services to provide power to the consumers as the need presents itself. For example, energy consumption increases during the daytime which is typically met by inefficient generation techniques, such as gas turbines [7]. As a result, off-peak power tends to be much more efficiently generated due to more stable production rates and consequently lower cost per kilowatt. By implementing energy storage systems both at the power source and at the location of end use, these fluctuations may be drastically reduced thereby lowering fuel consumption and cost.

While it is commonplace for batteries or pumped hydro storage (PHS) to come to mind at the mention of energy storage, other less common methods are also available, such as ultracapacitor energy storage to flywheel energy storage, which will be presented later. Since thermal energy is present during operation of most mechanical and electrical systems, thermal energy storage (TES) may be of use. There are two main applications of TES which include storing thermal energy (either hot or cold energy) for later use, or thermal management [8]. Currently the main application of TES is sensible heat TES (SHTES) where a TES material experiences a change in temperature during charging or discharging, such as for use with solar-thermal power plants [9]. However, SHTES requires a large mass and volume of the storage material which limits its use to stationary systems. The main drawback of SHTES is its low energy density which requires a large mass and volume of storage material to reach a desired energy storage capacity. The other main type of TES is latent heat TES (LHTES), which utilizes a phase change material (PCM) that stores both sensible and latent heat during operation, generally with a greater contribution from the latter.

LTHES is known for having high energy storage densities and nearly isothermal operation which allows for a broader range of applications relative to SHTES [10]. A few applications for LHTES in recent years include cooling of cell phones [11], vehicle waste heat recovery [12], building thermal management [13] and steam generation for electric power production [14] to name a few. In the future, TES, including both SHTES and LHTES, has the potential to shift the electrical consumption for heating and cooling from peak to off-peak power periods, which may offset the mismatch between the supply and demand experienced by the grid daily [15]. Currently, TES has many underutilized potential applications, which in the past has been limited mainly by cost and insufficient heat transfer rates (low energy density) in PCMs (SHTES materials).

In this work, a review of chemical, electrical, mechanical and thermal energy storage methods is presented. The sub-classifications of each are discussed along with its own unique advantages and disadvantages. In this work, the emphasis will be on TES, including SHTES and LHTES with a greater focus on the latter since it is a developing technology that has received more attention in recent years.

Overall, the goal of this work is to increase the knowledge base for energy storage techniques thereby increasing awareness, development and further utilization.

1.1.1. Energy storage types

In general, energy storage methods can be classified as one of the following: chemical, electrical, mechanical and thermal, of which can be further separated into the subdivisions seen in Fig. 1.1. Also, Table 1.1 presents a summary of typical parameters associated with each method. Overall, a high energy density, high overall efficiency (accounting for losses during the charging, storage and discharging periods), quick response time, low cost, little maintenance and a long lifetime are desirable in energy storage mechanisms [5,9,16,17]. One of the most important of the aforementioned traits is a high energy density, which allows for smaller volumes as well as a lesser amount of materials. A high energy density is desirable from both ergonomic and economic perspectives facilitating installation in existing as well as newly designed systems. As with any device, a compromise between the system cost, performance and efficiency must be made to determine if installation is appropriate. While all of the aforementioned traits are generally desirable, no single system comprises them all, which merits specific research tailored to each.

1.1.1.1. Chemical energy storage

Chemical energy storage refers to the process of converting electrical energy into chemical potential energy, which is generally converted back into electricity at the time of need. The chemical potential energy is stored by forming bonds between molecules and released upon the breaking of those bonds. The two main types of chemical energy storage are batteries (including conventional, metal-air and flow varieties) and regenerative fuel cells [4,6,18]. While other methods of chemical energy storage exist, such as biological energy storage, they will not be discussed here since their low efficiencies ($\sim 1\%$) limit their practical use [19].

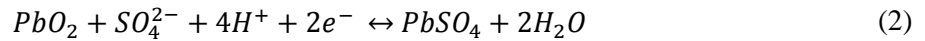
1.1.1.1.1. Conventional batteries

One of the oldest and most widely known types of energy storage is batteries. A battery consists of electrochemical cells with a positive electrode (anode) and a negative electrode (cathode) in contact with

an electrolyte. In a battery, electricity is converted to chemical potential energy through chemical reactions at the electrodes that is later discharged by the reverse process to produce electricity on demand. Advantages of batteries include reversible reactions, a rapid response to load changes, the potential for high efficiencies, commercial availability and can be manufactured quickly [4]. However, they also have low energy densities, small energy capacities, small discharge capabilities and contain toxic materials. Conventional batteries capable for use as utility energy storage applications are lead acid, lithium ion, nickel cadmium, nickel metal hydride, sodium sulphur and sodium nickel chloride. Batteries can be combined in series and parallel to provide the desired voltage and currents to meet the requirements of a particular system.

1.1.1.1.1 Lead acid

Lead acid batteries are the oldest type of rechargeable batteries that have been studied for more than 140 years [6,20]. This type of battery contains lead metal and lead oxide in a sulphuric acid electrolyte. When the battery is discharged the electrodes become lead sulphate and the electrolyte becomes mostly water. The chemical reactions describing a lead acid battery are:

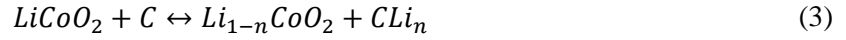


for the anode and cathode, respectively. The main advantages of lead acid batteries are their low cost (about \$50-310/kWh), high reliability and high efficiencies (~ 85 %) which have led to applications that provide up to 50 MW while the duration for lower power rating may last up to approximately 8 h [21]. However, their lifetime is short (3-12 years), they have a low energy density (about 40 Wh/kg) and are unable to function in low temperature applications which limits their use [1].

1.1.1.1.2. Lithium-ion

Lithium-ion batteries (Li-ion) operate with metal oxides containing lithium (LiCoO₂, LiMO₂, LiNiO₂, etc.) at the negative electrode and graphitic carbon at the positive electrode, while the electrolyte consists of lithium salts (LiPF₆ for example) dissolved in organic carbonates [22]. During charging, the lithium atoms at the negative electrode are ionized which move through the electrolyte to the positive

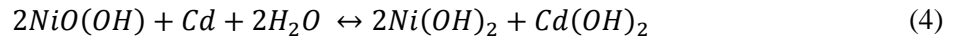
electrode where they join with an electron provided by an external power source. The reverse occurs during discharge thereby supplying power. One such example of a typical reaction for a Li-ion battery is:



However, the specific reaction depends on the type of metal oxide at the cathode. Li-ion batteries have an increased energy density (nearly 200 Wh/kg), lifetime (10,000 cycles) and a low memory effect relative to lead acid batteries [1,20]. Their main drawbacks are cost (\$900/kWh), vulnerability to damage from deep discharge and potential safety hazards if damaged. Currently, the main applications of Li-ion batteries are in portable electronics and the automotive industry due to their light weight and relatively high energy density [4].

1.1.1.1.1.3. Nickel cadmium (NiCd)

Relative to lead acid batteries, nickel cadmium batteries have higher energy densities (approximately 65 Wh/kg), a long lifetime, low maintenance costs and a high durability [20,23]. However, they are bulky, contain toxic materials, are subject to self-discharge and can cost up to \$1000/kWh. Therefore, more research efforts have been focused on Li-ion batteries due to lower costs and higher performance. The structure of a NiCd battery comprises a nickel hydroxide anode, cadmium hydroxide cathode, electrode separator and an alkaline electrolyte, which operate by the following reaction:



A large scale example of a NiCd battery storage system is seen in Alaska which is capable of providing 27 MW for approximately 30 min as a spinning reserve [24].

1.1.1.1.1.4. Nickel metal hydride (NiMH)

Since NiCd batteries are fairly toxic by containing cadmium, NiMH batteries provide an environmentally friendly alternative which has been shown to increase energy densities by about 30 % [23]. The energy density of NiMH batteries can reach 80 Wh/kg with 50 % longer lifecycles than lead-acid or NiCd batteries [25]. However, they do not have as high a performance as Li-ion and are subject to

self-discharge limiting their use for long term storage. Since the performance is not as good as Li-ion and are more costly than NiCd batteries, they are not likely a strong candidate for energy storage [18].

1.1.1.1.1.5. Sodium sulphur (NaS)

In a sodium sulphur battery, liquid sulphur and sodium occupy the positive and negative electrodes, respectively, separated by a beta alumina ceramic electrolyte. In NaS batteries, the electrolyte only allows flow of positive sodium ions, which combine with sulphur through the following reaction:



In order to maintain a liquid phase for its components, the temperature must remain between 300 °C and 400 °C resulting in parasitic losses in performance [18]. Additionally, they cost about \$350/kWh, operate with a slightly lower voltage than the aforementioned types and only one manufacturer currently produces these batteries [20,21]. Along with having a lifespan, energy density and efficiency of 2500 cycles, 100 Wh/kg and up to nearly 90 %, respectively, they have a significant advantage to other types since they can charge with a power source of up to six times their continuous power rating for short 30 s intervals [26]. An example of NaS in practical use is by the city of Tokyo, Japan, containing multiple installations with the largest installation capable of providing 9.6 MW for nearly 7 hours of discharging for load leveling.

1.1.1.1.1.6. Sodium nickel chloride (ZEBRA)

The sodium nickel chloride battery, commonly referred to as the ZEBRA battery due to its scientific birthplace in South Africa, is another high temperature system (about 300 °C) [4]. Nickel chloride is located at the positive electrode and sodium is at the negative electrode for the ZEBRA which operates by the following reaction:



Advantages of the ZEBRA battery include some overcharge and deep-discharge capabilities, a relatively higher cell voltage of 2.59V and a high degree of safety [18,20]. The energy density of the ZEBRA battery is about 120 Wh/kg with a cost of \$100-200/kWh making it a promising candidate for energy storage [27].

1.1.1.1.2. Metal-air batteries

Unlike the battery types discussed above, a metal-air battery consists of a common metal such as lithium, zinc, or aluminum at the anode while using air at the cathode that is typically constructed of a porous carbon material coated with a catalyst [26]. Therefore, one unique advantage of metal-air batteries is that they contain the highest theoretical energy densities since the oxygen in the air, for the cathode, does not need to be stored. In the past, focus has been on aqueous systems such as zinc-air, however, lithium air batteries have the potential for much larger capacities per mass relative to the former [28]. Decomposition of the solution for zinc-air batteries and corrosion of lithium metals are challenges that must be overcome before large scale utilization can be made possible. Lithium-air batteries are still a maturing technology which has yet to approach its theoretical values for energy capacity, specific power, etc. which requires more future research.

1.1.1.1.2. Flow batteries

An alternative subset of batteries that stores chemical energy in the electrolyte solution, instead of at the electrode, is that of flow batteries as seen in Fig. 1.2 [4]. The electrolytes are stored in external tanks and are pumped through the power cell containing the anode, membrane and cathode. Since flow batteries store their electrolyte in separate tanks, they have the advantage of large capacities, as well as high energy and power densities [29]. Inclusion of pumps for circulating the electrolytes induces parasitic losses which must be compensated for by the overall system performance. Also, toxic chemicals that are detrimental to the environment may be used in flow batteries and is not desirable. While a variety of flow batteries exist, they can be divided into two subgroups of redox (all-vanadium, vanadium-bromine, vanadium-cerium, iron-chromium, polysulphide-bromine, etc.) and hybrid (zinc-bromine, zinc-nickel, soluble lead acid, etc.) [17]. In general, flow batteries can have power ratings in the 100's of MW with discharging durations of up to 20 hours and a cost between \$180/kWh and \$250/kWh [29].

1.1.1.1.4. Regenerative fuel cells (RFC)

While both flow batteries and fuel cells can convert chemical potential energy to electrical energy, the distinguishing feature of fuel cells is the consumption of a fuel. In a fuel cell, there exists an anode

where fuel is supplied and ionized, an electrolyte that may be in the form of a membrane, and a cathode where the oxidant is supplied as seen in Fig. 1.3. Various types of fuel cells exist such as hydrogen fuel cells, direct-methanol fuel cells and solid oxide fuel cells. However, for energy storage, a regenerative fuel cell (RFC) is needed which consists of (i) a unitized fuel cell which can operate in both forward and reverse modes, or (ii) can be used in conjunction with an electrolyzer to produce fuel when electricity is supplied, in which case the entire device (fuel cell and electrolyzer) is termed a RFC [6]. Hence, the hydrogen fuel cell is one of the main types considered for energy storage as an RFC.

During charging, electricity can be utilized to convert water into hydrogen and oxygen, of which the former is stored. Since large tanks can be located on site, the capacity of a RFC can be relatively large. The main disadvantages are cost (more than \$10,000/kW) and efficiency (about 50 %) [20,30]. In order to lower costs, development of unitized RFCs have been studied by multiple researchers since the cell has both forward (fuel consumption) and reverse (fuel production) modes, eliminating the need for a separate electrolyzer [31]. An additional advantage to utilizing hydrogen fuel cells as RFCs, is that hydrogen is a chemical commodity with a variety of other uses such as for powering transportation vehicles [32].

1.1.1.2. Electrical energy storage

The process of converting electricity into electrostatic energy, such as by capacitors or superconducting magnetic energy storage (SMES) systems, is referred to as electrical energy storage [20]. Electrical energy storage is most advantageous when relatively smaller amounts of energy are needed instantaneously for a short duration on the order of seconds to minutes [33].

1.1.1.2.1. Capacitors/ultracapacitors

Ultracapacitors have high energy densities (up to 15 Wh/kg), long lifetime (20 years) and require no maintenance as compared to battery energy storage [27,34]. The lifecycle of ultracapacitors can be more than 100,000 charge/discharge cycles requiring little maintenance and have efficiencies up to 80 % [6]. Major problems which limit ultracapacitors to short term storage systems are the relatively high rate of self-discharge (around 20 % in 12 h) and the monotonically decreasing voltage during discharge

requiring additional electronics for conditioning. Typically capacitors are utilized for ride-through and bridging in power quality systems for shifting from one power source to another.

1.1.1.2.2. Superconducting magnetic energy storage (SMES)

SMES consists of an inductor made of a superconducting material that allows for electrical current to be stored and circulated through the inductor with near negligible losses [20]. The energy stored in a SMES system is defined as:

$$E = 0.5L_{coil}I_e^2 \quad (7)$$

where L_{coil} is the inductance of the coil and I_e is the electrical current. The system efficiency can be as high as 98 % and a lifetime of up to 30 years [27]. Currently, SMES systems can store up to about 10 MW while systems reaching up to 100 MW are in research with discharge durations on the order of minutes [20]. The main disadvantages of SMES are their high cost and the presence of a strong magnetic field which could be detrimental from an environmental perspective.

1.1.1.3. Mechanical energy storage

The two subsets of mechanical energy storage include kinetic and potential energy storage. Kinetic energy storage is only practical with flywheel energy storage (FES) for much smaller power ratings and capacities. Potential energy storage is utilized by pumped hydro storage (PHS) and compressed air energy storage (CAES) [17,35]. Both PHS and CAES are limited by their geographical locations (requiring reservoirs for water or air), however, currently provide the largest power ratings of all energy storage types [32].

1.1.1.3.1. Potential energy storage

As mentioned previously, potential energy storage comprises mainly pumped hydro storage (PHS) and compressed air energy storage (CAES). The main limitation to these systems is determining a suitable location which is more challenging than other storage systems since large reservoirs are needed for either water or air.

1.1.1.3.1.1 Pumped hydro storage (PHS)

Worldwide, pumped hydro storage comprises a total discharge power of approximately 127 GW, which is about 99 % of the planet's total energy storage capacity [4]. Hence, PHS comprises about 3 % of the total electric power production globally [20]. This method utilizes gravitational potential energy stored in water at different elevations as seen in Fig. 1.4 and described by the following equation:

$$E = mgh \quad (8)$$

where m , g and h are the mass of water, acceleration due to gravity and the change in height between the high and low reservoirs, respectively. In a PHS system, a pump consumes electrical energy to increase the gravitational potential energy of water, which is then converted back to electricity by a turbine.

The efficiency, power density, cost and lifetime of a PHS system may reach up to approximately 85 %, 1.5 Wh/kg, \$23/kWh and 60 years, respectively [27]. The efficiency of a PHS system is determined by the amount of power produced upon discharging divided by the input power to run the pumps, which includes evaporative losses. As expected, the geographical topography requirements, including two large water reservoirs at different altitudes, limits its utilization. A unique advantage of PHS systems is the supply of freshwater for the community [36].

1.1.1.3.1.2. Compressed air energy storage (CAES)

The second most utilized type of energy storage is compressed air energy storage with a total worldwide discharge capacity of about 440 MW [4]. CAES consists of utilizing electrical energy to compress air into a sealed, airtight cavern. Commonly, natural rock caverns, such as evacuated salt mines, gas fields or oil fields, are utilized [3]. The compressed air is then used to replace the compression stage of a gas turbine. Typical pressures in the CAES caverns are about 8 MPa with a power rating of 100-300 MW with efficiencies of approximately 80 % [20]. The sizing of a CAES system depends on the specific application, however, for wind power applications it is typically less than 25 % of the wind farm capacity [37]. A main advantage to CAES systems is the capability of a quick startup, associated with gas turbines, allowing for power demands to be met promptly. However, since the system also utilizes natural

gas to heat the compressed air, CAES is considered a hybrid energy storage system. Similar to PHS, the availability of an evacuated airtight cavern limits the possible locations of CAES systems.

1.1.1.3.2. Kinetic (Flywheel) energy storage

As mentioned previously, flywheel energy storage (FES) is the only suitable method for storing kinetic energy. During charging in a FES system, an electrical motor consumes electricity to increase the kinetic energy of a spinning mass, called a flywheel [2]. The stored kinetic energy is then converted back into electrical energy by the same electrical device, now acting as a generator, as seen in Fig. 1.5. The stored energy is described by:

$$E = \frac{1}{2} I \omega^2 \quad (9)$$

where I is the moment of inertia and ω is the angular velocity of the flywheel. Flywheel energy storage is characterized by low speed ($\omega < 10^4$ RPM) and high speed ($\omega > 10^4$ RPM) systems. Since the angular velocity is squared in Eq. (9), a small increase allows for a significant increase in stored energy. However, the angular velocity is limited based on the tensile strength of the flywheel material. Modern composite materials are used for high speed FES systems since they are lightweight and able to obtain much higher spinning speeds compared to metals, which are heavy. To reduce heat transfer losses, the flywheel enclosure may be under vacuum pressure as well as contain an active magnetic bearing [38]. The main advantages of FES include a long lifetime ($> 200,000$ cycles) and high efficiencies (90-95 %) [20]. Relative to the other methods, the cost is fairly high with values up to \$150,000/Wh for high speed FES systems [27]. Also the duration of FES systems is short on the order of magnitude of seconds. FES can provide uninterrupted power during the transfer of one power source to another or as a smoothing device such as for the power output of a wind turbine among other applications.

1.1.1.4. Thermal energy storage (TES)

Thermal energy storage (TES) allows for the storage of thermal energy (both hot and cold) for later utilization. TES may be separated into (i) sensible TES (SHTES) exhibited by a change in temperature (ii) latent heat TES (LHTES) by means of changing phase, (iii) chemical TES through

endothermic and exothermic reactions associated with the breaking of bonds between molecules, and (iv) sorption processes where energy is stored through Van Der Waals forces [39]. Since thermal energy is present in most systems, TES has numerous potential applications.

Thermal energy storage systems have proved to be a viable method to reduce inefficiencies in thermal systems by the capture of waste heat including direct power production through turbines, as well as improve thermal management of electronics [40], buildings [41], spacecraft [42] and vehicles [43]. Integration of TES systems into buildings (both residential and commercial) has the ability to provide some or all of the heating or cooling needs by utilizing energy during off-peak hours, thereby reducing costs and the demand of electricity during peak periods. One relatively unique feature of TES, relative to the aforementioned methods, is that the end product is not almost exclusively electrical energy, except for large scale thermal power production systems.

Two types of TES systems that will only be briefly discussed here are sorption and chemical TES [39]. A sorption system can be either physical (physisorption) or chemical (chemisorption) in which a substance becomes attached to another, thereby storing energy. In a physisorption system the adsorbate, a flowing gas or liquid, interacts with a surface, or adsorbent, and deposits a film on top of the adsorbent. Energy is stored in the Van Der Waals potential between the adsorbate and adsorbent. In a chemisorption system, new chemical bonds are formed between the adsorbate and adsorbent, storing more energy than Van Der Waals forces alone can manage. In a chemical TES system, a reversible chemical reaction is used to store energy by inducing an endothermic reaction which separates a chemical into two components that are stored separately and later recombined to release heat at the time of need by an exothermic reaction. In a simple chemical heat pump, low grade waste heat is used to decompose a solid, releasing a gas, which is then condensed to release higher grade heat. Chemisorption and chemical TES systems are more promising due to their higher energy density, and lower heat loss than physisorption, however, both technologies are not quite as mature as SHTES or LHTES and will not be further discussed.

1.1.1.4.1. Sensible heat thermal energy storage (SHTES)

Sensible heat thermal energy storage is the most established TES technology, especially for large scale solar-thermal power applications with existing plants capable of 7.5 h with a 50 MWe power capacity [44]. As previously mentioned, SHTES refers to the process of TES without a change in phase. This is generally associated with solids and liquids due to their much higher energy storage densities relative to gases. SHTES can be further classified into active, where the energy storage medium is used to flow (liquids only) through a heat exchanger, or passive where the energy storage medium is stationary (solid or liquid) [45]. Additionally, a direct active system is one in which the energy storage medium also serves as the heat transfer fluid (HTF). Since the materials used for SHTES have a low energy density without phase change, the large overall volume and mass limit its use to stationary (ground based) applications.

The amount of energy stored in a SHTES system is dependent on both the density and specific heat of the storage media as seen in Eq. (10). For a closed system, the amount of energy stored as heat, Q , (neglecting work as well as kinetic and potential energy changes) in a SHTES system can be written as:

$$\Delta E = Q = \int_{T_i}^{T_f} \rho V c_v(T) dT \quad (10)$$

where T_i , T_f , V , ρ and c_v are the initial temperature, final temperature, volume, density and specific heat capacity of the TES material, respectively [46]. If c_v is nearly constant over the given operating range, Equation (10) can be approximated as:

$$Q = V \rho c_v (T_f - T_i) \quad (11)$$

It is clear that for fixed operating conditions (constant Q , V and $(T_f - T_i)$), a SHTES material should be chosen with the higher volumetric heat capacity ($\rho \cdot c_v$) for a larger energy storage capacity.

1.1.1.4.2. Latent heat thermal energy storage (LHTES)

Relative to SHTES, LHTES is still a developing technology which operates by storing and releasing both sensible and latent heats, usually with a larger contribution by the latter, using a PCM [41]. LHTES systems are typically characterized by their high energy density, isothermal phase change and

small volume. However, most PCMs used in LHTES systems have low thermal conductivities requiring the use of an enhancement technique to increase overall heat transfer rates [47]. PCMs can be classified based on the phases (solid, liquid or gas) experienced during phase change which may be solid-solid, solid-liquid, solid-gas or liquid-gas [35]. While the latent heats of vaporization for solid-gas and liquid-gas PCMs are much higher than solid-solid or solid-liquid types, the relatively low density of gases and storage issues related to large volume changes renders their use impractical for most LHTES applications. However, solid-liquid PCMs are most common in recent studies since they generally have higher latent heats relative to solid-solid PCMs. Further classification of PCMs into organics, inorganics and eutectics will be discussed in more detail in later sections of this work.

During a complete charging process, a solid-liquid PCM, experiences three domains consisting of (i) sensible heating with a completely solid PCM, initially below its melting temperature, (ii) latent heating where both solid and liquid phases are present and (iii) further sensible heating of a completely liquid PCM until the final temperature of the heat source is reached, as described by:

$$\Delta E = Q = \int_{T_i}^{T_m} \rho V c_{v,s}(T) dT + \rho V h_{sl} + \int_{T_m}^{T_f} \rho V c_{v,l}(T) dT \quad (12)$$

where the subscripts s and l correspond to the solid and liquid phases, respectively, while T_m and h_{sl} are the melting temperature and latent heat stored during phase change, respectively [46]. If the solid and liquid specific heat capacities are assumed to be constant, Eq. (12) can be approximated as:

$$Q = \rho V \left(c_{v,s}(T_m - T_i) + h_{sl} + c_{v,l}(T_f - T_m) \right) \quad (13)$$

It should be noted that during operation of a LHTES system, it is not necessary for the PCM to experience all three domains and complete melting may not occur if the discharging, or solidification, process begins during the latent heating stage.

By comparing Eqs. (10) and (12), it can be seen that if the same operating temperature is observed by both a SHTES and LHTES system, the LHTES system will store a significantly larger amount of energy since it has an additional latent term along with the sensible term. While this statement is valid, it is not the method in which LHTES systems are implemented since large temperature swings

are not desirable as they induce additional stresses and fatigue on the enclosure. Rather, LHTES systems are designed to operate over a relatively small temperature range, containing the PCM melting temperature, for a certain energy storage capacity. In this method, the LHTES system mass and volume are greatly reduced relative to a SHTES system thereby increasing the potential applications that are not feasible for SHTES systems, such as for portable systems including handheld electronics, transportation vehicles and even spacecraft.

1.2. TES properties

Prior to the selection of a suitable TES material, the desired operating temperature range, enclosure function (only material storage or a storage tank with an integrated heat exchanger), system constraints (maximum allowable size, desired energy storage capacity, minimum required heat transfer rates, etc.) must be determined [48]. Once these variables are known, the selection of a given TES material can be chosen that meets the desired requirements. However, this may not be a simple task due to the overwhelmingly large number of TES materials including metal alloys, ceramics, glasses, polymers, elastomers and hybrids for SHTES, and paraffins, non-paraffin organics, salt hydrates, metallics and eutectics for LHTES [35,48]. In order to select the type of TES material, the desirable properties must be known. These properties will be discussed in the following sections and are separated based on thermal, physical, kinetic, chemical and economic aspects as summarized in Table 1.2. In general, these traits are all related to good heat transfer, energy storage, material safety and cost [49–51].

1.2.1. Thermal/physical

From a thermal perspective, a material should have a high thermal conductivity, high energy density per unit volume ($\rho \cdot c_p$), low vapor pressure, no deterioration with cycling, and for LHTES a PCM must have an acceptable phase change temperature within its operation range as well as a high latent heat and small volume change between phases [15,49]. If these conditions are met, then the size of the physical system can be decreased, thereby reducing the cost associated with bulk materials. Note that for LHTES, a low PCM thermal conductivity may be acceptable if an enhancement is implemented which increases the overall heat transfer rates to an appropriate level [52].

1.2.2. Kinetic

For SHTES materials, to the authors' knowledge, few if any kinetic limitations exist. On the other hand, for LHTES, a sufficient crystallization rate and negligible subcooling are desired [35]. Subcooling, also known as supercooling, is the phenomenon of lowering the temperature of a liquid below its melting temperature such as for a solid-liquid PCM. In a normal scenario without subcooling, the formation of crystals occurs at the PCM's melting temperature resulting in solidification. However, some materials lack nucleation sites thereby inhibiting phase change even as the system reaches its final system temperature. This is not desirable since without solidification, the PCM does not release its stored energy. It should also be noted that while a typical PCM may not experience subcooling at room temperature, when the scale is reduced to a micro-level, such as by micro-encapsulation, subcooling may occur [53]. In order to avoid this problem, inclusion of additives may facilitate nucleation in the PCM [54]. However, since subcooling is heavily dependent on the rate of cooling as well as the PCM type, an additive which is sufficient for a specific set of conditions may be completely ineffective in others requiring extensive research for a specific system [55].

1.2.3. Chemical

From a chemical perspective, the TES material should be non-toxic, non-corrosive, chemically compatible with all materials in contact with the TES material and be chemically stable without deterioration after cycling [13]. Also it should be non-flammable and non-explosive leading to a safe operating system.

1.2.4. Economic

In order for future utilization of TES systems to be practical, a TES material should also be inexpensive, easily obtainable, abundant and have a long lifetime [49].

1.3. SHTES systems

Research and development of thermal energy storage systems has been performed for more than 3 decades with the main area of concern being the energy storage medium [48]. Thousands of materials are known which can be classified into the following categories: metal and alloys, ceramics and glasses,

polymers and elastomers, and hybrids consisting of composites and natural materials. As with any type of TES system the operating range along with desired application determines the type of TES for a given system.

While SHTES systems generally require a larger volume and mass than LHTES systems, there exist many potential stationary applications where these issues are not a concern. Typical materials such as water, stone, sand, brick, concrete etc. are inexpensive, are not detrimental to the environment and have large operational temperature ranges [56]. Utilization of a solid SHTES material minimizes the possibility of leaks, while liquids may double as the HTF. When the energy storage material also acts as the HTF, a higher exergy efficiency may be realized due to a reduction in the temperature differences within the system [45].

Common SHTES materials can be seen in Table 1.3. With regards to the solid SHTES materials in the table, cast steel and cast iron have the two highest volumetric heating capacities ($\rho \cdot c_p$), yet cast steel costs more than 30 times that of cast iron. Therefore, cast iron is a more promising solid SHTES material. For the liquids, the most attractive of those listed in the table are the nitrate salts and mineral oil for their lower cost yet relatively high value for $\rho \cdot c_p$. Solar salts are commonly used in low temperature solar power applications. However their small temperature range limits the amount of sensible heat that can be stored, meaning that a large quantity of solar salt would have to be used to have an appreciable energy storage capacity.

1.3.1. Types of SHTES

Due to the different types of SHTES materials, there are a few common system configurations which usually comprise a bulk energy storage medium, packed bed arrangement, solar pond or thermocline [20,56].

1.3.1.1. Bulk energy storage medium

The simplest form of SHTES is through a bulk energy storage medium which is in contact with a heat exchanger or electric power source. Heat is generally transferred to or from an energy storage

medium mostly by HTF tubes embedded in the medium which may be a solid or liquid. If the medium is a liquid it may either be considered as passive, active or direct active as discussed above [45].

An example of a large scale active bulk energy storage system for solar power applications consists of two large tanks of molten salt [57]. In the two-tank system, one tank contains a cooler molten salt which is heated during charging and transported to a hotter tank. During discharging, thermal energy from the hot salt tank is transferred to the working fluid of a power plant and is subsequently sent to the cold storage tank. Aquifers comprise another large scale SHTES system in which water saturated permeable rock, located underground, may be used for seasonal thermal energy storage to reduce the burden of heating and air conditioning systems [58].

1.3.1.2. Packed beds

Since many abundant SHTES materials are of spherical construct, such as stone, a packed bed is a practical configuration as seen in Fig. 1.6. During charging, a hot fluid flows through the packed bed which stores thermal energy. Typical HTFs such as air, water or heat transfer oils may also act as an additional SHTES medium [58]. The parameters which must be varied for a given rock bed include the size of the particles, flow rate of the fluid, inlet temperature of the fluid, particle material and fluid type. The material and fluid choice determines the energy storage capacity of the system. The main disadvantage is the large pressure drop of the HTF flowing through the porous bed.

Packed bed systems may be utilized for low temperature residential applications as well as high temperature solar power applications among others [59]. For example, Hänchen et al. [60] studied a high temperature concentrating solar power (CSP) application of a packed bed with magnesium silicate rock and air as the working fluid for both the CSP and the energy storage system, thereby eliminating the need for expensive sealing gaskets and an additional heat exchanger since the system operated at near ambient pressure.

1.3.1.3. Solar ponds

A solar pond is a shallow body of water that stores energy from the sun. Natural solar ponds have been known to exist for about one century [61] while other types such as salt gradient, partitioned,

viscosity stabilized, membrane stratified and shallow solar ponds exist which operate in a similar manner. Solar radiation is absorbed by the dark bottom of a pond which retains heat by some means of stratification, such as a salt or viscosity gradient. Individual layers of a solar pond may be subject to natural convection as depicted in Fig. 1.7 [62]. If the water from the pond is not directly utilized, heat extraction must be accomplished through a heat exchanger, such as embedded HTF tubes or even heat pipe heat exchangers [63]. An optimum value for the salt content in a solar pond is about 80 g/kg of water [64]. Solar ponds are generally shallow on the order of about 2 m deep and may contain temperatures up to 100 °C [61]. In the past, industrial applications have made use of the water obtained from solar ponds for process heat. The main drawback is that they require a large area in order to have a substantial amount of useable water.

1.3.1.4. Thermocline

An alternative solution to the two-tank solar power SHTES systems is to utilize a one-tank thermocline design [65]. A thermocline is, to some extent, a combination of the aforementioned SHTES types which contains a thermal gradient due to buoyancy. However, a thermocline typically comprises an enclosure filled with a packed bed of a filler material saturated with a molten salt as the HTF, and both may act as energy storage mediums. Contrary to solar ponds, the highest temperature section resides at the top which diminishes with depth. During charging, cooler molten salt is removed from the bottom of the thermocline, heated and is then deposited at the top of the enclosure, while the reverse occurs during discharging. The filler material is ideally an inexpensive material with a high specific heat. Buoyancy forces keep the hot molten salt at the top of the tank while the cooler molten salt remains lower. Typical filler materials may include quartzite, marble and limestone [57]. The single tank storage in a thermocline SHTES system is generally slightly larger than the two individual tanks in a two-tank bulk SHTES system, which has the potential to reduce costs by up to 35 %.

The two main problems facing thermocline systems are that the salt must remain in the molten state and the effect of thermal ratcheting with cycling [66]. Generally the salt must be maintained above 150 °C to avoid altering its thermal and physical properties. On the other hand, thermal ratcheting occurs

due to the cyclic operation of system and results in plastic deformation and eventually failure of the tank, thereby shortening the lifetime of the system. Since large temperature gradients are experienced throughout its operation, expansion and contraction of the enclosure wall progressively increases its diameter (i.e. ratchets) to a larger size eventually leading to failure.

1.4. Latent heat thermal energy storage systems

As previously discussed, LHTES comprises utilizes a PCM to store and release both sensible and latent energies. Since a large amount of energy is needed to change phase relative to increase in temperature, it can be stored over a small temperature range. This can be effectively seen by comparing the values in Table 1.4. For example, water is commonly used for both SHTES and LHTES, however, more energy can be stored by changing phase than over a 50 °C temperature range. Table 1.4 clearly shows the advantage of a higher energy storage density for the LHTES with much less mass and volume required for a fixed capacity. Since LHTES has a high energy density, minimal mass and volume are required, facilitating its use for smaller and portable systems along with nearly any application utilizing SHTES. The other main advantage of LHTES is that the phase change is nearly isothermal, which is beneficial for improved thermal control.

1.4.1. Phase change materials (PCMs)

The key feature to any LHTES system is its phase change material (PCM) which stores and releases thermal energy by means latent heat. While solid-liquid PCMs are most common due to its higher latent heats, solid-solid PCMs have a unique advantage of negligible volume expansion between solid crystalline structures along with the elimination of leaks [49]. As previously mentioned solid-gas and liquid-gas phase transitions have much higher heats of fusion yet are impractical for most applications due to the large volume changes.

The two main requirements regarding utilization of PCMs for a LHTES are the determination of an appropriate phase change temperature and the latent heat of fusion. While single-component substances (also commonly referred to as laboratory or analytical grade PCMs) have a distinct melting temperature, most commercially available PCMs, comprise a mixture of components, such as various

paraffins, that melts over a relatively small temperature range depending on its composition [46]. Other factors which are considered for a particular application are the temperature range of operation, energy storage density, compatibility with the enclosure, chemical and thermal stability, cost and safety [41,67–69].

Generally, PCMs are classified into one of the following groups: organics, inorganics, and eutectics as seen in Fig. 1.8. A eutectic PCM is a minimum melting temperature composition consisting of two or more PCMs which may be any combination of organics or inorganics [70]. Table 1.5 shows the typical ranges for phase change temperatures and latent heats of fusion for commercially available PCMs which displays the broad ranges experienced for each subgroup. It is clear that a variety of PCM choices exist, as any listed in the table could apply for an operational temperature range from approximately 0 °C to 150 °C. Table 1.6 presents a variety of PCMs which have been studied in the past.

1.4.1.1. Organics

Organic PCMs are generally non-toxic, non-corrosive, chemically stable, thermally stable, have little to no subcooling, good compatibility with enclosure materials and have high latent heat per unit mass [13]. However, organics are known for their flammability as well as having relatively lower phase change enthalpies as compared to inorganics. Typically, organics are further categorized into paraffins and non-paraffins.

1.4.1.1.1. Paraffins

Paraffin waxes are one of the most common types of PCMs which are comprised of hydrocarbons and are derived from organic materials. Paraffin waxes are generally straight chain n-alkanes where a higher chain length corresponds to a higher melting temperatures and latent heats of fusion [35]. Commercial paraffin waxes are composed of a mixture of different chain length alkanes which have a range of melting temperatures (typically within a range of a few degrees centigrade) while laboratory grades are of higher purity with a single melting temperature [68]. Paraffins have melting temperatures typically between -10 °C to 120 °C and latent heat of fusions between about 130 – 250 kJ/kg [71]. Advantages include high latent heats, low volume changes upon melting, no phase segregation, low vapor

pressure, long lifetime of thermal cycling, are chemically inert, safe, reliable, have negligible subcooling, have well established properties, are relatively inexpensive and easily obtainable [13,68]. Their drawbacks are a low thermal conductivity (~ 0.2 W/mK) and moderate flammability; corresponding to the existence of paraffin wax candles.

1.4.1.1.2. Non-paraffins

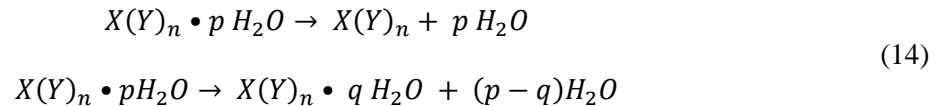
Non-paraffin organic PCMs are not easily classified with common characteristics as paraffins. There are many different types of non-paraffin organic PCMs which are generally grouped into fatty acids, alcohols, glycols and esters [35]. Non-paraffins commonly have a higher latent heat of fusion and are inflammable. The disadvantages of non-paraffins are low thermal conductivity, possible toxicity, unstable at high temperatures and can be considerably more expensive (approximately twice as much as paraffins).

1.4.1.2. Inorganics

Inorganic PCMs are classified into two main categories of salt hydrates and metallics. Inorganics have higher latent heats and thermal conductivities compared to organics and are also non-flammable [13]. However, they are plagued with subcooling, corrosion, phase separation, phase segregation and a lack of thermal stability after successive cycling.

1.4.1.2.1. Salt hydrates

One of the oldest and most studied classifications of PCMs is salt hydrates [72]. The combination of an inorganic salt (denoted $X(Y)_n$) and water consist of an aqueous solution as a liquid that is then hydrated to a crystalline matrix during discharging. The dehydration of the salt hydrate during melting is usually described by one of the following reactions [73]:



In the past salt hydrates have been preferred because of their high latent heat with typical values of approximately 300 kJ/kg. They have higher thermal conductivities than organic PCMs which are typically around 0.5 W/mK and undergo small volume changes during melting and solidification [35]. However,

salt hydrates have problems with subcooling and phase segregation, where the denser salt falls to the bottom and does not recombine with water, thereby degrading the system over time [74,75]. As previously mentioned, subcooling may be alleviated to some extent by addition of nucleating agents, yet it is an issue which must be addressed for a specific salt hydrate and operating temperature. While thickening agents may reduce the amount of phase segregation, they may also reduce the overall thermal conductivity. Lastly, from an economic perspective, salt hydrates are generally more expensive than paraffins.

1.4.1.2.2. Metallics

Metals considered for low temperature PCMs (high temperature PCMs will be discussed shortly) generally consist of low melting temperature metals, such as gallium with a latent heat of fusion and melting temperature of about 80 kJ/kg and 30 °C, respectively [35]. While this heat of fusion is much lower than that of other PCMs considered, in general metallics have high heats of fusion per unit volume due to the large densities [69]. Another advantage to metallics is their high thermal conductivities. However, they are not generally considered as PCMs due to large weight penalties.

1.4.1.3. Eutectics

A eutectic PCM is a minimum melting temperature composition of multiple PCMs (any combination of inorganics and organics) [69]. During solidification, the crystals of each component freeze as a mixture and later melt congruently without separation. Eutectics may consist of purely inorganics, organics or a combination whose composition result in the lowest melting point of the mixture [22]. Their volumetric energy storage density is also slightly higher than organics.

1.4.1.4. Solid-solid PCMs

Solid-solid PCMs typically change from one crystalline state to another by means of latent heat and usually do not experience significant volume changes. One such material which has exceptional qualities is high density polyethylene ($h_{sl} = 300$ kJ/kg) which is achieved by treating the material to induce cross linking, however, the treating process induces significant cost [54]. While solid-solid PCMs

generally do not have as high of latent heat per unit weight, as seen in Table 1.5, they can have high latent heat per unit volume making them attractive for stationary applications [49].

1.4.1.5. High temperature PCMs

High temperature PCMs, typically defined in the range of 120 °C to 1000 °C, may consist of any of the aforementioned types of PCMs and are of particular interest for solar applications. While many materials have been studied for use as low temperature PCMs, this is not the case regarding high temperature PCMs [76]. This may be attributed to safety hazards among other reasons relative to low melting temperature PCMs. However, in recent years they have received more attention due to research geared towards solar-thermal systems. Cárdenas and León [77] as well as Kenisarin [78] have performed literature reviews on high temperature PCMs and may be used as a reference for various thermophysical properties of high temperature PCMs. In the aforementioned works, the properties for high temperature PCMs vary widely from one material to another. Other than potentially high costs, chemical compatibility with various materials is a main challenge which must be overcome.

1.4.2. Enhancement techniques

Since the thermal conductivity of most PCMs is inherently low, a heat transfer enhancement is commonly implemented. The goal of an enhancement is to increase the overall heat transfer rates within the PCM and is usually achieved by the addition of a high thermal conductivity medium. Note that there is no single ideal enhancement method, however, the following are desired:

- ability to achieve high heat transfer rates
- contain minimal volume and mass
- compatible with PCM and enclosure
- resistant to corrosion and deterioration after repetitive cycling
- inexpensive, abundant and easily obtainable

Care must be taken when choosing an appropriate enhancement technique as the addition of a foreign material into the PCM may significantly suppress or even eliminate the positive contribution of natural

convection heat transfer on the melting process and could be detrimental to the overall performance [79]. Therefore, all domains (solid only, mixed solid and liquid, and liquid only) must be considered prior to the final selection of an enhancement method.

To achieve high heat transfer rates, a large interfacial surface area must exist between a heat transfer surface and the PCM. However, while the overall effective thermal conductivity increases proportionally to the mass of a high thermal conductivity additive, a larger mass does not guarantee improved heat transfer rates. Performance is also dependent on the thermal contact resistances as well as enhancer morphology within the PCM. If an enhancement method has insufficient thermal contact with a heat transfer surface, then it will not be effective. For example, Hamada et al. [80] found that carbon brushes with less mass outperformed carbon fiber chips due to insufficient thermal contact with the heat transfer surfaces for the latter. The physical construct of the enhancement technique, i.e. brushes vs. chips or fins vs. porous media, allows for different heat transfer pathways. For example, the heat transfer pathway for a fin is mainly two-dimensional while for a porous media is three-dimensional, which disperses heat differently. In certain applications, one type of pathway may be more desirable than another and the choice of an enhancement technique should be considered.

In the past, various approaches have been implemented as enhancement techniques such as the addition of fins [40], foils [81], foams or other porous media [82], particles [83], nanoparticles [84], carbon structures [85] and heat pipes [86]. Other enhancement methods include macro- or micro-encapsulation [87] or a cascaded configuration [88]. In order to improve the rates of heat transfer within the PCM to that beyond an individual enhancer, the combination of two or more has proven to be effective, depending on the type of enhancement and the particular configuration [89,90]. To illustrate the relative improvement in performance which can be achieved by the combination of aluminum foils and a heat pipe as enhancement methods, Allen et al. [91] experimentally decreased the melting and solidification time of a rod-enhanced PCM system in a vertical cylindrical enclosure from 200 min and 152 min to 13 and 11 min, respectively. In another study by Robak et al. [92], a 15 % reduction in capital costs relative to a SHTES, was reported to be achievable by the implementation of thermosyphons in a

LHTES, along with a reduced overall system volume for a large scale solar concentrating power CSP plant. Therefore, when sufficient heat transfer enhancement techniques are implemented into PCMs, LHTES may be both economically comparable and capable of achieving high energy storage rates relative to other energy storage systems.

1.5. Applications of TES

While the number of potential applications for TES is practically endless, some common applications will be discussed here. In general, there are two main uses for LHTES systems which are TES (including thermal energy recovery) or thermal management as seen in Fig. 1.9 [8]. Due to the large temperature fluctuations during operation, SHTES systems are limited to only TES applications. Note that there are many overlapping applications which may be considered for both SHTES and LHTES, or thermal energy storage and thermal management. However, the goal of a LTHES storage system for use in a thermal management application may not be to utilize the stored thermal energy but rather to reduce thermal fluctuations of a given system or increase heat dissipation (such as PCM integrated heat sinks). A few recent review papers which discuss the applications of TES include [5,13,41,58,67–69,93,94].

1.5.1. Thermal energy storage

When thermal energy is available, it may be stored in the form of hot or cold thermal energy by a LHTES or SHTES system. An advantage of LHTES relative to SHTES is that the temperature of the PCM may be closer to the environment temperature thereby minimizing unwanted heat loss or gain. Additionally, the driving temperature of a LHTES system can remain nearly constant between a heat transfer surface and the PCM phase change temperature during both charging and discharging which may vary greatly during operation for a SHTES system. These traits along with the higher energy density make LHTES an attractive form of TES, particularly for portable applications which is not practical for SHTES. Regardless, SHTES has found many applications where storage volume and mass are not limiting factors. Additionally, the main advantage of SHTES is the low cost of common materials (\$0.05/kg to \$5.00/kg) relative to PCMs (\$4.28/kg to \$334/kg) [5].

One of the main areas for TES is the field of solar energy which include but is not limited to high temperature solar power systems [9,65,95,96], solar heating / cooling [59,97], solar cooking [98,99] and solar greenhouses [100]. Other applications include non-solar power production [101], air conditioning [51,52,102], fuel cells [103], food processing [50], transportation of temperature sensitive goods [93] and ice storage for data center cooling [104]. Another main use for thermal energy storage is for integration with building materials [22,70,105]. While other TES applications exist, they will not be discussed here.

1.5.1.1. Thermal energy recovery

A more specific subset of TES is thermal energy recovery in either hot or cold forms. The process of waste heat (coolness) recovery is typically observed by the pre-heating (pre-cooling) of an incoming HTF by an outgoing HTF, or other medium. This usually occurs through a heat exchanger that may consist of segments of the same HTF at different points in a fluid line or may be two separate entities (comprised as a bulk solid, liquid, gas, etc.). Note that for SHTES systems, the HTF may act as the TES material which is stored in a separate storage tank when not in use. Without TES, a heat exchanger only recovers thermal energy effectively when both the hot and cold sources are active. However, if sensible or latent energy is stored, then the heat exchange device may have four possible operation modes: *charging* (only the hot source is active), *simultaneous charging and discharging* (both hot and cold sources are active), *storage* (hot and cold sources are inactive) and *discharging* (only the cold source is active). Note that for coolness recovery units, the roles of charging and discharging consist of removal and addition of thermal energy, respectively, which is contrary to conventional waste heat recovery terminology [93]. Therefore, the function of a thermal energy recovery device is to act as a thermal buffer which increases the overall efficiency of a system. Some examples of LHTES systems used for thermal energy recovery include low grade heat recovery [106], heat pipe heat exchangers [88,107], building materials [108,109], automotive [12,110,111], steel industries [112–114] and air conditioning [115].

1.5.1.2. Thermal management

As previously mentioned, the larger temperature fluctuations of a SHTES system renders it less useful relative to LHTES and consequently, will not be further discussed. By selecting an appropriate

phase change temperature, LHTES can be effectively used for thermal management of a system. The investigation of incorporating PCMs into building materials has received much interest in recent years [13,22,116]. Common building materials such as wallboards, cement, brick, etc. have included encapsulated PCM with little impact on the structural performance while contributing greatly to thermal comfort levels. On a summer day, energy is added to a building by both sunlight and through the building envelope. Without PCM the temperature of the room would increase, however, the increase can be greatly reduced (depending on the PCM properties, operating temperatures, etc.) reducing the demand of a traditional cooling system. This increase in energy is then dissipated during the night as the outdoor temperatures fall below the temperature within the building, and consequently discharges the PCM. During winter, a similar yet reciprocal behavior is observed where energy stored during the day due to sunlight is used to reduce the temperature drop during the night and the demand of the heating system. Therefore, the maximum and minimum temperatures experienced can be reduced to a more stable average temperature with less fluctuation, thereby increasing thermal comfort.

The other main area of thermal management using PCMs includes cooling of electronics. A PCM can be used to extend the duration in which an electronic heat generating source can operate prior to reaching a maximum allowable operating temperature. Many studies in the past 10 years have been focused on utilizing PCMs to achieve this goal through PCM based heat sinks which are cooled by convection to the ambient [40,117–119]. Additional thermal management studies using PCMs include but are not limited to integration with clothing [120], automotive [121], spacecraft [42], fuel cells [103], transportation of temperature sensitive goods (food, blood, organs, etc.) [93].

1.6. Conclusions

In this work, different energy storage systems with their unique advantages and disadvantages have been presented and discussed. While energy storage may be beneficial for a variety of systems, intermittent systems in particular require some type of energy storage in order for more stable operation that provide energy with a higher quality at the time of need. Currently, mechanical energy storage is the most widely used type of energy storage, including PHS and CAES, yet is limited by geographical

topography and mainly consists of large scale systems. Other smaller scale systems such as battery energy storage and LHTES have great potential to be utilized in residential applications, which may help alleviate the daily fluctuations experienced by power plants in the future. In general, LTHES is underutilized since the implementation of enhancement techniques has resolved its main drawback of insufficient heat transfer rates stemming from the low thermal conductivity of most PCMs. The high energy density, nearly isothermal operation and small temperature fluctuations experienced by a LHTES allows its implementation into a large variety of both small and large scale systems, as well as for stationary and portable applications. The lower cost of SHTES relative to LHTES has allowed its use in large scale power plants, however, a large system mass and volume is required due to the low energy storage density of SHTES materials. Overall, no single energy storage system comprises an ideal device, which emphasizes the need for various approaches. Hence, further research is needed to overcome the barriers that restrict further implementation of energy storage systems.

Nomenclature

c_v	specific heat capacity
E	energy
I	moment of inertia
I_e	electrical current
g	gravitational acceleration
h	height
h_{sl}	heat of fusion
L	length
L_{coil}	coil inductance
m	mass
p	numeric constant
q	numeric constant
Q	heat energy
t	time
T	temperature
V	volume
$X(Y)_n$	organic salt

Greek symbols

ρ	density
ω	angular velocity

Subscripts

<i>f</i>	final
<i>i</i>	initial
<i>l</i>	liquid
<i>m</i>	melting
<i>s</i>	solid, solidification

Acronyms

CAES	compressed air energy storage
CSP	concentrating solar power
FES	flywheel energy storage
HTF	heat transfer fluid
LHTES	latent heat thermal energy storage
PCM	phase change material
PHS	pumped hydro storage
RFC	regenerative fuel cell
SHTES	sensible heat thermal energy storage
SMES	superconducting magnetic energy storage
TES	thermal energy storage

References

- [1] Z. Zhou, M. Benbouzid, J. Frédéric Charpentier, F. Sculler, T. Tang, A review of energy storage technologies for marine current energy systems, *Renew. Sustain. Energy Rev.* 18 (2013) 390–400.
- [2] R. Sebastián, R. Peña Alzola, Flywheel energy storage systems: Review and simulation for an isolated wind power system, *Renew. Sustain. Energy Rev.* 16 (2012) 6803–6813.
- [3] H. Kim, J. Rutqvist, D. Ryu, B. Choi, C. Sunwoo, W.-K. Song, Exploring the concept of compressed air energy storage (CAES) in lined rock caverns at shallow depth: A modeling study of air tightness and energy balance, *Appl. Energy.* 92 (2012) 653–667.
- [4] B. Dunn, H. Kamath, J.-M. Tarascon, Electrical energy storage for the grid: a battery of choices, *Science.* 334 (2011) 928–35.
- [5] Y. Tian, C.Y. Zhao, A review of solar collectors and thermal energy storage in solar thermal applications, *Appl. Energy.* 104 (2013) 538–553.
- [6] A. Rabiee, H. Khorramdel, J. Aghaei, A review of energy storage systems in microgrids with wind turbines, *Renew. Sustain. Energy Rev.* 18 (2013) 316–326.
- [7] E.S. Rubin, H. Zhai, The cost of carbon capture and storage for natural gas combined cycle power plants, *Environ. Sci. Technol.* 46 (2012) 3076–84.

- [8] B. Zalba, J.M. Marín, L.F. Cabeza, H. Mehling, Review on thermal energy storage with phase change: materials, heat transfer analysis and applications, *Appl. Therm. Eng.* 23 (2003) 251–283.
- [9] A. Gil, M. Medrano, I. Martorell, A. Lázaro, P. Dolado, B. Zalba, et al., State of the art on high temperature thermal energy storage for power generation. Part 1 - Concepts, materials and modellization, *Renew. Sustain. Energy Rev.* 14 (2010) 31–55.
- [10] A.A. Al-abidi, S. Bin Mat, K. Sopian, M.Y. Sulaiman, A.T. Mohammed, CFD applications for latent heat thermal energy storage: a review, *Renew. Sustain. Energy Rev.* 20 (2013) 353–363.
- [11] S.C. Fok, W. Shen, F.L. Tan, Cooling of portable hand-held electronic devices using phase change materials in finned heat sinks, *Int. J. Therm. Sci.* 49 (2010) 109–117.
- [12] V. Pandiyarajan, M. Chinna Pandian, E. Malan, R. Velraj, R.V. Seeniraj, Experimental investigation on heat recovery from diesel engine exhaust using finned shell and tube heat exchanger and thermal storage system, *Appl. Energy.* 88 (2011) 77–87.
- [13] L.F. Cabeza, A. Castell, C. Barreneche, A. de Gracia, A.I. Fernández, Materials used as PCM in thermal energy storage in buildings: A review, *Renew. Sustain. Energy Rev.* 15 (2011) 1675–1695.
- [14] R. Adinberg, D. Zvegilsky, M. Epstein, Heat transfer efficient thermal energy storage for steam generation, *Energy Convers. Manag.* 51 (2010) 9–15.
- [15] A. Arteconi, N.J. Hewitt, F. Polonara, State of the art of thermal storage for demand-side management, *Appl. Energy.* 93 (2012) 371–389.
- [16] A. Khaligh, Z. Li, Battery, ultracapacitor, fuel cell, and hybrid energy storage systems for electric, hybrid electric, fuel cell, and plug-in hybrid electric vehicles: State of the art, *Veh. Technol. IEEE Trans.* 59 (2010) 2806–2814.
- [17] A. Evans, V. Strezov, T.J. Evans, Assessment of utility energy storage options for increased renewable energy penetration, *Renew. Sustain. Energy Rev.* 16 (2012) 4141–4147.
- [18] R.M. Dell, D.A.J. Rand, Energy storage — a key technology for global energy sustainability, *J. Power Sources.* 100 (2001) 2–17.
- [19] I. Dincer, M. Rosen, *Thermal energy storage: systems and applications*, John Wiley & Sons, West Sussex, 2002.
- [20] H. Chen, T.N. Cong, W. Yang, C. Tan, Y. Li, Y. Ding, Progress in electrical energy storage system: A critical review, *Prog. Nat. Sci.* 19 (2009) 291–312.
- [21] A. Poullikkas, A comparative overview of large-scale battery systems for electricity storage, *Renew. Sustain. Energy Rev.* 27 (2013) 778–788.
- [22] R. Baetens, B. Jelle, A. Gustavsen, Phase change materials for building applications: A state-of-the-art review, *Energy Build.* 42 (2010) 1361–1368.

- [23] N.-K.C. Nair, N. Garimella, Battery energy storage systems: Assessment for small-scale renewable energy integration, *Energy Build.* 42 (2010) 2124–2130.
- [24] D. Doughty, P. Butler, Batteries for large-scale stationary electrical energy storage, *Electrochem. Soc. Interface.* (2010) 49–53.
- [25] S. Vazquez, S.M. Lukic, E. Galvan, L.G. Franquelo, J.M. Carrasco, Energy storage systems for transport and grid applications, *IEEE Trans. Ind. Electron.* 57 (2010) 3881–3895.
- [26] K.C. Divya, J. Østergaard, Battery energy storage technology for power systems—An overview, *Electr. Power Syst. Res.* 79 (2009) 511–520.
- [27] D. Fernandes, F. Pitié, G. Cáceres, J. Baeyens, Thermal energy storage: “How previous findings determine current research priorities,” *Energy.* 39 (2012) 246–257.
- [28] A. Kraytsberg, Y. Ein-Eli, Review on Li–air batteries—Opportunities, limitations and perspective, *J. Power Sources.* 196 (2011) 886–893.
- [29] M. Skyllas-Kazacos, M.H. Chakrabarti, S. a. Hajimolana, F.S. Mjalli, M. Saleem, Progress in flow battery research and development, *J. Electrochem. Soc.* 158 (2011) R55–R79.
- [30] M. Gabbasa, K. Sopian, Review of the electrodes layer for unitized regenerative proton exchange membrane fuel cells, *Adv. Environ. Biotechnol. Biomed.* (2012) 163–168.
- [31] H. Matsushima, W. Majima, Y. Fukunaka, Three-phase interfacial phenomena in alkaline unitized regenerative fuel cell, *Electrochim. Acta.* 114 (2013) 509–513.
- [32] G. Zhang, X. Wan, A wind-hydrogen energy storage system model for massive wind energy curtailment, *Int. J. Hydrogen Energy.* 39 (2014) 1243–1252.
- [33] L. Qu, W. Qiao, Constant power control of DFIG wind turbines with supercapacitor energy storage, *IEEE Trans. Ind. Appl.* 47 (2011) 359–367.
- [34] X. Fang, N. Kutkut, J. Shen, I. Batarseh, Analysis of generalized parallel-series ultracapacitor shift circuits for energy storage systems, *Renew. Energy.* 36 (2011) 2599–2604.
- [35] A. Sharma, V.V. Tyagi, C.R. Chen, D. Buddhi, Review on thermal energy storage with phase change materials and applications, *Renew. Sustain. Energy Rev.* 13 (2009) 318–345.
- [36] J.S. Anagnostopoulos, D.E. Papantonis, Pumping station design for a pumped-storage wind-hydro power plant, *Energy Convers. Manag.* 48 (2007) 3009–3017.
- [37] P. Denholm, R. Sioshansi, The value of compressed air energy storage with wind in transmission-constrained electric power systems, *Energy Policy.* 37 (2009) 3149–3158.
- [38] J.G. Bai, X.Z. Zhang, L.M. Wang, A flywheel energy storage system with active magnetic bearings, *Energy Procedia.* 16 (2012) 1124–1128.
- [39] A.H. Abedin, M.A. Rosen, A critical review of thermochemical energy storage systems, *Open Renew. Energy J.* 4 (2011) 42–46.

- [40] L.-W. Fan, Y.-Q. Xiao, Y. Zeng, X. Fang, X. Wang, X. Xu, et al., Effects of melting temperature and the presence of internal fins on the performance of a phase change material (PCM)-based heat sink, *Int. J. Therm. Sci.* 70 (2013) 114–126.
- [41] A. Waqas, Z. Ud Din, Phase change material (PCM) storage for free cooling of buildings—A review, *Renew. Sustain. Energy Rev.* 18 (2013) 607–625.
- [42] T.Y. Kim, B.-S. Hyun, J.-J. Lee, J. Rhee, Numerical study of the spacecraft thermal control hardware combining solid–liquid phase change material and a heat pipe, *Aerosp. Sci. Technol.* 27 (2013) 10–16.
- [43] A. Jamekhorshid, S.M. Sadrameli, Application of phase change materials (PCMs) in maintaining comfort temperature inside an automobile, *World Acad. Sci. Eng. Technol.* 61 (2012) 400–402.
- [44] S. Kuravi, J. Trahan, D.Y. Goswami, M.M. Rahman, E.K. Stefanakos, Thermal energy storage technologies and systems for concentrating solar power plants, *Prog. Energy Combust. Sci.* 39 (2013) 285–319.
- [45] M. Haider, A. Werner, An overview of state of the art and research in the fields of sensible, latent and thermo-chemical thermal energy storage, *Elektrotechnik und Informationstechnik*. 130 (2013) 153–160.
- [46] A. Faghri, Y. Zhang, *Transport Phenomena in Multiphase Systems*, Elsevier Academic Press, Burlington, MA, 2006.
- [47] L. Fan, J.M. Khodadadi, Thermal conductivity enhancement of phase change materials for thermal energy storage: A review, *Renew. Sustain. Energy Rev.* 15 (2011) 24–46.
- [48] A.I. Fernandez, M. Martínez, M. Segarra, I. Martorell, L.F. Cabeza, Selection of materials with potential in sensible thermal energy storage, *Sol. Energy Mater. Sol. Cells*. 94 (2010) 1723–1729.
- [49] T. Nomura, N. Okinaka, T. Akiyama, Technology of Latent Heat Storage for High Temperature Application: A Review, *ISIJ Int.* 50 (2010) 1229–1239.
- [50] L.M. Bal, S. Satya, S.N. Naik, Solar dryer with thermal energy storage systems for drying agricultural food products: A review, *Renew. Sustain. Energy Rev.* 14 (2010) 2298–2314.
- [51] A. a. Al-Abidi, S. Bin Mat, K. Sopian, M.Y. Sulaiman, C.H. Lim, A. Th, Review of thermal energy storage for air conditioning systems, *Renew. Sustain. Energy Rev.* 16 (2012) 5802–5819.
- [52] G. Chaxiu, D. Hexin, W. Xinli, Performance enhancement of a PCM cold storage under condition of heat flux, *Challenges Environ. Sci. Comput. Eng.* (2010) 499–502.
- [53] L. Huang, E. Günther, C. Doetsch, H. Mehling, Subcooling in PCM emulsions—Part 1: Experimental, *Thermochim. Acta*. 509 (2010) 93–99.
- [54] M.M. Farid, A.M. Khudhair, S.A.K. Razack, S. Al-Hallaj, A review on phase change energy storage: materials and applications, *Energy Convers. Manag.* 45 (2004) 1597–1615.

- [55] A. García-Romero, G. Diarce, J. Ibarretxe, A. Urresti, J.M. Sala, Influence of the experimental conditions on the subcooling of Glauber's salt when used as PCM, *Sol. Energy Mater. Sol. Cells.* 102 (2012) 189–195.
- [56] S.M. Hasnain, Review on sustainable thermal energy storage technologies, Part I: heat storage materials and techniques, *Energy Convers. Manag.* 39 (1998) 1127–1138.
- [57] Z. Yang, S. V. Garimella, Thermal analysis of solar thermal energy storage in a molten-salt thermocline, *Sol. Energy.* 84 (2010) 974–985.
- [58] P. Pinel, C. a. Cruickshank, I. Beausoleil-Morrison, A. Wills, A review of available methods for seasonal storage of solar thermal energy in residential applications, *Renew. Sustain. Energy Rev.* 15 (2011) 3341–3359.
- [59] H. Singh, R.P. Saini, J.S. Saini, A review on packed bed solar energy storage systems, *Renew. Sustain. Energy Rev.* 14 (2010) 1059–1069.
- [60] M. Hänchen, S. Brückner, A. Steinfeld, High-temperature thermal storage using a packed bed of rocks – Heat transfer analysis and experimental validation, *Appl. Therm. Eng.* 31 (2011) 1798–1806.
- [61] A.A. El-Sebaei, M.R.I. Ramadan, S. Aboul-Enein, A.M. Khallaf, History of the solar ponds: A review study, *Renew. Sustain. Energy Rev.* 15 (2011) 3319–3325.
- [62] R. Singh, M. Mochizuki, T. Nguyen, A. Akbarzadeh, Applications of heat pipes in thermal management and energy conservation, *Front. Heat Pipes.* 2 (2011) 1–13.
- [63] S. Tundee, P. Terdtoon, P. Sakulchangsattajai, R. Singh, A. Akbarzadeh, Heat extraction from salinity-gradient solar ponds using heat pipe heat exchangers, *Sol. Energy.* 84 (2010) 1706–1716.
- [64] A.A. El-Sebaei, S. Aboul-Enein, M.R.I. Ramadan, A.M. Khallaf, Thermal performance of shallow solar pond under open and closed cycle modes of heat extraction, *Sol. Energy.* 95 (2013) 30–41.
- [65] Z. Yang, S. V. Garimella, Cyclic operation of molten-salt thermal energy storage in thermoclines for solar power plants, *Appl. Energy.* 103 (2013) 256–265.
- [66] S.M. Flueckiger, Z. Yang, S. V. Garimella, Review of molten-salt thermocline tank modeling for solar thermal energy storage, *Heat Transf. Eng.* 34 (2013) 787–800.
- [67] F. Agyenim, N. Hewitt, P. Eames, M. Smyth, A review of materials, heat transfer and phase change problem formulation for latent heat thermal energy storage systems (LHTESS), *Renew. Sustain. Energy Rev.* 14 (2010) 615–628.
- [68] M. Iten, S. Liu, A work procedure of utilising PCMs as thermal storage systems based on air-TES systems, *Energy Convers. Manag.* 77 (2014) 608–627.
- [69] M.K. Rathod, J. Banerjee, Thermal stability of phase change materials used in latent heat energy storage systems: A review, *Renew. Sustain. Energy Rev.* 18 (2013) 246–258.

- [70] N. Soares, J.J. Costa, a. R. Gaspar, P. Santos, Review of passive PCM latent heat thermal energy storage systems towards buildings' energy efficiency, *Energy Build.* 59 (2013) 82–103.
- [71] Rubitherm, Phase Change Material - RT, (2013).
- [72] S.D. Sharma, K. Sagara, Latent heat storage materials and systems: A review, *Int. J. Green Energy.* 2 (2005) 1–56.
- [73] P.A. Prabhu, N.N. Shinde, P.S. Patil, Review of phase change materials for thermal energy storage applications, *Int. J. Eng. Res. Appl.* 2 (2012) 871–875.
- [74] C.Y. Zhao, D. Zhou, Z.G. Wu, Heat transfer of phase change materials (PCMs) in porous materials, *Front. Energy.* 5 (2011) 174–180.
- [75] Z. Duan, H. Zhang, L. Sun, Z. Cao, F. Xu, Y. Zou, et al., CaCl₂·6H₂O/Expanded graphite composite as form-stable phase change materials for thermal energy storage, *J. Therm. Anal. Calorim.* 115 (2014) 111–117.
- [76] A. Hoshi, D.R. Mills, A. Bittar, T.S. Saitoh, Screening of high melting point phase change materials (PCM) in solar thermal concentrating technology based on CLFR, *Sol. Energy.* 79 (2005) 332–339.
- [77] B. Cárdenas, N. León, High temperature latent heat thermal energy storage: Phase change materials, design considerations and performance enhancement techniques, *Renew. Sustain. Energy Rev.* 27 (2013) 724–737.
- [78] M.M. Kenisarin, High-temperature phase change materials for thermal energy storage, *Renew. Sustain. Energy Rev.* 14 (2010) 955–970.
- [79] C.Y. Zhao, Z.G. Wu, Heat transfer enhancement of high temperature thermal energy storage using metal foams and expanded graphite, *Sol. Energy Mater. Sol. Cells.* 95 (2011) 636–643.
- [80] Y. Hamada, W. Ohtsu, J. Fukai, Thermal response in thermal energy storage material around heat transfer tubes: effect of additives on heat transfer rates, *Sol. Energy.* 75 (2003) 317–328.
- [81] M. Sugawara, Y. Komatsu, D. Onodera, H. Beer, Three-dimensional freezing of water in a copper foils porous layer around a coolant-carrying tube, *Heat Mass Transf.* 48 (2012) 1847–1854.
- [82] A. Gyekenyesi, A.C. Wroblewski, Numerical study of a thermal energy storage device utilizing graphite foam infiltrated with a phase change material, *J. Mater. Eng. Perform.* 23 (2013) 1–6.
- [83] S. Jegadheeswaran, S.D. Pohekar, T. Kousksou, Performance enhancement of solar latent heat thermal storage system with particle dispersion - an exergy approach, *Clean - Soil, Air, Water.* 39 (2011) 964–971.
- [84] Z. Rao, S. Wang, F. Peng, Molecular dynamics simulations of nano-encapsulated and nanoparticle-enhanced thermal energy storage phase change materials, *Int. J. Heat Mass Transf.* 66 (2013) 575–584.

- [85] P.M. Gilart, Á.Y. Martínez, M.G. Barriuso, C.M. Martínez, Development of PCM/carbon-based composite materials, *Sol. Energy Mater. Sol. Cells.* 107 (2012) 205–211.
- [86] N. Sharifi, S. Wang, T.L. Bergman, A. Faghri, Heat pipe-assisted melting of a phase change material, *Int. J. Heat Mass Transf.* 55 (2012) 3458–3469.
- [87] P.B. Salunkhe, P.S. Shembekar, A review on effect of phase change material encapsulation on the thermal performance of a system, *Renew. Sustain. Energy Rev.* 16 (2012) 5603–5616.
- [88] H. Shabgard, C.W. Robak, T.L. Bergman, A. Faghri, Heat transfer and exergy analysis of cascaded latent heat storage with gravity-assisted heat pipes for concentrating solar power applications, *Sol. Energy.* 86 (2012) 816–830.
- [89] X. Wang, Q. Guo, J. Wang, Y. Zhong, L. Wang, X. Wei, et al., Thermal conductivity enhancement of form-stable phase-change composites by milling of expanded graphite, micro-capsules and polyethylene, *Renew. Energy.* 60 (2013) 506–509.
- [90] Y.Q. Xie, J. Song, P.T. Chi, J.Z. Yu, Performance enhancement of phase change thermal energy storage unit using fin and copper foam, *Appl. Mech. Mater.* 260 (2013) 137–141.
- [91] M.J. Allen, T.L. Bergman, A. Faghri, N. Sharifi, Robust heat transfer enhancement during melting and solidification of a pcm using a combined heat pipe-metal foam or foil configuration, *J. Heat Transfer.* (2014) Submitted.
- [92] C.W. Robak, T.L. Bergman, A. Faghri, Economic evaluation of latent heat thermal energy storage using embedded thermosyphons for concentrating solar power applications, *Sol. Energy.* 85 (2011) 2461–2473.
- [93] E. Oró, a. de Gracia, a. Castell, M.M. Farid, L.F. Cabeza, Review on phase change materials (PCMs) for cold thermal energy storage applications, *Appl. Energy.* 99 (2012) 513–533.
- [94] P. Tatsidjodoung, N. Le Pierrès, L. Luo, A review of potential materials for thermal energy storage in building applications, *Renew. Sustain. Energy Rev.* 18 (2013) 327–349.
- [95] C.W. Robak, T.L. Bergman, A. Faghri, Enhancement of latent heat energy storage using embedded heat pipes, *Int. J. Heat Mass Transf.* 54 (2011) 3476–3484.
- [96] H. Shabgard, T.L. Bergman, N. Sharifi, A. Faghri, High temperature latent heat thermal energy storage using heat pipes, *Int. J. Heat Mass Transf.* 53 (2010) 2979–2988.
- [97] L. a. Chidambaram, A.S. Ramana, G. Kamaraj, R. Velraj, Review of solar cooling methods and thermal storage options, *Renew. Sustain. Energy Rev.* 15 (2011) 3220–3228.
- [98] A. Lecuona, J.-I. Nogueira, R. Ventas, M.-C. Rodríguez-Hidalgo, M. Legrand, Solar cooker of the portable parabolic type incorporating heat storage based on PCM, *Appl. Energy.* 111 (2013) 1136–1146.

- [99] R.M. Muthusivagami, R. Velraj, R. Sethumadhavan, Solar cookers with and without thermal storage—A review, *Renew. Sustain. Energy Rev.* 14 (2010) 691–701.
- [100] A. Vadiee, V. Martin, Thermal energy storage strategies for effective closed greenhouse design, *Appl. Energy*. 109 (2013) 337–343.
- [101] S. Sanaye, A. Fardad, M. Mostakhdemi, Thermoeconomic optimization of an ice thermal storage system for gas turbine inlet cooling, *Energy*. 36 (2011) 1057–1067.
- [102] P. Charvát, L. Klimeš, M. Ostrý, Numerical and experimental investigation of a PCM-based thermal storage unit for solar air systems, *Energy Build.* 68 (2014) 488–497.
- [103] A.P. Sasmito, T. Shamim, A.S. Mujumdar, Passive thermal management for PEM fuel cell stack under cold weather condition using phase change materials (PCM), *Appl. Therm. Eng.* 58 (2013) 615–625.
- [104] X.P. Wu, M. Mochizuki, K. Mashiko, T. Nguyen, T. Nguyen, V. Wuttijumnong, et al., Cold energy storage systems using heat pipe technology for cooling data centers, *Front. Heat Pipes*. 2 (2011) 1–7.
- [105] H. Caliskan, I. Dincer, A. Hepbasli, Thermodynamic analyses and assessments of various thermal energy storage systems for buildings, *Energy Convers. Manag.* 62 (2012) 109–122.
- [106] Y. Ammar, S. Joyce, R. Norman, Y. Wang, A.P. Roskilly, Low grade thermal energy sources and uses from the process industry in the UK, *Appl. Energy*. 89 (2012) 3–20.
- [107] Z. Liu, Z. Wang, C. Ma, An experimental study on the heat transfer characteristics of a heat pipe heat exchanger with latent heat storage. Part II: Simultaneous charging/discharging modes, *Energy Convers. Manag.* 47 (2006) 967–991.
- [108] V.V. Tyagi, S.C. Kaushik, S.K. Tyagi, T. Akiyama, Development of phase change materials based microencapsulated technology for buildings: A review, *Renew. Sustain. Energy Rev.* 15 (2011) 1373–1391.
- [109] M. Santamouris, D. Kolokotsa, Passive cooling dissipation techniques for buildings and other structures: The state of the art, *Energy Build.* 57 (2013) 74–94.
- [110] J. Shon, H. Kim, K. Lee, Improved heat storage rate for an automobile coolant waste heat recovery system using phase-change material in a fin–tube heat exchanger, *Appl. Energy*. 113 (2014) 680–689.
- [111] H. Tan, Y. Li, H. Tuo, M. Zhou, B. Tian, Experimental study on liquid/solid phase change for cold energy storage of Liquefied Natural Gas (LNG) refrigerated vehicle, *Energy*. 35 (2010) 1927–1935.
- [112] N. Maruoka, T. Mizuochi, H. Purwanto, T. Akiyama, Feasibility study for recovering waste heat in the steelmaking industry using a chemical recuperator, *ISIJ Int.* 44 (2004) 257–262.

- [113] H. Zhang, H. Wang, X. Zhu, Y.-J. Qiu, K. Li, R. Chen, et al., A review of waste heat recovery technologies towards molten slag in steel industry, *Appl. Energy*. 112 (2013) 956–966.
- [114] T. Nomura, N. Okinaka, T. Akiyama, Waste heat transportation system, using phase change material (PCM) from steelworks to chemical plant, *Resour. Conserv. Recycl.* 54 (2010) 1000–1006.
- [115] X. Zhang, S. Yu, M. Yu, Y. Lin, Experimental research on condensing heat recovery using phase change material, *Appl. Therm. Eng.* 31 (2011) 3736–3740.
- [116] C. Barreneche, A. de Gracia, S. Serrano, M. Elena Navarro, A.M. Borreguero, a. Inés Fernández, et al., Comparison of three different devices available in Spain to test thermal properties of building materials including phase change materials, *Appl. Energy*. 109 (2013) 421–427.
- [117] Z.G. Qu, W.Q. Li, J.L. Wang, W.Q. Tao, Passive thermal management using metal foam saturated with phase change material in a heat sink, *Int. Commun. Heat Mass Transf.* 39 (2012) 1546–1549.
- [118] R. Baby, C. Balaji, Experimental investigations on thermal performance enhancement and effect of orientation on porous matrix filled PCM based heat sink, *Int. Commun. Heat Mass Transf.* 46 (2013) 27–30.
- [119] J. Finn, D.J. Ewing, L.M.L. Ma, J. Wagner, Thermal protection of vehicle payloads using phase change materials and liquid cooling, *Am. Control Conf.* (2010) 1204–1210.
- [120] H. Yoo, J. Lim, E. Kim, Effects of the number and position of phase-change material-treated fabrics on the thermo-regulating properties of phase-change material garments, *Text. Res. J.* 83 (2012) 671–682.
- [121] K. Kim, K. Choi, Y. Kim, K. Lee, K. Lee, Feasibility study on a novel cooling technique using a phase change material in an automotive engine, *Energy*. 35 (2010) 478–484.
- [122] C.J. Rydh, Environmental assessment of vanadium redox and lead-acid batteries for stationary energy storage, *J. Power Sources*. 80 (1999) 21–29.
- [123] A. Faghri, Y. Zhang, J. Howell, *Advanced Heat and Mass Transfer*, Global Digital Press, Columbia, Missouri, 2010.
- [124] K. Nithyanandam, R. Pitchumani, Computational studies on a latent thermal energy storage system with integral heat pipes for concentrating solar power, *Appl. Energy*. 103 (2013) 400–415.
- [125] C. Alkan, E. Günther, S. Hiebler, Ö.F. Ensari, D. Kahraman, Polyurethanes as solid–solid phase change materials for thermal energy storage, *Sol. Energy*. 86 (2012) 1761–1769.

Table 1.1. Summary of recent studies on energy storage techniques.

Type	Reference	Capacity (MWh)	Power rating (MW)	Duration	Power density (Wh/kg) (Wh/m ³) (W/m ³)	Lifetime (years)	Capital cost (\$/kW) (\$/kWh)	Cycle efficiency (%)
Chemical								
Pb-acid battery	[4,20]	Up to 48 MWh	Up to 20 MW	hours	30-50 Wh/kg	5-15	300-600 \$/kW	75-90
Ni-Cd battery	[4,20]	46 MWh	Up to 40 MW	hours	50-75 Wh/kg	10-20	1000 \$/kW	60-70
Li-ion battery	[4,20]	4-24 MWh	Up to 10 MW	hours	75-200 Wh/kg	5-15	1800-4100 \$/kW	90-94
Flow batteries								
V-redox	[4,20,122]	4-40 MWh	1-10 MW	hours	20 Wh/kg	20	1950-2150 \$/kW	<85%
Fuel Cell								
Hydrogen PEM	[4,20]	-	Up to 50 MW	days	600-1200 Wh/kg	5-15	6-20 \$/kWh	45-65
Electrical								
Capacitors	[4,20]	-	Up to 50 kW	1 hour	20000 Wh/m ³	~5	200-400 \$/kW 500-1000 \$/kWh	60-70
SMES	[4,20]	-	~1-100 MW	1 hour	~30 Wh/kg	~2.3	200-300 \$/kW 1000-10,000 \$/kWh	~ 97
Mechanical								
PHS	[4,20]	184 MWh	10 MW to 5 GW	days	~30 Wh/kg	>60	600-2000 \$/kW 5-100 \$/kWh	60-90
CAES	[4,20]	250 MWh	10 MW- 1 GW	days	2200 W/m ³	>40	400-800 \$/kW 2-50 \$/kWh	70-89
FES	[4,20]	25 kWh	~10 kW- 1 MW	minutes	~30 Wh/kg	~15	250-350 \$/kW 1000-5000 \$/kWh	90-95
Thermal								
SHTES	[29,92]	450 MWh	100's MW	hours	10000 Wh/m ³	20	840-1680 \$/kW	60
LHTES	[29,92]	450 MWh	100's MW	hours	26000 Wh/m ³	20	680-1620 \$/kW	60

Table 1.2. Desired characteristics of a thermal energy storage system.

Property	Desired characteristics
Thermal aspects	Uniform T_m (LHTES only) High h_{sl} (LHTES only) Small volume change with temperature or phase change High thermal conductivity High heat transfer rates High energy density ($\rho \cdot c_v$) Minimal thermal degradation with time (rates and capacity) Minimal temperature gradients within the system Minimal heat loss to the environment
Kinetic aspects	Suitable TES storage container No subcooling (LHTES only) No phase segregation (LHTES only)
Chemical aspects	Completely reversible melting/solidification processes Nonflammable Non-toxic Non-corrosive
Economic aspects	Inexpensive High energy storage efficiency (charge/discharge cycle) Long lifetime Compact design

Table 1.3. Common materials used in SHTES systems.

Material	Reference	Temperature range (°C)	Density, ρ^* (kg/m ³)	Specific heat capacity, c_p^* (kJ/kg·K)	$\rho \cdot c_p^*$ (kJ/m ³ ·K)	Thermal conductivity, k^* (W/m·K)	Cost (\$/kg)
Solids							
concrete	[27]	200-400	2200	0.9	1870	1.5	
NaCl	[27]	200-500	2160	0.9	1836	7	0.05
cast iron	[27]	200-400	7200	0.6	4032	37	0.15
silica fire brick	[27]	200-700	1820	1	1820	1.5	1.00
sand-rock minerals	[5]	200-300	1700	1.3	2210	1	0.15
cast steel	[5]	200-700	7800	0.6	4680	40	5.00
magnesia fire bricks	[5]	200-1200	3000	1.2	3450	5	2.00
Liquids							
HITEC solar salt	[27]	120-133	1990	-	-	0.6	-
mineral oil	[9]	200-300	770	2.6	2002	0.1	0.30
nitrate salts	[9]	265-565	1870	1.6	2992	0.5	0.50
sodium carbonate salts	[9]	270-530	850	1.3	1105	71	2.00
silicone oil	[44]	300-400	900	2.1	1890	0.1	-
lithium salt	[44]	180-1300	510	4.2	2137	38	-
Dowtherm A	[44]	15-400	867	2.2	1907	0.1	-
Therminol 66	[44]	0-345	750	2.1	1575	-	-

*Note that the values in this table are approximate as the thermophysical properties vary with temperature.

Table 1.4. Comparison of common SHTES and LHTES materials with $\Delta T = 50\text{ }^{\circ}\text{C}$ [46].

Material (phase)	Reference	Density (kg/m^3)	Specific heat (kJ/kgK)	Temperature range (T_m)	Latent heat (kJ/kg)	Mass required for 1 MJ of storage (kg)	Volume required for 1 MJ of storage (m^3)
aluminum - sensible (solid)	[27]	2702	1.076	$< 600\text{ }^{\circ}\text{C}$	-	186	0.069
water - sensible only (liquid)	[35]	1000	4.23	$0\text{-}100\text{ }^{\circ}\text{C}$	-	47	0.047
water - latent only (liquid)	[123]	1000	4.23	($T_m = 0\text{ }^{\circ}\text{C}$)	334	18	0.018
n-octadecane - latent only (liquid)	[46]	774	2.16	($T_m = 27.5^{\circ}\text{C}$)	244	28	0.035

Table 1.5. Typical PCM melting temperature and enthalpy ranges [72].

PCM type	Melting temperature range (°C)	Latent heat of fusion range (kJ/kg)
organic: paraffins	-15 - 100	150-250
organic: non-paraffins	5-80	125-300
inorganic: salt hydrates	5-137	100-400
inorganics: non-salt hydrates	0-900	125-425
eutectics	5 - 140	100-250
solid-solid PCMs	20-185	25-275

Table 1.6. Common PCM materials.

Type	References	Melting temperature (kJ/kg)	Latent heat (kJ/kg)
Paraffins			
octadecane	[95]	27.5 °C	243.5
RT100	[9]	112 °C	213
RT25	[41]	24°C	164
RT20	[41]	20-22°C	172
FM20	[41]	20-23°C	130
Non-paraffin organics			
A164	[9]	112 °C	306
polyglycol E400	[8]	8 °C	99.6
dimethyl-sulfoxide	[8]	16.5 °C	85.7
polyglycol E6000	[8]	16.5 °C	190
biphenyl	[8]	71 °C	119.2
propionamide	[8]	79 °C	168.2
naphthalene	[8]	80 °C	147.7
erythritol	[8]	118 °C	339.8
Hydrated salts			
ClimSel C 23	[8]	23 °C	148
STL27	[8]	27 °C	213
S27	[8]	27 °C	207
TH29	[8]	29 °C	188
ClimSel C 32	[8]	32 °C	212
STL47	[8]	47 °C	221
STL52	[8]	52 °C	201
STL55	[8]	55 °C	242
PCM72	[8]	72 °C	n.a.
Non-hydrated salt inorganics			
KNO ₃	[124]	335	9500
NaNO ₃	[5]	307	172
AlSi ₁₂	[5]	576	560
MgCl ₂	[5]	714	452
NaCl	[5]	800	492
LiF	[5]	850	n.a
Na ₂ CO ₃	[5]	854	275.7
K ₂ CO ₃	[5]	897	235.8
KF	[8]	857	452
Metallics (wt. %, alloys)			
46.3Mg-53.7Zn	[78]	340	185
96Zn-4Al	[78]	381	138
34.65Mg-65.35Al	[78]	497	285
68.5Al-5.0Si-26.5Cu	[78]	525	364

64.3-34.0Cu-1.7Sb	[78]	545	331
46.3Al-4.6Si-49.1Cu	[78]	571	406
49Zn-45Cu-6Mg	[77]	703	176
84Mg-16Ca	[77]	790	272
83Cu-10P-7Si	[77]	840	92
56Si-44Mg	[77]	946	757
Eutectics			
KNO ₃ -NaNO ₂ -NaNO ₃	[5]	141	275
LiNO ₃ -NaNO ₃	[5]	195	252
MgCl ₂ -KCl-NaCl	[5]	380	149.7
Solid-solid PCMs			
n-alkyl ammonium tetrachlorometallates	[54]	37-93°C	122-340
high density polyethylene	[54]	127 °C	300
polyethylene glycol 1000- hexamethylene diisocyanate	[125]	19 °C (heating cycle) 26.3 °C (cooling cycle)	109 (heating cycle) 113 (cooling cycle)
polyethylene glycol 6000- hexamethylene diisocyanate	[125]	176 °C (heating cycle) 177 °C (cooling cycle)	59.9 (heating cycle) 47.2 (cooling cycle)
polyethylene glycol 10000- hexamethylene diisocyanate	[125]	171 °C (heating cycle) 173 °C (cooling cycle)	57.7 (heating cycle) 48.9 (cooling cycle)
polyethylene glycol 10000- isophorone diisocyanate	[125]	166 °C (heating cycle) 165 °C (cooling cycle)	57.4 (heating cycle) 41.2 (cooling cycle)
polyethylene glycol 10000- isophorone diisocyanate	[125]	169 °C (heating cycle) 168 °C (cooling cycle)	58.8 (heating cycle) 46.7 (cooling cycle)
polyethylene glycol 6000- toluene diisocyanate	[125]	161 °C (heating cycle) 164 °C (cooling cycle)	57 (heating cycle) 44.1 (cooling cycle)
polyethylene glycol 10000- toluene diisocyanate	[125]	162 °C (heating cycle) 162 °C (cooling cycle)	57.1 (heating cycle) 46 (cooling cycle)
n.a.: not available			

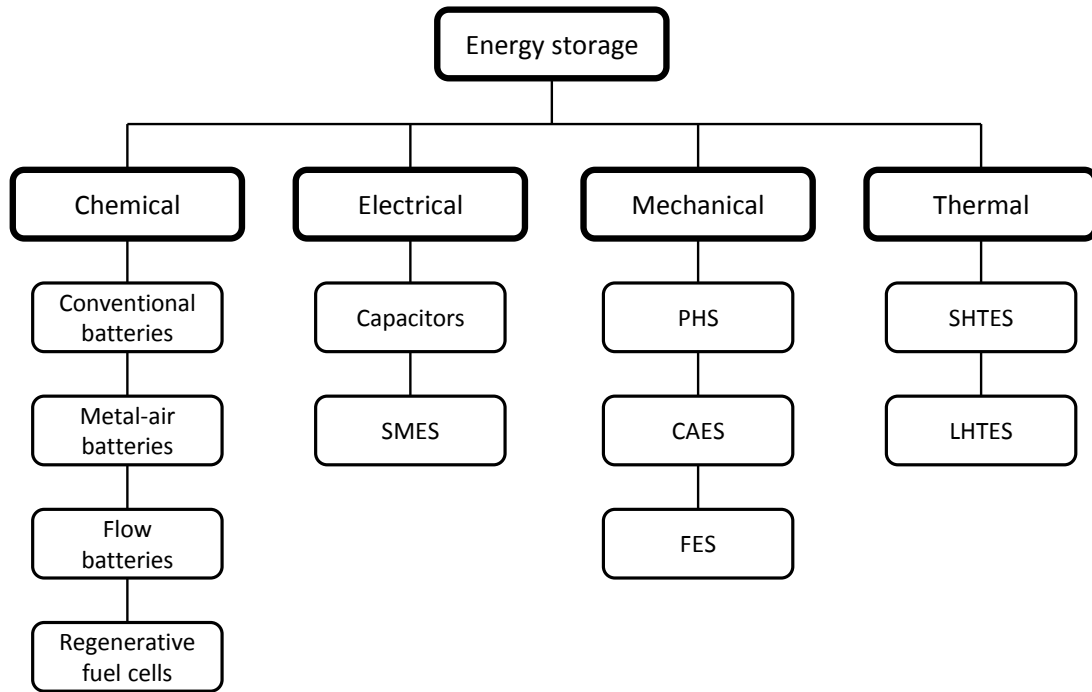


Fig. 1.1. Energy storage types.

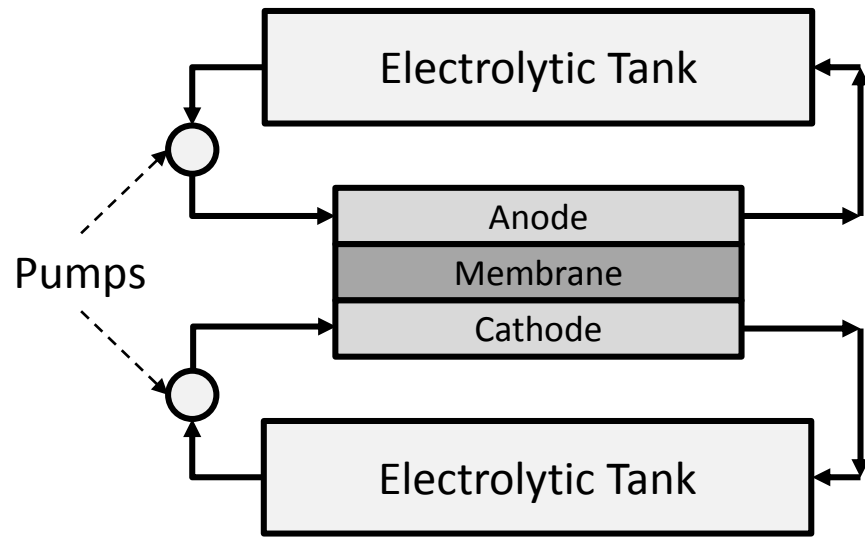


Fig. 1.2. Schematic of a typical flow battery.

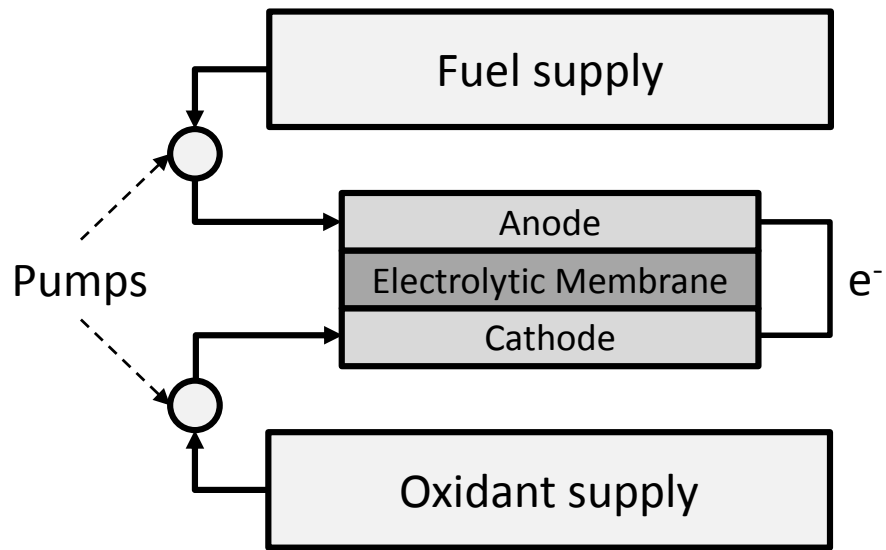


Fig. 1.3. Schematic of hydrogen regenerative fuel cell.

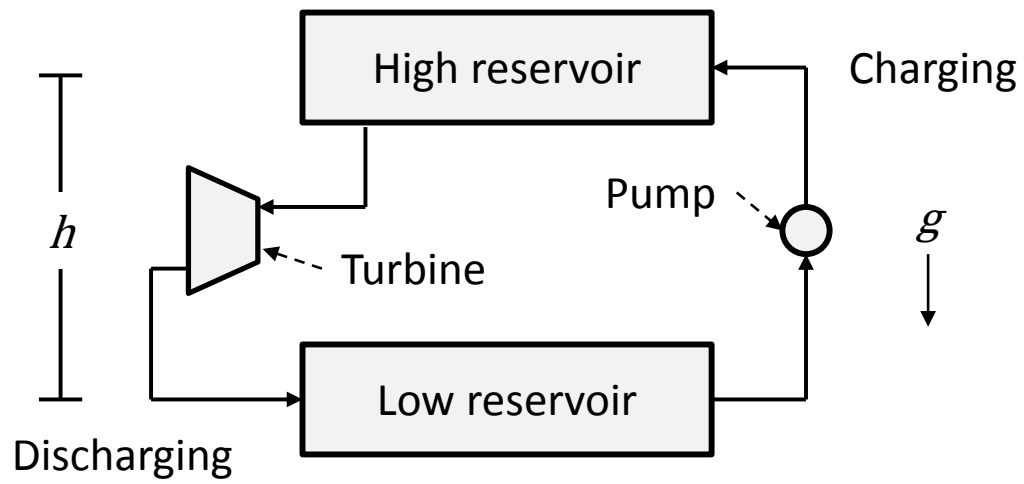


Fig. 1.4. Schematic of a pumped hydro storage system.

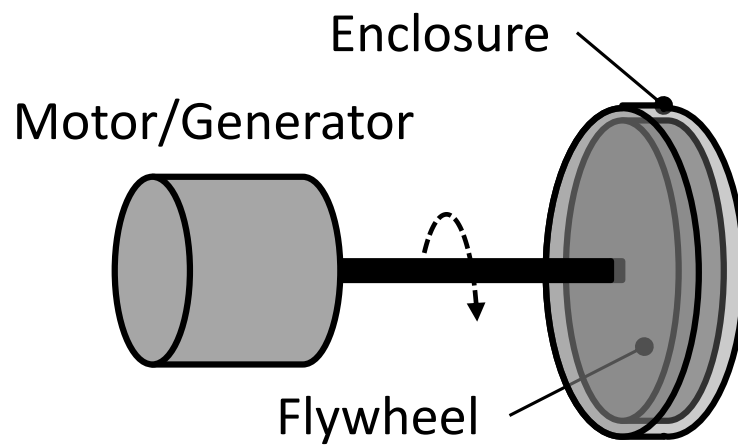


Fig. 1.5. Schematic of a flywheel energy storage system.

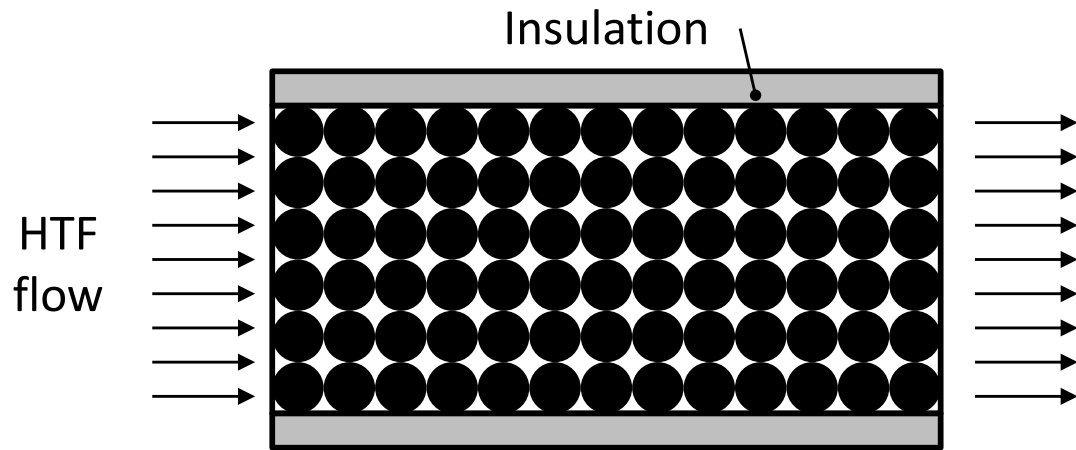


Fig. 1.7. Schematic of a packed bed SHTES.

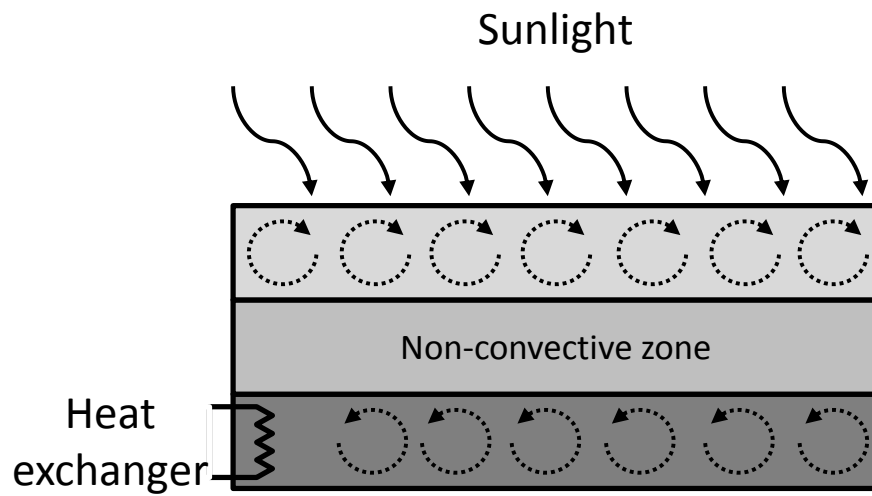


Fig. 1.7. Schematic of a solar pond.

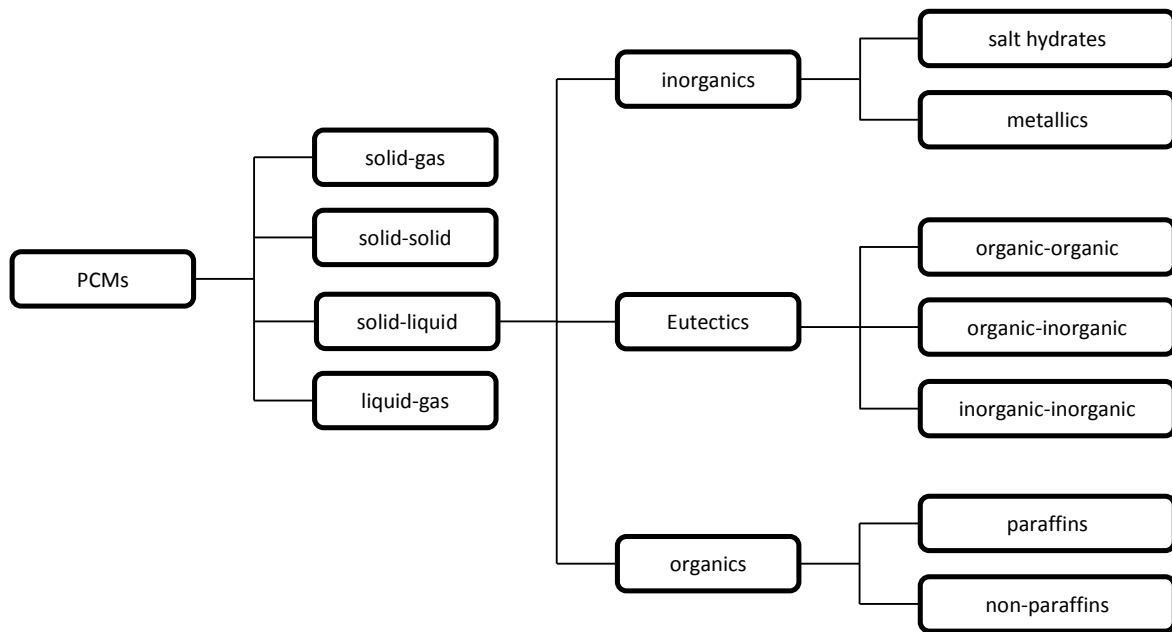


Fig. 1.8. Classification of PCMs.

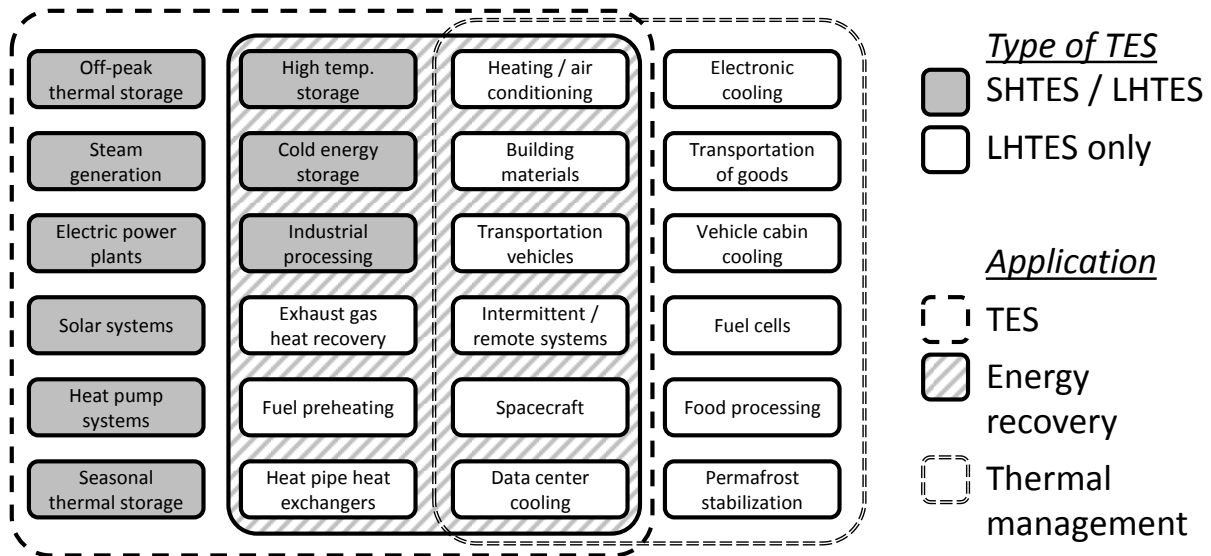


Fig. 1.9. Applications of TES.

Chapter 2. Challenges and Applications of Latent Heat Thermal Energy Storage Systems

Including Enhancement Techniques: Approach and Methodology

Latent heat thermal energy storage (LHTES) utilizing phase change materials (PCMs), has been an emerging technology in the past few decades that could be a pivotal solution for the utilization of alternative energies. LHTES is characterized by its high energy density and isothermal characteristics which make it suitable for both large scale terrestrial based applications as well as for small scale portable devices. However, the inherently low thermal conductivity of most PCMs requires the integration of heat transfer enhancement techniques. Heat transfer can be increased by two main methods: increasing the thermal penetration depth or by increasing heat diffusion. Common enhancement techniques include addition of high thermal conductivity extended surfaces, nanoparticles, structures and heat pipes, as well as utilizing encapsulation and cascaded configurations. By combining two or more of the aforementioned techniques, heat transfer rates can be further improved. This work reviews the various enhancement techniques that have been investigated in recent years including the advantages and disadvantages along with the challenges and unresolved issues for implementation.

2.1. Introduction

A renewed interest in latent heat thermal energy storage (LHTES) technologies implementing phase change materials (PCMs), has been observed in the last few decades due to the demand for alternative energy and thermal management systems [1–3]. A phase change material operates by storing latent energy during charging, which is later released at the time of demand. The types of phase change processes that are desirable for LHTES consist of solid-liquid and solid-solid, since liquid-gas and solid-gas experience large volume changes [4]. Since solid-solid PCMs do not have as high of latent heats relative to solid-liquid PCMs, only the latter will be of focus here [5].

Solid-liquid PCMs are desirable as thermal energy storage (TES) materials since they can have a high energy density, nearly isothermal operation and require minimal temperature differences to facilitate heat transfer relative to sensible heat thermal energy storage (SHTES) materials [6]. While SHTES is a more mature technology relative to LHTES, a large volume and mass of a SHTES material is required

limiting its use for mainly large scale terrestrial based applications [7]. On the other hand, the high energy density of LHTES allows its range of uses to extend into portable markets, such as handheld electronics and vehicle systems, as well as have the potential to reduce overall volume and capital cost relative to SHTES systems [8]. Researchers have studied implementation of PCMs in numerous applications including TES [2], power generation [9], solar systems [10], waste heat recovery [11], electronic cooling [12], heating ventilation and air conditioning [13], thermal management of buildings [14], automotive [15], aircraft [16], spacecraft [17], food industries [18,19] and heat exchangers [20]. Past review papers that discuss the different types and applications of PCMs include but are not limited to [3,13,21–24]. Generally, PCMs have the potential to be beneficial in systems where excess thermal or electrical energy is desired to be stored or dissipated and also experiences intermittent heating and cooling periods.

However, the real-world applications of LHTES systems are limited at best [25]. The reason being that most PCMs have low thermal conductivities, typically falling below about 1.5 W/mK [22]. Therefore, PCMs require some type of heat transfer enhancement technique to facilitate faster charging and discharging rates [26]. In recent years, the development of various heat transfer enhancement techniques has been the focus of many studies, as made evident by recent review articles [27–29]. Other problems encountered by PCMs may include deterioration of properties (thermal, storage and chemical) with successive cycling, subcooling, phase segregation, corrosion, incongruent melting, large volume changes, and high cost [8]. While there are numerous low temperature PCMs, a limited number of commercially available high temperature PCMs exist which limit the technology, especially for solar thermal power plants [10]. Additionally, a particular PCM, enclosure, heat transfer enhancement and heat exchanger must all be chemically compatible. All of these issues must be overcome prior to more widespread usage of LHTES systems.

In the past, numerous investigators have completed comprehensive reviews of PCM materials and applications [1,8,21–24,26,30] in which solid-liquid PCMs are separated into organics (such as paraffins), inorganics (such as salt hydrates) and eutectics. However, few have focused on the various approaches utilized to increase the heat transfer rates in PCMs [27,29]. In this work, recent investigations involving

PCM heat transfer enhancement techniques will be reviewed and each method will be thoroughly analyzed. As with the extensive number of PCMs for potential use, there also exist a significant variety of heat transfer enhancement techniques, which will be separated into several classifications. Each enhancement technique will be evaluated based on its performance and challenges along with its opportunities for improvement. However, it should be noted that there are no standard metrics for evaluating a specific enhancement technique which makes a direct comparison relatively difficult. Regardless, the reported improvements and challenges associated with the implementation of a specific technique will be presented.

2.2. Numerical modeling of PCMs

One of the major challenges associated with the mathematical modeling of a phase change process is to accurately represent the location of the solid-liquid interface. The moving boundary of the solid-liquid interface is accompanied with the latent heat absorption (during melting) or release (during solidification) and a sharp variation in the thermophysical properties of the liquid and solid PCM. Multi-dimensional configurations in real applications and the effect of natural convection in the molten PCM are additional physical phenomena which add to the complexity of the problem.

Numerical modeling schemes are separated into two major categories: deforming grid and fixed grid schemes [31]. The deforming grid schemes utilize a transformed grid to describe the solid-liquid interface. The grid density may be adapted to be higher near the solid-liquid interface and lower elsewhere in computational domain. However, the deforming grid scheme is more challenging to implement than the fixed grid scheme. In the latter, a fixed grid covers the entire computational domain including the solid, liquid and mushy (containing solid and liquid) regions of the PCM. Additionally, the solid-liquid interface is accounted for using an enthalpy-temperature relation.

There are three different methods to solve the phase change problem using a fixed grid scheme [31]: enthalpy method [32–34], the equivalent heat capacity method [35,36], and the temperature transforming model (TTM) [37–39]. It was reported that when using the enthalpy method, the temperature at a typical grid point may oscillate with time and that the equivalent heat capacity methods

suffered in selecting the grid size and time step, as well as often produced physically unrealistic oscillatory results. The TTM encountered inconsistencies [40] which led to unreasonable results or solution divergence. Also, different methods were presented to force the velocities to be negligibly small in the solid region of the PCM during phase change, classified as the [40–42]: source term, switch-off, ramped source term, ramped switch-off and variable viscosity methods. Each of these methods employed a large value (e.g. 10^{30}) in their algebraic equations to approximate the large viscosity of a solid or to scale the solid velocities, which results in numerical singularities and difficulty in solution convergence and accuracy. Straightforward methods, such as introducing a solid velocity correction, are commonly used to resolve this challenge [43–45]. In one such study, Shimin et al. [46] integrated a pressure decoupled solid-velocity correction into the TTM and determined that it provided a more robust solution compared to other methods such as: source term, switch-off, ramped source term, ramped switch-off and variable viscosity methods.

Advantages

- Practical engineering correlations may be developed by the results of numerical modeling.
- Comprehensive parametric studies may be performed by simply changing parameters and material properties.
- Numerical modeling is particularly attractive for high temperatures applications since experiments may be more difficult to perform and have a higher potential for safety hazards.
- Modeling is much more cost effective compared to experimental measurements.
- User friendly software may commonly be utilized for modeling.

In terms of detailed numerical modeling:

- Fixed grid schemes are relatively simple to implement compared to adaptive or moving grid schemes.
- The TTM does not suffer from temperature oscillation or unrealistic results compared to other methods such as enthalpy and equivalent heat capacity.

- TTM is not as sensitive as other phase change models in selecting grid size and time steps.
- Computational times may be reduced by orders of magnitude using the TTM with the standard under relaxation version of the consistent update technique algorithm.
- Integrating the TTM with the pressure decoupled solid-velocity correction [46] provides a more robust solution compared to the source term, switch-off, ramped source term, ramped switch-off and variable viscosity methods.

Disadvantages/Challenges

- Adaptive or moving grid schemes are relatively more difficult to implement compared to fixed grid schemes.
- The enthalpy and equivalent heat capacity methods may suffer from temperature oscillation or unrealistic results.
- The equivalent heat capacity method may also suffer for selecting the grid size and time step.
- The current TTM is for pure PCM (constant phase change temperature) modeling, however, it must be modified for PCMs comprised of a mixture of components with varying phase change temperatures.
- The enthalpy method was widely used for PCM modeling, even to solve benchmark problems, however, it was reported in the literature that this method suffers from temperature oscillation.
- The current TTM is not capable of predicting the shape of the dendrites for the PCM during the solidification.
- The TTM is limited for a fixed grid approach, not a moving boundary approach.

Unresolved issues

- For studies involving PCM melting in a 2D computational domain heated from below, most investigators neglected the 3D effect of Benard cellular convection flows which exists in the molten PCM at early stages of melting.

- For the fin-enhanced PCM configurations, most investigators neglected the 3D effects present at the fin tips, even for 2D computational domains
- An innovative method is needed to model the PCM expansion or contraction with a fixed grid approach since the moving boundary method is relatively complicated.
- In most applications, the turbulent nature of the natural convection currents is present which is more time consuming to model relative to laminar flows. Therefore, developed correlations are needed for the effects of turbulent flow.

2.3. Enhancement techniques

In the past, researchers have studied a myriad of enhancement techniques which aim to increase the overall heat transfer rates within a PCM, as reported in [1,13,21,27,29]. In this work, the various methods are categorized as: extended surfaces (fins or foils), nanoparticles, structures (foam, expanded graphite (EG)), heat pipes (HPs) or thermosyphons (TSs) (and other reflux systems), encapsulation (macro and micro/nano) and cascaded arrangements as presented in Fig. 2.1. The improved heat transfer mechanism generally consists of increasing either the thermal penetration depth or heat diffusion within a PCM. Increasing the thermal penetration depth is a necessity for utilizing the PCM farther from the heat source while thermal diffusion is more localized to the heat transfer surfaces (HTSs). Enhancement methods such as extended surfaces and heat pipes increase the thermal transport capabilities within the PCM to emulate a HTS far from the original heat sink or source. Other enhancements such as the addition of particles and structures affect the effective thermal conductivity of the enhancer-PCM composite, thereby increasing heat diffusion. Since increasing either the thermal penetration depth or the heat diffusion in a PCM system are each effective, their combination may allow for further improvement beyond the scope of each individually.

While it is intuitive that a higher effective thermal conductivity increases heat transfer, it does not guarantee improved performance. This is due to the morphology of the enhancement method which may include fins, foils, foam, EG, matrices or nanoparticles which is not taken into account into calculation of the effective thermal conductivity [47]. Therefore, if the same high thermal conductivity material is

implemented as two different forms into a PCM, the improvement in heat transfer performance may be drastically different. For example, Hamada et al. [48] observed that including carbon brushes was more effective at increasing the overall heat transfer rates than adding fiber chips, even though the effective thermal conductivity using the chips was larger than that of the brushes. It was determined that the carbon fiber brushes had superior contact with the HTS relative to the chips which allowed for better performance.

It should be noted that integration of foreign objects into the PCM may significantly suppress the positive contribution of natural convection on the melting process and has the potential to actually decrease the melting rates. For example, Zhao and Wu [49] found that while porous materials (high thermal conductivity foams, EG, etc.) can increase conduction heat transfer during melting, it may not outweigh the suppression of natural convection in a completely liquid domain, thereby decreasing the performance of the PCM system post melting. Therefore, care must be taken when choosing an enhancement technique to ensure that all domains of energy storage (completely solid PCM, presence of both solid and liquid PCM, and completely liquid PCM) are considered. Regardless of the enhancement method, it is of the utmost importance that the thermal contact resistance at the interface between the HTS and an enhancer be maintained at a minimum. If separation occurs between the enhancer and HTS after successive cycling, system failure may transpire. However, during solidification, natural convection has negligible impact, hence, any type of enhancement technique increases the solidification rate. Overall, the ideal enhancement technique would most effectively utilize the mass of the enhancer while occupying a minimal volume to maintain a high storage density of the LHTES system.

2.3.1. Extended surfaces

The addition of extended surfaces, including fins and foils, is one of the simplest methods used to increase the surface area of the HTSs in thermal systems. Fins typically comprise geometries such as rectangular, cylindrical (pin fins), or cones and are relatively thicker and more rigid compared to foils. Foils on the other hand, are defined here as thin fins with thicknesses (t) on the order of magnitude of a few microns to below approximately $t = 0.1$ mm. The flexibility of foils also resolves the stress related

problems induced by the PCM volume expansion and contraction with phase change [50]. Another main difference between foils and fins arises from the method of attachment to a HTS. Annularly shaped foils may be easily manufactured and installed with existing technologies, such as a press-fit method. This is contrary to fins which are generally fixed by a more permanent means, such as welding or adhesive epoxies. While it is possible to attach foils to a planar surface, it increases the cost and difficulty of installation which may not be desirable. The final major attribute which distinguishes the two enhancement techniques is that foils can have a much smaller pitch for the same metal volume fraction, thereby changing the intended form of enhancement, from increasing the thermal penetration for fins to increasing the thermal diffusion with foils.

As previously discussed, the effective thermal conductivity of foils and fins may be calculated to be identical if the same material and porosity are implemented [31]. However, different melting and solidification rates would occur due to the varying heat transfer mechanisms of each method. The smaller foil pitch would result in mainly conduction-dominated heat transfer, while the relatively larger fin spacing results in some degree of natural convection between fins for a fixed enhancer volume. Hence, fins are preferred for increasing the thermal penetration depth while foils are preferred for increasing heat diffusion.

2.3.1.1. Fins

In LHTES, the role of different fin configurations in enhancing performance has been studied extensively by various researchers. The two main devices for transferring heat between a PCM are a heat transfer fluid (HTF) (used in water heaters, power plants, waste heat recovery systems, etc.) or a hot or cold boundary wall (electronic cooling, etc.). The location of the fins in systems where there is no HTF is obviously on the PCM side. But if the PCM transfers heat with a HTF, the location of the fins is generally based on the relative heat transfer coefficient. This is because, the efficiency of a fin increases with a decrease in the heat transfer coefficient [51]. In most systems, the heat transfer coefficient on the PCM side is less than that on the HTF side, and thus it is a general practice that fins are on the PCM side. However, it is important to understand whether or not the presence of fins actually provides an

appreciable performance enhancement. This improvement depends on the fin properties, PCM properties, fin-PCM configuration and thermal boundary conditions. Fins should have high thermal conductivity and good corrosion resistance as well as occupy minimum volume and mass. Moreover, the heat transfer mechanisms during phase change depend upon the configuration as well as the orientation of the system and fins. The proceeding discussions in this section deal with the heat transfer mechanisms and the role of fins in determining the modes of heat transfer during melting and solidification separately. A summary of experimental and numerical investigations involving fins in recent years are presented in Table 2.1 and Table 2.2, respectively. The advantages, disadvantages and unresolved issues for fin type systems are as follows:

Advantages

- Fins are a simple yet effective method to provide a significant degree of thermal penetration into a PCM.
- The techniques regarding the implementation of fins in both experiments and modeling are well established.
- The manufacturing techniques for fins are well established.
- Fins are available to be constructed from a wide variety of materials.

Disadvantages/Challenges

- Typically requires some type of attachment method, such as welding or a thermal adhesive, which increases the manufacturing costs. This may also induce undesired thermal contact resistances.
- The presence of fins may significantly suppress natural convection in the molten PCM.
- The fin efficiency decreases as the length of the fins increase. This issue becomes more exaggerated for fins with lower thermal conductivity such as those typically used in higher temperature LHTES systems (stainless steel or more expensive nickel and super alloys).

Unresolved issues

- Stress issues related to PCM expansion and contraction during phase change may cause fractures at the location of attachment, especially for high temperature systems in which the fin itself also expands and contracts.
- In high temperature environments, common high thermal conductivity materials such as copper and aluminum may not be used and lower thermal conductivity materials must be utilized.
- While a greater fin thickness can achieve higher heat transfer rates, it also occupies more volume and mass which is detrimental to the overall energy storage capacity. Therefore, optimization should be carried out to obtain the preferred fin specifications.

2.3.1.2. Foils

As discussed previously, foils are thin ($t < 0.1$ mm) flexible fins which generally have a smaller pitch. Since melting in a foil-PCM composite is mainly conduction dominated, the enhancement in heat diffusion must outweigh the suppression in natural convection. Hence, the attachment method of the foils to the HTS must maintain contact after successive cycling to ensure that a minimal thermal contact resistance exists. Since a press-fit method is most likely the most economical approach to attach foils to a tubular surface, this consideration would need to be extensively studied for a foil-PCM system. Since PCMs may undergo significant volume changes, foils may experience movement along the HTS. This movement is not ideal as it may result in a larger contact resistance after successive cycling and may be detrimental to long term system performance. One proposed method to mitigate this problem is to implement a foil shape with a cutout at the foil root where it contacts the HTS to act as a pressure relief slot. This would facilitate a pathway for liquid PCM to flow between foils along the HTS towards the location of lowest pressure, such as compressible air at the top of an enclosure (which is common in PCM systems). Methods such as this may be essential to avoid PCM leaching into the contact joint between the HTS and the foil and expanding, thereby creating a gap between the foil root and the HTS which would increase the thermal contact resistance. Therefore, further study regarding the structural analysis of foil-PCM systems is suggested for optimal foil design.

A summary of studies involving foil-PCM systems can be seen in Table 2.3. An incredible improvement in heat transfer was achieved for solidification of water as a PCM by Sugawara et al. [52]. The authors studied the effect of adding copper foils ($t = 0.035$ mm) onto a HTF tube and found that the total solidification time can be reduced to an eighteenth that without the foils. It was also reported that the foils had a larger impact on melting than on solidification, however, this was most likely attributed to the lower thermal conductivity of the liquid water vs. ice. As the thermal conductivity of a PCM decreases, a higher achievement in performance is capable of being achieved by a specific enhancer. In another study by Sugawara et al. [53] copper foils of the same thickness were utilized in a different manner in which the foils were not in direct contact with a HTF tube for all but one case studied. However, this is an ineffective manner to utilize foils as a large thermal resistance is introduced by the PCM filling the space between the HTF tube and foil root.

From a fundamental heat transfer perspective, a fin, or foil, may not be useful if the resistance of the fin is greater than that of the base [51]. While the other studies presented in the table specify the enhancement as a “foil”, the “foil” thickness encountered in each is 0.5 mm or greater which is too thick to be flexible, therefore they are more like fins and will not be further discussed here. The advantages, disadvantages and unresolved issues for PCM systems involving foils are as follows:

Advantages

- Foils are effective at increasing the effective thermal conductivity (heat diffusion) within the PCM. Only a small volume fraction of foils (~1%) is needed to significantly increase the melting and solidification rates.
- Relative to other enhancement techniques which increase thermal diffusion within the PCM, foils may be the most effective since it comprises the most direct heat transfer pathway that is relatively orthogonal to the HTS.
- Similar to fins, the technologies for manufacturing foils are well developed and the installation methods such as press-fitting may be achieved in a cost effective manner for tubular surfaces compared to other methods.

- A large variety of inexpensive high thermal conductivity materials are available for production of foils.
- With the same effective porosity, foils affect a much larger volume of PCM due to a larger surface area density than fins.
- Foils minimize the stress issues arising from the PCM volume expansion and contraction during phase change.

Disadvantages/Challenges

- With a press-fit method of installation, a thermal contact resistance between the HTF and foil root may present itself after successive cycling.
- Difficulties may arise for installation on non-tubular surfaces.
- Foils may significantly suppress natural convection due to a small foil pitch with a small spacing between foils.
- Relative to fins, foils have low structural strength which may limit their practical length.
- The effectiveness of a foil decreases with length due to its relatively thin structure.
- Due to small thicknesses, foils may be susceptible to corrosion.

Unresolved issues

- Optimal foil shapes as well as long term structural and thermal stability is yet to be investigated.
- In high temperature environments, common high thermal conductivity materials such as copper and aluminum may not be used and lower thermal conductivity materials must be utilized.

2.3.2. Nanoparticles

The addition of high thermal conductivity nanoparticles to PCMs has attracted much attention for increasing the effective thermal conductivity in the last decade. Numerous nanoparticle types including graphite nanofibers, multi-walled carbon nanotubes, and graphite nanoplatelets, metals such as Al, Cu, Ag, and metal oxides including Al_2O_3 , CuO, MgO and TiO_2 , among others, have been explored. Four major factors affect the increase in heat diffusion by the addition of high conductivity nanoparticles to the

PCMs and consist of: type, concentration, geometry and long term stability within the PCM. Addition of nanoparticles to the PCM forms a mixture whose thermophysical properties are different than those related to the base PCM. For example, the addition of nanoparticles results in an increase (decrease) in the effective thermal conductivity and viscosity (latent and specific heats) of the nanoparticle-enhanced PCM. Therefore, the enhancement in conduction within the nanoparticle-enhanced PCM must outweigh the reduction in natural convection and heat storage capacity.

As shown in Fig. 2.2 and adopted from Valan Arasu et al. [54], nanoparticle dispersion has a much more profound effect on heat transfer enhancement during the solidification as compared to melting. This is expected regarding the suppression of natural convection within the molten PCM due to the increased viscosity of the liquid PCM. Hence, the improvement in conduction heat transfer must outweigh the suppression in natural convection in order for the addition of nanoparticles to be viable enhancement technique. As the nanoparticle concentration increases, the viscosity also increases in which case this issue is of greater importance.

The most important challenge associated with nanoparticle-enhanced PCMs is the long-term stability of the suspension after multiple charge-discharge cycles. Most of the investigations on nanoparticle-enhanced PCMs are performed for a relatively short period of time and a limited number of melting-solidification cycles; hence, the long-term stability of these nanoparticle-enhanced PCMs has not yet been addressed. Moreover, most of the investigations to date are concerned with low temperature PCMs, mainly paraffin and deionized water, and the effect of nanoparticle addition to high temperature PCMs remains to be addressed. A recent review of the theoretical and experimental studies on nanoparticle-enhanced PCMs for LHTES applications has been presented by Khodadadi et al. [55]. Recent investigations involving the addition of nanoparticles into PCMs are presented in Table 2.4. To summarize, the advantages, disadvantages and unresolved issues involving LHTES systems with nanoparticle-enhanced PCMs are as follows:

Advantages

- Increases the effective thermal conductivity (heat diffusion) of the nanoparticle-enhanced PCM.

- May be easily added to any LHTES without adding complexity to the storage unit.
- Nanoparticles serve as nucleating agents during solidification which may significantly reduce the degree of subcooling.
- Nanoparticle addition comprises a high surface area density with the PCM.

Disadvantages/Challenges

- Long-term stability of nanoparticle-enhanced PCMs is questionable, especially pertaining to agglomeration and sedimentation of particles.
- Relatively high thermal resistances exist between distinct particles as well as with the HTSs, hence farther from the HTSs, the addition of nanoparticles may not be effective.
- Addition of nanoparticles may significantly increase the viscosity of the nanoparticle-enhanced PCM relative to the pure PCM. Hence the increase in the effective thermal conductivity should outweigh the suppression in natural convection heat transfer.
- The latent heat of fusion of the nanoparticle-enhanced PCM is usually reduced relative to the pure PCM. However, this decrease may be small as the mass fraction of nanoparticles is usually less than 10 wt%.

Unresolved issues

- Performance of the nanoparticle-enhanced high temperature PCMs has not been addressed in literature.
- More research is required to identify the effect of nanoparticle addition on the PCM properties such as melting temperature, viscosity, and latent heat of fusion.
- The appropriate combination of particle thermal conductivity and particle mass fraction is important and needs to be investigated to enhance the performance of the LHTES system.

2.3.3. High thermal conductivity structures

Relative to adding particles that may experience agglomeration after time, addition of rigid structures made from materials of high thermal conductivity, such as copper, aluminum and carbon, can

resolve this problem while also increasing heat transfer rates within PCMs [56]. While there exist many high thermal conductivity structures which have been studied in the past, such as carbon brushes [57], only those studied in more recent years will be presented here. Typical structures that have been utilized for enhancing heat transfer within PCMs are presented in Table 2.5 and include porous media (matrices, foams, expanded graphite, wools) and metal matrices. In general, structures are relatively rigid, constructed to form one piece and usually contain larger enhancer volume fractions than other enhancement techniques such as nanoparticles.

In all the structures discussed here, an increase in the effective thermal conductivity of the enhancer-PCM composite is achieved along with a high surface area density. The performance enhancement is dependent on both the porosity and material, relating to the effective thermal conductivity of the matrix. Although lower porosity values lead to a higher effective thermal conductivity, it also reduces the contribution of natural convection in the molten PCM on the overall melting rate. As previously discussed, the calculation of effective thermal conductivity is not dependent on the structure morphology, therefore, one structure made from the same material may be more effective than another. The main disadvantages of structures include the difficulty of attachment to an HTS and the random orientation of the struts or fibers as opposed to straight fins. Hence, in numerical studies the thermal conductivity is commonly estimated by assuming that approximately $1/3$ of the struts are oriented in any orthogonal direction [58]. This is not beneficial as the pathway for heat transfer consists of a tortuous structure which increases the effective length of a strut as well as significantly suppressing natural convection. In order to minimize the thermal resistances within the structure, the metal structure is desired to be distributed uniformly and aligned parallel to the desired direction of heat flow [27].

Due to non-planar surface of most high thermal conductivity structures, attaching the device to an enclosure may be more difficult. If the attachment method fails for some reason then both natural convection and conduction would be suppressed and may cause system failure. Other factors which should be noted for high thermal conductivity structures integrated into PCMs is that (i) the efficiencies of the structure decreases with distance from the HTS [51], (ii) as pore sizes decrease in a porous media, the

entrapment of gases may occur thereby decreasing the storage capacity and (iii) anisotropy and structural discontinuities may exist potentially resulting in hot spots, such as for EG [59]. The advantages, disadvantages, and unresolved issues for embedding high thermal conductivity structures into PCMs are as follows:

Advantages

- High thermal conductivity structures increase the effective thermal conductivity (heat diffusion) in PCM systems.
- High surface area densities may be achieved with porosities reaching up to 0.98.
- Structures may be manufactured to unique geometries which may be difficult for extended surface type enhancements.

Disadvantages/Challenges

- Structures may significantly suppress or even eliminate natural convection in the PCM depending on the effective pore size of the structure.
- The attachment method of a structure to a HTS may be difficult, especially for non-planar morphologies. Hence, a thermal contact resistance may exist at the location of attachment.
- For structures with small pore sizes, such as foams and EG, air entrapment may arise which decrease the performance of the storage system.
- Manufacturing costs may be significantly higher relative to other methods, and the choice of materials may be limited.
- The effectiveness of the structure decreases with increasing distance from the HTS.
- The tortuous morphology of structures, such as foams, may result in less effective heat transfer with relative to other methods such as foils. For typical structures, heat transfer is three-dimensional relative to two-dimensional heat transfer for foils.

Unresolved issues

- The appropriate methods for attaching distinct structures to a HTS, such as EG, to effectively transfer heat from a HTS to the PCM remain to be determined.

2.3.4. Heat pipes, thermosyphons and reflux systems

It is well known that heat pipes (HPs) and thermosyphons (TSs) can have high effective thermal conductivities which have led to their use in LHTES systems. HPs, TSs (also known as wickless HPs) and other reflux systems operate by utilizing a working fluid which undergoes evaporation and condensation at the hot and cold sections, respectively. Reflux systems differ from HPs and TSs in that the evaporation and condensation of an internal working fluid occurs directly on the HTF tubes, which are located within the reflux system, rather than within a HP or TS and subsequently transferred to the HTF. Since the internal working fluid is maintained in a reduced pressure environment, the liquid-vapor phase change process can occur at reduced temperatures, allowing use of fluids like water at or below room temperature [60]. The presence of a wick in a HP or reflux system allows the liquid working fluid to be pulled towards an evaporator which is located away from the pool of working fluid (that is typically positioned at the lowest region of a HP due to gravity). The integration of an internal working fluid within a HP, TS or reflux system allows for efficient operation in which the thermal conductivity may greatly exceed that of similarly-dimensioned solid materials [60].

Utilizing HPs is one approach to reduce the relatively high thermal resistance posed by the PCM. Sharifi et al., 2012 [37] numerically simulated the melting of a PCM that is contained in a vertical cylindrical enclosure, heated by a concentrically-located HP. The melting rate for the HP-enhanced case is compared to that induced by heating from an isothermal surface and with a solid rod or a hollow tube with the same exterior dimensions. The melting effectiveness was defined as the ratio of the PCM liquid fraction induced by an isothermal surface, HP or tube to the liquid fraction of a rod-enhanced system. Figure 2.3 shows the time histories of the effectiveness for isothermal condition, the HP, and the tube for one case study. As can be seen from this figure, the effectiveness for the HP case is above unity, indicating an improved heat transfer performance relative to the rod-enhanced case. The upper limit of performance is represented by an isothermal surface (with identical temperature to that of the HP

evaporator) while the lower limit for an ineffective HP is a tube which has slightly lower performance relative to the rod-enhanced case.

Overall, HPs make excellent candidates for improving heat transfer in PCMs. The only main disadvantage of adding HPs/TSs to PCMs is the cost and the possibility of failure, however, the cost of a HP or TS may be less than that of a typical extended surface due to the lesser amount of bulk material needed for the HP or TS. Also, the failure of a single HP or TS has little effect on the overall performance of an LHTES with many HPs/TSs. Some studies involving HPs, TSs or other reflux systems are presented in Table 2.6 and Table 2.7 while typical advantages, disadvantages, and unresolved issues are as follows:

Advantages

- Heat pipes and thermosyphons are by far the most effective means to increase the thermal penetration depth in PCM systems. The effective thermal conductivity of a HP or TS can greatly exceed that of a similarly dimensioned solid material.
- Large amounts of heat can be transferred through a small cross sectional area over great distances.
- A variety of HP/TS shapes are available.
- A large variety of materials for the HP wall, wick and working fluid allow for a vast range of operating conditions.
- HPs/TSs are highly reliable, durable and have long lifetimes. The failure of individual HPs/TSs has little impact on the overall system performance. HPs have been reported to show negligible deterioration after 13+ years [61].
- Relative to extended surfaces, their performance does not significantly deteriorate by increasing their length.
- The presence of a wick allows HPs to effectively operate in any orientation.
- If TSs are implemented, then one directional heat transfer may be utilized which may be advantageous for certain systems.

Disadvantages/Challenges

- The method for attaching a HP/TS to a HTS or enclosure may be challenging which may induce thermal contact resistances.
- Selecting compatible materials for the HP wall, wick and working fluid, as well as the PCM, heat source and sink and the enclosure is an issue which must be addressed for each system. This may be a more challenging for high temperature LHTES systems.
- Performing both melting and solidification with only one set of TSs is challenging. Hence, TS-assisted LHTES systems require either multiple HTF channels or sets of TSs (for charging and discharging).
- If a HP/TS fails it may need to be replaced.
- The limitations pertaining to HPs/TSs, such as the sonic and boiling limits among others, may limit the performance of a PCM system involving HPs/TSs.
- Frozen startup, referring to an initially solid HP/TS working fluid, may cause some problems during the onset of operation with an initially cold HP/TS.

Unresolved issues

- The utilization of a thermal network model for a HP/TS-enhanced PCM system requires the effect of the vapor pressure drop to be considered for a more comprehensive analysis.
- Suitable HP/TS working fluids for intermediate temperature applications in the range of 200 °C to 400 °C remain to be adequately identified.
- Since welding of HPs/TSs is challenging due to the superior heat dissipation of HPs/TSs, alternative technologies for assembling HP/TS-enhanced LHTES systems must be developed.

2.3.5. Encapsulation

Encapsulation, or enclosing, a PCM inside a shell material has been extensively studied for LHTES systems due to its characteristically large surface area density. Length scales for encapsulation are classified as macro ($>1\text{mm}$), micro ($1\text{ }\mu\text{m} - 1\text{ mm}$), and nano ($1\text{ nm} - 1\text{ }\mu\text{m}$) [62]. While the main

purpose is to encase the PCM, encapsulation can resolve the problem of PCM expansion and contraction by allowing for it to occur in a minimum volume [29]. For lower temperature ($< 200\text{ }^{\circ}\text{C}$) applications, a flexible shell material (typically plastic) may be utilized. However, as the operating temperature increase, the available materials may be more limited, in which a rigid shell is general implemented. When a non-flexible shell is implemented, the fill ratio of PCM should not exceed 80% in order to withstand the pressure variation during phase change [63].

Typically, encapsulation is achieved by either physical or chemical manufacturing methods as described in [64]. However, chemical methods are required for smaller capsule sizes and may contain more consistent shell structures. The shapes of the encapsulated PCMs can vary including spheres, cylinders and rectangular prisms among others, however, spheres are more common for micro- or nano-encapsulation.

Encapsulation may provide a rather simple design solution that can be applied to a wide range of PCMs and operating temperatures by selecting chemically compatible PCMs and shell materials. Important design factors for macro-encapsulated systems include the effect of capsule size, HTF inlet temperature, HTF mass flow rate and the thermal conductivity of the materials [62]. Generally, as the diameter of the capsule decreases, heat transfer rates increase since the interfacial surface area between the HTS and PCM increases. Likewise, as the temperature difference between the HTF and the PCM melting temperature as well as the mass flow rates increase, the heat transfer rates also increase. In a numerical study by Karthikeyan et al. [65], the HTF inlet temperature was reported to have a greater effect than the latter and is presented in Fig. 2.4. In the figure, it may be deduced that an increase in the HTF temperature from $67\text{ }^{\circ}\text{C}$ to $80\text{ }^{\circ}\text{C}$ can reduce the charging time by approximately 60%.

While it is ideal to have a metal shell due to high thermal conductivity and strength, manufacturing processes limit its use as the size decreases generally resulting in non-metallics used for micro- or nano-encapsulation. One of the major challenges is the high cost of encapsulation for PCMs, while others include the reduction in performance over successive thermal cycles, change in properties as length scale decreases and a completely sealed shell to eliminate leaks.

Common building materials have been used for both macro- and micro-encapsulation such as masonry, concrete, gypsum and others. By encapsulating PCM into the walls of a building, energy savings and improved thermal management can be achieved such as reducing maximum room temperatures and humidity by approximately 4 °C and 16%, respectively in Shenzhen, China [66]. For example, Foran and Wu [67] reported that microencapsulation of PCMs into gypsum wallboards is one of the more attractive and efficient methods for utilizing microencapsulation of PCMs. Another common area of study, which is still in the development stage, is direct use of microencapsulated PCMs into an HTF, referred to as a slurry [68]. In this way, the heat exchanger between the PCM and HTF is eliminated and a high surface area density is achieved. With regards to macro-encapsulation, the most common configuration is a packed bed in which the PCM is contained in spherical capsules over which an HTF flows [69]. The relevant experimental and theoretical investigations concerning the encapsulated PCM systems are presented in Table 2.8 and Table 2.9, respectively. Advantages, disadvantages, and unresolved issues for the encapsulation of PCMs include:

Advantages

- A high degree of thermal penetration into a packed bed may be achieved by encapsulation.
- High surface area densities may be achieved, especially for micro-encapsulation.
- A large variety of sizes (with length scales on the order of a few micrometers to a few centimeters), shapes (spherical, cylindrical, etc.) and materials may be utilized.
- Encapsulation may minimize the problems related to PCM expansion and contraction.

Disadvantages/Challenges

- Compatibility between the PCM, shell material and any other secondary medium may be challenging.
- If the thermal resistance within the PCM itself is large, encapsulation may not significantly increase heat transfer rates, especially for larger capsule sizes.

Macro-encapsulation

- Higher possibility of leaks.
- High pressure drops for the HTF along flow direction.
- The driving temperature decreases with HTF flow direction.
- Systems generally have lower porosities for a packed bed of PCM-filled capsules which increases the overall system volumes. As the porosities decrease, the total volume and pressure drop also increase.

Micro- and nano-encapsulation

- Micro- and nano-encapsulation may weaken the structural properties of a substrate material.
- Subcooling may present itself as the length scale decreases for some PCMs.

Unresolved issues

- Erosion of the thin walls in micro-encapsulated PCMs may reduce the system lifetime.
- Manufacturing of micro- and nano-encapsulated PCMs may be difficult, particularly for controlling the internal void fraction and PCM mass.
- Thermal stresses exist in the tank wall and capsule shell due to system temperature gradients along the tank.

2.3.6. Cascaded

In systems involving HTFs, employing a single PCM results in both a monotonically decreasing HTF temperature and heat flux between the HTF and PCM in the direction of flow. This undesirable trait may be resolved by cascading multiple PCMs so that the melting temperatures decrease (increase) in the direction of flow during melting (solidification). The underlying idea is to maintain a more uniform spatial temperature difference between the HTF and the PCM. Thus, during melting (solidification) the PCMs with relatively higher (lower) melting temperature are positioned in an upstream region. It has been postulated that a more uniform temperature difference between the HTF and the PCM in a cascaded configuration improves the exergy efficiency and heat transfer rates in LHTES systems. However, contradicting results have been reported with regard to the possibility and the extent of exergy efficiency

and heat transfer enhancement achieved by using cascaded configuration [70–72]. In general, it can be said that the heat transfer and exergy efficiency enhancements achieved by using multiple PCMs in a cascaded configuration are not as significant as suggested by some early lumped capacitance models. Moreover, any potential improvement in heat transfer and/or exergy efficiency strongly depends on the precise selection of the melting point and relative portion of each PCM in the cascaded system. This poses another limitation to this method as identification of a practical PCM to match the calculated optimal melting temperature may be challenging. Regardless, cascaded PCM configurations allows for a more favorable heat flux between the PCM and the HTF. As shown in Fig. 2.5 and adopted from Shabgard et al. [72], the performance of a cascaded LHTES system lies between that of two single-PCM LHTES systems with the lowest and highest melting temperatures of the cascaded system. Table 2.10 presents the recent investigations on utilizing a cascaded PCM configuration into LHTES systems while some pros and cons as well as unresolved issues include:

Advantages

- Cascaded PCM configurations allow for a more favorable heat flux along the direction of the HTF flow.
- Potentially, less fluctuation for the HTF outlet temperatures over time can be provided by a cascaded PCM configuration.
- The amount of PCM that melts and solidifies during consecutive charging-discharging cycles can be increased in cascaded LHTES systems. This can potentially reduce the size and mass of the storage system by more effective use of the latent heats of fusion of PCMs.

Disadvantages/Challenges

- Accurate numerical simulation is required to identify the number of PCMs, size of each segment and melting temperatures for an optimal cascaded configuration.
- The optimal design conditions are dependent on the hot and cold HTF inlet conditions and any change in the HTF inlet conditions may result in less than optimal operation.

- Challenges may arise in determining practical PCMs to match those acquired by numerical simulation.
- The potential enhancement achieved by using cascaded configurations may not be enough to offset the additional cost, as well as the higher probability of leaks, related to multiple PCM container/tanks.

Unresolved issues

- There are contradicting results related to the effect of cascaded configurations on the exergy efficiency and heat transfer rates.
- The operating and design parameters causing the different energy and exergy performances reported in the literature need to be identified.

2.4. Combined enhancement

In this review it is made evident that of all the PCM enhancements, there is no perfect method to enhance heat transfer in PCM systems. It is clear that each is limited by some factors whether it is cost, difficulty in implementation or only allowing for thermal transport. While the latter may not seem like a significant disadvantage, an increase in both thermal transport and thermal diffusion are necessary for a PCM system to maximize heat transfer rates. A simple approach for achieving this feat is to implement a combination of the aforementioned techniques. For example, Liu et al. [73] reported that to further increase the heat transfer rates in a HP heat exchanger integrated with PCM, an additional enhancement technique in the PCM was needed for practical use in solar applications.

The combination of two or more enhancers allows for an increase in performance beyond the scope of a single technique. This is achieved by exploiting the individual improvements for each enhancer. An effective combination implements at least one enhancement to increase thermal transport within the PCM while another technique increases diffusion. A particularly attractive method to enhance PCMs including a combined enhancement of HPs with aluminum foils (0.017 mm thickness) was investigated by Sharifi et al. [74]. The combination of a HP with foils (with a porosity of 0.987) was reported to achieve an

increase in heat transfer rates by 3 and 9 times relative to a similar rod-enhanced PCM system during melting and solidification, respectively. In a further study, Allen et al. [75,76] investigated the effect of porosity on the combined HP and foil and combined HP and foam configurations and determined that a HP and foil (HP and foam) case with a porosity of 0.957 (0.890) was able to increase the melting and solidification rates by nearly 15 and 7 times that of the rod-enhanced case with minimal variation with a change in inclination angle. Other studies involving a combination of heat transfer enhancement techniques for PCM systems can be seen in Table 2.11. The advantages, disadvantages and unresolved issues for combined enhancement techniques are as follows:

Advantages

- The combination of an enhancement technique which increases the thermal penetration depth with one that increases the effective thermal conductivity
- Combined enhancement techniques may increase the overall melting and solidification rates much more than is possible with a single heat transfer enhancement technique.
- A large variety of combinations may be achieved using the aforementioned techniques.

Disadvantages/Challenges

- The overall cost increases as additional enhancement techniques are included.
- The addition of multiple enhancement techniques that are made from different materials may increase the concerns regarding material compatibilities due to a greater number of interfaces.
- The optimization of systems involving combined enhancement techniques is more difficult than for a single enhancement technique.

Unresolved issues

- The long term structural and thermal properties are yet to be determined for combined enhancement techniques.

2.5. Comparison of various techniques

A schematic for many of the heat transfer enhancement techniques that have been implemented into PCM systems and reviewed in this work are presented in Fig. 2.1. It is clear from the figure that the mechanisms for heat transfer may vary widely depending on the utilized enhancement method. Some important considerations for selecting a specific enhancement technique include: the desired improvement in heat transfer (thermal transport, diffusion or both), thermal contact resistance and heat transfer pathway. In each section above, the advantages, disadvantages and unresolved issues for each type of enhancement is provided, and is also summarized in Table 2.12, which help to determine the extent of which an enhancer can affect heat transfer in an LHTES system. Again it should be noted that there is not an ideal enhancement technique which makes the combination of multiple enhancements an attractive solution especially for larger scale systems, yet some methods may be preferred compared to others.

In general, a compromise must be made between the performance (increase in heat transfer rates) and cost (including the material, manufacture and installation) of an enhancer. It should also be noted that as the operating temperature of a LHTES system increases (such as above 800 °C), it becomes more difficult to determine both an appropriate material and enhancement technique. Fins are one of the most commonly investigated methods since they are well established, yet manufacturing and installation costs (machining, welding, etc.) may be high. Foils are an attractive option since they require minimal mass and volume and can be manufactured by cost effective means, such as die stamping. The press-fit method of installation is cost effective for tubular structures, such as HPs, TSs, HTF tubes or pin-fins, however, installation of foils on planar or other non-tubular geometries may be challenging. Of the methods investigated, it seems that foils may be the most attractive at increasing heat diffusion in PCM systems as they provide a relatively orthogonal heat transfer pathway from a HTS, which is more effective than others such as foams which comprise undesirable morphologies for heat transfer. With regards to high thermal conductivity structures, some may be expensive and less effective compared to more traditional extended surface type enhancements while the method of attachment is also more difficult. While the addition of high thermal conductivity particles can increase the effective thermal conductivity, other

thermophysical properties are also affected which may be detrimental to the overall performance enhancement. The high surface area density between the HTSs and the PCM in encapsulation is setback by the high costs associated with the encapsulation process. Relative to solid materials, HPs/TSs, which utilize the latent heat transport of an internal working fluid, comprise significantly higher thermal conductivities, yet the additional costs may make some hesitant to implement them. While cascaded arrangements allow for more favorable heat transfer rates between a PCM and a HTF, it may increase the cost and chance of leaks.

In order to determine the effect of utilizing a single enhancement technique relative to a combined technique, Fig. 2.6 and Fig. 2.7 are adopted from Allen et al. [76] which is also presented in Table 2.11. A vertical cylindrical enclosure contained n-octadecane while heat transfer was ultimately driven by an underlying HTF (water) that was in contact with a copper disc at the base of the cylinder as well as a HP or rod. In Fig. 2.6, the liquid fraction histories for cases involving a HP, rod or aluminum foam ($\phi = 0.95$, 20 PPI) individually as an enhancement techniques are compared to a non-enhanced PCM system. From the figure, the necessity for a heat transfer enhancement technique in PCM systems is clearly evident by the long duration required for phase change, particularly during solidification. Since the system includes base heat transfer, the effect of natural convection is significant during melting which accounts for the drastic difference in the complete melting and solidification times, even though the liquid PCM thermal conductivity is lower than that of the solid PCM. Hence, in Fig. 2.6, the improvement in heat diffusion within the foam-PCM composite indeed outweighs the suppression in natural convection heat transfer. For the range of conditions studied, the HP-enhanced case has the highest melting and solidification rates followed by the rod- and then foam-enhanced systems.

Further, Allen et al. [76] also investigated the effect of combining a HP with either aluminum foils ($t = 24 \mu\text{m}$) or foam (20 PPI) where the foil-PCM and foam-PCM composites each had a porosity of $\phi = 0.95$. In Fig. 2.7, the combined enhancement techniques were able to achieve significantly higher heat transfer rates than the HP or foam individually. It can also be inferred from the figure that the foils are preferred relative to the foam. This was also determined in the previous work by Allen et al. [75], in

which the foils combined with the HP were able to achieve higher heat transfer rates than the combined HP and foam case using only one-third of the foil volume relative to the foam volume. The combined HP and foil system was able to reduce the complete melting and solidification times from approximately 150 min and 500 min, respectively to approximately 15 min, which is an incredible achievement [76].

Regardless of the type of enhancement technique, it is clear at this point that the combination of two or more methods is a key concept to effectively utilizing LHTES systems. Each individual enhancement method has its own limitations which must be addressed and in general, the performance decreases as length scales increase (except for nano-particles which are independent of the system size). In order to circumvent this decrease in performance, the combination of a technique which allows for an increase in the thermal penetration depth combined with another that increases thermal diffusion is necessary to significantly increase heat transfer rates in an effective manner for large scale systems. If this is achieved, then heat transfer rates can be increased by more than an order of magnitude and the melting and solidification times can be reduced to a fraction of that for non-enhanced PCM systems.

2.6. Conclusions

In this paper, various enhancement methods for improving heat transfer rates within PCMs have been presented. Since first implementation of PCMs, the methods of enhancement have been ever improving to better suit the desired capabilities of LHTES systems with current technologies ranging from thermal management of handheld electronic devices to electric power production. Since each type of enhancer has its own limitations, the combination of multiple methods is a vital concept for substantially increasing heat transfer rates in PCM systems. It seems that the past limiting factor of low thermal conductivity is no longer an issue as simple and innovative enhancement techniques are capable of increasing heat transfer rates by more than an order of magnitude relative to pure PCM systems. In the future, new materials and improved methods of implementation for heat transfer enhancements must be developed for successful operation of LHTES systems, especially in harsher environments.

Nomenclature

d	diameter (m)
h	height (m)
L	length (m)
m	mass (g)
N	number of fins
r	radius (m)
T	temperature (°C)
t	time (s), thickness (mm)
V	volume (m ³)

Greek symbols

ϕ	porosity
ω	pore density (PPI)

Subscripts

a	adiabatic
c	condenser
e	evaporator
$fiber$	fiber
i	inner
in	in
mat	mat
m	melting
o	outer
out	out
p	pore
pcm	phase change material
s	solidification
$wall$	wall
$wick$	wick

Acronyms

CSP	concentrating solar power
DSC	Differential Scanning Calorimetry
EG	expanded graphite
EXP	experimental
FD	finite difference
FE	finite element
FV	finite volume
HP	heat pipe
HTF	heat transfer fluid
HTS	heat transfer surface

LHTES	latent heat thermal energy storage
NUM	numerical
PCM	phase change material
PPI	pores per inch
SHTES	sensible heat thermal energy storage
TES	thermal energy storage
TS	thermosyphon
TTM	temperature transforming model

References

- [1] F. Agyenim, N. Hewitt, P. Eames, M. Smyth, A review of materials, heat transfer and phase change problem formulation for latent heat thermal energy storage systems (LHTESS), *Renew. Sustain. Energy Rev.* 14 (2010) 615–628.
- [2] M. Iten, S. Liu, A work procedure of utilising PCMs as thermal storage systems based on air-TES systems, *Energy Convers. Manag.* 77 (2014) 608–627.
- [3] M.M. Kenisarin, High-temperature phase change materials for thermal energy storage, *Renew. Sustain. Energy Rev.* 14 (2010) 955–970.
- [4] M.K. Rathod, J. Banerjee, Thermal stability of phase change materials used in latent heat energy storage systems: A review, *Renew. Sustain. Energy Rev.* 18 (2013) 246–258.
- [5] B. Cárdenas, N. León, High temperature latent heat thermal energy storage: Phase change materials, design considerations and performance enhancement techniques, *Renew. Sustain. Energy Rev.* 27 (2013) 724–737.
- [6] a. F. Regin, S.C. Solanki, J.S. Saini, Heat transfer characteristics of thermal energy storage system using PCM capsules: A review, *Renew. Sustain. Energy Rev.* 12 (2008) 2438–2458.
- [7] C.W. Robak, T.L. Bergman, A. Faghri, Enhancement of latent heat energy storage using embedded heat pipes, *Int. J. Heat Mass Transf.* 54 (2011) 3476–3484.
- [8] S.D. Sharma, K. Sagara, Latent heat storage materials and systems: A review, *Int. J. Green Energy.* 2 (2005) 1–56.
- [9] R. Adinberg, D. Zvegilsky, M. Epstein, Heat transfer efficient thermal energy storage for steam generation, *Energy Convers. Manag.* 51 (2010) 9–15.
- [10] A. Gil, M. Medrano, I. Martorell, A. Lázaro, P. Dolado, B. Zalba, et al., State of the art on high temperature thermal energy storage for power generation. Part 1 - Concepts, materials and modellization, *Renew. Sustain. Energy Rev.* 14 (2010) 31–55.
- [11] J. Shon, H. Kim, K. Lee, Improved heat storage rate for an automobile coolant waste heat recovery system using phase-change material in a fin–tube heat exchanger, *Appl. Energy.* 113 (2014) 680–689.

- [12] Z.G. Qu, W.Q. Li, J.L. Wang, W.Q. Tao, Passive thermal management using metal foam saturated with phase change material in a heat sink, *Int. Commun. Heat Mass Transf.* 39 (2012) 1546–1549.
- [13] A. a. Al-Abidi, S. Bin Mat, K. Sopian, M.Y. Sulaiman, C.H. Lim, A. Th, Review of thermal energy storage for air conditioning systems, *Renew. Sustain. Energy Rev.* 16 (2012) 5802–5819.
- [14] L.F. Cabeza, A. Castell, C. Barreneche, A. de Gracia, A.I. Fernández, Materials used as PCM in thermal energy storage in buildings: A review, *Renew. Sustain. Energy Rev.* 15 (2011) 1675–1695.
- [15] P. Kauranen, T. Elonen, L. Wikström, J. Heikkinen, J. Laurikko, Temperature optimisation of a diesel engine using exhaust gas heat recovery and thermal energy storage (diesel engine with thermal energy storage), *Appl. Therm. Eng.* 30 (2010) 631–638.
- [16] E. Lohse, G. Schmitz, Experimental investigation of temporary electronics cooling with regularly structured composite latent heat storage, *HVAC&R Res.* 19 (2013) 814–822.
- [17] T.Y. Kim, B.-S. Hyun, J.-J. Lee, J. Rhee, Numerical study of the spacecraft thermal control hardware combining solid–liquid phase change material and a heat pipe, *Aerosp. Sci. Technol.* 27 (2013) 10–16.
- [18] J.H. Johnston, J.E. Grindrod, M. Dodds, K. Schimitschek, Composite nano-structured calcium silicate phase change materials for thermal buffering in food packaging, *Curr. Appl. Phys.* 8 (2008) 508–511.
- [19] L.M. Bal, S. Satya, S.N. Naik, Solar dryer with thermal energy storage systems for drying agricultural food products: A review, *Renew. Sustain. Energy Rev.* 14 (2010) 2298–2314.
- [20] A. Lazaro, P. Dolado, J.M. Marin, B. Zalba, PCM-air heat exchangers for free-cooling applications in buildings: Empirical model and application to design, *Energy Convers. Manag.* 50 (2009) 444–449.
- [21] S.M. Hasnain, Review on sustainable thermal energy storage technologies, Part I: heat storage materials and techniques, *Energy Convers. Manag.* 39 (1998) 1127–1138.
- [22] A. Sharma, V.V. Tyagi, C.R. Chen, D. Buddhi, Review on thermal energy storage with phase change materials and applications, *Renew. Sustain. Energy Rev.* 13 (2009) 318–345.
- [23] B. Zalba, J.M. Marín, L.F. Cabeza, H. Mehling, Review on thermal energy storage with phase change: materials, heat transfer analysis and applications, *Appl. Therm. Eng.* 23 (2003) 251–283.
- [24] M.M. Farid, A.M. Khudhair, S.A.K. Razack, S. Al-Hallaj, A review on phase change energy storage: materials and applications, *Energy Convers. Manag.* 45 (2004) 1597–1615.

- [25] C.W. Robak, T.L. Bergman, A. Faghri, Economic evaluation of latent heat thermal energy storage using embedded thermosyphons for concentrating solar power applications, *Sol. Energy*. 85 (2011) 2461–2473.
- [26] E. Oró, a. de Gracia, a. Castell, M.M. Farid, L.F. Cabeza, Review on phase change materials (PCMs) for cold thermal energy storage applications, *Appl. Energy*. 99 (2012) 513–533.
- [27] L. Fan, J.M. Khodadadi, Thermal conductivity enhancement of phase change materials for thermal energy storage: A review, *Renew. Sustain. Energy Rev.* 15 (2011) 24–46.
- [28] M. Liu, W. Saman, F. Bruno, Review on storage materials and thermal performance enhancement techniques for high temperature phase change thermal storage systems, *Renew. Sustain. Energy Rev.* 16 (2012) 2118–2132.
- [29] S. Jegadheeswaran, S.D. Pohekar, Performance enhancement in latent heat thermal storage system: A review, *Renew. Sustain. Energy Rev.* 13 (2009) 2225–2244.
- [30] P.A. Prabhu, N.N. Shinde, P.S. Patil, Review of phase change materials for thermal energy storage applications, *Int. J. Eng. Res. Appl.* 2 (2012) 871–875.
- [31] A. Faghri, Y. Zhang, *Transport Phenomena in Multiphase Systems*, Elsevier Academic Press, Burlington, MA, 2006.
- [32] N. Shamsundar, E.M. Sparrow, Analysis of Multidimensional Conduction Phase Change Via the Enthalpy Model, *J. Heat Transfer*. 97 (1975) 333–340.
- [33] V.R. Voller, A fixed grid numerical modelling methodology for convection-diffusion mushy region phase-change problems, *Int. J. Heat Mass Transf.* 30 (n.d.) 1709–1719.
- [34] Y. Cao, A. Faghri, A numerical analysis of Stefan problems for generalized multi-dimensional phase-change structures using the enthalpy transforming model, *Int. J. Heat Mass Transf.* 32 (1989) 1289–1298.
- [35] K. Morgan, A numerical analysis of freezing and melting from a vertical wall, *Comput. Methods Appl. Mech. Eng.* 28 (1981) 275–284.
- [36] J.S. Hsiao, B.T.F. Chung, An efficient algorithm for finite element solution to two-dimensional heat transfer with melting and freezing, *J. Heat Transf.* 108 (1986) 462–464.
- [37] N. Sharifi, S. Wang, T.L. Bergman, A. Faghri, Heat pipe-assisted melting of a phase change material, *Int. J. Heat Mass Transf.* 55 (2012) 3458–3469.
- [38] N. Sharifi, T.L. Bergman, A. Faghri, Enhancement of PCM melting in enclosures with horizontally-finned internal surfaces, *Int. J. Heat Mass Transf.* 54 (2011) 4182–4192.
- [39] N. Sharifi, C.W. Robak, T.L. Bergman, A. Faghri, Three-dimensional PCM melting in a vertical cylindrical enclosure including the effects of tilting, *Int. J. Heat Mass Transf.* 65 (2013) 798–806.

- [40] Z. Ma, Y. Zhang, Solid velocity correction schemes for a temperature transforming model for convection phase change, *Int. J. Numer. Methods Heat Fluid Flow*. 16 (2006) 204–225.
- [41] V. VR, C. M, M. NC, An enthalpy method for convection/diffusion phase change, *Int. J. Numer. Methods Eng*. 24 (1987) 271–284.
- [42] A.D. Brent, V.R. Voller, K.J. Reid, Enthalpy-porosity technique for modeling convection-diffusion phase change: application to the melting of a pure metal, *Numer. Heat Transf*. 13 (1988) 297–318.
- [43] S. Wang, A. Faghri, T.L. Bergman, Numerical Modeling of Alternate Melting and Solidification, *Numer. Heat Transf*. 58 (2010) 393–418.
- [44] P. Taylor, S. Wang, A. Faghri, T.L. Bergman, Melting in Cylindrical Enclosures : Numerical Modeling and Heat Transfer Correlations, *Numer. Heat Transf*. 61 (2012) 837–859.
- [45] S. Wang, A. Faghri, T.L. Bergman, A comparison study of sensible and latent thermal energy storage systems for concentrating solar power applications, *Numer. Heat Transf*. 61 (2012) 860–871.
- [46] S. Wang, A. Faghri, T.L. Bergman, A comprehensive numerical model for melting with natural convection, *Int. J. Heat Mass Transf*. 53 (2010) 1986–2000.
- [47] W.Q. Li, Z.G. Qu, Y.L. He, W.Q. Tao, Experimental and numerical studies on melting phase change heat transfer in open-cell metallic foams filled with paraffin, *Appl. Therm. Eng*. 37 (2012) 1–9.
- [48] Y. Hamada, W. Ohtsu, J. Fukai, Thermal response in thermal energy storage material around heat transfer tubes: effect of additives on heat transfer rates, *Sol. Energy*. 75 (2003) 317–328.
- [49] C.Y. Zhao, Z.G. Wu, Heat transfer enhancement of high temperature thermal energy storage using metal foams and expanded graphite, *Sol. Energy Mater. Sol. Cells*. 95 (2011) 636–643.
- [50] S. Mahmoud, A. Tang, C. Toh, R. AL-Dadah, S.L. Soo, Experimental investigation of inserts configurations and PCM type on the thermal performance of PCM based heat sinks, *Appl. Energy*. 112 (2013) 1349–1356.
- [51] T.L. Bergman, A.S. Lavine, F.P. Incropera, D.P. DeWitt, *Fundamentals of Heat and Mass Transfer*, 7th ed., John Wiley & Sons, Hoboken, 2011.
- [52] M. Sugawara, Y. Komatsu, Y. Takahashi, H. Beer, Freezing enhancement around a horizontal tube using copper foil disks, *Heat Mass Transf*. 47 (2011) 1691–1698.
- [53] M. Sugawara, Y. Komatsu, D. Onodera, H. Beer, Three-dimensional freezing of water in a copper foils porous layer around a coolant-carrying tube, *Heat Mass Transf*. 48 (2012) 1847–1854.

- [54] A. Valan Arasu, A.P. Sasmito, A.S. Mujumdar, Numerical performance study of paraffin wax dispersed with alumina in a concentric pipe latent heat storage system, *Therm. Sci.* 17 (2013) 419–430.
- [55] J.M. Khodadadi, L. Fan, H. Babaei, Thermal conductivity enhancement of nanostructure-based colloidal suspensions utilized as phase change materials for thermal energy storage: A review, *Renew. Sustain. Energy Rev.* 24 (2013) 418–444.
- [56] K. Chintakrinda, R.D. Weinstein, A.S. Fleischer, A direct comparison of three different material enhancement methods on the transient thermal response of paraffin phase change material exposed to high heat fluxes, *Int. J. Therm. Sci.* 50 (2011) 1639–1647.
- [57] Y. Hamada, W. Otsu, J. Fukai, Y. Morozumi, O. Miyatake, Anisotropic heat transfer in composites based on high-thermal conductive carbon fibers, *Energy*. 30 (2005) 221–233.
- [58] E.K. Summers, M. a. Antar, J.H. Lienhard, Design and optimization of an air heating solar collector with integrated phase change material energy storage for use in humidification–dehumidification desalination, *Sol. Energy*. 86 (2012) 3417–3429.
- [59] Y. Tian, C.Y. Zhao, A review of solar collectors and thermal energy storage in solar thermal applications, *Appl. Energy*. 104 (2013) 538–553.
- [60] A. Faghri, *Heat Pipe Science and Technology*, Taylor & Francis Group, Washington, D.C., 1995.
- [61] J.H. Rosenfeld, D.M. Ernst, J.E. Lindemuth, J.L. Sanzi, S.M. Geng, J. Zuo, An Overview of Long Duration Sodium Heat Pipe Tests, *New Front. Futur. Concepts*. 699 (2004) 1–10.
- [62] P.B. Salunkhe, P.S. Shembekar, A review on effect of phase change material encapsulation on the thermal performance of a system, *Renew. Sustain. Energy Rev.* 16 (2012) 5603–5616.
- [63] W.-D. Steinmann, R. Tamme, Latent Heat Storage for Solar Steam Systems, *J. Sol. Energy Eng.* 130 (2008) 011004.
- [64] V.V. Tyagi, S.C. Kaushik, S.K. Tyagi, T. Akiyama, Development of phase change materials based microencapsulated technology for buildings: A review, *Renew. Sustain. Energy Rev.* 15 (2011) 1373–1391.
- [65] S. Karthikeyan, G. Ravikumar Solomon, V. Kumaresan, R. Velraj, Parametric studies on packed bed storage unit filled with PCM encapsulated spherical containers for low temperature solar air heating applications, *Energy Convers. Manag.* 78 (2014) 74–80.
- [66] X. Shi, S.A. Memon, W. Tang, H. Cui, F. Xing, Experimental Assessment of Position of Macro Encapsulated Phase Change Material in Concrete Walls on Indoor Temperatures and Humidity Levels, *Energy Build.* 71 (2013) 80–87.
- [67] R. Foran, M. Wu, The Capabilites and Barriers of Incorporating Phase Change Material into Residential Building Design in Sydney , Australia, *Int. J. Eng. Pract. Res.* 2 (2013) 170–173.

- [68] Z. Chen, G. Fang, Preparation and heat transfer characteristics of microencapsulated phase change material slurry: A review, *Renew. Sustain. Energy Rev.* 15 (2011) 4624–4632.
- [69] N.A.M. Amin, F. Bruno, M. Belusko, Effectiveness–NTU correlation for low temperature PCM encapsulated in spheres, *Appl. Energy*. 93 (2012) 549–555.
- [70] J.S. Lim, A. Bejan, J.H. Kim, Thermodynamic optimization of phase-change energy storage using two or more materials, *J. Energy Resour. Technol.* 114 (1992) 84.
- [71] H. Michels, R. Pitz-Paal, Cascaded latent heat storage for parabolic trough solar power plants, *Sol. Energy*. 81 (2007) 829–837.
- [72] H. Shabgard, C.W. Robak, T.L. Bergman, A. Faghri, Heat transfer and exergy analysis of cascaded latent heat storage with gravity-assisted heat pipes for concentrating solar power applications, *Sol. Energy*. 86 (2012) 816–830.
- [73] Z. Liu, Z. Wang, C. Ma, An experimental study on the heat transfer characteristics of a heat pipe heat exchanger with latent heat storage. Part II: Simultaneous charging/discharging modes, *Energy Convers. Manag.* 47 (2006) 967–991.
- [74] N. Sharifi, A. Faghri, T.L. Bergman, M.J. Allen, Melting and solidification enhancement using heat pipe with foils, *Int. J. Heat Mass Transf.* (2014) Submitted.
- [75] M.J. Allen, T.L. Bergman, A. Faghri, N. Sharifi, Robust heat transfer enhancement during melting and solidification of a pcm using a combined heat pipe-metal foam or foil configuration, *J. Heat Transfer*. (2014) Submitted.
- [76] M.J. Allen, N. Sharifi, A. Faghri, T.L. Bergman, Effect of inclination angle on the melting and solidification of a phase change material enhanced with a heat pipe and either metal foam or foils, *To Be Submitt. TBD* (2014) TBD.
- [77] R. Baby, C. Balaji, A Neural Network-Based Optimization Of Thermal Performance Of Phase Change Material-Based Finned Heat Sinks—An Experimental Study, *Exp. Heat Transf.* 26 (2013) 431–452.
- [78] A. a. Al-Abidi, S. Mat, K. Sopian, M.Y. Sulaiman, A.T. Mohammad, Experimental study of melting and solidification of PCM in a triplex tube heat exchanger with fins, *Energy Build.* 68 (2014) 33–41.
- [79] R. Baby, C. Balaji, Thermal optimization of PCM based pin fin heat sinks: An experimental study, *Appl. Therm. Eng.* 54 (2013) 65–77.
- [80] L.-W. Fan, Y.-Q. Xiao, Y. Zeng, X. Fang, X. Wang, X. Xu, et al., Effects of melting temperature and the presence of internal fins on the performance of a phase change material (PCM)-based heat sink, *Int. J. Therm. Sci.* 70 (2013) 114–126.

- [81] G.R. Solomon, R. Velraj, Analysis of the heat transfer mechanisms during energy storage in a Phase Change Material filled vertical finned cylindrical unit for free cooling application, *Energy Convers. Manag.* 75 (2013) 466–473.
- [82] A. a. Al-Abidi, S. Mat, K. Sopian, M.Y. Sulaiman, A.T. Mohammad, Internal and external fin heat transfer enhancement technique for latent heat thermal energy storage in triplex tube heat exchangers, *Appl. Therm. Eng.* 53 (2013) 147–156.
- [83] A.A. Al-Abidi, S. Mat, K. Sopian, M.Y. Sulaiman, A.T. Mohammad, Numerical study of PCM solidification in a triplex tube heat exchanger with internal and external fins, *Int. J. Heat Mass Transf.* 61 (2013) 684–695.
- [84] P.H. Biwole, P. Eclache, F. Kuznik, Phase-change materials to improve solar panel's performance, *Energy Build.* 62 (2013) 59–67.
- [85] N.H.S. Tay, F. Bruno, M. Belusko, Comparison of pinned and finned tubes in a phase change thermal energy storage system using CFD, *Appl. Energy.* 104 (2013) 79–86.
- [86] R. Bayón, E. Rojas, L. Valenzuela, E. Zarza, J. León, Analysis of the experimental behaviour of a 100 kWth latent heat storage system for direct steam generation in solar thermal power plants, *Appl. Therm. Eng.* 30 (2010) 2643–2651.
- [87] C. Guo, W. Zhang, Numerical simulation and parametric study on new type of high temperature latent heat thermal energy storage system, *Energy Convers. Manag.* 49 (2008) 919–927.
- [88] G. Chaxiu, D. Hexin, W. Xinli, Performance enhancement of a PCM cold storage under condition of heat flux, *Challenges Environ. Sci. Comput. Eng.* (2010) 499–502.
- [89] S. Jegadheeswaran, S.D. Pohekar, T. Kousksou, Performance enhancement of solar latent heat thermal storage system with particle dispersion - an exergy approach, *Clean - Soil, Air, Water.* 39 (2011) 964–971.
- [90] M. Abolghasemi, A. Keshavarz, M.A. Mehrabian, Thermodynamic analysis of a thermal storage unit under the influence of nano-particles added to the phase change material and/or the working fluid, *Heat Mass Transf.* 48 (2012) 1961–1970.
- [91] N.S. Dhaidan, J.M. Khodadadi, T. a. Al-Hattab, S.M. Al-Mashat, Experimental and numerical investigation of melting of phase change material/nanoparticle suspensions in a square container subjected to a constant heat flux, *Int. J. Heat Mass Transf.* 66 (2013) 672–683.
- [92] N.S. Dhaidan, J.M. Khodadadi, T. a. Al-Hattab, S.M. Al-Mashat, Experimental and numerical study of constrained melting of n-octadecane with CuO nanoparticle dispersions in a horizontal cylindrical capsule subjected to a constant heat flux, *Int. J. Heat Mass Transf.* 67 (2013) 523–534.
- [93] C.J. Ho, J.Y. Gao, An experimental study on melting heat transfer of paraffin dispersed with Al₂O₃ nanoparticles in a vertical enclosure, *Int. J. Heat Mass Transf.* 62 (2013) 2–8.

- [94] M. Jourabian, M. Farhadi, A.A. Rabienataj Darzi, Outward melting of ice enhanced by Cu nanoparticles inside cylindrical horizontal annulus: Lattice Boltzmann approach, *Appl. Math. Model.* 37 (2013) 8813–8825.
- [95] P. Chandrasekaran, M. Cheralathan, V. Kumaresan, R. Velraj, Solidification behavior of water based nanofluid phase change material with a nucleating agent for cool thermal storage system, *Int. J. Refrig.* Accepted m (2014).
- [96] Z. Duan, H. Zhang, L. Sun, Z. Cao, F. Xu, Y. Zou, et al., $\text{CaCl}_2 \cdot 6\text{H}_2\text{O}$ /Expanded graphite composite as form-stable phase change materials for thermal energy storage, *J. Therm. Anal. Calorim.* 115 (2014) 111–117.
- [97] X. Xiao, P. Zhang, M. Li, Preparation and thermal characterization of paraffin/metal foam composite phase change material, *Appl. Energy.* 112 (2013) 1357–1366.
- [98] J.J. Wu, J. Li, X. Xu, L. Yang, F. Zhao, C. Li, Molten salts/ceramic-foam matrix composites by melt infiltration method as energy storage material, *J. Wuhan Univ. Technol. Sci. Ed.* 24 (2009) 651–653.
- [99] N. Khodabandeh, H. Shokouhmand, Two-Temperature Model for Improvement of Heat Transport in PCMs Using Porous Matrix, *World Appl. Sci. J.* 18 (2012) 208–213.
- [100] R. Baby, C. Balaji, Experimental investigations on thermal performance enhancement and effect of orientation on porous matrix filled PCM based heat sink, *Int. Commun. Heat Mass Transf.* 46 (2013) 27–30.
- [101] M. Moeini Sedeh, J.M. Khodadadi, Thermal conductivity improvement of phase change materials/graphite foam composites, *Carbon N. Y.* 60 (2013) 117–128.
- [102] M. Sugawara, T. Onodera, Y. Komatsu, M. Tago, H. Beer, Freezing of water saturated in aluminum wool mats, *Heat Mass Transf.* 44 (2008) 835–843.
- [103] P.M. Gilart, Á.Y. Martínez, M.G. Barriuso, C.M. Martínez, Development of PCM/carbon-based composite materials, *Sol. Energy Mater. Sol. Cells.* 107 (2012) 205–211.
- [104] Z. Li, Z.-G. Wu, Numerical study on the thermal behavior of phase change materials (PCMs) embedded in porous metal matrix, *Sol. Energy.* 99 (2014) 172–184.
- [105] W.Q. Li, Z.G. Qu, B.L. Zhang, K. Zhao, W.Q. Tao, Thermal behavior of porous stainless-steel fiber felt saturated with phase change material, *Energy.* 55 (2013) 846–852.
- [106] L. Xia, P. Zhang, R.Z. Wang, Preparation and thermal characterization of expanded graphite/paraffin composite phase change material, *Carbon N. Y.* 48 (2010) 2538–2548.
- [107] Y.-C. Weng, H.-P. Cho, C.-C. Chang, S.-L. Chen, Heat pipe with PCM for electronic cooling, *Appl. Energy.* 88 (2011) 1825–1833.

- [108] G. Fang, X. Liu, S. Wu, Experimental investigation on performance of ice storage air-conditioning system with separate heat pipe, *Exp. Therm. Fluid Sci.* 33 (2009) 1149–1155.
- [109] H. Shabgard, T.L. Bergman, N. Sharifi, A. Faghri, High temperature latent heat thermal energy storage using heat pipes, *Int. J. Heat Mass Transf.* 53 (2010) 2979–2988.
- [110] K. Nithyanandam, R. Pitchumani, Thermal energy storage with heat transfer augmentation using thermosyphons, *Int. J. Heat Mass Transf.* 67 (2013) 281–294.
- [111] K. Nithyanandam, R. Pitchumani, Computational studies on a latent thermal energy storage system with integral heat pipes for concentrating solar power, *Appl. Energy*. 103 (2013) 400–415.
- [112] K. Nithyanandam, R. Pitchumani, Cost and performance analysis of concentrating solar power systems with integrated latent thermal energy storage, *Energy*. 64 (2014) 793–810.
- [113] J.P. Bédécarrats, J. Castaing-Lasvignottes, F. Strub, J.P. Dumas, Study of a phase change energy storage using spherical capsules. Part II: Numerical modelling, *Energy Convers.* 50 (2009) 2537–2546.
- [114] L. Karim, F. Barbeon, P. Gegout, a. Bontemps, L. Royon, New phase-change material components for thermal management of the light weight envelope of buildings, *Energy Build.* 68 (2014) 703–706.
- [115] A.S. Sundaram, R.V. Seeniraj, R. Velraj, An experimental investigation on passive cooling system comprising phase change material and two-phase closed thermosyphon for telecom shelters in tropical and desert regions, *Energy Build.* 42 (2010) 1726–1735.
- [116] L. Pan, Q. Tao, S. Zhang, S. Wang, J. Zhang, S. Wang, et al., Preparation, characterization and thermal properties of micro-encapsulated phase change materials, *Sol. Energy Mater. Sol. Cells*. 98 (2012) 66–70.
- [117] L. Bayés-García, L. Ventolà, R. Cordobilla, R. Benages, T. Calvet, M. a. Cuevas-Diarte, Phase Change Materials (PCM) microcapsules with different shell compositions: Preparation, characterization and thermal stability, *Sol. Energy Mater. Sol. Cells*. 94 (2010) 1235–1240.
- [118] J. Li, P. Xue, W. Ding, J. Han, G. Sun, Micro-encapsulated paraffin/high-density polyethylene/wood flour composite as form-stable phase change material for thermal energy storage, *Sol. Energy Mater. Sol. Cells*. 93 (2009) 1761–1767.
- [119] X.-Y. Li, L. Li, J.-W. Yu, J.-Q. Liu, Y.-Y. Wu, Investigation of the dynamic characteristics of a storage tank discharging process for use in conventional air-conditioning system, *Sol. Energy*. 96 (2013) 300–310.
- [120] M. Jradi, M. Gillott, S. Riffat, Investigation of the dynamic characteristics of a storage tank discharging process for use in conventional air-conditioning system, *Appl. Therm. Eng.* 59 (2013) 211–222.

- [121] K. Nithyanandam, R. Pitchumani, a. Mathur, Analysis of a latent thermocline storage system with encapsulated phase change materials for concentrating solar power, *Appl. Energy*. 113 (2014) 1446–1460.
- [122] E. Oró, J. Chiu, V. Martin, L.F. Cabeza, Comparative study of different numerical models of packed bed thermal energy storage systems, *Appl. Therm. Eng.* 50 (2013) 384–392.
- [123] W. Zhao, A.F. Elmozughi, A. Oztekin, S. Neti, Heat transfer analysis of encapsulated phase change material for thermal energy storage, *Int. J. Heat Mass Transf.* 63 (2013) 323–335.
- [124] H. Peng, H. Dong, X. Ling, Thermal investigation of PCM-based high temperature thermal energy storage in packed bed, *Energy Convers. Manag.* 81 (2014) 420–427.
- [125] M. Wu, C. Xu, Y.-L. He, Dynamic thermal performance analysis of a molten-salt packed-bed thermal energy storage system using PCM capsules, *Appl. Energy*. 121 (2014) 184–195.
- [126] H. Bindra, P. Bueno, J.F. Morris, R. Shinnar, Thermal analysis and exergy evaluation of packed bed thermal storage systems, *Appl. Therm. Eng.* 52 (2013) 255–263.
- [127] J. Yang, C.Y. Zhao, Solidification analysis of a single particle with encapsulated phase change materials, *Appl. Therm. Eng.* 51 (2013) 338–346.
- [128] Y.-Q. Li, Y.-L. He, Z.-F. Wang, C. Xu, W. Wang, Exergy analysis of two phase change materials storage system for solar thermal power with finite-time thermodynamics, *Renew. Energy*. 39 (2012) 447–454.
- [129] Y.Q. Li, Y.L. He, H.J. Song, C. Xu, W.W. Wang, Numerical analysis and parameters optimization of shell-and-tube heat storage unit using three phase change materials, *Renew. Energy*. 59 (2013) 92–99.
- [130] J.N.W. Chiu, V. Martin, Multistage latent heat cold thermal energy storage design analysis, *Appl. Energy*. 112 (2013) 1438–1445.
- [131] X. Wang, Q. Guo, J. Wang, Y. Zhong, L. Wang, X. Wei, et al., Thermal conductivity enhancement of form-stable phase-change composites by milling of expanded graphite, micro-capsules and polyethylene, *Renew. Energy*. 60 (2013) 506–509.
- [132] Y.Q. Xie, J. Song, P.T. Chi, J.Z. Yu, Performance enhancement of phase change thermal energy storage unit using fin and copper foam, *Appl. Mech. Mater.* 260 (2013) 137–141.
- [133] N. Calvet, X. Py, R. Olivès, J.-P. Bédécarrats, J.-P. Dumas, F. Jay, Enhanced performances of macro-encapsulated phase change materials (PCMs) by intensification of the internal effective thermal conductivity, *Energy*. 55 (2013) 956–964.
- [134] L. Yang, X. Zhang, G. Xu, Thermal performance of a solar storage packed bed using spherical capsules filled with PCM having different melting points, *Energy Build.* 68 (2014) 639–646.

- [135] H. Yin, X. Gao, J. Ding, Z. Zhang, Experimental research on heat transfer mechanism of heat sink with composite phase change materials, *Energy Convers. Manag.* 49 (2008) 1740–1746.
- [136] K. Siva, M.X. Lawrence, G.R. Kumares, P. Rajagopalan, H. Santhanam, Experimental and numerical investigation of phase change materials with finned encapsulation for energy-efficient buildings, *J. Build. Perform. Simul.* 3 (2010) 245–254.
- [137] M. Chinnapandiana, V. Pandiyarajan, R. Velraj, Experimental Investigation of A Latent Heat Storage System For Diesel Engine Waste Heat Recovery With and Without Cascaded Arrangement, in: *Int. Conf. Mech. Automob. Robot. Eng.*, 2011: pp. 239–243.
- [138] H. Shabgard, A. Faghri, T.L. Bergman, C.E. Andraka, Numerical simulation of heat pipe-assisted latent heat thermal energy storage unit for dish-stirling systems, *J. Sol. Energy Eng.* 136 (2014) 021025–1–12.
- [139] Y. Tian, C.Y. Zhao, Thermal and exergetic analysis of metal foam-enhanced cascaded thermal energy storage (MF-CTES), *Int. J. Heat Mass Transf.* 58 (2013) 86–96.
- [140] S.M. Flueckiger, S. V. Garimella, Latent heat augmentation of thermocline energy storage for concentrating solar power – A system-level assessment, *Appl. Energy.* 116 (2014) 278–287.

Table 2.1. Experimental investigations involving fin enhanced PCM systems.

Reference	PCM properties	Fin properties	Operation mode and applications	Configuration	Conclusions
[77]	• n-eicosane ($T_m = 36.5\text{ }^{\circ}\text{C}$, $m = 0.05\text{ kg}$)	• aluminum • flat fin (thickness, $t = 2\text{ mm}$) • number, $N = 0-7$ • porosity, $\phi = 0.79-1.00$	• melting • electric heater • electronic cooling applications	A rectangular heat sink with vertical fins is filled with PCM and heated from below.	The operational time of the heat sink (until a temperature of $55\text{ }^{\circ}\text{C}$) was extended by a factor of 3 using a finned relative to non-finned heat sink.
[78]	• RT82 ($T_m = 77-85\text{ }^{\circ}\text{C}$, $m = 5.6\text{ kg}$)	• copper • flat fin ($t = 1\text{ mm}$, length, $L = 42\text{ mm}$) • $N = 8$	• melting / solidification • HTF (water) • solar TES applications	A triple tube heat exchanger has the PCM contained in the middle section and the HTF in the inner and outer sections.	The melting time was decreased to 58% as the HTF increased from 8 kg/min to 16 kg/min . As the inlet temperature increased from $85\text{ }^{\circ}\text{C}$ to $100\text{ }^{\circ}\text{C}$, the melting time was reduced to 86%.
[79]	• n-eicosane ($T_m = 36.5\text{ }^{\circ}\text{C}$) • paraffin wax ($T_m = 53-57\text{ }^{\circ}\text{C}$, $m = 39-50\text{ g}$)	• aluminum • pin fin • $N = 0 - 120$	• melting / solidification • electric heater • electronic cooling applications	A rectangular heat sink with vertical pin fins is filled with PCM and heated from below.	The time for the heat sink to reach a set point temperature was increased by a factor of 24 with $N = 72$ relative to without the fins. An optimum configuration was obtained based on the PCM volume fraction and the modified dimensionless temperature utilizing an artificial neural network genetic algorithm.
[80]	• n-eicosane ($T_m = 37\text{ }^{\circ}\text{C}$) • 1-hexadecan-ole ($T_m = 49\text{ }^{\circ}\text{C}$, $m \approx 0.15\text{ kg}$)	• aluminum • flat fin ($t \approx 2\text{ mm}$, $L \approx 40\text{ mm}$) • $N = 4$	• melting / solidification • electric heater • electronic cooling applications	A rectangular aluminum cavity is filled with PCM and heated from below.	PCMs with higher melting temperatures were reported to extend operation times until a set point temperature was reached. For the conditions considered, the maximum temperature rise was reduced by up to $10\text{ }^{\circ}\text{C}$ for the finned heat sink.
[50]	• 6 PCMs comprising hydrated salts, organics or mixtures • $29\text{ }^{\circ}\text{C} < T_m < 41\text{ }^{\circ}\text{C}$ • $V_{pcm} = 25\text{ ml}$	• aluminum • flat fin ($t = 2\text{ mm}$)	• melting • electric heater • electronic cooling applications	A rectangular cavity with vertical fins is filled with PCM and heated from below. Six heat sink arrangements were investigated.	Adding fins reduced the heat sink peak temperature relative to that without the fins. A honeycomb heat sink made from aluminum foils ($t = 0.060\text{ mm}$) showed comparable performance to the fin cases. The PCM with the lowest T_m had the longest operation time and lowest heat sink temperature.
[81]	• RT 21 ($T_m = 19-22\text{ }^{\circ}\text{C}$)	• copper • axial fin ($t = 3\text{ mm}$, $L = 240\text{ mm}$, height, $h = 10-26\text{ mm}$)	• solidification • HTF (air) • electronic cooling applications	A vertical double tube heat exchanger with the HTF in the inner tube and the PCM with axial fins between the tubes.	A finned heat sink was able to provide a 22% reduction in the complete solidification time relative to that without the fins with $h = 20\text{ mm}$ ($\approx 60\%$ length of the annular gap the outer section).

Table 2.2. Numerical investigations involving fin enhanced PCM systems.

Reference	Method	PCM properties	Fin properties	Operation mode and application	Configuration	Conclusions
[38]	<ul style="list-style-type: none"> • 2D • finite volume (FV) • TTM (including natural convection) 	<ul style="list-style-type: none"> • n-octadecane ($T_m = 30\text{ }^{\circ}\text{C}$) 	<ul style="list-style-type: none"> • copper • flat fin (dimension-less) 	<ul style="list-style-type: none"> • melting • constant side wall temperature • solar TES applications 	A rectangular enclosure is filled with PCM and horizontal fins extend outward from the heated wall into a portion of the PCM domain.	A rapid melting regime is initially present due to the finned region followed by a slow melting regime as the solid-liquid interfaces advance to the non-finned regions. New correlations were developed to predict the melting rates for both regimes. A dimensionless total melting time was reduced by 60% with 6 fins that were 80% of the length of the enclosure.
[82]	<ul style="list-style-type: none"> • FLUENT • 2D • FV • enthalpy-porosity (including natural convection) 	<ul style="list-style-type: none"> • RT82 ($T_m = 77\text{--}85\text{ }^{\circ}\text{C}$) 	<ul style="list-style-type: none"> • copper, aluminum and steel • axial fin ($t = 1\text{--}4\text{ mm}$, $L = 10\text{--}42\text{ mm}$) • $N = 0\text{--}8$ 	<ul style="list-style-type: none"> • melting • HTF (water) • solar TES applications 	A triple tube heat exchanger has the PCM contained in the middle section and the HTF in the inner and outer sections.	The effect of fin thickness during melting is small compared to the fin length and number. With $N = 8$, the complete melting time was reduced to 34.7% relative to that of the case without fins.
[83]	<ul style="list-style-type: none"> • FLUENT • 2D • FV • enthalpy-porosity (including natural convection) 	<ul style="list-style-type: none"> • RT82 ($T_m = 77\text{--}85^{\circ}\text{C}$, $m = 5.6\text{ kg}$) 	<ul style="list-style-type: none"> • copper • axial fin ($t = 0.5\text{--}4\text{ mm}$, $L = 10\text{--}42\text{ mm}$) • $N = 0\text{--}8$ 	<ul style="list-style-type: none"> • solidification • HTF (water) • solar TES applications 	A triple tube heat exchanger has the PCM contained in the middle section and the HTF in the inner and outer sections.	The effect of fin thickness during solidification is small compared to the fin length and number. The complete solidification time was decreased to 35% of the pure PCM case with $N = 8$ and $t = 1\text{ mm}$.
[84]	<ul style="list-style-type: none"> • 2D • finite element (FE) • enthalpy-porosity (including natural convection) 	<ul style="list-style-type: none"> • RT25 ($T_m = 26.5^{\circ}\text{C}$, $m \approx 2.35\text{ kg}$) 	<ul style="list-style-type: none"> • aluminum • flat fin ($t = 4\text{ mm}$) 	<ul style="list-style-type: none"> • melting • solar irradiation • solar panel applications 	A rectangular cavity is filled with PCM and horizontal fins.	Integration of a PCM with a solar panel can help to maintain its temperature below $40\text{ }^{\circ}\text{C}$ for 80 min with constant solar irradiation.
[85]	<ul style="list-style-type: none"> • ANSYS software • 2D and 3D • FV 	<ul style="list-style-type: none"> • paraffin 	<ul style="list-style-type: none"> • copper • pin fin ($d = 3\text{--}9\text{ mm}$, $L = 20\text{--}40\text{ mm}$) • radial ($d = 52\text{--}92\text{ mm}$, $t = 0.3\text{--}1\text{ mm}$) 	<ul style="list-style-type: none"> • solidification • HTF (water with dissolved ionic solids) 	A vertical shell (PCM) and tube (HTF) heat exchanger utilizes horizontal fins in the PCM.	The finned tube with annular fins achieved 25% faster phase change duration relative to that with pin fins. Yet both annular and pin finned tubes achieved better performance relative to without fins.

Table 2.3. Recent investigations involving foil enhanced PCM systems.

Reference	Method	PCM properties	Foil properties	Operation mode and application	Configuration	Conclusions
[53]	EXP NUM • PHOENICS code commercial software • 3D	• water ($T_m = 0^\circ\text{C}$)	• copper • radial ($t = 0.035$ mm) • porosity, $\phi = 0.925$	• solidification • HTF (aqueous glycol solution)	A rectangular cavity with a horizontal HTF tube is surrounded with PCM and foils without tube contact.	While foils are not in thermal contact with the HTF tube, a small foil volume fraction (0.5%) has a significant impact on solidification. The solidification rate can be doubled with $\phi = 0.925$.
[52]	EXP NUM • 2D	• water ($T_m = 0^\circ\text{C}$)	• copper • radial ($d = 94$ mm, $t = 0.030$ mm) • $\phi = 0.975$	• solidification • HTF (aqueous glycol solution)	A rectangular cavity with a horizontal HTF tube is surrounded by the PCM and foils.	The solidification time reduced to an eighteenth (tenth) compared with that of a bare tube, even with a small copper volume fraction of $\phi = 0.95$ ($\phi = 0.975$). Foils were reported to increase melting rates greater than the solidification rates.
[50]	EXP	• 6 PCMs comprising hydrated salts, organics or mixtures of both. • $29^\circ\text{C} < T_m < 41^\circ\text{C}$ • $V_{pcm} = 25$ ml	• aluminum • honeycomb structure (cell size = 6 mm, $t = 0.06$ mm, $h = 12$ mm)	• melting / solidification • electric heater • electronic cooling applications	A rectangular cavity with vertical fins is filled with PCM and heated from below. Six heat sink arrangements were investigated.	Honeycomb inserts show a similar thermal performance as a machined finned heat sink with less weight, greater ease of assembly and reduced cost.
[86]	EXP NUM • 1D	• $\text{KNO}_3/\text{NaNO}_3$ eutectic mixture ($m = 2100$ kg)	• expanded graphite (EG) • rectangular ($t = 1$ mm)	• melting / solidification • HTF (water/steam) • solar power applications	A horizontal shell (PCM) and tube (HTF) heat exchanger utilizes vertical foils in the PCM.	The thermal conductivity was increased from 0.5 W/mK for the pure PCM to approximately 8 W/mK for the EG foil-PCM composite.
[87]	NUM • FLUENT • 2D • enthalpy-porosity method • FV	• $\text{KNO}_3/\text{NaNO}_3$ eutectic mixture ($T_m = 220^\circ\text{C}$)	• aluminum • radial ($d_o = 56$ mm, $t = 0.5$ -4mm)	• solidification • HTF (water/steam) • solar power generation	A horizontal shell (PCM) and tube (HTF) heat exchanger utilizes vertical foils in the PCM.	The thermal conductivity of the PCM increased from 0.5 W/mK for the pure PCM to 10 W/mK for the foil-PCM composite. The complete solidification time decreased to approximately 25% by increasing thickness from 0.5 mm to 4 mm or decreasing foil pitch from 10 mm to 2.5 mm.
[88]	NUM • FLUENT • 2D • enthalpy-porosity method • FV	• eutectic salt ($T_m = 5$ -9 $^\circ\text{C}$)	• aluminum • radial ($d_o = 46$ mm, $t = 0.5$ -4 mm)	• solidification • HTF (air) • cold TES and building applications	A horizontal shell (PCM) and tube (HTF) heat exchanger utilizes vertical foils in the PCM.	Foils can greatly reduce solidification time by thermally penetrating the PCM. Also, as the heat flux was doubled, the complete solidification time was reduced by nearly 50%.

Table 2.4. Studies involving nano-particle enhanced PCMs.

Reference	Method	PCM	Particle properties	Operation mode and applications	Configuration	Conclusions
[89]	NUM • FLUENT • 2D	• RT58 ($T_m = 55-59\text{ }^{\circ}\text{C}$)	• Cu ($L < 50\text{ nm}$) • 0-20 wt%	• melting • HTF (water)	A vertical shell (PCM) and tube (HTF) heat exchanger is studied.	Both the heat transfer rate and exergy efficiency are improved by adding nanoparticles. Up to 21% decrease in the total melting time was obtained for 20 vol% nanoparticle.
[90]	NUM • 2D	• $\text{CaCl}_2\cdot 6\text{H}_2\text{O}$ ($T_m = 30\text{ }^{\circ}\text{C}$)	• Cu • Al_2O_3 • CuO • 0-20vol%	• melting • HTF (water)	A horizontal shell (PCM) and tube (HTF) heat exchanger is studied.	Entropy generation and melting duration were decreased by 43% and 42%, respectively, by adding 20 vol% nanoparticle. Adding nanoparticles to the PCM is much more advantageous compared to adding them to the HTF. The reduction of specific heat and latent heat of the PCM due to addition of nanoparticles was more than compensated by increase in heat transfer rate.
[91]	EXP NUM • COMSOL • 2D	• n-octadecane ($T_m = 28\text{ }^{\circ}\text{C}$)	• CuO ($L = 9\text{ nm}$) • 0-5 wt%	• melting • electric heater	A square cavity is heated from the side.	The heat transfer rate increases with increasing the weight fraction of nanoparticles due to the improvement of the thermal conductivity. A 9% reduction in melting time was achieved by addition of 5 wt% nanoparticle.
[92]	EXP NUM • COMSOL • 2D	• n-octadecane ($T_m = 28\text{ }^{\circ}\text{C}$)	• CuO ($L = 9\text{ nm}$) • 0-5 wt%	• melting • electric heater	A horizontal tube is heated from the curved wall.	About 13% reduction in melting time was achieved by the addition of 5 wt% nanoparticles. The rate of increase of heat transfer due to the addition of nanoparticles decreased with increasing concentration of particles due to intensified effects of viscosity, agglomeration and sedimentation.
[93]	EXP	• n-octadecane ($T_m = 28\text{ }^{\circ}\text{C}$)	• Al_2O_3 • 0-10 wt%	• melting • electric heater / cold HTF (water)	A vertical square enclosure is heated from one side and cooled from opposite side.	For a cold wall temperature close to the melting temperature of the PCM, the average Nusselt number decreased by about 60% for a particle concentration of 10 wt%. The suppression of natural convection heat transfer due to the addition of nanoparticles is even greater when the cold wall is maintained at temperatures lower than the PCM melting temperature.
[94]	NUM • 2D	• water ($T_m = 0\text{ }^{\circ}\text{C}$)	• Cu ($L=100\text{nm}$) • 0-4 vol%	• melting • inner cylinder at constant temperature	A concentric and non-concentric horizontal shell (PCM) and tube (HTF) system are investigated.	In general, the melting rate was increased by increasing the volume fraction of nanoparticles in the range of conditions studied. Quantitatively up to 11% more melt volume fraction was achieved by the addition of 4 vol% nanoparticle at a time instant corresponding to about 60% melt volume fraction in base system. The increase in the melting rate was more profound when the hot inner cylinder was positioned in the upper region of the shell. The reason is the more important role of conduction in this configuration.

Table 2.4. Studies involving nano-particle enhanced PCMs, cont.

Reference	Method	PCM	Particle properties	Operation mode and applications	Configuration	Conclusions
[95]	EXP	<ul style="list-style-type: none"> • water ($T_m = 0\text{ }^{\circ}\text{C}$) 	<ul style="list-style-type: none"> • multiwall carbon nanotubes • 0.1 wt% 	<ul style="list-style-type: none"> • solidification • HTF bath (aqueous glycol solution) 	The PCM is contained in a spherical enclosure immersed in an HTF bath.	A 25% reduction in the complete solidification time was achieved using water enhanced with nanoparticles as a phase change material.

Table 2.5. LHTES systems involving high thermal conductivity structures.

Reference	Method	PCM properties	Structure properties	Operation mode and applications	Configuration	Conclusions
[47]	EXP NUM • 2D • FV • enthalpy method	• paraffin ($T_m = 46-60$ °C)	foam • copper • $\phi = 0.9-0.98$ • $\omega = 10-40$ pores per inch (PPI)	• melting • electric heater • electronic cooling applications	A rectangular cavity is heated from the side.	The average hot wall temperature was reduced by 30 °C with the copper foam compared to only PCM.
[96]	EXP	• $\text{CaC}_{12} \cdot 6\text{H}_2\text{O}$ ($T_m = 29-37$ °C)	expanded graphite (EG) • 10-50 wt%	• thermal conductivity measurement	A cylindrical disk is heated from below for thermal conductivity measurement using the transient plate source method.	The effective thermal conductivity was increased by 14 times from 0.6 W/mK of pure PCM to 8.8 W/mK with a 50 wt% EG. The addition of surfactant increases the bonding energy between the PCM and EG. Differential Scanning Calorimetry (DSC) and thermal gravimetric analysis show good thermal stability and energy storage properties.
[97]	EXP	• paraffin ($T_m = 60$ °C)	foam • nickel, copper • $\phi = 0.97$ • $\omega = 5-25$ PPI	• thermal conductivity measurement	A rectangular foam-PCM sample is used for thermal conductivity measurement using the transient plate source and steady-state methods.	The effective thermal conductivity was increased by a factor of 3 and 15 for the nickel and copper foam, respectively, compared to the pure PCM. Degassing the PCM by melting under vacuum pressure increases the impregnation of PCM into foam by about 7%. A slight shift in the phase change temperature (~ 1 °C) was observed. Also the latent heat of the composite is about 22-30% less than the paraffin for the composite.
[98]	EXP	• Na_2SO_4 ($T_m = 888$ °C)	foam • SiC ceramic	• thermal conductivity measurement • high temperature TES applications	This work determined the foam-PCM composite thermal conductivity using DSC.	The Na_2SO_4 / SiC composite thermal conductivity was around 5.5 W/mK (from about 0.55 W/mK [14] for the pure PCM).
[99]	NUM • 2D • FV • enthalpy method	• paraffin	metal matrix • aluminum, nickel, stainless steel, copper • $\phi = 0.85-0.95$	• melting • constant temperature	A rectangular enclosure contains PCM with a hot side wall that is held at constant temperature.	Metal matrices with higher thermal conductivities, lower porosities, and lower pore diameters have faster melting times. The complete melting time was reduced to one fourth when $\phi = 0.95$ was reduced to $\phi = 0.80$. The complete melting time with the copper matrix is one half of that for the stainless steel matrix.

Table 2.5. LHTES systems involving high thermal conductivity structures, cont.

Reference	Method	PCM properties	Structure properties	Operation mode and applications	Configuration	Conclusions
[100]	EXP	• n-eicosane ($T_m = 36.5\text{ }^{\circ}\text{C}$,)	foam • copper • $\phi = 0.86$ • $\omega = 10\text{ PPI}$	• melting • electric heater • electronic cooling applications	A rectangular enclosure contains the PCM and foam while heated from the bottom. The entire system may be tilted.	The orientation was shown to only slightly alter the complete melting time from about 100 min to 120 min. After 90 min, each orientation has a temperature within $0.5\text{ }^{\circ}\text{C}$ of one another. Similar performance is repeated for aluminum foam.
[12]	EXP	• paraffin ($T_m = 47\text{-}59^{\circ}\text{C}$)	foam • copper • $\phi = 0.90\text{-}0.98$ • $\omega = 5\text{-}20\text{ PPI}$	• melting • electric heater • electronic cooling applications	A rectangular enclosure filled with PCM and foam is heated from below and cooled with external fins from above.	Lower surface temperatures are observed for lower porosities and pore densities while the former has a greater effect. Natural convection was suppressed by at least 55.3% relative to the pure PCM heat sink without foam.
[101]	EXP NUM • FLUENT • 3D • FV	• cyclohexane ($T_m \approx 6.5\text{ }^{\circ}\text{C}$)	foam • graphite (pore diameter, $d_p = 400\text{ }\mu\text{m}$) • $\phi = 0.75$	• melting • electric heater	A rectangular enclosure is filled with PCM and heated from below.	The graphite foam-PCM composite had a highest reported thermal conductivity of approximately 30 W/mK while the pure PCM was 0.13 W/mK . Natural convection in foam was negligible.
[102]	EXP NUM • 2D • FV • enthalpy method	• water ($T_m = 0\text{ }^{\circ}\text{C}$)	wool mats • aluminum • radial disk- or roll-types ($d_{\text{fiber}} = 120\text{ }\mu\text{m}$, $t_{\text{mat}} = 6\text{ mm}$) • $\phi = 0.9\text{-}0.95$	• solidification • HTF (brine)	A rectangular enclosure with a horizontal HTF tube is filled with PCM.	After 3 hours of operation the mass of ice is twice that of the system without wool mats with a porosity of $\phi = 0.95$. The disk type arrangement was far superior to the method of wrapping the wool around the HTF tube. The model predicted the disk-type fairly well, yet under-predicted the roll type by 25%
[103]	EXP	• RT50 ($T_m = 49\text{ }^{\circ}\text{C}$) • RT60 ($T_m = 59\text{ }^{\circ}\text{C}$)	EG • $\phi = 0.25$	• thermal conductivity measurement	A disc shaped EG-PCM composite is used for thermal conductivity measurement.	The thermal conductivity was increased by a factor of 5.76 and 2.24 for RT50 and RT60, respectively with EG relative to without it.
[104]	NUM • FLUENT • 3D • FV • enthalpy method	• NaNO_3 ($T_m = 306\text{ }^{\circ}\text{C}$)	metal matrix • copper • ideal cube shaped • $\phi = 0.90\text{-}0.95$ • $\omega = 5\text{-}30\text{ PPI}$	• melting / solidification • constant temperature sidewall • solar applications	A cuboid matrix structure is embedded in PCM and heated on two sides.	The heat transfer coefficient can be increases by up to 28 times in the solid phase with the copper matrix relative to that without it. The complete melting and solidification times are reduced to 20% and 4% of that for the pure PCM with $\phi = 0.90$.

Table 2.5. LHTES systems involving high thermal conductivity structures, cont.

Reference	Method	PCM properties	Structure properties	Operation mode and applications	Configuration	Conclusions
[105]	EXP	<ul style="list-style-type: none"> • paraffin ($T_m = 48-59$ °C) 	fiber felt <ul style="list-style-type: none"> • stainless steel ($d_{fiber} = 100-200$ μm) • $\phi=0.80-0.90$ 	<ul style="list-style-type: none"> • melting • constant surface temperature • thermal management applications 	A rectangular fiber felt-PCM composite heated on one side.	As the porosity increased from 0.80 to 0.90, the dominant mechanism shifted from combined conduction and convection to natural convection only. A lower surface temperature was observed for a smaller fiber diameter at a fixed porosity due to a higher interfacial surface area. A higher porosity of 0.90 resulted in a larger surface temperature but also a greater amount of PCM melting due to natural convection.
[106]	EXP	<ul style="list-style-type: none"> • paraffin ($T_m = 48.7$ °C) 	EG <ul style="list-style-type: none"> • $\phi=0.95-0.99$ 	<ul style="list-style-type: none"> • melting / solidification • electric heater / cold HTF (water) 	A vertical shell (PCM) and tube (HTF) is studied with EG embedded in the PCM.	The melting point changed by 1.2 °C. The total melting and solidification time was reduced by 48.9% and 66.5%, respectively, with a porosity of 0.95. Also the thermal conductivity was increased by more than a factor of 10.

Table 2.6. Experimental investigations involving heat pipes and reflux systems integrated with PCMs.

Reference	Method	PCM properties	Enhancement properties	Operation mode and applications	Configuration	Conclusions
[7]	EXP	• paraffin wax ($m \approx 1$ kg)	HP • copper-water ($L = 0.2$ m, $d = 6$ mm)	• melting / solidification • HTF (water) • solar applications	A vertical cylinder with PCM has five vertical HPs that extended into an underlying HTF.	The heat transfer rates were increased by 60% and 100% by use of five heat pipes during charging and discharging, respectively.
[107]	EXP	• lauric acid ($T_m \approx 43$ °C) • palmitic acid ($T_m \approx 60$ °C) • tricosane ($T_m \approx 45$ °C)	HP • copper-water ($L = 120$ mm, $d = 6$ mm)	• melting / solidification • electric heater / cold HTF (air) • electronic cooling applications	A horizontal HP extends through a rectangular PCM enclosure. The HP is heated on one side and is subject to forced convection on the other.	The HP-enhanced PCM system can reduce fan power consumption up to nearly 46% while reducing the average heater temperature by about 12.3 °C compared to without the PCM.
[73]	EXP	($T_m = 52.1$ °C)	HP ($L = 1$ m)	• melting / solidification • HTF (water) • heat exchanger/ solar applications	A HP extends through the PCM and is also in contact with the HTF.	A HP heat exchanger with integrated PCM is investigated to study the charging, discharging, and simultaneous operation modes. A thermal resistance network analysis is performed for the system.
[9]	EXP	• Zn (70)-Sn(30) eutectic mixture ($T_m=200-370$ °C, $m = 210$ ton)	reflux • water	• melting / solidification • HTF (water) • solar applications	The PCM is positioned in between the HTF channels of a reflux system.	The proof of concept was experimentally tested and was able to provide up to 12 MW for about 20 min.
[108]	EXP	• water ($T_m = 0$ °C)	loop HP • helical evaporator • copper-R22 ($L_{pcm} = 15$ m, $d_o=12.7$ mm, $d_i=10.2$ mm)	• solidification • HTF (water) • ice storage, air conditioning applications	A helical HP evaporator is placed in an ice storage tank while a helical condenser is placed inside a helical HTF tube.	A charge and discharge rate of up to 3.5 kW can be achieved with the proposed ice storage system. A latent and sensible capacity of 25MJ and 10MJ are present with a total of 35 MJ. An outlet air temperature into the room of about 8-9 °C. An outlet water temperature from the tank of about 5 °C was achieved.

Table 2.7. Numerical studies on LHTES systems utilizing heat pipes and reflux systems.

Reference	Method	PCM properties (wt%)	Enhancement Properties	Operation mode and applications	Configuration	Conclusions
[37]	<ul style="list-style-type: none"> • 2D • FV • TTM (including natural convection) 	<ul style="list-style-type: none"> • NaNO₃ ($T_m=307$ °C) 	HP <ul style="list-style-type: none"> • stainless steel-potassium ($L_e = 25$mm, $L_a = 20$mm, $L_c = 23$-70mm, $d_o = 9$-14mm, $t_{wall} = 1$mm, $t_{wick} = 1$mm) 	<ul style="list-style-type: none"> • melting • HP is in contact with HTF (constant wall temperature) 	A vertical cylinder is filled with PCM with a concentrically-located HP that is also in contact with an HTF.	The melting rate induced by the HP was significantly higher than that of a similarly dimensioned rod or tube. The average HP effectiveness (ratio of the liquid fraction relative to that of the rod case) over the duration of complete PCM melting could attain a value greater than 2. The HP was also the most effective for heating from above the PCM relative to the rod or tube.
[109]	<ul style="list-style-type: none"> • 1D • thermal network (including natural convection) 	<ul style="list-style-type: none"> • KNO₃ ($T_m=335$ °C) 	HP <ul style="list-style-type: none"> • stainless steel-mercury ($L_e = 100$ mm, $L_a = 60$ mm, $L_c = 140$ mm, $d_o = 18$ mm, $t_{wall} = 1$mm, $t_{wick} = 1$mm) 	<ul style="list-style-type: none"> • melting / solidification • HP is in contact with HTF (Therminol VP-1) • CSP applications 	A shell and tube is investigated with HPs embedded in the tube: <ul style="list-style-type: none"> • shell (PCM) and tube (HTF) • shell (HTF in cross flow) and tube (PCM) 	HPs significantly improved the thermal performance compared to a non-HP configuration for both melting and solidification. The charging (discharging) effectiveness was increased by approximately 60% (40%) compared to a case without the HPs.
[110]	<ul style="list-style-type: none"> • FLUENT • 2D • FV • enthalpy-porosity method (including natural convection) 	<ul style="list-style-type: none"> • KNO₃ ($T_m=335$ °C) 	TS <ul style="list-style-type: none"> • stainless steel-Therminol VP-1 ($L_e = 100$ mm, $L_a = 60$ mm, $L_c = 140$mm, $d_o = 9$ mm, $t_{wall} = 2$ mm) 	<ul style="list-style-type: none"> • melting / solidification • TS is in contact with hot HTF (Therminol VP-1) • CSP applications 	A shell and tube is investigated with HPs embedded in the tube: <ul style="list-style-type: none"> • shell (PCM) and tube (HTF) • shell (HTF in cross flow) and tube (PCM) 	The energy stored / retrieved and the effectiveness was presented for both modules and different TS arrangements. The Configurations that lead to improved effectiveness and energy storage / retrieval rates per unit cost of TSs are identified.
[111]	<ul style="list-style-type: none"> • FLUENT • 2D • FV • enthalpy-porosity method (including natural convection) 	<ul style="list-style-type: none"> • KNO₃ ($T_m=335$ °C) 	HP <ul style="list-style-type: none"> • stainless steel-Therminol VP-1 ($L_e = 100$mm, $L_a = 60$ mm, $L_c = 140$mm, $d_o = 18$ mm, $t_{wall} = 1$ mm, $t_{wick} = 1$ mm) 	<ul style="list-style-type: none"> • melting / solidification • HP and tube ARE in contact with hot HTF (Therminol VP-1) • CSP applications 	A shell and tube is investigated with HPs embedded in the tube: <ul style="list-style-type: none"> • shell (PCM) and tube (HTF) • shell (HTF in cross flow) and tube (PCM) 	The energy stored/retrieved and effectiveness were presented for both modules and different HP arrangements. Configurations that lead to improved effectiveness and energy storage/retrieval rates per unit HP cost are identified.

Table 2.7. Numerical studies on LHTES systems utilizing heat pipes and reflux systems, cont.

Reference	Method	PCM properties (wt%)	Enhancement Properties	Operation mode and applications	Configuration	Conclusions
[112]	<ul style="list-style-type: none"> • 1D • FV • enthalpy method (conduction only) 	<ul style="list-style-type: none"> • Li_2CO_3 (35)- Na_2CO_3 (65) ($T_m=505$ °C) • Li_2CO_3 (32)- K_2CO_3 (35)- Na_2CO_3 (33) ($T_m=397$ °C) • K_2CO_3 (51) - Na_2CO_3 (49) ($T_m=710$ °C) 	HP <ul style="list-style-type: none"> • stainless steel-sodium ($L_e = 200\text{mm}$, $L_a = 42$ mm, $L_c = 800\text{mm}$, $d = 10$ mm, $t_{wick} = 1$ mm) 	<ul style="list-style-type: none"> • melting / solidification • HTF (NaNO_3- KNO_3 or KCL- MgCl_2) • CSP applications 	HPs extend through a rectangular PCM enclosure with HTF channels above and below PCM.	The cost and performance of a HP-enhanced PCM system and encapsulated PCM system were investigated. Optimum designs of the storage system were based on the minimum levelized cost of electricity, maximum exergetic efficiency, and maximum capacity factor are reported and compared with the results of two-tank molten salt storage systems. The cost should be less than \$4 per unit HP to meet SunShot Initiative 2020 requirements.

Table 2.8. Studies involving encapsulation of PCMs.

Reference	Method	PCM properties	Encapsulation properties	Operation mode and applications	Configuration	Conclusions
[113]	EXP	<ul style="list-style-type: none"> • water ($T_m = 0\text{ }^{\circ}\text{C}$, $m = 500\text{ kg}$) 	macro <ul style="list-style-type: none"> • polyolefin • sphere ($d_o = 77\text{ mm}$, $t = 2\text{ mm}$) 	<ul style="list-style-type: none"> • melting / solidification • HTF (aqueous glycol solution) • cold TES applications 	A vertical cylindrical tank is packed with spherical PCM capsules through which a HTF flows.	A significant degree of subcooling is observed. Increased solidification rates were observed for lower inlet coolant temperature and higher flow rate.
[114]	EXP	<ul style="list-style-type: none"> • shape stabilized paraffin (85)-styrene-butadiene-styrene (15) ($T_m = 27\text{ }^{\circ}\text{C}$) 	macro <ul style="list-style-type: none"> • concrete • cylinder ($d = 2.5\text{ cm}$, $l = 28\text{ cm}$) 	<ul style="list-style-type: none"> • melting / solidification • electric heater • building material applications 	A rectangular concrete slab had horizontal cylinders filled with PCM.	The PCM allows for a reduced rate in which the surface temperature increases. Also a thermal lag of about 3.7 hours to reach the maximum surface temperature is observed with the PCM relative without it.
[115]	EXP	<ul style="list-style-type: none"> • hydrated salt: HS 29 ($T_m = 28\text{-}30\text{ }^{\circ}\text{C}$) 	macro <ul style="list-style-type: none"> ($d = 75\text{ mm}$) 	<ul style="list-style-type: none"> • melting / solidification • TS heat exchanger • electronic cooling applications 	A tank contains a packed bed of spherical PCM capsules saturated with water are in contact with TSs that are not in direct contact with the capsules.	The total system capacity was 7462 kJ which operates passively by the thermal diode effect of TSs with the diurnal temperature variation thereby discharging energy at night.
[116]	EXP	<ul style="list-style-type: none"> • palmitic acid ($T_m = 66\text{ }^{\circ}\text{C}$) 	micro <ul style="list-style-type: none"> • ALOOH • sphere ($d = 200\text{ nm}$) 	<ul style="list-style-type: none"> • building material applications 	The thermal properties of a micro-encapsulated PCM were investigated using DSC.	T_m is reduced by more than $50\text{ }^{\circ}\text{C}$ from about $66\text{ }^{\circ}\text{C}$ to $14\text{ }^{\circ}\text{C}$ due to the strong interfacial interactions. The thermal storage capacity of the micro encapsulated material is approximately 20% of that of the pure PCM.
[117]	EXP	<ul style="list-style-type: none"> • RT 27 ($T_m = 25\text{-}28\text{ }^{\circ}\text{C}$) 	micro <ul style="list-style-type: none"> • arabic gum, gelatin, arag-agar ($d = 4\text{-}12\text{ }\mu\text{m}$) nano <ul style="list-style-type: none"> • arabic gum, arag-agar ($d = 104\text{ nm}$) 	-	Microcapsule production was investigated.	Two methods are utilized to obtain microcapsules of PCMs with two different shell materials with an encapsulation ratio of nearly 50%. Both shell materials and methods are recommended for use in TES systems.

Table 2.8. Studies involving encapsulation of PCMs, cont.

Reference	Method	PCM properties	Encapsulation properties	Operation mode and applications	Configuration	Conclusions
[118]	EXP	• paraffin ($T_m = 11-16$ °C)	micro ($d = 7.29$ μm)	• melting / solidification • HTF (air)	A rectangular high-density polyethylene/wood composite was embedded with PCM microcapsules. The composite is heated (cooled) with a convective oven (refrigerator).	The addition of microencapsulated PCMs was found to be thermally stable and the physical properties of the fiberboard were unaltered. By including graphite particles (38 μm and 8.8 wt%) into the fiberboard, the thermal conductivity was increased by 17.7%. A small fraction of micro-encapsulated particles had ruptured after successive cycling as observed by SEM photographs. Also subcooling was observed for about 6 °C below the melting temperature range.

Table 2.9. Numerical studies investigating the encapsulation of PCMs.

Reference	Method	PCM properties	Encapsulation properties	Operation mode and applications	Configuration	Conclusions
[65]	<ul style="list-style-type: none"> • 1D • FD • enthalpy method (conduction only) 	<ul style="list-style-type: none"> • paraffin wax ($T_m = 56-67\text{ }^{\circ}\text{C}$) 	macro <ul style="list-style-type: none"> • sphere ($d = 60-100\text{ mm}$) 	<ul style="list-style-type: none"> • melting • HTF (air) • solar air heating applications 	A vertical cylindrical tank is packed with spherical PCM capsules through which a HTF flows.	Increasing (decreasing) the HTF initial temperature and flow rate (diameter) decrease the overall charging time. The HTF inlet temperature has a greater influence than the mass flow rate. Increasing the thermal conductivity beyond 1 W/mK had a minimal effect as the major thermal resistance was between the spheres and the HTF for the conditions studied.
[119]	<ul style="list-style-type: none"> • 1D • FD • equivalent heat capacity method (conduction only) 	<ul style="list-style-type: none"> • organic HS-2 ($T_m = 8.5\text{ }^{\circ}\text{C}$) 	macro <ul style="list-style-type: none"> • sphere ($d = 74\text{ mm}$) 	<ul style="list-style-type: none"> • solidification • cold HTF (water) • air conditioning applications 	A vertical cylindrical tank is packed with spherical PCM capsules through which a HTF flows.	Increasing the HTF inlet mass flow rate or temperature increased the total storage capacity. However, the influence of the mass flow rate is not as appreciable as the HTF inlet temperature. Melting was 36% faster when the inlet temperature was increased from $12\text{ }^{\circ}\text{C}$ to $16\text{ }^{\circ}\text{C}$.
[120]	<ul style="list-style-type: none"> • 1D • FD • enthalpy method (conduction only) 	<ul style="list-style-type: none"> • $\text{CaCl}_2 \cdot 6\text{H}_2\text{O}$ ($T_m = 29.9\text{ }^{\circ}\text{C}$) • paraffin wax C18 ($T_m = 28.2\text{ }^{\circ}\text{C}$) 	macro <ul style="list-style-type: none"> • rectangular ($L = 20\text{ mm}$, $W = 10\text{ cm}$, $t = 2\text{ cm}$) 	<ul style="list-style-type: none"> • melting / solidification • HTF (air) 	A rectangular capsule was filled with PCM subject to forced convection with the HTF.	The paraffin wax mass takes approximately three times the melting time and provides 1.2 times the thermal storage capacity compared to a similar mass of $\text{CaCl}_2 \cdot 6\text{H}_2\text{O}$.
[121]	<ul style="list-style-type: none"> • 1D • FD • enthalpy method (conduction only) 	- (dimension-less)	macro <ul style="list-style-type: none"> • sphere ($d = 0.5-5\text{ mm}$) 	<ul style="list-style-type: none"> • melting / solidification • HTF (solar salt) • CSP applications 	A vertical cylindrical tank is packed with spherical PCM capsules through which a HTF flows.	Decreasing the capsule radii by approximately 80% increases the total utilization by 45% and latent utilization by ~50% with $Re_h = 50000$. A parametric study on maximizing the total energy and latent utilizations was performed.
[122]	<ul style="list-style-type: none"> • 1D • FV • enthalpy method (conduction only) 	<ul style="list-style-type: none"> • organic PCM ($T_m = 3-7\text{ }^{\circ}\text{C}$) 	macro <ul style="list-style-type: none"> • sphere ($d = 3.6\text{ mm}$) 	<ul style="list-style-type: none"> • melting / solidification • HTF (water) • industrial and domestic TES applications 	A vertical cylindrical tank is packed with spherical PCM capsules through which a HTF flows.	Three different Nusselt correlations found in the literature were analyzed and compared. For a low HTF flow rate, natural convection becomes important and the Brinkman equation may be useful in mathematical modeling.

Table 2.9. Numerical studies investigating the encapsulation of PCMs, cont.

Reference	Method	PCM properties	Encapsulation properties	Operation mode and applications	Configuration	Conclusions
[123]	<ul style="list-style-type: none"> • FLUENT • 2D • FV • enthalpy-porosity and front-tracking methods (including natural convection) 	<ul style="list-style-type: none"> • NaNO₃ ($T_m = 307\text{ °C}$) 	macro <ul style="list-style-type: none"> • stainless steel • cylinder ($d=76.2\text{ mm}$, $l=508\text{ mm}$) 	<ul style="list-style-type: none"> • melting • HTF (air or Therminol VP-1) • CSP applications 	A cylindrical shell is filled with PCM and is subject to HTF flow in two arrangements: cross flow and axially flow.	The solid-liquid interface dynamics, temperature distribution and the time of energy storage and retrieval predicted by the front-tracking method agrees well with enthalpy-porosity method. The heat transfer process inside the capsule is affected by the capsule size and HTF.
[112]	<ul style="list-style-type: none"> • 1D • FV • enthalpy method (conduction only) 	<ul style="list-style-type: none"> • Li₂CO₃(35)-Na₂CO₃ (65)- ($T_m=505\text{ °C}$) • Li₂CO₃(32)-K₂CO₃(35)-Na₂CO₃(33) ($T_m=397\text{ °C}$) • K₂CO₃(51)-Na₂CO₃(49) ($T_m=710\text{ °C}$) 	macro <ul style="list-style-type: none"> • sphere ($d=10\text{-}160\text{ mm}$) 	<ul style="list-style-type: none"> • melting / solidification • HTF (NaNO₃-KNO₃ or KCL-MgCl₂) • CSP applications 	A vertical cylindrical tank is packed with spherical PCM capsules through which a HTF flows.	A HP-enhanced PCM system with a packed bed of PCM filled capsules was optimized based on the minimum levelized cost of electricity, maximum exergetic efficiency, and maximum capacity factor are reported and compared to that of a two-tank molten salt storage system. Smaller capsule sized reduce cost, have higher exergetic efficiency and lowest levelized cost of electricity.
[124]	<ul style="list-style-type: none"> • 1D • finite difference (FD) • enthalpy method 	<ul style="list-style-type: none"> • NaNO₂ • (solid-solid transition temperature is 277.32 °C, $T_m = 304\text{ °C}$) 	macro <ul style="list-style-type: none"> • sphere ($d=5\text{-}45\text{ mm}$) 	<ul style="list-style-type: none"> • melting • HTF (molten salt mixture: NaNO₃ and KNO₃) • high temperature TES applications 	A vertical cylindrical tank is packed with spherical PCM capsules through which a HTF flows.	A numeric-dispersion model for a packed bed system can successfully predict the system performance for a packed bed system. Increasing the inlet velocity by 27 times reduces the phase change time by 41%.
[125]	<ul style="list-style-type: none"> • 2D • FV • TTM • conduction model with an effective thermal conductivity to include natural convection 	<ul style="list-style-type: none"> ($T_m = 330\text{ °C}$) 	macro <ul style="list-style-type: none"> • stainless steel • sphere ($d = 40\text{ mm}$) 	<ul style="list-style-type: none"> • solidification • HTF (molten salt: mixture NaNO₃ (60) and KNO₃ (40)) • CSP applications 	A vertical cylindrical tank is packed with spherical PCM capsules through which a HTF flows.	A packed bed thermocline can save 35% of the capital cost compared to the two-tank system. The discharging efficiency can be increased from 36% to 97% by increasing the phase change temperature from 330 °C to 380 °C , respectively. The efficiency decreases from 98 % to 73% by increasing the HTF inlet velocity from $5.55 \times 10^{-5}\text{ m/s}$ to $1.295 \times 10^{-2}\text{ m/s}$, respectively. Increasing the capsule diameter from 0.02 m to 0.1 m decreases the efficiency from 98% to 73.78%, respectively.

Table 2.9. Numerical studies investigating the encapsulation of PCMs, cont.

Reference	Method	PCM properties	Encapsulation properties	Operation mode and applications	Configuration	Conclusions
[126]	<ul style="list-style-type: none"> • 1D • equivalent heat capacity method • conduction only 	<ul style="list-style-type: none"> • KCl-KBr-KNO₃ • NaCl-KCl-LiCl (dimension-less) 	<ul style="list-style-type: none"> • macro • sphere (dimension-less) 	<ul style="list-style-type: none"> • melting • HTF (air) • high temperature TES applications 	A vertical cylindrical tank is packed with spherical PCM capsules through which a HTF flows.	The effect of pressure drop on fractional exergy destruction is about 2-6%. The analysis reveals that under identical conditions, a sensible heat packed bed has a higher exergy recovery relative to one including PCM capsules.
[127]	<ul style="list-style-type: none"> • 1D • FD 	<ul style="list-style-type: none"> • RT27 ($T_m = 28\text{ }^{\circ}\text{C}$) 	<ul style="list-style-type: none"> • micro • sphere ($d = 30\text{-}500\text{ }\mu\text{m}$) 	<ul style="list-style-type: none"> • solidification • constant wall temperature • solar heating applications 	A single sphere is filled with PCM and subject to a constant wall temperature.	The particle size has a significant effect on the solidification time even with small Stefan numbers.

Table 2.10. Recent studies involving cascaded PCM systems.

Reference	Method	PCMs (wt%)	Operation mode and applications	Configuration	Conclusions
[128]	NUM • analytical finite-time thermodynamics	two hypothetical PCMs: • $527\text{ }^{\circ}\text{C} < T_m < 1227\text{ }^{\circ}\text{C}$ • $127\text{ }^{\circ}\text{C} < T_m < 727\text{ }^{\circ}\text{C}$	• melting / solidification • HTF (air) • CSP applications	A HTF collects thermal energy from a solar receiver which then flows through two PCM containers.	Using two PCMs instead of a single PCM can increase the overall exergetic efficiency by up to 53.8%.
[129]	NUM • FLUENT • 2D • FV • enthalpy method	• $\text{K}_2\text{CO}_3(51)\text{-Na}_2\text{CO}_3(49)$ ($T_m = 710\text{ }^{\circ}\text{C}$) • $\text{Li}_2\text{CO}_3(20)\text{-Na}_2\text{CO}_3(60)\text{-K}_2\text{CO}_3(20)$ ($T_m = 550\text{ }^{\circ}\text{C}$) • $\text{Li}_2\text{CO}_3(32)\text{-K}_2\text{CO}_3(35)\text{-Na}_2\text{CO}_3(33)$ ($T_m = 397\text{ }^{\circ}\text{C}$)	• melting • HTF (air) • CSP applications	A horizontal shell (PCM) and tube (HTF) heat exchanger contains three PCM sections along the HTF flow.	The melting times for each PCM section decreases with increasing the air inlet temperatures. The optimal length for each PCM segment should be determined in such a way that the total melting time for each PCM is similar. However, no comparison is made with a single-PCM configuration.
[130]	NUM • COMSOL • 2D • FE • effective heat capacity method	paraffin mixtures: • ($T_m = 7\text{ }^{\circ}\text{C}$) • ($T_m = 9\text{ }^{\circ}\text{C}$) • ($T_m = 11\text{ }^{\circ}\text{C}$)	• melting / solidification, simultaneous • cold TES applications	A vertical finned tube with three PCM segments. The PCMs with the highest T_m and lowest T_m are at the top and bottom of the TES module, respectively.	The heat transfer rates of a cascaded LHTES may be improved by 10% to 40% compared to a single-PCM system during complete melting and solidification domains. At the midway point during melting and solidification, the cascaded LHTES does not show a significant improvement in the performance relative to the single-PCM TES.
[71]	EXP	• KNO_3 ($T_m = 335\text{ }^{\circ}\text{C}$) • $\text{KNO}_3(95.5)\text{-KCl}(4.5)$ ($T_m = 320\text{ }^{\circ}\text{C}$) • NaNO_3 ($T_m = 306\text{ }^{\circ}\text{C}$) • $\text{MgCl}_2(60)\text{-KCl}(20.4)\text{-NaCl}(19.6)$ ($T_m = 380\text{ }^{\circ}\text{C}$)	• melting / solidification • HTF (oil) • solar power applications	A vertical shell (PCM) and tube (HTF) heat exchanger is separated into three PCM sections.	A cascaded LHTES can utilize a higher percentage of its storage capacity (57.2%) relative to a non-cascaded system (44.9-53.4%).

Table 2.11. LHTES systems utilizing combined enhancement techniques.

Reference	Method	PCM properties	Enhancement properties	Operation mode and applications	Configuration	Conclusions
[74]	EXP NUM • 2D • FV • TTM	• n-octadecane ($T_m = 28\text{ }^{\circ}\text{C}$, $m = 72\text{-}90\text{ g}$)	HP • copper-water ($L=175\text{ mm}$, $L_{pcm}=72\text{-}90\text{ mm}$, $d_o=6\text{mm}$) foils • aluminum • radial ($d_o=39\text{mm}$, $t = 17\text{ }\mu\text{m}$) • $\phi = 0.987$	• melting / solidification • heat transfer driven by a HTF (water) in contact with a HP	A vertical cylindrical enclosure is filled with PCM and contains a concentrically- located HP or rod. The HP has horizontal radial foils installed.	The melting and solidification rates could be increased with the combined HP and foils (ϕ $=0.987$) by 3 and 9 times that of a similarly dimensioned rod-enhanced system. The system performance was reported to increase as the ratio of the HP embedded in the PCM increased.
[75]	EXP	• n-octadecane ($T_m = 28\text{ }^{\circ}\text{C}$, $m = 80\text{ g}$)	HP • copper-water ($L=175\text{mm}$, $L_{pcm} = 82\text{mm}$, $d_o=6\text{mm}$) foils • aluminum • radial ($d_o=39\text{mm}$, $t=17\text{-}24\text{ }\mu\text{m}$) • $\phi = 0.957\text{-}0.987$ foam • aluminum • annular ($d_o = 39\text{ mm}$) • $\phi = 0.870\text{-}0.957$ • $\omega=5\text{-}40\text{ PPI}$	• melting / solidification • heat transfer driven by a HTF (water) in contact with a HP	A vertical cylindrical enclosure is filled with PCM and contains a concentrically- located HP or rod. The HP has horizontal radial foils installed.	Melting and solidification rates were increased by about 15 and 7 times that of a rod-enhanced system. The melting and solidification times were reduced from 200 (152) min to as low as 13 (11) min during melting and solidification for a combined HP and foil case with $\phi = 0.957$. The combined enhancement was able to increase the melting rates by a factor of 10 relative to the HP- enhanced PCM configuration.
[76]	EXP	• n-octadecane ($T_m = 28\text{ }^{\circ}\text{C}$, $m = 60\text{ g}$)	HP • copper-water ($L = 175\text{mm}$, $L_{pcm} = 60\text{mm}$, $d_o = 6\text{mm}$) foils • aluminum • radial ($d_o= 39\text{ mm}$, $t= 24\text{ }\mu\text{m}$) • $\phi = 0.948$ foam • aluminum • annular ($d_o = 39\text{mm}$) • $\phi = 0.948$ • $\omega = 20\text{ PPI}$	• melting / solidification • heat transfer driven by a HTF (water) in contact with a HP and copper base	A cylindrical enclosure is filled with PCM and contains a concentrically- located HP or rod. The HP has radial foils installed. The effect of system inclination angle is investigated.	The complete melting and solidification times were reduced from about 150 min and 400 min to as low as 16 min and 13 min with $\phi = 0.948$. The effect of system inclination angle was found to have minimal impact on the system performance for the combined HP and foil and the combined HP and foam configurations relative to the others studied. The melting rate for the combined HP and foam case increased by a factor of approximately 9 compared to that of a non- enhanced PCM system.

Table 2.11. LHTES systems utilizing combined enhancement techniques, cont.

Reference	Method	PCM properties	Enhancement properties	Operation mode and applications	Configuration	Conclusions
[131]	EXP	• n-eicosane ($T_m \approx 37$ °C)	micro-encapsulation ($d = 3\text{-}20\mu\text{m}$) EG • $\phi = 0.80\text{-}0.95$ • 0-20 wt%	Mechanical and thermophysical property measurement	Micro-encapsulated PCM and EG were embedded in a high density polyethylene matrix.	The thermal conductivity of the composites with 20 wt% EG loaded could be enhanced by 22 times compared to polyethylene matrix-MPCM composites without EG. Thermal conductivity of the composite could be increased by 10 times at a loading of 10 wt% EG.
[132]	EXP	• n-eicosane ($T_m \approx 37$ °C)	Fins • brass • flat ($t = 0.8$ mm) foam • copper • $\phi = 0.96$	• melting • electric heater • electronic cooling applications	Rectangular enclosure contains vertical fins and foam which is heated from below.	A fin is used to increase the thermal penetration and then dispersed through the foam. The inclusion of the foam more than doubles the thermal conductivity relative to the fins alone. The most uniform temperature distribution is observed with both the fins and foam.
[133]	EXP NUM • COMSOL • 2D	• water ($T_m = 0$ °C)	macro-encapsulation • polyolefin • sphere ($d = 98$ mm) graphite flakes or EG	• solidification • HTF (aqueous glycol solution) • building cooling, solar water heating applications	Single spherical PCM capsule cooled by a variable temperature bath.	The storage and discharge durations were reduced by up to 35% and 58%, respectively, with 13 wt% of EG. It was determined that the EG had slightly improved performance relative to graphite flakes but were not as easy to implement and may be more costly.
[134]	NUM • 1D • enthalpy method	• ($T_m = 61$ °C) • ($T_m = 51$ °C) • ($T_m = 43$ °C)	macro-encapsulation • polycarbonate • sphere ($d = 55$ mm) cascaded	• melting • HTF (water) • solar collector applications	A vertical cylindrical tank containing PCM filled spheres with a flowing HTF.	The cascaded configuration had a shorter melting time, higher energy transfer efficiency and lower exergy transfer efficiencies during melting compared to a single PCM system. However, once complete melting occurred, a higher exergy transfer efficiency is observed.
[135]	EXP	• paraffin ($T_m = 57\text{-}61$ °C)	EG • 6.7 wt% HP ($L = 150\text{mm}$, $d_o = 6\text{mm}$)	• melting / solidification • electric heater • electronic cooling applications	A rectangular EG-PCM composite is in contact with a HP's condenser section and a finned heat sink.	The thermal conductivity of the EG-PCM composite was about 4.7 W/mK. The times for melting and solidification were reduced by 63% and 26%, respectively, with EG. The overall heat transfer coefficient for the heat sink with the EG-PCM composite was increased by up to a factor of 3 relative to without it.

Table 2.11. LHTES systems utilizing combined enhancement techniques, cont.

Reference	Method	PCM properties	Enhancement properties	Operation mode and applications	Configuration	Conclusions
[136]	EXP NUM • FLUENT • 3D • enthalpy method	• formic acid ($T_m = 7\text{ }^{\circ}\text{C}$)	macro-encapsulation • high density polythene • cylinder ($d = 40\text{ mm}$, $h = 150\text{ mm}$) • sphere ($d = 70\text{ mm}$) pins • copper • axial ($t = 1\text{ mm}$)	• melting / solidification • HTF (aqueous glycol solution) • building cooling applications	The cylindrical (sphere) capsule contains axial (vertical) fins and is filled with PCM and heated by a HTF bath with a controlled temperature.	A cylinder has 38% more surface area than a sphere and solidified in approximately 53 % of the time for the latter. The melting and solidification time for the cylinder could be further reduced by up to 72% and 51%, respectively, with internal fins.
[137]	EXP	• d-sorbitol ($T_m \approx 95\text{ }^{\circ}\text{C}$, $m = 19\text{ kg}$) • paraffin ($T_m \approx 37\text{ }^{\circ}\text{C}$, $m = 15\text{ kg}$)	macro-encapsulation • cylindrical ($d = 80\text{ mm}$, $h = 100\text{ mm}$) cascaded	• melting • HTF (castor oil) • exhaust gas waste heat recovery applications	Two cylindrical tanks contain cylindrical PCM capsules in which the HTF flows.	The cascaded (single PCM) storage system recovered about 20% (15%) of the thermal energy of the exhaust gas. However, the overall PCM mass was significantly less for the single PCM than the cascaded system which does not provide an ideal comparison.
[138]	NUM • 2D • FV • TTM (conduction only)	• NaCl ($T_m = 800\text{ }^{\circ}\text{C}$)	HP • stainless steel-sodium ($L_{pcm} = 1000\text{ mm}$, $d_o = 20\text{ mm}$, $t_{wall} = 2\text{ mm}$, $t_{wick} = 2\text{ mm}$) pins • nickel • radial ($t = 0.15\text{ mm}$) • $\phi = 0.93$	• melting / solidification, simultaneous • hot HP in contact with radiation source / cold HP in contact with Stirling engine • TES for solar dish-Stirling systems	The PCM is contained in between two vertical sets of HPs (for charging and discharging). Radial fins in contact with both sets of HPs are embedded in the PCM.	The system with the greatest (smallest) heat pipe spacing was found to have the greatest (smallest) temperature drops across the LHTES, as well as the maximum (minimum) amount of PCM melting and solidification. The exergy efficiency for all cases was greater than 97%, with the maximum exergy efficiency associated with the system having the minimum HP spacing.
[72]	NUM • 1D • thermal network (including natural convection)	($m \approx 70,000\text{ kg}$) • NaOH (73.3) - NaCl (26.7) ($T_m = 370\text{ }^{\circ}\text{C}$) • KCl (22.9) - MnCl_2 (60.6) - NaCl (16.5) ($T_m = 350\text{ }^{\circ}\text{C}$) • NaOH (65.2) - NaCl (20) - Na_2CO_3 (14.8) ($T_m = 318\text{ }^{\circ}\text{C}$)	TS • stainless steel-biphenyl ($L = 1000\text{ mm}$, $d_o = 20\text{ mm}$, $t_{wall} = 2\text{ mm}$) Cascaded	• melting / solidification • TS is in contact with HTF (Therminol VP-1) and PCM • CSP applications	TSs extend through a rectangular PCM enclosure with HTF channels above and below PCM.	LHTES with the lowest melting temperature PCM yields the highest exergy efficiency. However, a cascaded LHTES recovers the largest amount of exergy during a 24 h charging / discharging cycle. The cascaded LHTES recovers about 10% more exergy during a 24 h charging / discharging cycle compared to the best non-cascaded LHTES considered in this work.

Table 2.11. LHTES systems utilizing combined enhancement techniques, cont.

Reference	Method	PCM properties	Enhancement properties	Operation mode and applications	Configuration	Conclusions
[139]	NUM • 2D • enthalpy method	single-PCM • RT55 ($T_m = 55$ °C) cascaded • RT31 ($T_m = 31$ °C) • RT50 ($T_m = 31$ °C) • RT82 ($T_m = 31$ °C)	foam • copper • $\phi = 0.85$ -0.95 • $\omega = 10$ -30 PPI cascaded	• melting • HTF (water) • solar applications	A rectangular enclosure is filled with foam embedded in PCM and is contained between two HTF channels.	Heat exchange and exergy rates of a single-PCM LHTES is improved by a cascaded LHTES system up to 30% and 23%, respectively, and is further improved by adding metal foam by 2-7 times. The exergy efficiency of a single-PCM LHTES cannot be significantly improved by cascaded LHTES, nor by metal foam cascaded LHTES.
[140]	NUM • 1D • FV	Eight sets of three hypothetical PCMs • 300 °C < T_m < 600 °C	macro-encapsulation • sphere ($d = 10$ mm) cascaded	• melting / solidification • HTF (NaNO_3 (60)- KNO_3 (40)) • CSP applications	A thermocline tank is filled with a packed bed of spherical PCM capsules over which the HTF flows. The PCM capsules are cascaded with three sections.	Thermocline tanks filled with a single PCM show a similar performance to rock-filled tank of equal size in terms of the annual storage or plant output. A three-stage cascade structure of the bed potentially yields a 9.7% increase in the annual power output and a 16% decrease in the thermocline tank diameter relative to a rock-filled tank, provided that the melting temperatures of PCMs are tuned precisely.

Table 2.12. Advantages, disadvantages, challenges and unresolved issues for each enhancement technique.

Enhancement method	Advantages	Disadvantages/challenges	Unresolved issues
Fins	<ul style="list-style-type: none"> • Increase thermal penetration depth • Well established methodology for experiments and modeling • Well established manufacturing techniques • Available from a wide variety of materials 	<ul style="list-style-type: none"> • Requires attachment method on HTS (e.g. welding, thermal adhesive) • Cost of machining • Thermal contact resistances may exist • May suppress natural convection • Performance decreases as the length of the fins increase 	<ul style="list-style-type: none"> • Possible deformation or cracks during PCM expansion or contraction especially in high temperature applications in which the metal itself expands • May be difficult to find suitable materials for high temperature environments • Optimization is needed to find a suitable compromise between the fin thickness, heat transfer rates, and overall energy storage capacity
Foils	<ul style="list-style-type: none"> • Increase heat diffusion • Large increases in heat transfer rates with small foil volume fractions (~ 1%) • Direct 2D heat transfer pathway • Well established methodology for experiments and modeling • High surface area density • Low costs for materials and manufacturing • Low cost for installment on tubular surfaces using a press-fit method • Flexible (eliminates stress issues arising from PCM expansion or contraction) 	<ul style="list-style-type: none"> • Thermal contact resistances may exist • May be difficult to install on non-tubular surfaces • May significantly suppress natural convection • Structural strength may limit its practical length • Performance decreases as the foil length increases • Corrosion may be an issue due to the small thickness of foils 	<ul style="list-style-type: none"> • Optimal foil shapes and long term structural and thermal stability are yet to be investigated • May be difficult to find suitable materials for high temperature environments
Nanoparticles	<ul style="list-style-type: none"> • Increase heat diffusion • Implementation is unproblematic and does not add complexity to the system • Nanoparticles act as nucleating agents during solidification which may reduce subcooling • High surface area density 	<ul style="list-style-type: none"> • Agglomeration and sedimentation of particles may occur after time • Relatively high thermal resistance between particles and HTSs • May significantly suppress natural convection due to an undesired increase in viscosity of the particle-PCM composite • May decrease the overall storage capacity per volume by decreasing the effective latent and specific heats of the particle-PCM composite 	<ul style="list-style-type: none"> • Performance of the nanoparticle dispersion in high temperature PCMs has not been addressed in the literature • More research is required to identify the effect of nanoparticle addition on the PCM properties such as melting temperature, viscosity, and latent heat of fusion • The appropriate combination of particle thermal conductivity and mass fraction must be investigated

Table 2.12. Advantages, disadvantages, challenges and unresolved issues for each enhancement technique, cont.

Enhancement method	Advantages	Disadvantages/challenges	Unresolved issues
Structures	<ul style="list-style-type: none"> • Increase heat diffusion • High surface area density • May be manufactured for unique geometries 	<ul style="list-style-type: none"> • May significantly suppress natural convection • May be difficult to attach to HTSs which may subsequently present thermal contact resistances • Air entrapment may occur for smaller pore sizes • Relatively expensive to fabricate • Limited material selection • Performance decreases with distance from the HTS • The tortuous morphology of most structures results in 3D heat transfer which may be less effective than foils 	<ul style="list-style-type: none"> • The preferred methods to attach certain structures to a HTS, such as EG, remain to be determined
Heat pipes/ Thermosyphons	<ul style="list-style-type: none"> • Increase thermal penetration depth more than any other method since HPs/TSs may have much higher thermal conductivities than solid materials • Large amounts of heat can be transferred through a small cross sectional area over great distances • Variety of shapes available • Variety of operational conditions • High reliability / lifetime / durability • Failure of an individual HP/TS has little impact on overall system with many HPs/TSs • Unlike fins / foils, performance does not significantly deteriorate by increasing length • HPs can effectively operate regardless of orientation • The thermal diode feature of TSs may be advantageous for one-directional heat transfer 	<ul style="list-style-type: none"> • May be difficult to attach a HP/TS to a HTS • Thermal contact resistances may exist • Material compatibility issues between HP wall, wick and working fluid, as well as PCM, PCM enclosure and HTF • More than one set of TSs is required to perform both melting and solidification requiring two HTF channels • HPs/TSs may fail and require replacement • TSs require two separate HTF channels • Performance limitations for HPs/TSs also apply in PCM systems involving HPs/TSs • Frozen startup, referring to an initially solid HP/TS working fluid, may cause some problems during the onset of operation with an initially cold HP/TS 	<ul style="list-style-type: none"> • The utilization of a thermal network model for a HP-enhanced PCM system requires the effect of vapor pressure to be considered for a more comprehensive analysis • Suitable HP/TS working fluids for intermediate temperature applications in the range of 200 °C to 400 °C remain to be adequately identified • Since welding of HPs/TSs is challenging due to the superior heat dissipation of HPs/TSs, alternative technologies for assembling HP/TS-enhanced LHTES systems must be developed

Table 2.12. Advantages, disadvantages, challenges and unresolved issues for each enhancement technique, cont.

Enhancement method	Advantages	Disadvantages/challenges	Unresolved issues
Encapsulation	<ul style="list-style-type: none"> • Increase thermal penetration depth in a packed bed system • High surface area density • High thermal penetration into packed bed • Variety of sizes and shapes from a few micrometers to a few centimeters • Variety of materials may be utilized for shell material • Minimizes problem of PCM expansion and contraction 	<ul style="list-style-type: none"> • Chemical compatibility must exist between PCM, capsule shell and any other secondary medium • If the PCM thermal resistance is large, encapsulation may not significantly increase heat transfer rates <p>Macro-encapsulation</p> <ul style="list-style-type: none"> • Possibility of leaks • High HTF pressure drop • Driving temperature decreases with HTF flow direction • Relatively lower porosities require the greatest overall system volumes for the same thermal storage capacity <p>Micro- or nano-encapsulation</p> <ul style="list-style-type: none"> • May deteriorate structural properties of the substrate material • Subcooling may present itself in the PCM 	<ul style="list-style-type: none"> • Erosion of the thin walls in micro-encapsulated PCMs would reduce the lifetime of the PCM system • Manufacturing of micro- and nano-encapsulated PCMs may be difficult, particularly for controlling the internal void fraction and PCM mass • Thermal stresses exist in the tank wall and capsule shell due to thermal gradients and phase change
Cascaded	<ul style="list-style-type: none"> • Provide nearly constant heat flux along HTF flow direction • Reduce the outlet HTF temperature fluctuations • A larger amount of PCM may undergo phase change relative to a non-cascaded PCM system resulting in a higher overall utilization of energy 	<ul style="list-style-type: none"> • Accurate numerical simulation is required to identify the optimal cascaded configuration • Actual conditions may differ from design conditions limiting the actual increase in performance • Determination of practical PCMs to match the design conditions • The increase in performance must offset additional costs related to PCM partitions and the higher probability of leaks 	<ul style="list-style-type: none"> • There are contradicting results related to the effect of cascaded configurations on the exergy efficiency and heat transfer rates • The operating and design parameters causing the different energy and exergy performances need to be identified

Table 2.12. Advantages, disadvantages, challenges and unresolved issues for each enhancement technique, cont.

Enhancement method	Advantages	Disadvantages/challenges	Unresolved issues
Combined enhancement	<ul style="list-style-type: none"> • May increase both thermal penetration and thermal diffusion • Overall performance may be significantly increased relative to a single enhancement technique • Variety of combinations are possible using the aforementioned techniques 	<ul style="list-style-type: none"> • The overall cost increases as additional enhancement techniques are included • The addition of multiple enhancement techniques that are made from different materials may increase the concerns regarding material compatibilities due to a greater number of interfaces • The optimization of systems involving combined enhancement techniques is more difficult than for a single enhancement technique 	<ul style="list-style-type: none"> • The long term structural and thermal properties are yet to be determined for combined enhancement techniques

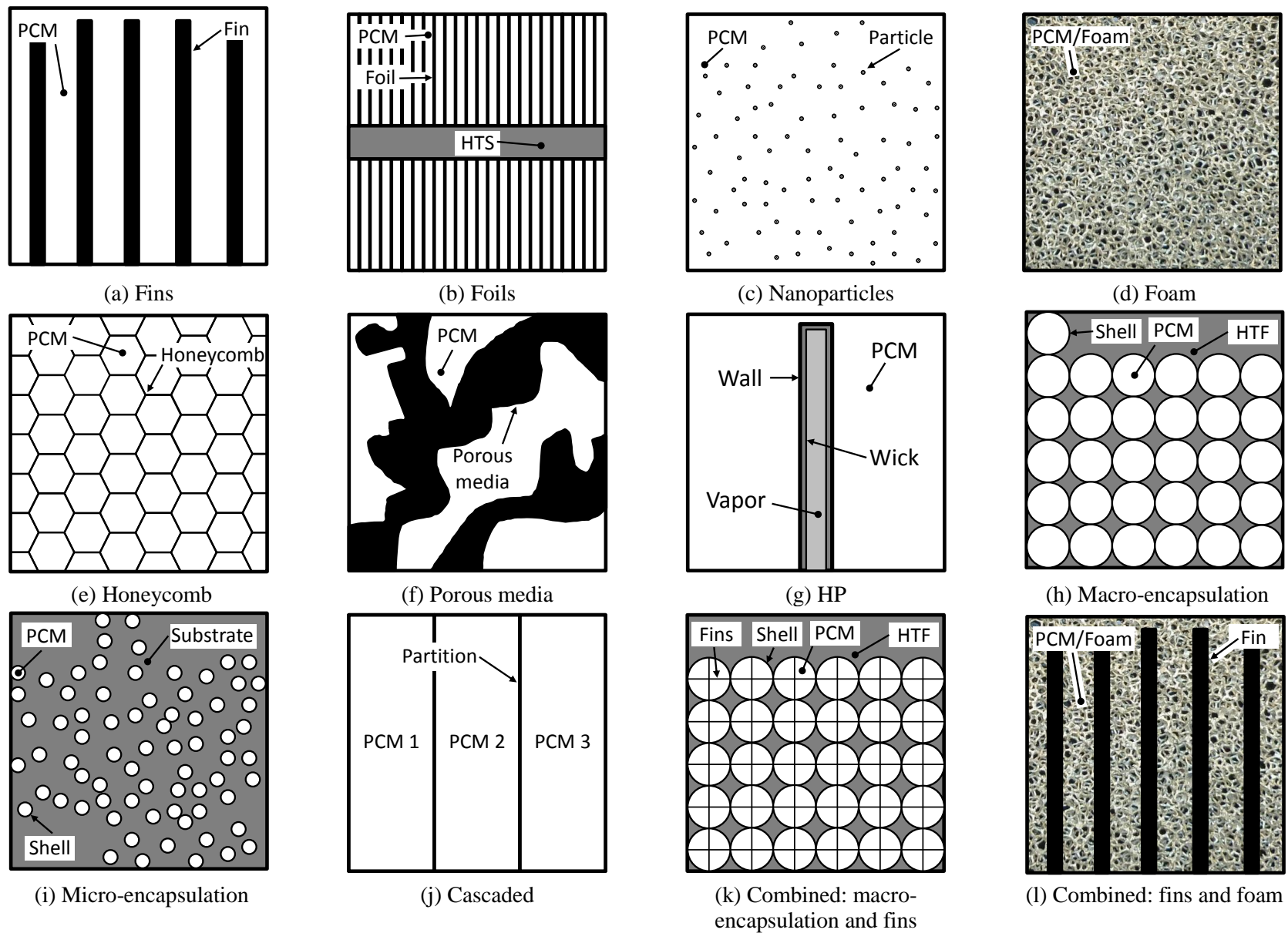


Fig. 2.1. Various heat transfer enhancement techniques implemented in PCM systems.

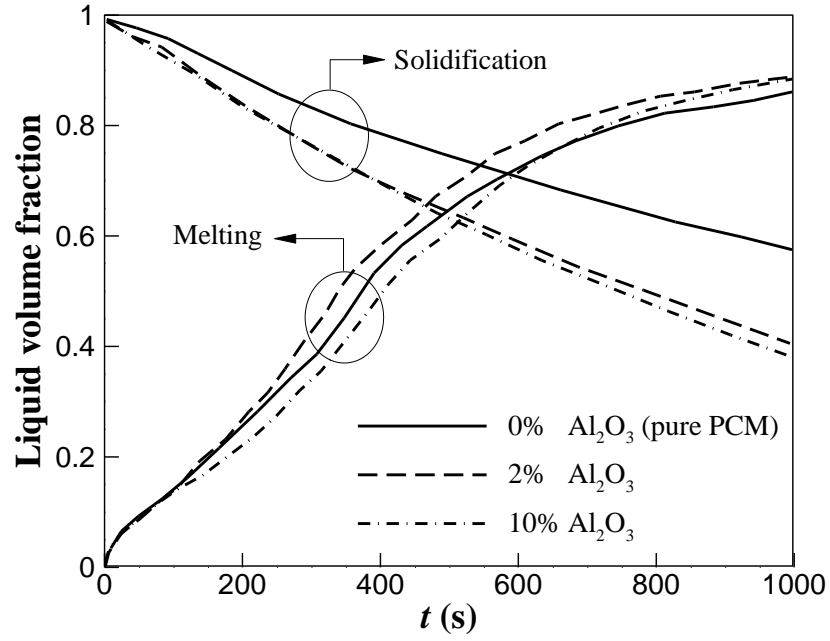


Fig. 2.2. Effect of nanoparticle concentration on the melting and solidification of a PCM (adopted from [54]).

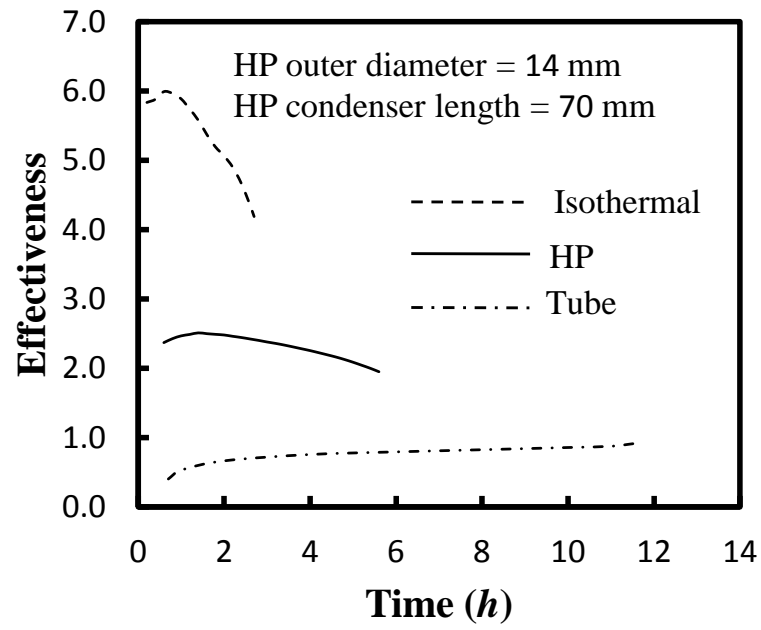


Fig. 2.3. Effectiveness histories for isothermal, HP and tube cases (adopted from [37]).

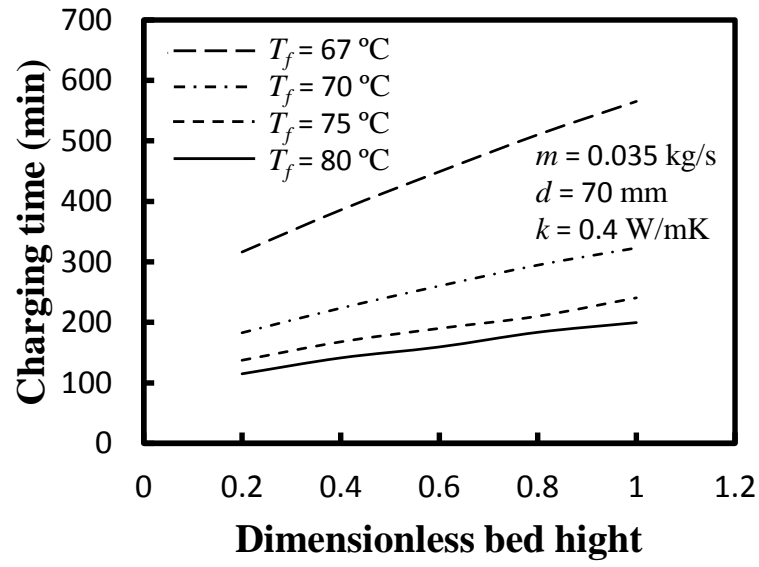


Fig. 2.4. Effect of the HTF inlet temperature on charging time (adopted from [65]).

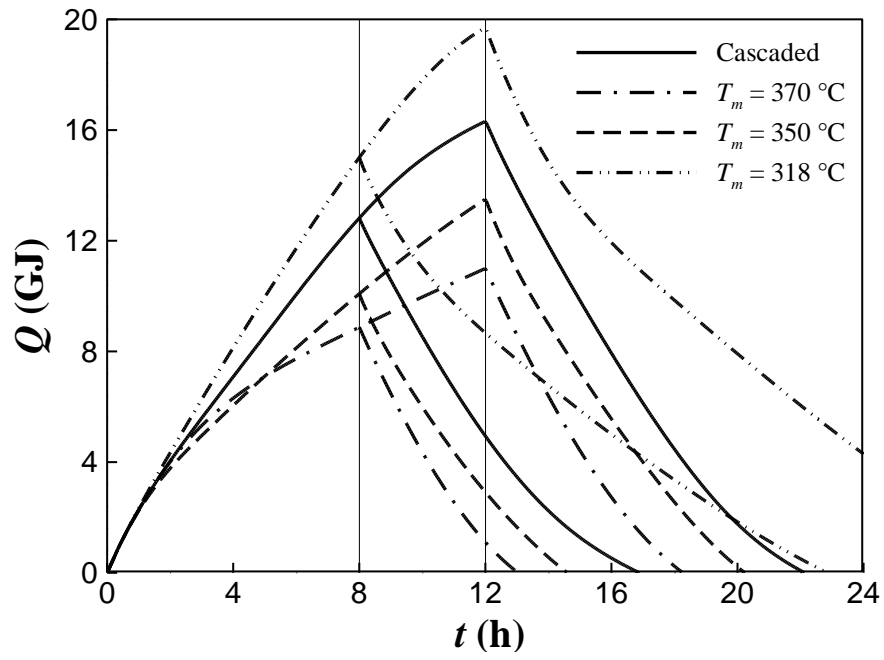
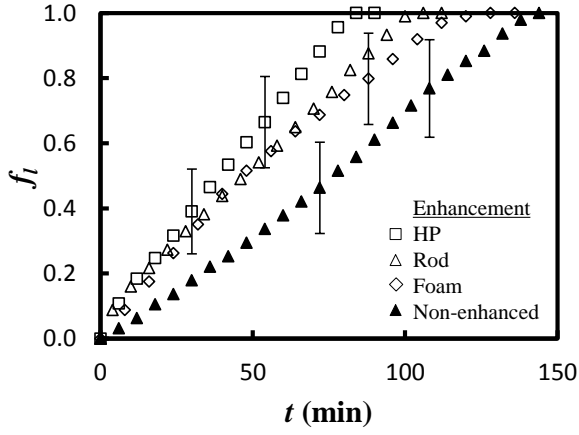
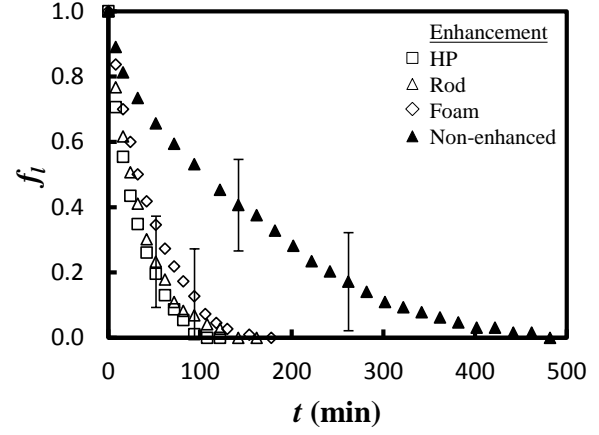


Fig. 2.5. Energy storage and recovery during charging–discharging cycles with charging periods of 8 and 12 h (adopted from [72]).

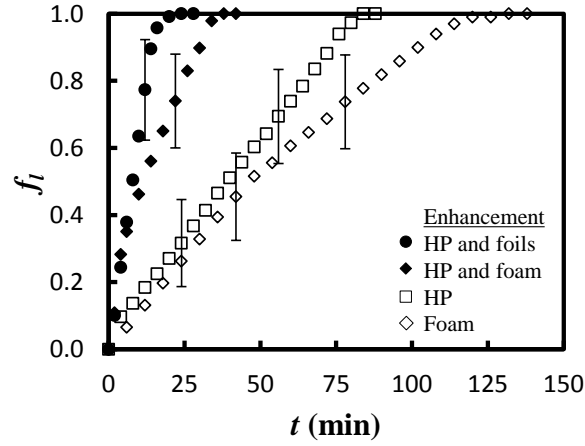


(a) melting

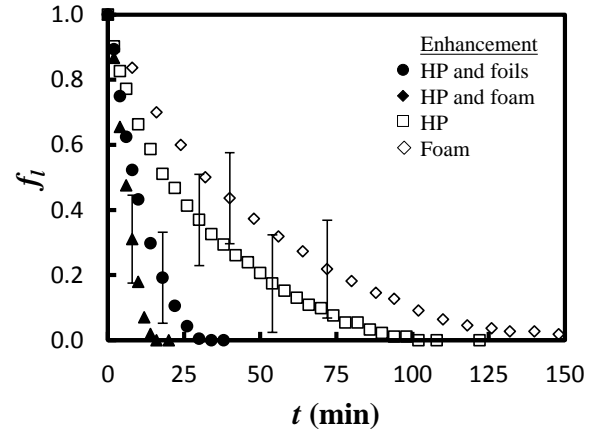


(b) solidification

Fig. 2.6. Comparison between enhancement techniques for a vertical cylindrical PCM system ($d = 41$ mm, $h = 60$ mm) with heat transfer through the base using a HP (copper-water, $d = 6$ mm), rod (solid-copper, $d = 6$ mm) and aluminum foam ($\phi = 0.95$, $\omega = 20$ PPI) during (a) melting and (b) solidification (adopted from [76]).



(a) melting



(b) solidification

Fig. 2.7. Comparison of enhancement techniques in a vertical cylindrical PCM system ($d = 41$ mm, $h = 60$ mm) with heat transfer through the base using a HP (copper-water, $d = 6$ mm) alone or combined with aluminum foils ($\phi = 0.95$, $t = 24$ μm) or foam ($\phi = 0.95$, $\omega = 20$ PPI) during (a) melting and (b) solidification (adopted from [76]).

Chapter 3. Robust Heat Transfer Enhancement during Melting and Solidification of a PCM using a Combined Heat Pipe-Metal Foam or Foil Configuration

Experiments are performed to analyze melting and solidification of a phase change material (PCM) enclosed in a vertical cylinder by a concentrically-located heat pipe (HP) surrounded by either aluminum foam or foils. The liquid fraction, temperature distribution, melting (solidification) rates and effectiveness are reported to quantify the improvement in performance relative to a base case, a Rod-PCM configuration. Parameters of interest include the porosity of the PCM-metal composite, the foil thickness, the number of foils and the foam pore density. The main contributor to enhanced performance is shown to be the porosity for both the HP-Foil-PCM and HP-Foam-PCM configurations. Both of these configurations improve heat transfer rates relative to either the HP-PCM or the Rod-PCM configuration. However, the HP-Foil-PCM configuration is shown to have approximately the same performance as the HP-Foam-PCM configuration with one third of the metal mass, for the range of porosities studied here (0.870 to 0.987). The HP-Foil-PCM configuration, with a porosity of 0.957 using 162 foils of thickness 0.024 mm, attained an overall rate of phase change that is about 15 times greater than that of the Rod-PCM configuration and about 10 times greater than that of the HP-PCM configuration. The greatest degree of enhancement was achieved with the HP-Foil-PCM configuration (with porosity 0.957) yielding an average effectiveness during melting (solidification) of 14.7 (8.4), which is an extraordinary improvement over the base case.

3.1. Introduction

Latent heat thermal energy storage (LHTES), utilizing phase change materials (PCMs), is characterized by high energy density, relatively small storage volume, and nearly isothermal operation compared to sensible heat thermal energy storage [1–5]. LHTES can be utilized in applications ranging from cooling of portable electronic devices [6,7] to energy storage for large scale solar power production [8–13].

More widespread usage of LHTES technology has been limited by the low thermal conductivity of many PCMs [1–5]. In order to circumvent this limitation, various approaches have been taken such as

adding high thermal conductivity enhancers to the PCM, thereby increasing the effective thermal conductivity of the enhancer-PCM composite. Other strategies include but are not limited to using fins, honeycomb structures, Lessing rings or porous media (such as metal or graphite foams) [3,14,15]. Nanoparticles, PCM encapsulation and heat pipes (HPs) have also been used to increase heat transfer rates in PCMs [1,2,4,9].

The concept of incorporating HPs into PCMs to reduce thermal resistances has been patented by Faghri [16,17]. HPs have been shown to increase phase change rates by 40 % relative to comparably-sized solid fins embedded in a PCM [12,18–20]. Alternatively, high porosity, open-celled metal foams that are infiltrated with a PCM have the potential to improve LHTES heat transfer rates due to the relatively large metal-PCM interfacial surface area [21]. The morphology of metal foam is typically described by its porosity, ϕ , or pore volume fraction, and pore density, ω , which describes the number and size of its pores. Metal foams typically have porosities greater than 0.85 with surface area densities exceeding $1000 \text{ m}^2 / \text{m}^3$ [21]. Rather than specify the surface area density, metal foam manufacturers report the pore density, defined as the number of pores per inch (PPI) [22]. Foams can be constructed from a wide variety of solid materials to yield various combinations of porosity and pore density. Foams of the same porosity can have different pore densities, where a smaller porosity corresponds to larger interconnecting solid strut thicknesses.

Table 3.1 includes a brief literature review of heat transfer investigations involving metal foam-PCM composites. All of the studies have shown that decreasing the porosity reduces the melting (solidification) time. However, a lower porosity reduces the energy storage capacity for a fixed LHTES system volume. Natural convection, which can enhance melting, may be suppressed when foams are used, depending on the type of PCM and the foam pore density. In all cases, metal foams can increase the melting and solidification rates, compared to rates involving a pure PCM system due to the higher percentage of the available energy being stored or released as latent heat rather than sensible heat (even for constant heat flux conditions). However, use of metal foams may decrease the overall heat transfer performance relative to pure PCM if the enhancement of conduction does not outweigh the suppression of natural convection.

Among the studies presented in Table 3.1, only one work considered the combination of two distinctive enhancement techniques. Xie et al. [23] investigated use of brass fins (0.8 mm thickness, 75 mm length and 25 mm height) in conjunction with copper foam ($\phi = 0.96$) embedded in eicosane ($T_m = 36.8$ °C). The combination of fins and foam in a rectangular container reduced the temperature gradient within the PCM in both horizontal and vertical orientations relative to systems without the fins and foams. With this combination, the fins promote deeper thermal penetration into the PCM (compared to foam alone) and the foam promotes diffusion of thermal energy into the PCM (compared to fins alone). The effective thermal conductivity of the fin-and-foam enhanced LHTES was increased by a factor of 2.6, compared to that of the PCM enhanced with only foam.

Similarly, Sharifi et al. [34] performed an experimental and numerical investigation of the melting and solidification of n-octadecane in a vertically-oriented cylindrical configuration which included a vertical HP that penetrated through an overlying, horizontally-layered set of aluminum foils. The bottom of the HP extended into a heat transfer fluid (HTF) which was held at a constant temperature to induce heat transfer to or from the PCM. An effectiveness was defined which enabled comparison of the melting rates to those using a conventional PCM enhancement approach utilizing a solid copper pin fin (rod). Melting (solidification) rates increased by 3 (9) times compared to a Rod-PCM configuration with a foil-PCM porosity of 0.987 (1.3 % solid foil volume fraction).

Results reported in [34], along with those obtained by infiltrating metal foams with PCM as summarized in Table 3.1, motivate this study. To the authors' knowledge, phase change in a HP-Foam-PCM configuration has not been previously reported. More specifically, melting and solidification in systems involving the HP-Foil-PCM, HP-Foam-PCM, HP-PCM and Rod-PCM configurations are investigated experimentally in a vertically-oriented cylindrical system. The objective is to determine the effectiveness of each approach by comparing the thermal performance of each configuration to that of a base case, the Rod-PCM system. The influence of the porosity and pore density (or foil thickness) is also reported.

3.2 Experimental Apparatus

Experiments were performed to quantify the thermal performance of a PCM system enhanced by the combination of a HP and either foils or foam. N-octadecane of 99 % purity ($T_m \approx 28^\circ\text{C}$) was used as the PCM; a list of its thermophysical properties is presented in Table 3.2. As is well known, this particular PCM has been employed in many heat transfer studies.

The experimental apparatus is shown in Fig. 3.1 and consists of a PCM housed within a vertical cylindrical enclosure that is heated (cooled) by a concentrically-located HP or rod. Foam or foil can be embedded in the PCM, while heat transfer to or from the PCM is ultimately driven by a HTF passing through an enclosure that includes the bottom section of the HP or rod. The enclosure is constructed of 10 mm thick welded aluminum plates with overall dimensions of 140 mm \times 100 mm \times 100 mm, using water as the HTF. A HP (or rod) of 175 mm length and 6 mm diameter transfers heat between the HTF and the PCM. The lower section of the HP (or rod) is immersed in the HTF which, in turn, is housed in the rectangular enclosure. The PCM enclosure is formed by (i) an acrylic cylinder with an inner (outer) diameter of 41 mm (50 mm) and height 125 mm, (ii) a bottom acrylic disc of 5 mm thickness and 50 mm diameter and (iii) an upper aluminum plate of 10 mm thickness.

An air gap of 2 mm thickness exists between the acrylic disc and an underlying acrylic plate to minimize heat transfer through the bottom of the enclosure. The combination of a hermetically-sealed HTF chamber and placement of the HTF inlet / outlet below the bottom of the acrylic plate results in an additional insulating air gap with a measured thickness of approximately 20 mm between the plate and water surface. The enclosure mating surface between the cylinder and upper aluminum plate was sealed using a combination of a synthetic rubber O-ring and vacuum grease. Silicone aquarium sealant was used to seal and secure the HP (rod), acrylic disc and acrylic cylinder in place. The entire apparatus was compressed using four all-threaded rods and wing nuts. Fiberglass insulation was wrapped around the acrylic cylinder, and the entire system was placed in a box constructed of 37 mm thick extruded polystyrene boards.

During melting, the PCM ($m_{pcm} = 0.080$ kg) expands, causing a reduction in the air volume above the

PCM, thereby increasing the air pressure. The differential air pressure was measured with a pressure transducer (Sper Scientific, model PS100 – 2 BAR) mounted on the upper aluminum plate, and was recorded using Lutron801 software. The measured pressure change, in conjunction with the measured air temperature, allows for the determination of the PCM liquid volume fraction as described in [34]. A total of 12 K-type thermocouples (TCs) were installed in the enclosure (10 in the PCM, 2 in the air) by inserting them into the pre-drilled (1.6 mm diameter) acrylic cylinder (and foam for the HP-Foam-PCM system) at the proper radial distance. The TC insertion holes were subsequently filled with silicone sealant. In addition, two TCs (T_{13} and T_{14}) were installed on the bottom section of the HP, one TC (T_{15}) on the HP tip, and one TC each within the HTF flow (T_{16} and T_{17}). The TC locations are shown in Table 3.3.

Heat transfer to and from the PCM occurs through either a solid copper rod or copper-water HP (Enertron, model HP-HD06DI17500BA, groove wick). The length of the HP (or rod) exposed to the PCM, L_{pcm} , is fixed at 82 mm. The adiabatic section of the HP (or rod), L_a , is considered to be the 28 mm distance measured from the top of the acrylic disk to the water surface and the remainder of the HP (or rod), L_{htf} , extends 65 mm into the HTF.

In order to compare the performance of the HP-Foil-PCM and HP-Foam-PCM configurations, the porosity of the enhancer-PCM composite should be the same. For each configuration, the level of PCM when completely solid is slightly below the top surface of the metal enhancer (foam or foil), while when completely liquid, the level is above the enhancer. Since for all cases the PCM mass is fixed and all of the solid PCM lies within the region occupied by the metal enhancer, the porosity used here is defined for both melting and solidification by the following relationship:

$$\varphi = \frac{V_{void}}{V_{total}} = \frac{V_{pcm}}{V_{pcm} + V_{me}} \approx \frac{m_{pcm}/\rho_{pcm,s}}{m_{pcm}/\rho_{pcm,s} + m_{me}/\rho_{me}} \quad (1)$$

Note that if the liquid density replaces the solid density in Eq. (1), the calculated porosity differs by approximately 0.3 %. The preceding definition allows for a consistent method to compare the foam and foils as metal enhancers.

To study the HP-Foam-PCM configuration, Duocel® aluminum foam (alloy 6101-T6, with 98 % aluminum content) was utilized. The foam samples were obtained from K.R. Reynolds Company [35] as 102 mm × 102 mm × 12.5 mm rectangular samples that were fabricated into annular discs of inner diameter 5.9 mm, outer diameter 39 mm and thickness 12.5 mm. The foam discs were stacked six pieces high (axially) around the HP to achieve a total height of approximately 75 mm. The commercially-available foam samples are available within a range of foam porosities, rather than an exact value, due to variability in the manufacture of the foam. Since the foam is of rigid construction, its porosity is fixed. The influence of pore density is studied using four aluminum foam samples with reported pore densities of 5, 10, 20 and 40 PPI and reported (measured) porosities in the range of 0.94 to 0.96 (0.943 to 0.957). The effect of porosity is determined for a pore density of 20 PPI with measured porosities between 0.870 and 0.957.

In this study, foil (alloy 8011) containing approximately 98 % aluminum is used in the HP-Foil-PCM configuration allowing for an appropriate comparison with the HP-Foam-PCM configuration. Two foil thicknesses are considered here: $t_1 = 0.017$ mm and $t_2 = 0.024$ mm with an outer diameter of 39 mm, allowing sufficient clearance to overlay the acrylic cylinder during test cell assembly. The foils were cut to form, with an inner diameter of 5 mm which results in an overlap onto the exterior of the HP (6 mm outer diameter) with a press-fit installation method. Unlike the foam, the porosity of the foil-PCM composite, in a fixed annular volume, can be easily adjusted by changing the foil thickness (t) and number of foils (N). The number of foils for a particular case is specified to match the porosity of the foil-PCM composite to that of the foam-PCM composite allowing for appropriate comparison. The range of porosity studied here for the foil-PCM composite is 0.957 to 0.987.

3.3. Experimental Procedure

Solidification and melting were investigated for the Rod-PCM, HP-PCM, HP-Foil-PCM and HP-Foam-PCM configurations. As previously described, a press-fit installation method was used to install the foils and foam, while a thin layer of thermal paste (Arctic Silver 5) was applied to the HP in the HP-Foam-PCM configuration to ensure sufficient thermal contact. A fixed PCM mass of 80 ± 0.2 g was de-

gassed by exposing the liquid PCM to a reduced pressure environment for approximately 2 hours before filling the enclosure. Prior to the onset of solidification, the system was shaken to remove any air voids within the foils or foam.

During melting (solidification) the initial temperature of the PCM was set to a value of 24 °C (31 °C) by circulating the HTF with a Lauda Brinkmann RM5 water bath circulator with a flow rate of about 0.1 kg / s. Once the system was equilibrated at the initial temperature (with all TCs in the PCM being within 0.2 °C of the desired initial temperature) the experiment was initiated by flowing water at a temperature of 45 °C (11 °C) which is about 17 °C above (below) T_m . Throughout each experiment, the TC and pressure transducer measurements are recorded. The liquid fraction can be determined by using the analysis of [34] wherein a PCM volume change is correlated to a change in the air volume as determined by the measured air pressure and temperature, assuming the air behaves as an ideal gas. Each experiment is concluded when all of the PCM melts (solidifies) as indicated by a constant air differential pressure.

3.4. Results and discussion

The main figure of merit reported here is the PCM volumetric liquid fraction (f_l) which is the ratio of the liquid PCM volume to the total PCM volume. The liquid fraction is determined in the same manner as in [34], utilizing a combination of the measured air pressure and air temperature to calculate the change in air volume which correlates to a PCM volume change. The same uncertainty analysis is used, as in [34], and will not be discussed in detail here. The resulting uncertainty of the liquid fraction in these experiments ranges from ± 0.1 to ± 0.15 . The uncertainty is calculated based on the sequential perturbation method utilizing a root-sum-squares calculation at each time instant. An effectiveness for melting or solidification provides a direct comparison of various configurations relative to the base case, subscript “bc”, the Rod-PCM configuration:

$$\varepsilon_m(t) = \frac{f_l(t)}{f_{l,bc}(t)} \quad (2)$$

$$\varepsilon_s(t) = \frac{f_s(t)}{f_{s,bc}(t)} = \frac{1 - f_l(t)}{1 - f_{l,bc}(t)} \quad (3)$$

Also by averaging the effectiveness over the duration of phase change, $\varepsilon_{m,avg}$ and $\varepsilon_{s,avg}$ are defined. The complete melting (solidification) time, t_m (t_s), is defined as the time when the liquid fraction reaches 0.95 (0.05) during melting (solidification).

3.4.1. Temperature distribution within the PCM

Representative temperature histories during melting and solidification are shown in Fig. 3.2 and Fig. 3.3, respectively, for the (a) HP-Foil-PCM, (b) HP-Foam-PCM, (c) HP-PCM and (d) Rod-PCM configurations. A high degree of symmetry was observed about the centerline of the enclosure. As such, each of the five sets of data points shown represents the average of two symmetrically-placed TCs. Melting and solidification phenomena can be inferred from the measured temperatures. A sharp increase (decrease) in the slope of the temperature history indicates the completion of melting (solidification) at that TC location.

The PCM temperature distribution in the HP-Foil-PCM configuration is presented in Fig. 3.2 (a) with an order of melting occurring at locations T_1 , T_4 , T_5 , T_2 and lastly T_3 . Since T_1 and T_4 experience melting at nearly the same time, and are located at two different axial locations but at the same radial location, conduction-dominated melting is inferred. Note that the vertical distance between foils is too small for any significant amount of natural convection to occur, and therefore the outer radii TC locations T_2 and T_5 also melt at a similar time. While it would be expected that the order of melting would occur at locations with increasing radius, this was not observed for T_3 . Most likely, the manual press-fit method of installation resulted in a larger than desired foil spacing, with a higher local porosity at that axial location.

The HP-Foam-PCM configuration in Fig. 3.2 (b) exhibits an order of melting as T_4 , T_1 , T_3 , T_5 and T_2 . The solid-liquid interface progresses mainly in the radial direction however, some degree of buoyancy-induced flow is apparent since upper locations have slightly higher temperatures and melt sooner than in the vicinity of lower TCs. Regardless, T_2 and T_5 melt at nearly the same time, confirming that the process is mainly conduction-dominated.

The PCM temperatures during melting for the HP-PCM and Rod-PCM configurations are presented in Fig. 3.2 (c) and (d), respectively. Each exhibits the same order in which the TC locations experience

melting (T_4 , T_5 , T_3 , T_1 and T_2) suggesting similar melting phenomena for the two configurations. The absence of foils or foam results in natural convection-dominated heat transfer, with the uppermost regions melting first, followed by a downward propagating melting front. Consequently, a large axial temperature gradient is displayed in the figure.

The temperature distribution histories during solidification for the (a) HP-Foil-PCM, (b) HP-Foam-PCM, (c) HP-PCM and (d) Rod-PCM configurations can be seen in Fig. 3.3. Since natural convection is insignificant during solidification, each case is conduction-dominated. Hence, for all cases the solid-liquid interface progresses primarily in the radial direction. The higher effective thermal conductivity of a HP relative to the rod results in more axial uniformity for each case involving a HP. On the other hand, the rod case exhibits a slightly conical solidification front since the lower outermost location is the third location to experience phase change. This phenomenon can be attributed to the large temperature drop experienced by the rod.

3.4.2. Temperature drops along the HP / Rod

The temperature drop along the HP or rod is defined using the temperatures at the TC locations in Fig. 1 as:

$$\Delta T_{HP/rod} = |T_{15} - 0.5(T_{13} + T_{14})| \quad (4)$$

where the second term represents the average temperature of the HP embedded in the HTF. The temperature drop is presented in Fig. 3.5 for the HP-Foam-PCM, HP-PCM and Rod-PCM configurations during (a) melting and (b) solidification. Note that for all cases studied, the temperature of the HP or rod embedded in the HTF (second term of Eq. (4)) is similar to that of the HTF, and the major variations of $\Delta T_{HP/rod}$ are attributed to the HP or rod temperature within the PCM (T_{15}).

The $\Delta T_{HP/rod}$ histories for the HP-PCM and Rod-PCM cases of Fig. 3.4 (a) display an initially conduction-dominated regime, followed by a natural convection-dominated heat transfer regime with a nearly constant value of $\Delta T_{HP/rod,m}$, as similarly observed previously [18,19]. For the HP-Foam-PCM configuration, the HP experiences a significantly larger temperature drop relative to the HP-PCM configuration that is attributed to its higher melting rate. In Fig. 3.4 (b), all cases experience a

monotonically decreasing temperature drop since solidification is conduction-dominated. During melting(solidification) in the HP-PCM configuration, the HP is nearly isothermal with a temperature drop of about 1 °C (2 °C) due to its high thermal conductivity relative to a rod. However, when foam is implemented with the HP, the improved thermal conductivity of the foam-PCM composite brings the HP temperature in the PCM closer to T_m , resulting in a larger temperature drop along the HP for the HP-Foam-PCM configuration relative to the HP-PCM configuration.

3.4.3. Effect of foil number and thickness on the HP-Foil-PCM configuration performance

As noted previously, the porosity of $\phi = 0.957$ for the foam-PCM composite is fixed (with $\omega = 20$ PPI), so the foil number and thickness must be adjusted for the foil-PCM composite to match the porosities of the two configurations. Additionally, the effect of the porosity will also be studied by considering the 0.987 case for the foil-PCM composite used in [34]. Two foil thicknesses ($t_1 = 0.017$ mm and $t_2 = 0.024$ mm) are also considered here to determine its effect on performance.

The measured liquid fraction and effectiveness histories for the HP-Foil-PCM configuration are reported in Fig. 3.5 for (a) melting and (b) solidification. By comparing the open and filled square symbols, it can be seen that for a fixed porosity ($\phi = 0.987$), similar melting (and solidification) rates are observed, even though the foil number and thickness are changed. The complete melting (solidification) time for the HP-Foil-PCM configuration with $\phi = 0.987$ is about 30 min (22 min) which is close to the results reported in [34] for a similar PCM mass. The effectiveness is increased from about 6.5 to 14.5 (5 to 8.5) during melting (solidification) as the porosity is decreased from 0.987 to 0.957. While solidification occurs faster for each case compared to melting due to the higher solid PCM thermal conductivity, the solidification effectiveness is lower than that of melting due to the smaller liquid fraction for the base case during melting at any given time. The complete melting (solidification) time for the HP-Foil-PCM configuration, with $\phi = 0.957$, is around 13 min (11 min), which is much faster than for the Rod-PCM configuration, approximately 200 min (150 min). For the range of parameters considered here, porosity is observed to have the most important influence on the heat transfer rates for the HP-Foil-

PCM configuration. It can be seen in Fig. 3.5 that as the porosity is decreased by adding more foils, the melting and solidification rate can be increased substantially.

3.4.4. Effect of pore density and porosity for HP-Foam-PCM performance

The liquid fraction behavior during both melting and solidification for HP-Foam-PCM cases with reported pore densities of 5, 10, 20 and 40 PPI and measured porosities ranging from 0.943 to 0.957 are displayed in Fig. 3.6. As evident, all cases yield similar behavior and the complete melting (solidification) time and average melting (solidification) effectiveness are 29 (24) min and 7.4 (4.2), respectively. There is no clear indication as to whether a higher or lower pore density induces a faster rate of phase change for either melting or solidification. Therefore, the pore density is not very significant in the HP-Foam-PCM configuration for the range of pore densities considered here.

The effect of porosity on the (a) melting and (b) solidification processes in the HP-Foam-PCM configuration can be established from Fig. 3.7. The measured porosities range from 0.870 to 0.949 with a constant reported pore density of 20 PPI. It can be observed that an increase in the melting and solidification rate occurs for the lower porosities. The average effectiveness (from lowest to highest porosity) is $\varepsilon_{m,avg} = 11.2, 9.3$ and 7.9 ($\varepsilon_{s,avg} = 6.4, 5.7$ and 4.2) during melting (solidification). Since the effective thermal conductivity of the foam-PCM composite increases with metal mass, a lower porosity promotes a higher rate of phase change in a fixed volume.

3.4.5. Comparison between the HP-Foam-PCM and HP-Foil-PCM configuration performance

At this point, it is clear that, for the range of conditions considered here, the porosity is the most influential parameter contributing to the effectiveness, while the pore density of the foam (or the foil number and thickness) has a negligible impact, for a fixed porosity. Both the HP-Foil-PCM and HP-Foam-PCM configurations lead to significantly enhanced melting and solidification rates relative to the Rod-PCM and HP-PCM cases. However, it is important to compare the two configurations when they are of the same porosity to determine which can best improve the overall heat transfer rates. Even though the porosity of the foil-PCM and foam-PCM composites in the HP-Foil-PCM and HP-Foam-PCM cases is the same, the morphology of the metal enhancer affects performance. The thin metal struts that comprise

the foam have a small contact area with the HP, which is on the order of 10 % of the HP surface area [36,37]. Since a large number of foils are installed and a slight overlap exists between adjacent foils at the HP-foil interface, a larger contact area is achieved with the HP relative to the foam case. Additionally, the effective thermal conductivity of the foam is more isotropic than that of the foil which also affects how heat is transferred in each metal enhancer.

In Fig. 3.8, the HP-Foil-PCM and HP-Foam-PCM cases are compared. It is clear that with a fixed porosity of $\phi = 0.957$, the HP-Foil-PCM case melts (solidifies) in less than half of the time of the HP-Foam-PCM case. Also by comparing the open squares and filled circles, the HP-Foil-PCM case has a similar melting and solidification rate as the HP-Foam-PCM case with only one third of the metal volume. When the porosity of the foam-PCM composite is decreased to $\phi = 0.870$, the HP-Foam-PCM does not perform as well as the HP-Foil-PCM case with $\phi = 0.957$ (which also has approximately one third the metal volume). Therefore, the combination of the HP and foils is the preferred method of enhancement relative to all others studied here.

Table 3.4 is a summary of all the cases considered here. The table displays the complete (95 %) phase change time (t_m, t_s), the average effectiveness ($\epsilon_{m,avg}, \epsilon_{s,avg}$) and the average rates of phase change ($r_{m,avg}, r_{s,avg}$) during both melting and solidification. The average melting (solidification) rate, $r_{m,avg}$ ($r_{s,avg}$), of phase change is defined as the total PCM mass divided by the time corresponding to complete melting (solidification):

$$r_{m,avg} = \frac{m_{PCM}}{t_m} \quad (5)$$

$$r_{s,avg} = \frac{m_{PCM}}{t_s} \quad (6)$$

The most effective configuration to enhance phase change rates is the HP-Foil-PCM case ($\phi = 0.957$) due to its highest melting (solidification) rate of 6.15 g / min (7.27 g / min) and average effectiveness of 14.74 (8.43) with the lowest melting (solidification) time of 13 (11) min. Due to the small separation distance between foils, less than 1 mm, natural convection is essentially eliminated and both phase change processes are conduction-dominated. The time required for complete phase change is smaller for

solidification since the solid PCM has a higher thermal conductivity than the liquid PCM. Since phase change rates of the base case during solidification are significantly higher than during melting, the effectiveness during solidification is lower than during melting. These results show that the melting and solidification rates for the HP-Foil-PCM configuration can be increased by about 15.4 and 13.8 (9.7 and 9.3) times, respectively, compared to the Rod-PCM (HP-PCM) case. The complete melting and solidification times for the HP-Foil-PCM configuration are reduced to 6.5 % and 7.2 % (10.3 % and 10.7 %), respectively, of the time for the Rod-PCM (HP-PCM) configuration, which is an extraordinary improvement.

3.5. Conclusions

An experimental investigation of melting and solidification in HP-Foil-PCM and HP-Foam-PCM configurations was conducted to determine average melting rates and a relative effectiveness compared to a base case configuration consisting of a Rod-PCM system. Overall, both types of enhancement techniques, for all conditions studied, significantly improved the melting and solidification rates relative to those of the Rod-PCM and HP-PCM configurations. In the HP-Foil-PCM or HP-Foam-PCM configurations, the HP acts to thermally penetrate the PCM while the foils or foam allow for improved thermal diffusion within the PCM. The influence of the foam pore density and foil thickness was shown to be negligible compared to the effect of porosity for both configurations. The largest average effectiveness, $\varepsilon_{m,avg} = 14.7$ ($\varepsilon_{s,avg} = 8.4$) during melting (solidification), was achieved for the HP-Foil-PCM configuration ($\varphi = 0.957$) which outperformed the HP-Foam-PCM configuration ($\varphi = 0.870$) with a lower porosity. The melting and solidification rates for the HP-Foil-PCM configuration were about 15 (10) times larger than that of the Rod-PCM (HP-PCM) configurations.

Nomenclature

c_p	specific heat (J/kg·K)
f_l	liquid fraction
h_{sl}	latent heat (kJ/kg)
k	thermal conductivity (W/m·K)
L	length (mm)
m	mass (kg)
N	number of foils
r	radial coordinate direction (mm)
r_m	melting rate (g/min)
r_s	solidification rate (g/min)
T	temperature (°C)
ΔT	driving temperature between HTF and PCM (°C)
$\Delta T_{HP/rod}$	temperature drop along the HP or Rod (°C)
t	time (min), thickness (mm)
t_m	time for 95 % complete melting (min)
t_s	time for 95 % complete solidification (min)
V	volume (m ³)
z	axial coordinate direction (mm)

Greek symbols

ε_m	melting effectiveness
ε_s	solidification effectiveness
μ	dynamic viscosity (Pa·s)
ρ	density (kg/m ³)
φ	porosity
ω	pore density (PPI)

Subscripts

a	adiabatic
avg	average
bc	base case
htf	heat transfer fluid
l	liquid
m	melting
me	metal enhancer
pcm	phase change material
s	solidification, solid
$total$	total
$void$	void

Acronyms

EXP	experimental
HP	heat pipe
HTF	heat transfer fluid
LHTES	latent heat thermal energy storage
MF	metal foam
NUM	numerical
PCM	phase change material
PPI	pores per inch
TC	thermocouple

References

- [1] Farid M. M., Khudhair A. M., Razack S. A. K., and Al-Hallaj S., 2004, "A review on phase change energy storage: materials and applications," *Energy Convers. Manag.*, 45, pp. 1597–1615.
- [2] Sharma A., Tyagi V. V., Chen C. R., and Buddhi D., 2009, "Review on thermal energy storage with phase change materials and applications," *Renew. Sustain. Energy Rev.*, 13, pp. 318–345.
- [3] Agyenim F., Hewitt N., Eames P., and Smyth M., 2010, "A review of materials, heat transfer and phase change problem formulation for latent heat thermal energy storage systems (LHTES)," *Renew. Sustain. Energy Rev.*, 14, pp. 615–628.
- [4] Cabeza L. F., Castell A., Barreneche C., de Gracia A., and Fernández A. I., 2011, "Materials used as PCM in thermal energy storage in buildings: A review," *Renew. Sustain. Energy Rev.*, 15, pp. 1675–1695.
- [5] Hasnain S.M., 1998, "Review on sustainable thermal energy storage technologies, Part I: heat storage materials and techniques," *Energy Convers. Manag.*, **39**(11), pp. 1127–1138.
- [6] Baby R. and Balaji C., 2012, "Experimental investigations on phase change material based finned heat sinks for electronic equipment cooling," *Int. J. Heat Mass Transf.*, 55, pp. 1642–1649.
- [7] Yang Y.-T. and Wang Y.-H., 2012, "Numerical simulation of three-dimensional transient cooling application on a portable electronic device using phase change material," *Int. J. Therm. Sci.*, 51, pp. 155–162.
- [8] Zhao W., Elmozughi A. F., Oztekin A., and Neti S., 2013, "Heat transfer analysis of encapsulated phase change material for thermal energy storage," *Int. J. Heat Mass Transf.*, 63, pp. 323–335.
- [9] Robak C. W., Bergman T. L., and Faghri A., 2011, "Economic evaluation of latent heat thermal energy storage using embedded thermosyphons for concentrating solar power applications," *Sol. Energy*, 85, pp. 2461–2473.
- [10] Oró E., Gil A., Gracia A. De, Boer D., and Cabeza L. F., 2012, "Comparative life cycle assessment of thermal energy storage systems for solar power plants," *Renew. Energy*, 44, pp. 166–173.

- [11] Bayón R., Rojas E., Valenzuela L., Zarza E., and León J., 2010, "Analysis of the experimental behaviour of a 100 kWth latent heat storage system for direct steam generation in solar thermal power plants," *Appl. Therm. Eng.*, 30, pp. 2643–2651.
- [12] Nithyanandam K. and Pitchumani R., 2013, "Computational studies on a latent thermal energy storage system with integral heat pipes for concentrating solar power," *Appl. Energy*, 103, pp. 400–415.
- [13] Shabgard H., Robak C. W., Bergman T. L., and Faghri A., 2012, "Heat transfer and exergy analysis of cascaded latent heat storage with gravity-assisted heat pipes for concentrating solar power applications," *Sol. Energy*, 86, pp. 816–830.
- [14] Zhao C. Y., Lu W., and Tian Y., 2010, "Heat transfer enhancement for thermal energy storage using metal foams embedded within phase change materials (PCMs)," *Sol. Energy*, 84, pp. 1402–1412.
- [15] Sharifi N., Bergman T. L., and Faghri A., 2011, "Enhancement of PCM melting in enclosures with horizontally-finned internal surfaces," *Int. J. Heat Mass Transf.*, 54, pp. 4182–4192.
- [16] Faghri A., 1990, "Thermal Energy Storage Heat Exchanger," Patent # 4976308.
- [17] Faghri A., 1991, "Micro Heat Pipe Energy Storage System," Patent # 5000252.
- [18] Shabgard H., Bergman T. L., Sharifi N., and Faghri A., 2010, "High temperature latent heat thermal energy storage using heat pipes," *Int. J. Heat Mass Transf.*, 53, pp. 2979–2988.
- [19] Robak C. W., Bergman T. L., and Faghri A., 2011, "Enhancement of latent heat energy storage using embedded heat pipes," *Int. J. Heat Mass Transf.*, 54, pp. 3476–3484.
- [20] Sharifi N., Wang S., Bergman T. L., and Faghri A., 2012, "Heat pipe-assisted melting of a phase change material," *Int. J. Heat Mass Transf.*, 55, pp. 3458–3469.
- [21] Zhao C. Y., 2012, "Review on thermal transport in high porosity cellular metal foams with open cells," *Int. J. Heat Mass Transf.*, 55, pp. 3618–3632.
- [22] Han X.-H., Wang Q., Park Y.-G., T'Joene C., Sommers A., and Jacobi A., 2012, "A review of metal foam and metal matrix composites for heat exchangers and heat sinks," *Heat Transf. Eng.*, **33**(12), pp. 991–1009.
- [23] Xie Y., Song J., Chi P., and Yu J., 2013, "Performance enhancement of phase change thermal energy storage unit using fin and copper foam," *Appl. Mech. Mater.*, 260, pp. 137–141.
- [24] Tian Y. and Zhao C. Y., 2013, "Thermal and exergetic analysis of metal foam-enhanced cascaded thermal energy storage (MF-CTES)," *Int. J. Heat Mass Transf.*, 58, pp. 86–96.
- [25] Liu Z., Yao Y., and Wu H., 2013, "Numerical modeling for solid–liquid phase change phenomena in porous media: Shell-and-tube type latent heat thermal energy storage," *Appl. Energy*, 112, pp. 1222–1232.

- [26] Li W. Q., Qu Z. G., He Y. L., and Tao W. Q., 2012, "Experimental and numerical studies on melting phase change heat transfer in open-cell metallic foams filled with paraffin," *Appl. Therm. Eng.*, 37, pp. 1–9.
- [27] Cui H. T., 2012, "Experimental investigation on the heat charging process by paraffin filled with high porosity copper foam," *Appl. Therm. Eng.*, 39, pp. 26–28.
- [28] Qu Z. G., Li W. Q., Wang J. L., and Tao W. Q., 2012, "Passive thermal management using metal foam saturated with phase change material in a heat sink," *Int. Commun. Heat Mass Transf.*, 39, pp. 1546–1549.
- [29] Tian Y. and Zhao C. Y., 2011, "A numerical investigation of heat transfer in phase change materials (PCMs) embedded in porous metals," *Energy*, 36, pp. 5539–5546.
- [30] Zhao C. Y. and Wu Z. G., 2011, "Heat transfer enhancement of high temperature thermal energy storage using metal foams and expanded graphite," *Sol. Energy Mater. Sol. Cells*, 95, pp. 636–643.
- [31] Wu Z. G. and Zhao C. Y., 2011, "Experimental investigations of porous materials in high temperature thermal energy storage systems," *Sol. Energy*, 85, pp. 1371–1380.
- [32] Zhou D. and Zhao C. Y., 2011, "Experimental investigations on heat transfer in phase change materials (PCMs) embedded in porous materials," *Appl. Therm. Eng.*, 31, pp. 970–977.
- [33] Chen Z., Gu M., and Peng D., 2010, "Heat transfer performance analysis of a solar flat-plate collector with an integrated metal foam porous structure filled with paraffin," *Appl. Therm. Eng.*, 30, pp. 1967–1973.
- [34] N. Sharifi, T. Bergman, A. Faghri, M.J. Allen, Melting and solidification enhancement using heat pipe with foils, *Int. J. Heat Mass Transf.* (2014) Submitted.
- [35] 2013, "K.R. Reynolds Company" <http://www.krreynoldscompany.com/>.
- [36] De Jaeger P., T'Joel C., Huisseune H., Ameel B., De Schampheleire S., and De Paepe M., 2012, "Assessing the influence of four cutting methods on the thermal contact resistance of open-cell aluminum foam," *Int. J. Heat Mass Transf.*, 55, pp. 6142–6151.
- [37] De Jaeger P., T'Joel C., Huisseune H., Ameel B., De Schampheleire S., and De Paepe M., 2012, "Assessing the influence of four bonding methods on the thermal contact resistance of open-cell aluminum foam," *Int. J. Heat Mass Transf.*, 55, pp. 6200–6210.

Table 3.1. Summary of studies on PCMs enhanced with metal foams.

Ref., date	Nature of work: EXP/ NUM	System geometry, boundary conditions	PCM type (M: melting, S: solidification)	Enhancement technique	Parameters studied	Observations
[24] 2013	Numerical (NUM), Experimental (EXP) validation	Rectangular, convective boundary, 3 PCM cascaded, enthalpy method, exergy analysis	M: Paraffin RT31, RT50, RT82 ($31^{\circ}\text{C} < T_m < 82^{\circ}\text{C}$)	Copper foam ($10 < \omega < 30$ PPI, $0.85 < \phi < 0.95$)	Addition of metal foam (MF)	Adding metal foam to a cascaded system can increase the heat exchange and exergy transfer rates by 2-7 times. The exergy efficiency is not significantly improved by adding MF.
[23] 2013	EXP	Rectangular, heated base	M: Eicosane ($T_m = 36.8^{\circ}\text{C}$)	Brass fins (0.8 mm thick), copper foam ($\phi = 0.96$)	Effect of combining fins with MF	Combining fins and foam more than doubled heat transfer rates compared to the MF alone. A more uniform temperature distribution is observed with both.
[25] 2013	NUM	Shell and tube, HTF in the tube, enthalpy method	M: RT58 ($48^{\circ}\text{C} < T_m < 62^{\circ}\text{C}$)	Copper foam ($0.85 < \phi < 0.95$, $10 < \omega < 60$ PPI)	Effect of adding foam	Effect of pore density is minimal and reducing porosity increases the melting rate. Addition of foam can increase heat transfer rates by more than 7 times.
[26] 2012	NUM, EXP validation	Rectangular, heated wall, constant heat flux, enthalpy method	M: Paraffin ($46.5^{\circ}\text{C} < T_m < 60.4^{\circ}\text{C}$)	Copper foam ($10 < \omega < 40$ PPI, $0.90 < \phi < 0.98$)	Effect of pore density and porosity	A lower wall temperature is observed for a lower porosity and higher pore density. Porosity is dominant relative to pore density.
[27] 2012	EXP	Vertical cylinder, concentrically located HTF tube	M: PS58	Copper foam ($\omega = 20$ PPI, $\phi = 0.96$)	Effect of adding MF	MF promotes more uniform temperature distribution. The heat transfer was enhanced by 36 % during melting.
[28] 2012	EXP	Rectangular, PCM-heat sink, heated from base, constant heat flux	M: Paraffin ($47^{\circ}\text{C} < T_m < 59^{\circ}\text{C}$)	Copper foam ($5 < \omega < 20$ PPI, $0.90 < \phi < 0.98$)	Effect of pore density, porosity and orientation	Lower surface temperatures are reported for lower porosities and pore densities. Effect of porosity is greater than pore density. Natural convection heat transfer was reported to be suppressed by at least 55.3 % with foam.
[29] 2011	NUM, EXP validation	Rectangular, heated base, constant heat flux, enthalpy method	M: Paraffin RT58 ($48^{\circ}\text{C} < T_m < 62^{\circ}\text{C}$)	Copper foam ($10 < \omega < 30$ PPI, $0.85 < \phi < 0.95$)	Effect of pore density and porosity	Addition of MF to PCM increased the heat conduction rate while suppressing natural convection. Smaller porosities and pore sizes result in higher conduction heat transfer rates.
[30] 2011	EXP	Vertical cylinder, heated base, constant heat flux	M/S: NaNO_3 (solid-solid phase change temperature = 276°C , $T_m = 306^{\circ}\text{C}$)	Steel alloy foam ($20 < \omega < 30$ PPI, $0.90 < \phi < 0.95$)	Effect of adding MF, effect of corrosion	MFs can reduce phase change times by about 25 % to 30 %. After complete melting, the enhancement in conduction should compensate for the suppression of natural convection by the addition of foam. Corrosion of MF in PCM may eventually limit performance.

Table 3.1. Summary of studies on PCMs enhanced with metal foams, cont.

Ref., date	Nature of work: EXP/NUM	System geometry, boundary conditions	PCM type (M: melting, S: solidification)	Enhancement technique	Parameters studied	Observations
[31] 2011	EXP	Vertical cylinder, heated from below or above, constant heat flux	M/S: NaNO_3 (solid-solid phase change temperature 276°C , $T_m = 306^\circ\text{C}$)	Steel alloy foam ($20 < \omega < 30$ PPI, $0.90 < \phi < 0.95$)	Effect of adding MF, heating from below or above,	MF can enhance conduction heat transfer by 120 %. Porosity is the dominant factor. Natural convection heat transfer could be reduced by half in the liquid region by addition of MF.
[32] 2011	EXP	Rectangular, heated base, constant heat flux	M: paraffin RT27 ($25^\circ\text{C} < T_m < 28^\circ\text{C}$) and $\text{CaCl}_2 \cdot 6\text{H}_2\text{O}$ (29°C)	Copper foam ($\omega = 30$ PPI, $\phi = 0.825$)	Effect of adding MF	Total melting time is reduced to one quarter (third) for RT27 ($\text{CaCl}_2 \cdot 6\text{H}_2\text{O}$) by adding MF. Inclusion of MF can reduce the effect of subcooling by one half for $\text{CaCl}_2 \cdot 6\text{H}_2\text{O}$.
[33] 2010	NUM	Inclined rectangular, solar irradiation from above, equivalent heat capacity method	M: Paraffin ($70^\circ\text{C} < T_m < 80^\circ\text{C}$)	Aluminum foam ($\phi = 0.90$)	Effect of adding MF	MFs significantly improve heat transfer performance in LHTES systems. The more uniform temperature also facilitates lower heat losses from the solar collector.
[14] 2010	EXP	Rectangular, heated base, constant heat flux, top and side walls subject to ambient	M/S: Paraffin RT58 ($48^\circ\text{C} < T_m < 62^\circ\text{C}$)	Copper foam ($10 < \omega < 30$ PPI, $0.85 < \phi < 0.95$)	Effect of pore density and porosity	The temperature difference from the base to 8 mm into PCM was reduced from 30°C for pure PCM to less than 1°C with foam. MFs can increase conduction heat transfer rates by 3-10 times. The solidification time was reduced by more than one-half.

Table 3.2. Thermophysical properties of n-octadecane [19].

Parameter	Value
Melting point, T_m [K]	301
Latent heat, h_{sl} [kJ/kg]	243.5
Liquid thermal conductivity, k_l [W/m·K]	0.148
Liquid density, ρ_l [kg/m ³]	770
Liquid specific heat, $c_{p,l}$ [J/kg·K]	2160
Dynamic viscosity, μ [Pa·s]	3.09×10^{-3}
Solid thermal conductivity, k_s [W/m·K]	0.358
Solid density, ρ_s [kg/m ³]	800
Solid specific heat, $c_{p,s}$ [J/kg·K]	1912

Table 3.3. Location of thermocouples.

Thermocouple	r -coordinate (mm)	z -coordinate (mm)
T_1, T_6	9	105
T_2, T_7	19	105
T_3, T_8	14	120
T_4, T_9	9	145
T_5, T_{10}	19	145
T_{11}, T_{12}	19	195
T_{13}	3	25
T_{14}	3	55
T_{15}	3	165

Table 3.4. Phase change time (t_m, t_s), average effectiveness ($\varepsilon_m, \varepsilon_s$), average melting rate ($r_{m,avg}$) and solidification rate ($r_{s,avg}$) for 95 % completion of phase change.

Enhancement	φ	ω (PPI)	N, t	Fig.	t_m (min)	$\varepsilon_{m,avg}$	$r_{m,avg}$ (g/min)	t_s (min)	$\varepsilon_{s,avg}$	$r_{s,avg}$ (g/min)
Rod	1.00	-	-	-	200	1.0	0.4	152	1.0	0.53
HP	1.00	-	-	-	126	1.4	0.63	102	1.5	0.78
HP-Foil	0.987	-	62, t_1	5	28	6.7	2.86	23	4.8	3.48
HP-Foil	0.987	-	49, t_2	5	31	6.4	2.58	21	5.2	3.81
HP-Foil	0.957	-	162, t_2	5	13	14.7	6.15	11	8.4	7.27
HP-Foam	0.943	5	-	6	29	7.4	2.76	24	4.2	3.33
HP-Foam	0.957	10	-	6	30	6.9	2.67	26	4.0	3.08
HP-Foam	0.949	20	-	6	29	7.6	2.76	23	4.5	3.48
HP-Foam	0.948	40	-	6	29	7.9	2.76	25	4.2	3.20
HP-Foam	0.870	20	-	6	21	11.2	3.81	14	6.4	5.71
HP-Foam	0.912	20	-	7	23	9.3	3.48	18	5.7	4.44

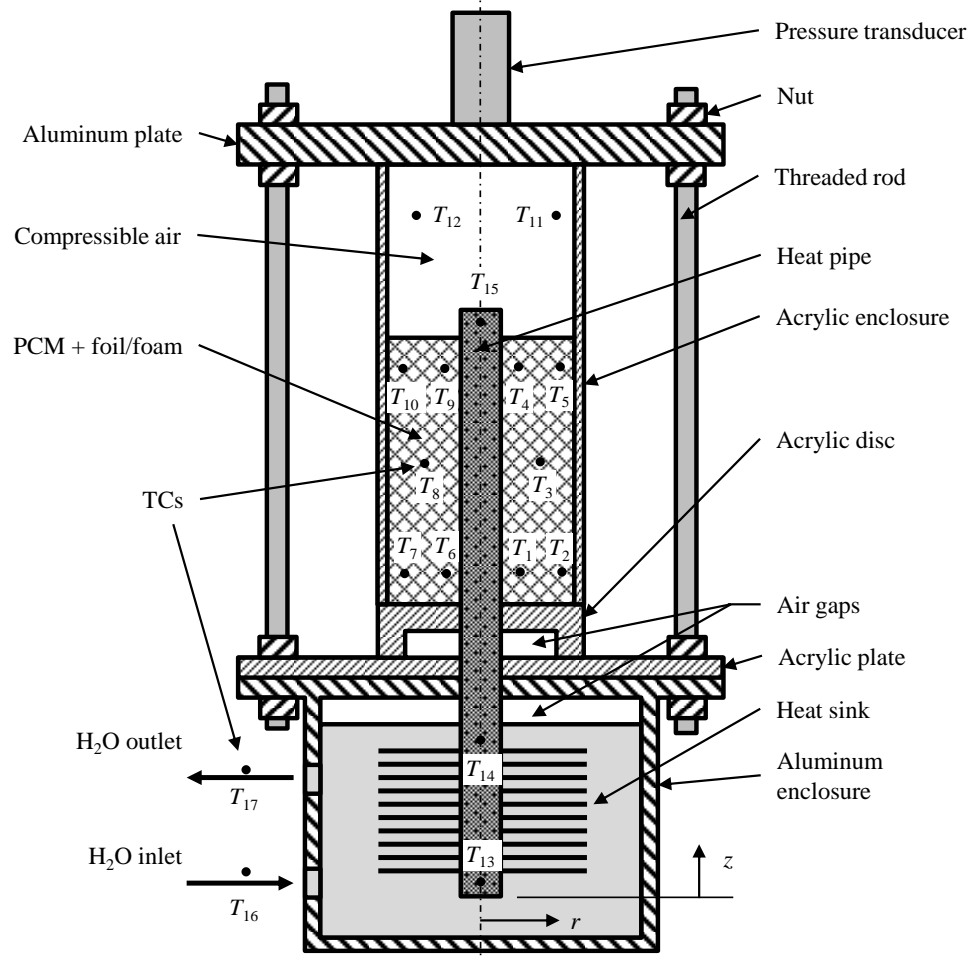
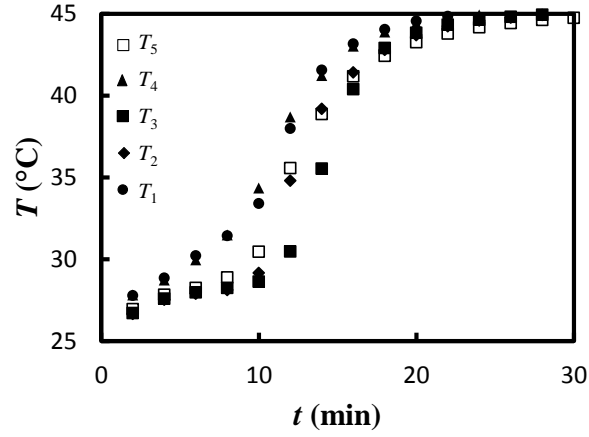
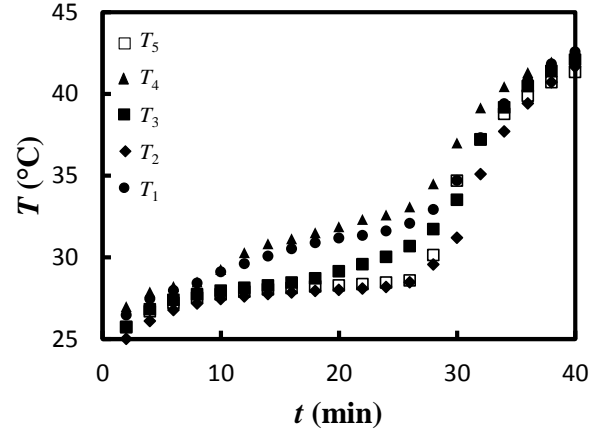


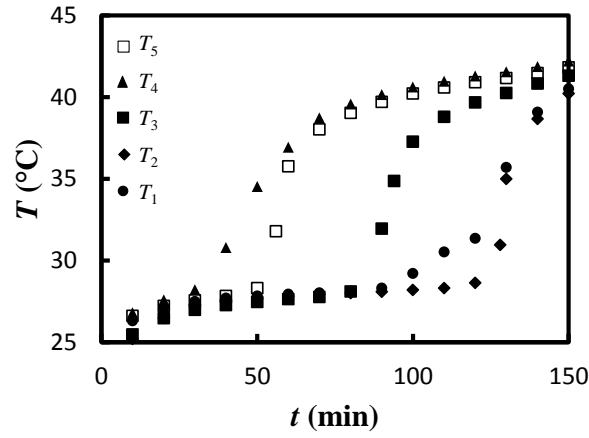
Fig. 3.1. Schematic of the experimental apparatus.



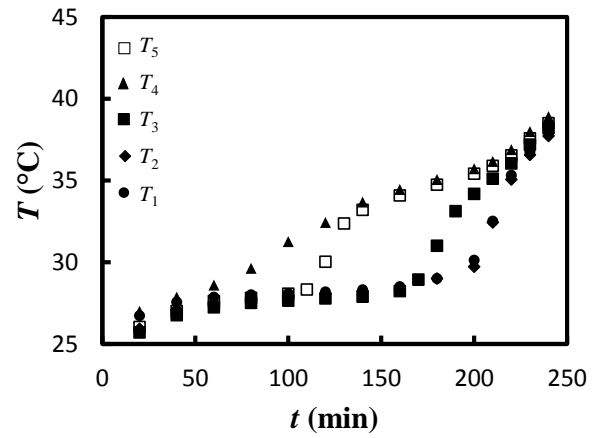
(a) HP-Foil-PCM



(b) HP-Foam-PCM

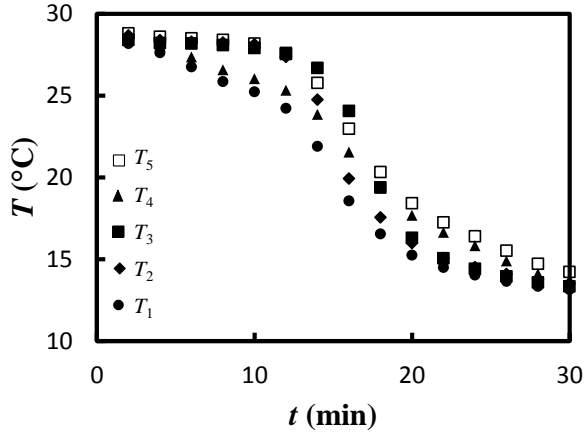


(c) HP-PCM

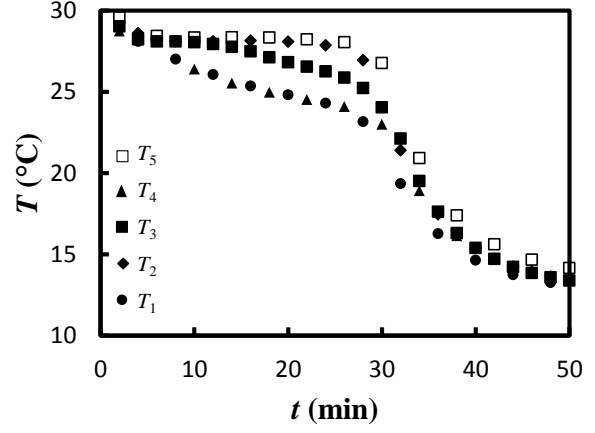


(d) Rod-PCM

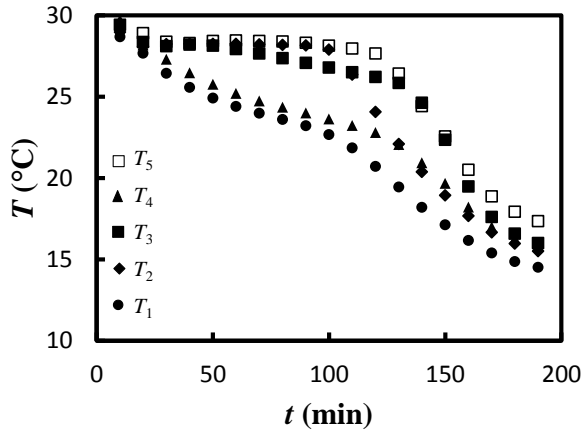
Fig. 3.2. Temperature distribution histories during melting for the (a) HP-Foil-PCM ($\phi = 0.957$, $N = 162$, $t_2 = 0.024$) (b) HP-Foam-PCM ($\phi = 0.949$, $\omega = 20$ PPI), (c) HP-PCM and (d) Rod-PCM configurations.



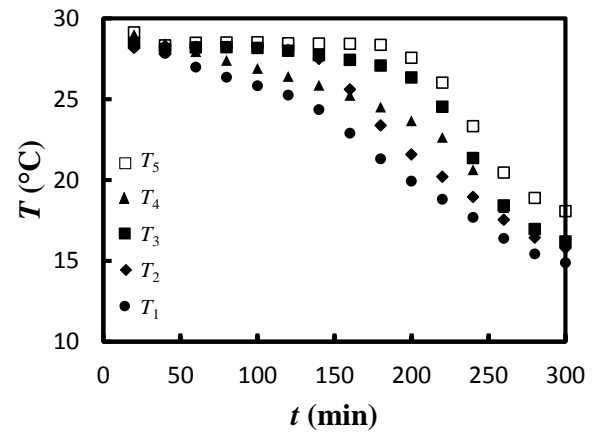
(a) HP-Foil-PCM



(b) HP-Foam-PCM

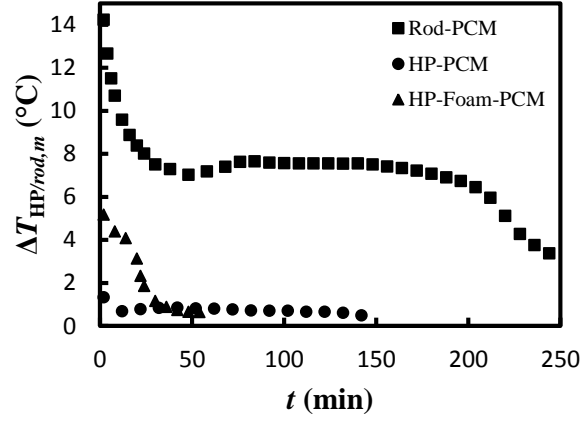


(c) HP-PCM

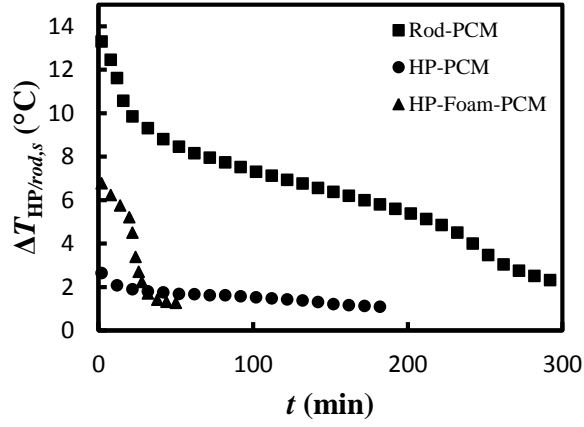


(d) Rod-PCM

Fig. 3.3. Temperature distribution histories during solidification for the (a) HP-Foil-PCM ($\phi = 0.957$, $N = 162$, $t_2 = 0.024$) (b) HP-Foam-PCM ($\phi = 0.949$, $\omega = 20$ PPI), (c) HP-PCM and (d) Rod-PCM configurations.

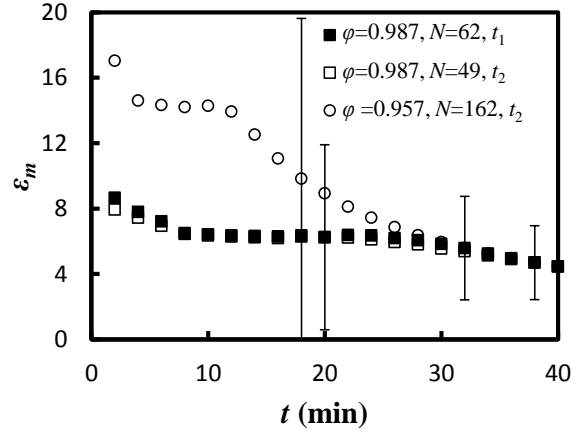
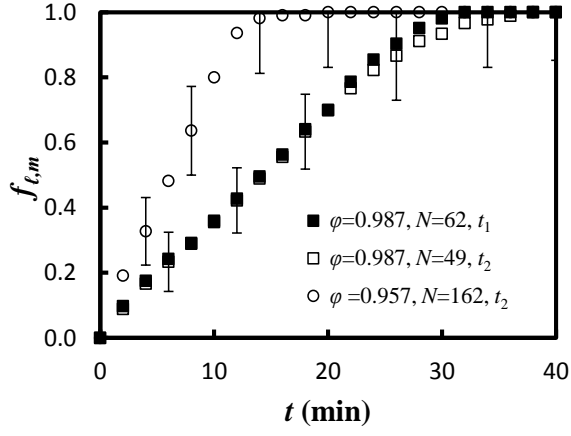


(a) melting

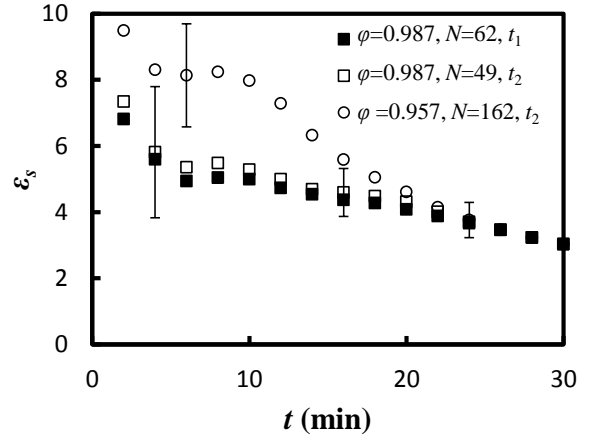
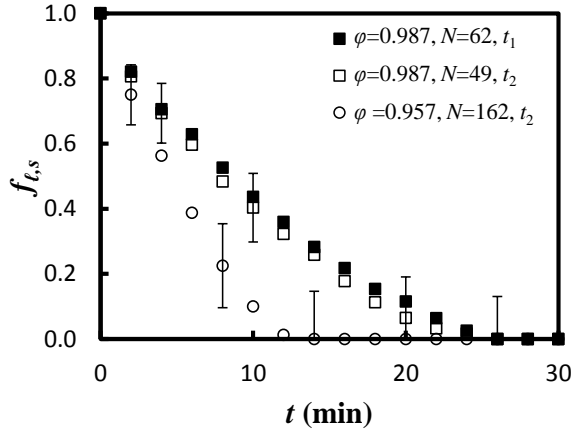


(b) solidification

Fig. 3.4. Temperature drop along the HP (or rod) in the Rod-PCM, HP-PCM and HP-Foam-PCM ($\varphi = 0.912$, $\omega = 20$ PPI) configurations during (a) melting and (b) solidification.

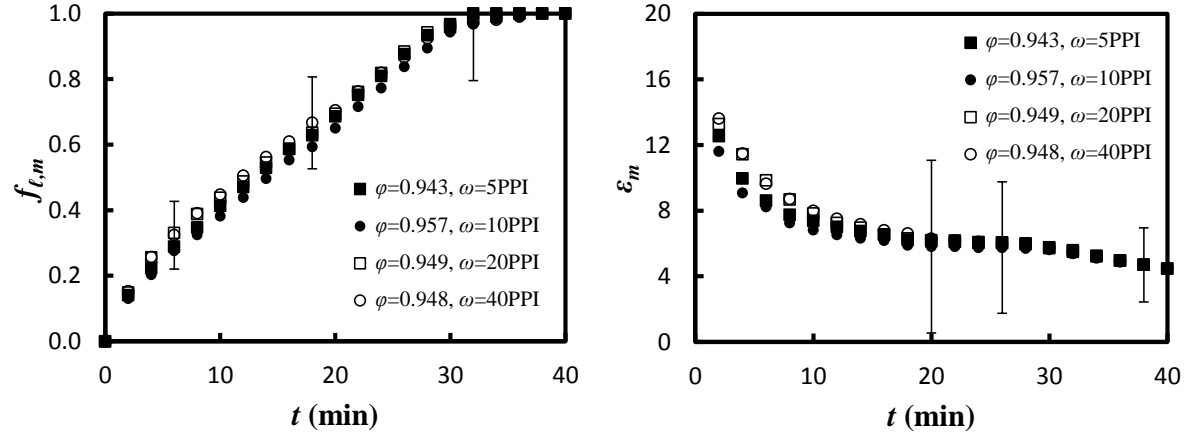


(a) melting

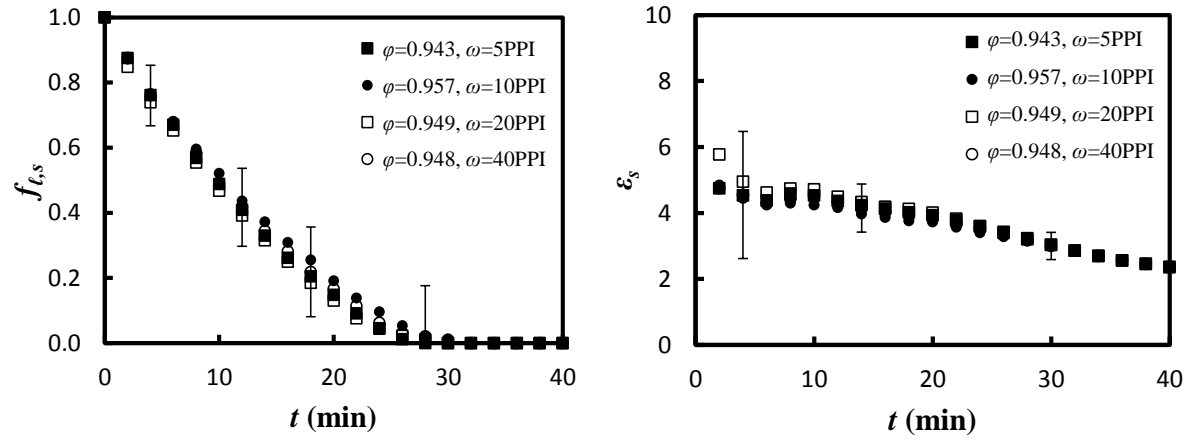


(b) solidification

Fig. 3.5. Volumetric liquid fraction (left) and effectiveness (right) for the HP-Foil-PCM cases for various porosities, foil numbers and foil thicknesses during (a) melting and (b) solidification.

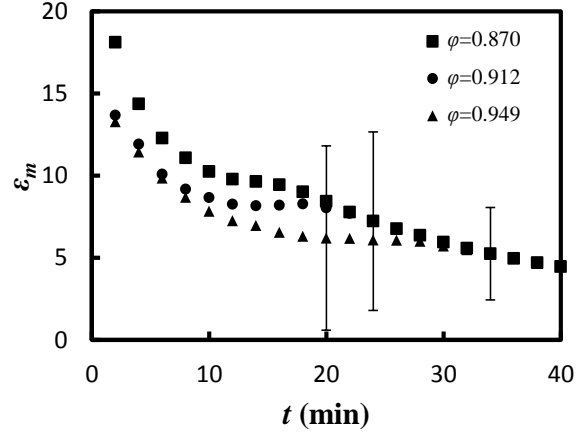
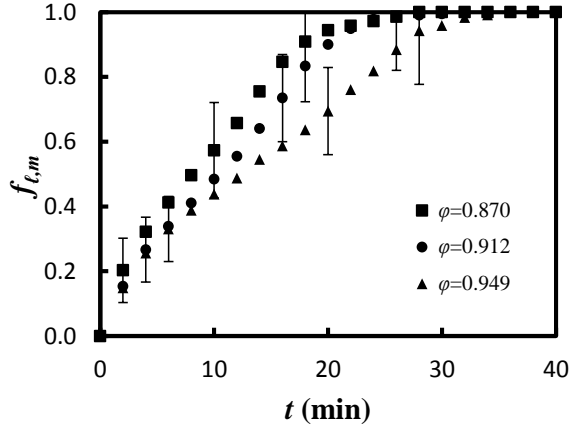


(a) melting

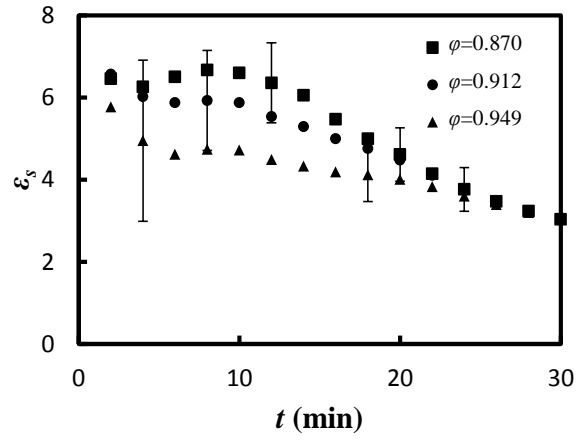
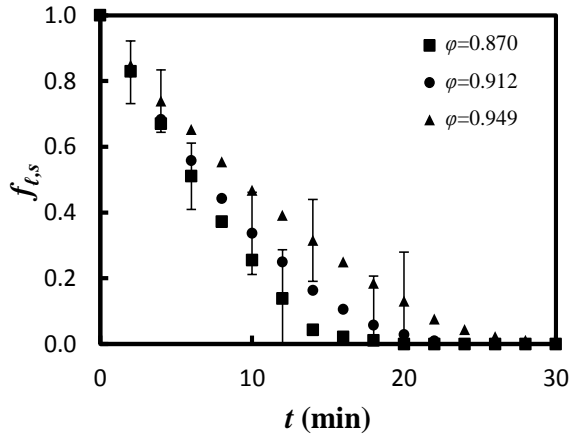


(b) solidification

Fig. 3.6. Volumetric liquid fraction (left) and effectiveness (right) for HP-Foam-PCM cases with a similar porosity ($0.943 < \phi < 0.957$) during (a) melting and (b) solidification.

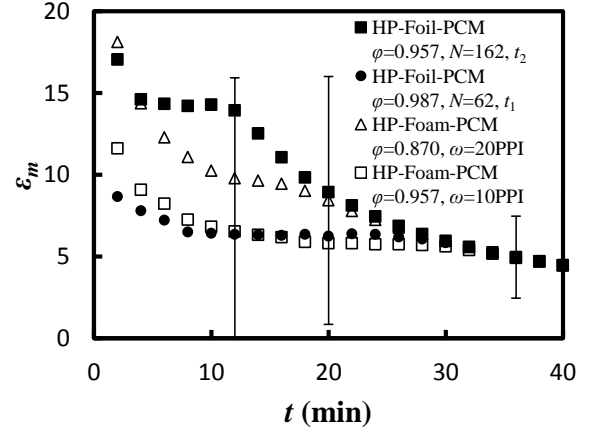
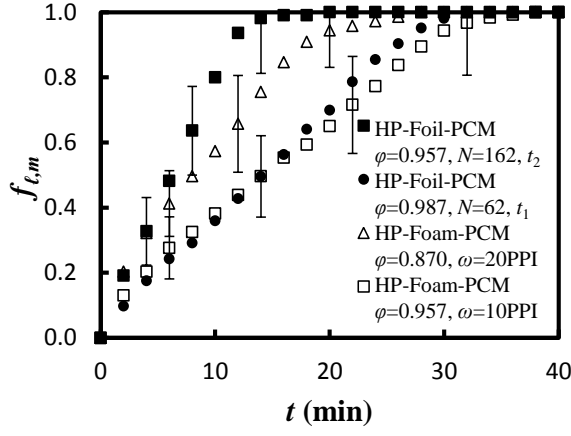


(a) melting

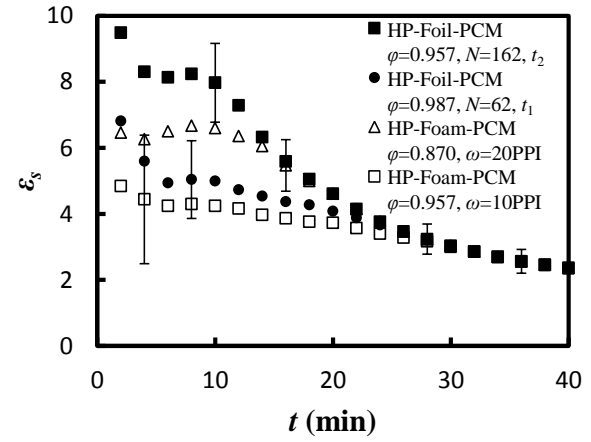
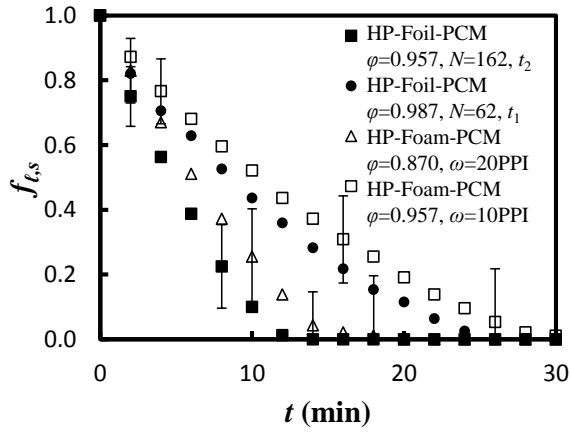


(b) solidification

Fig. 3.7. Volumetric liquid fraction (left) and effectiveness (right) for HP-Foam-PCM cases for various porosities with $\omega = 20$ PPI during (a) melting and (b) solidification.



(a) melting



(b) solidification

Fig. 3.8. Comparison of volumetric liquid fraction (left) and effectiveness (right) for the HP-Foil-PCM and HP-Foam-PCM configurations during (a) melting and (b) solidification.

Chapter 4. Effect of Inclination Angle during Melting and Solidification of a Phase Change

Material using a Combined Heat Pipe-Metal Foam or Foil Configuration

Experiments are performed to analyze the impact of system inclination angle (ranging from 0° to 90°) on the melting and solidification of a phase change material (PCM) in a cylindrical enclosure. Heat transfer occurs through a concentrically located heat pipe (HP) or rod and an underlying copper disc. The HP may also be combined with aluminum foils and foam. Six configurations are investigated: HP-Foil-PCM, HP-Foam-PCM, HP-PCM, Rod-PCM, Foam-PCM, and non-enhanced PCM. The PCM liquid fraction histories, temperature distribution, and photographs provide insight into the varying performance with inclination angle and three-dimensional melting. Experimental measurements indicate that the system orientation is insignificant during solidification, except for two HP-Foil-PCM cases, since it is conduction-dominated. When the HP-Foil-PCM was oriented vertically during solidification, the HP evaporator was above its condenser which reduced the value of the liquid fraction up to 0.11 relative to the horizontal orientation.

System orientation was observed to have a significantly larger impact during melting which may be attributed to (i) varying three-dimensional natural convection currents for systems without foils and foam, and (ii) the HP operation for cases involving the combination of a HP with foils or foam. The HP-Foil-PCM and HP-Foam-PCM configurations achieved a slightly higher liquid fraction by about 0.03 and 0.05, respectively, for a vertical relative to horizontal orientation. This minor variation is negligible relative to the overall performance of each configuration. During melting for the HP-PCM configuration, the horizontal case resulted in higher liquid fractions by approximately 0.09 (0.20) relative to the vertical cases with (without) heat transfer through a copper disc until the remaining solid PCM was below the HP or rod. Overall, the time for complete melting and solidification for the HP-Foil-PCM configuration was reduced to 12 % and 3 % that of a non-enhanced system, respectively regardless of orientation. Further, the minor variation in performance due to orientation for systems involving the combination of HPs and foils or foam renders them an attractive heat transfer enhancement techniques for phase change materials.

4.1. Introduction

As the increase in the demand of alternative energies, such as solar power production, utilizing energy storage may play a pivotal role in economically cost competitive and efficient systems. Of the various approaches, latent heat thermal energy storage (LHTES) using a phase change material (PCM) is attractive for thermal systems. While sensible heat thermal energy storage is more common in current application, LHTES has a higher potential utilization due to its higher energy density, lower operating temperatures, isothermal operation and reduced size [1]. However, most PCMs have low thermal conductivities which limit the use of LHTES systems [2]. Therefore, various enhancement techniques have been proposed and implemented such as: heat transfer fins [3,4], foils (fin thickness less than 0.5 mm) [5], micro-encapsulation [6], macro-encapsulation [7], nanoparticles [8], porous media (such as metal foams and expanded graphite) [9] and heat pipes (HPs) [10,11].

The implementation of HPs into PCMs has been patented by Faghri [12,13], as they can efficiently transfer large amounts of heat passively through small cross-sectional areas [14]. The impact of HPs on the melting and solidification of a PCM has been investigated by [1,10,11,15–18]. As enhancers, HPs allow for deeper thermal penetration into the PCM which increases the effective thermal conductivity of the HP-PCM composite. Other approaches, such as embedding foam or foils into the PCM, increase the effective thermal conductivity of a PCM-enhancer composite. For example, Zhao et al. [19] reported that the overall heat transfer rates can be increased by up to 10 times with the inclusion of metal foam depending on the choice of foam and PCM. Similarly, Sugawara et al. [5] reported that installing 0.03 mm thick copper foils onto a heat transfer fluid (HTF) tube embedded in PCM can decrease the complete melting (solidification) time to a tenth (eighteenth) of that for a pure PCM system using a foil volume fraction of only 5 %. Other studies involving metallic heat transfer enhancers have shown comparable results which will not be discussed here.

However, embedding metal enhancers, such as foam or foils, into PCMs may significantly suppress the positive contribution of natural convection during melting. Hence, the increase in the overall heat transfer rates must be substantial. Since the rate of heat transfer due to conduction decreases with an

increasing distance from the heat transfer surface, the improvement in heat transfer by adding a metal enhancer decreases as the solid-liquid interface advances. Since many studies of Foam-PCM systems have been focused towards electronic cooling, small length scales perpendicular to the heat source in the range of about 15 mm to 50 mm is acceptable [19–24]. However, as the length scale from the heat source increases for larger scale systems, foams or foils may be ineffective, hence the need to increase the thermal penetration depth within the foam.

The combination of HPs and aluminum foils was first proposed by Sharifi et al [25]. The authors experimentally and numerically investigated the solidification and melting in a vertical cylindrical enclosure heated / cooled by a concentric HP which penetrated an array of horizontal foils within the PCM enclosure. Heat transfer rates were increased with a HP-Foil-PCM configuration by 3 and 9 times compared to a similar Rod-PCM system during melting and solidification, respectively, with a foil volume fraction of 1.2 %.

A similar system was further investigated by Allen et al. [26] which included the combination of a HP and aluminum foam where the foam porosities ranged from 0.870 to 0.987. The HP-Foil-PCM configuration was reported to have improved performance relative to the HP-Foam-PCM configuration. The HP-Foil-PCM configuration was capable of reducing the complete melting and solidification times from 200 min and 150 min for a Rod-PCM configuration to 13 min and 11 min, respectively. The heat transfer rates for the HP-Foil-PCM and HP-Foam-PCM configurations were increased by nearly 15 and 7 (8 and 6) times relative to the Rod-PCM configuration during melting (solidification), respectively, with a porosity of approximately 0.957 for the foil-PCM and foam-PCM composites.

At this point, the combined HP and foam or foil systems were only studied in the vertical orientation. However, if an enhancement technique is to be implemented into systems which experience varying inclination angles, such as portable electronics, it must operate regardless of its orientation. For example, Sandia National Laboratories investigated the use of a HP assisted-LHTES for use with a dish-Stirling system [27]. The authors propose attachment of the LHTES directly onto the dish which will impose a varying inclination angle with the time of day, as the dish is designed to follow the trajectory of

the sun. Further investigation by Shabgard et al. [28] revealed that exergy efficiencies greater than 97% could be achieved with finned-HPs.

In conduction-dominated systems, orientation is mainly insignificant. However, for systems involving HPs, the internal evaporation and condensation processes vary depending on the HP orientation. Also, natural convection strongly depends on the respective locations of the hot and cold mediums. Therefore, melting rates may change significantly with different orientations.

Ye et al. [29] numerically investigated the effect of system inclination angle on the melting of a paraffin ($T_m \approx 27\text{ }^{\circ}\text{C}$) in a quadrantal cavity heated from the curved wall. Without any type of heat transfer enhancement within the PCM, the complete melting time for the system heated from below was about 13 % of that compared to heating from above. In a related study, Kamkari et al. [30] experimentally melted a paraffin ($T_m \approx 45\text{ }^{\circ}\text{C}$) in a rectangular enclosure with varying tilt angles, with 0° corresponding to heating from below. The complete melting time was reduced by approximately 35 % and 53 % for the 0° and 45° orientations, respectively, relative to 90° with side wall heating. Hence, orientation angle alone may significantly alter the heat transfer rates in PCM systems due to changing natural convection flow patterns. Similar observations have been reported by [31–34].

With regards to HP-PCM systems, few have considered HP orientation with the exception of Nithyanandam and Pitchumani [35–37] and Shabgard et al. [16]. These works numerically investigated the effects of the orientation and number of HPs in a shell and tube PCM system. In [35], a case with two horizontal HPs penetrating the tube on opposite sides took about 30 % longer to melt relative to vertical HPs. While Shabgard et al. [16] observed improved heat transfer with vertical heat pipes, hence the need for a more fundamental study containing a single HP.

The improved heat transfer rates in PCM systems obtained for a combined enhancement including a HP and foam or foils in [25,26], and the contradictory results regarding the orientation of a HP-assisted PCM system motivate this work. Furthermore, in order to compare the effect of adding a HP vs. aluminum foam to a PCM, heat transfer through the base that secures the HP is essential and is implemented here. In this study, the orientation of the HP-Foil-PCM, HP-Foam-PCM, HP-PCM, Rod-

PCM, Foam-PCM and non-enhanced PCM configurations are experimentally investigated. The PCM temperature distribution, volumetric liquid fraction and photographs are acquired, while the complete phase change times and melting rates allow for a relative comparison between cases.

4.2. Experimental apparatus

A layout of the experimental apparatus is shown in Fig. 4.1. The PCM (n-octadecane, properties in Table 4.1) is contained in an acrylic tube (41 mm inner diameter, 60 mm height, and 4.6 mm wall thickness) and is subject to heat transfer from a copper disc (63 mm outer diameter, 5 mm thickness) at the base of the tube, as well as a concentrically located HP or rod further enhanced with either foam or foils. To further investigate the HP-PCM configuration without heat transfer through the base of the tube, the copper disc was replaced with the combination of an acrylic plate (5 mm thickness) and acrylic disc (50.2 mm diameter, 5 mm thick) with a 2 mm recess for air insulation were implemented in a manner consistent with [26].

A Lauda Brinkmann RE107 water bath circulator is used to circulate water as a HTF to provide the driving potential for heat transfer. The HTF is contained in an enclosure fabricated from 10 mm thick acrylic plates with overall dimensions of 140 mm \times 100 mm \times 100 mm. A HP (Fujikura: copper-water, grooved wick) or rod of length 150 mm and outer diameter 6 mm, and a copper disc of thickness 4 mm and diameter 65 mm facilitate heat transfer between the HTF and the PCM. Additionally, 25 copper foils (39 mm outer diameter, 5 mm inner diameter and 0.025 mm thickness) were press-fit onto the HP within the HTF.

The acrylic tube contained the PCM between the underlying disc (copper or acrylic) and an acrylic plate of thickness 25 mm. The acrylic plate contained a fabricated pathway leading to a network of aluminum pipes, with an outer diameter (thickness) of 14 mm (2 mm), which constructs an air chamber to accommodate the volume change of the PCM due to different solid and liquid densities. At each interface, silicone aquarium sealant was used to seal and secure each device, while four all-threaded rods compress the entire system. After assembly, the entire apparatus is placed in an acrylic enclosure of dimensions 200 mm \times 130 mm \times 300 mm to thermally insulate the system from the environment as well as allow for

visual observation of the melting and solidification processes. Additionally, fiberglass insulation (80 mm thick) was wrapped around the network of aluminum pipes which extended beyond the acrylic enclosure.

In this study, Duocel® aluminum foam (alloy 6101-T6 containing about 98 % aluminum) with a porosity (ϕ) of 0.945 (0.948) and a pore density of 20 pores per inch were utilized for the HP-Foam-PCM (Foam-PCM) configuration. Aluminum foils (alloy 8011, also with approximately 98 % aluminum content) with outer diameter 0.39 mm and thickness 0.024 mm were used in the HP-Foil-PCM configuration with $\phi = 0.945$. The foils and foam, of annular construction, had an inner diameter of 5 mm to maintain thermal contact with a concentric HP after a press-fit installation. In order to secure and thermally bond the foam to the copper disc, a thin layer of Omegabond® 101 thermal epoxy was implemented [38].

Upon melting, expansion of the PCM (mass, $m = 60 \pm 0.2$ g) causes a reduction in the air volume within the aluminum pipe network thereby increases the air pressure. To measure the air pressure change, a Sper Scientific (model PS100 – 2 bar) differential pressure transducer is attached to the air expansion chamber, collected with a pressure meter (Sper Scientific, Model 840065) and recorded using Lutron801 software.

During assembly, a total of 18 Teflon-coated, 254 μ m diameter chromel-alumel (K-type) thermocouples were inserted into through-holes in the acrylic tube at the proper radial ($r_1 = 9$ mm, $r_2 = 15$ mm), axial ($z_1 = 15$ mm, $z_2 = 30$ mm, $z_3 = 45$ mm) and polar ($\theta_1 = 0^\circ$, $\theta_2 = 90^\circ$, $\theta_3 = 180^\circ$) coordinates within the PCM domain with an estimated placement accuracy of ± 1 mm, and then secured with silicone sealant as seen in Fig. 4.1. Thermocouples were also installed on the HP in the PCM ($z = 55$ mm), on the HP in the HTF ($z = -20$ mm and $z = -80$ mm) and on the copper disc (two on both the PCM and HTF sides at $r = 12$ mm with $\theta_1 = 0^\circ$ and $\theta_3 = 180^\circ$) using a small drop of thermal epoxy (Omegabond® 101) and aluminum foil tape. A thermocouple was also installed in the air chamber and at the water inlet and outlet. Each thermocouple was calibrated using the freezing and boiling points of distilled water, and were also constructed from the same spool of wire to minimize bias errors. The thermocouple temperature

uncertainty was estimated as ± 1 °C while a National Instruments data acquisition (NI CDAQ-9172) system and LabVIEW software were used to collect and record data at 1 sec intervals, respectively.

In order to set the system inclination angle, a protractor angle finder is utilized to ensure that it is within $\pm 2^\circ$ of the desired angle. The following system inclination angles are considered: $\alpha = 0^\circ, 30^\circ, 60^\circ$ and 90° , with $\alpha = 0^\circ$ denoting the vertical orientation as seen in Fig. 4.1. To quantify the performance of each configuration, the volumetric liquid fraction is calculated using the measured air temperature and pressure change as described in [25]. To further analyze the effect of tilting, photographs were taken periodically, using a Panasonic Lumix (model: DMC-FH24) camera.

For a valid comparison between the HP-Foil-PCM and HP-Foam-PCM configurations, the porosity of the foil-PCM and foam-PCM composites must be held constant. Since the porosity of the metal foam is fixed, the mass of the foils must be adjusted to that of the foam which results in a similar metal enhancer-PCM porosity, calculated by:

$$\varphi = \frac{V_{void}}{V_{total}} = \frac{V_{pcm}}{V_{pcm} + V_{me}} \approx \frac{m_{pcm}/\rho_{pcm,s}}{m_{pcm}/\rho_{pcm,s} + m_{me}/\rho_{me}} \quad (1)$$

Note that individual foils are not porous as they are fabricated from common household aluminum foil, and the PCM occupies the region between foils.

4.3. Experimental procedure

Melting and solidification of the HP-Foil-PCM, HP-Foam-PCM, Foam-PCM, HP-PCM, Rod-PCM and non-enhanced PCM configurations were investigated in this study. As previously mentioned, the HP and rod were secured using silicone sealant, the foils and foam were press-fit onto the HP while thermal epoxy was used to secure the foam to the copper disc. A fixed mass of 60 g of PCM was degassed in a reduced pressure environment before filling the enclosure. The entire system was also shaken to remove any entrapped air within the foam or between foils. In the study, the foil-PCM and foam-PCM composites for the HP-Foil-PCM and HP-Foam-PCM configurations had a porosity of about 0.95. As previously described, the entire assembly was placed into an acrylic enclosure to isolate the system from the ambient environment and then the network of aluminum pipes (containing air) were wrapped with

fiberglass insulation. Finally, the desired system inclination angle is established using a protractor angle finder and then securing the entire system.

The initial temperature of the PCM was set as 24 °C (31 °C) during melting (solidification) for all cases by using a Lauda Brinkmann RE107 water bath circulator to provide flow and control the temperature of the HTF. After equilibration at the set point temperature, solidification (melting) was initiated by flowing water at 11 °C (45 °C) to establish a nominal driving temperature of $\Delta T = 17$ °C between the PCM melting temperature and the HTF temperature. Two additional driving temperatures of $\Delta T = 8$ °C and $\Delta T = 25$ °C were also studied which correspond to inlet HTF temperatures of 20 °C and 3 °C (36 °C and 53 °C), respectively, during solidification (melting). Each experiment is terminated once a constant differential air pressure is observed, indicating complete melting or solidification. The thermocouple and pressure transducer measurements were recorded during each experiment which allowed for determination of the liquid fraction as described in [25]. In the analysis, a PCM volume change correlates to a change in air pressure and temperature assuming that the air acts as an ideal gas and is well mixed within the aluminum pipe.

To ensure repeatability, each experiment was conducted twice with minor (approximate 1 %) differences in the liquid fraction between two distinct cases. Hence, the average measured values obtained from two experiments are presented here.

4.4. Results and discussion

The temperature distribution, photographs, liquid fraction (f_l), and time for 95 % complete melting (t_m) and solidification (t_s) are the main figures of merit used to quantify the performance of each system. Of these parameters, the liquid fraction is defined based on the change in air pressure and temperature in the same manner as [25]. An uncertainty analysis [39] is carried out in a similar manner as [25] and will not be repeated in detail. The uncertainty analysis is based on a sequential perturbation method at each time instant. The average uncertainty in liquid fraction ranged from approximately ± 0.10 to ± 0.15 . From the liquid fraction histories, a few additional parameters may be defined including a relative effectiveness, melting rate and time ratio for 95 % complete phase change.

With respect to the base case of the non-enhanced PCM configuration, the relative effectiveness at 95 % complete phase change is defined as:

$$\varepsilon_m = \frac{f_l(t_m)}{f_{l,bc}(t_m)} \quad (2)$$

$$\varepsilon_s = \frac{1 - f_l(t_s)}{1 - f_{l,bc}(t_s)} \quad (3)$$

Similar to [26], the period pertaining to 95 % phase change provides a more relevant time instant since the outer diameter of the foils and foam is slightly less than that of the inner diameter of the acrylic tube containing the PCM and end effects are not of interest.

An additional figure of merit is the melting rate. Since the liquid fraction histories are fairly linear for the range of conditions studied, with the exception of the HP-PCM, Rod-PCM and Foam-PCM cases with $\alpha = 90^\circ$, the melting rate may be defined as:

$$r_m = \frac{m_{pcm}}{t_m} \quad (4)$$

Note that a solidification rate could be similarly defined as Eq. (5), however, it is not a good measure of performance as the liquid fraction history is non-linear due to the conduction-dominated heat transfer, as will be shown later.

The final figure of merit which will be used in this work is the time ratio (t/t_{bc}) for 95 % complete phase change. This value can be compared between each configuration and the base case defined as:

$$\left(\frac{t}{t_{bc}}\right)_m = \frac{t_m}{t_{m,bc}} \quad (5)$$

$$\left(\frac{t}{t_{bc}}\right)_s = \frac{t_s}{t_{s,bc}} \quad (6)$$

The magnitude of the time ratio indicates the percentage of time in which a particular configuration melts or solidifies relative to the non-enhanced PCM case. Overall, the liquid fraction, temperature distribution, effectiveness, phase change rates and time for 95 % complete phase change allow for comparison to determine which configuration and orientation is preferred.

4.4.1 Temperature distribution in the PCM

The measured local temperatures are presented in Fig. 4.2 through Fig. 4.4. In these figures, the open and filled markers represent the temperature at a radius of $r_1 = 9$ mm and $r_2 = 15$ mm, respectively. Note that in the following figures, the dashed line represents the HP temperature at $z = 55$ mm, and the solid line represents the average temperature between two thermocouple measurements on the copper disc at $\theta_1 = 0^\circ$ and $\theta_3 = 180^\circ$ on the PCM side at $r = 12$ mm. During melting with $\alpha = 0^\circ$ and all cases of solidification, a high degree of symmetry was observed and each (r, z) location in Fig. 4.2 and Fig. 4.3 and each value presented represents the average value between the 3 polar (θ) locations as seen in Fig. 4.1 (b).

The temperature distribution during solidification is presented with $\alpha = 0^\circ$ for the Foam-PCM, HP-PCM and HP-Foam-PCM cases in Fig. 4.2. The Foam-PCM configuration in Fig. 4.2 (a) displays a one-dimensional solidification front that advances axially from the copper disc, as indicated by the convergence of the inner and outer radii locations at the same axial location. In the HP-PCM case, the HP acts to increase the available heat transfer surface area in contact with the PCM as observed by the similar temperature between the HP and copper disc in Fig. 4.2 (b). The effect of heat transfer through the copper disc is observed by the sooner indication of solidification for the thermocouple locations at $z_1 = 15$ mm (square symbols) at the $r_2 = 15$ mm prior to the other axial locations. However, heat transfer through the HP is shown to be dominant as the last two thermocouple locations infer solidification at a similar time. When foam is added onto the HP for the HP-Foam-PCM configuration in Fig. 4.2 (c), a similar solidification phenomenon is observed as for the HP-PCM case except that the higher thermal conductivity of the enhancer-PCM composite results in a faster solidification rate.

Representative temperature histories during melting for the Foam-PCM, HP-PCM and HP-Foil-PCM cases with $\alpha = 0^\circ$ are presented in Fig. 4.3. The Foam-PCM case exhibits a one-dimensional melting front that advances axially from the copper disc, as seen in Fig. 4.3 (a). Natural convection-dominated heat transfer for the HP-PCM case is inferred from Fig. 4.3 (b) since the uppermost thermocouple locations (circles) melt prior to those at the mid-height (triangles); especially since melting occurs at $(r_2 =$

15 mm, $z_3 = 45$ mm) prior to ($r_1 = 9$ mm, $z_2 = 30$ mm). For the HP-Foam-PCM case, a conduction-dominated melting process is inferred from the temperature distribution in Fig. 4.3 (c). Natural convection is severely suppressed in the foam, since the thermocouple locations infer melting with increasing axial and radial locations rather than the uppermost thermocouple locations melting prior to the lower locations. The combination of the HP with foam allows for the HP to transfer heat further into the PCM which is then dispersed in a conduction-dominated manner within the foam-PCM composite.

In Fig. 4.2 and Fig. 4.3 with $\alpha = 0^\circ$, the average values for each (r, z) position are displayed since symmetry about the central axis was present. However, when $\alpha = 90^\circ$, three-dimensional melting is present. In Fig. 4.4, the temperature distribution for the HP-Foil-PCM (left) and HP-Foam-PCM (right) cases with $\alpha = 90^\circ$ are presented at (a) $z_1 = 15$ mm, (b) $z_2 = 30$ mm and (c) $z_3 = 45$ mm.

In Fig. 4.4, a few key distinctions can be noted for both configurations. First, the temperature gradient at each axial location is approximately 3 °C for the HP-Foil-PCM case and may be greater than 10 °C for the HP-Foam-PCM case. Another discrepancy is noted by comparing the solid and dotted lines for the temperature of the copper disc and the HP within the PCM, respectively. These values are similar for the HP-Foam-PCM case with the temperature of the copper disc being slightly less (within 1 °C after the first 10 min) than the HP temperature in the PCM, indicating a greater amount of heat transfer from the disc. Yet, for the HP-Foil-PCM configuration the opposite is observed, indicating higher heat transfer through the HP. Also, the order in which each (r, z) location surpasses the melting temperature indicates that heat transfer through the HP is dominant relative to the disc for the HP-Foil-PCM.

As mentioned previously, there are two distinct methods in which heat transfer rates are improved for PCM systems that consist of increasing thermal penetration or thermal diffusion. By combining a HP with foils or foam, heat transfer rates are shown to be drastically improved relative to each enhancement individually. Since solidification is many conduction-dominated, orientation is rather insignificant, however, orientation may significantly affect melting due to varying natural convection currents. However, inclusion of metal enhancers, such as foils or foam, may significantly suppress natural convection which renders orientation as less significant.

4.4.2 Photographic observations

Photographic observations during solidification and melting allow for a fundamental understanding of each process. The influence of system inclination angle during melting is observed in this section for the HP-PCM, Rod-PCM and non-enhanced PCM configurations. Each photograph is taken from the right side view as indicated in Fig. 4.1 (b) and is parallel to the cross section view containing the plane of symmetry in Fig. 4.1 (a). It should be noted that the brightness and contrast of each black-and-white photo has been adjusted to provide a clear distinction between the white solid PCM and transparent liquid PCM. The silicone that was used to seal and secure the thermocouples at $\theta_2 = 90^\circ$ on the back of the acrylic tube also appear somewhat white in each photograph. However, upon inspection, the solid-liquid interface is more distinct and is easily discernible for most of the photographs. Lastly, the aluminum foil tape utilized to secure the TCs to the HP after the application of the thermal epoxy also appears in the photographs at the tip and base of the HP and rod. The original intent was to measure the temperature at the base of the HP or rod, however, problems relating to that specific thermocouple location resulted in omission of the measurements at that location.

Photographs during solidification for the (a) HP-PCM, (b) Rod-PCM and (c) non-enhanced PCM cases at $t = 15$ min (left) and $t = 30$ min (right) with $\alpha = 0^\circ$ are seen in Fig. 4.5. Experimental measurements indicate that the orientation has minimal influence during solidification, therefore, only the vertical orientation is presented for brevity. The solidification front which advances from the copper base is shown to be relatively similar for each case which indicates a similar degree of heat transfer. Therefore, the increase in heat transfer surface area by adding the HP or rod, results in a greater amount of solidification relative to the non-enhanced PCM case. It can also be seen that the HP is superior to the rod by the larger, more uniform radius of solid PCM at all axial distances for the HP in Fig. 4.5 (a), while the rod has a conical shape that slightly decreases in diameter at increasing axial locations in Fig. 4.5 (b). As time progresses from $t = 15$ min (left) and $t = 30$ min (right), both solidification fronts independently advance in the HP-PCM and Rod-PCM configurations, as seen in Fig. 4.5 (a) and (b).

In Fig. 4.6, photographs during melting are presented for the (a) HP-PCM, (b) Rod-PCM and (c) non-enhanced PCM configurations at $t = 60$ min with $\alpha = 0^\circ$ (left) and $\alpha = 90^\circ$ (right). The inclination angle is shown to influence the shape of the solid-liquid interface in each case due to the complex three-dimensional natural convection currents. The effect of symmetry about the center of the tube is seen for the vertical cases, however, for all non-vertical cases, only symmetry about the plane of Fig. 4.1 (a) is observed. It is interesting to note that the solid-liquid interfaces closest to the copper disc is similar for the Rod-PCM and non-enhanced PCM cases with $\alpha = 0^\circ$ and $\alpha = 90^\circ$ in Fig. 4.6. Inclusion of the HP or rod increases the rate of melting by increasing the overall heat transfer surface area in contact with the PCM and allows for natural convection to provide an additional downward melting front relative to the non-enhanced case.

The effect of system inclination angle during melting for the HP-PCM configuration can be seen in Fig. 4.7 with 30 min intervals. For each case, natural convection significantly alters the solid-liquid interfaces. The accumulation of warmer PCM at the top of the enclosure results in an additional downward melting front which is not present during solidification. This interface is clear for each case by the upper horizontal solid-liquid interface. For $\alpha = 0^\circ$ (left), melting is symmetric about the center of the HP as observed by the similar axial height of each upper and lower solid liquid interface while for all other inclination angles, only plane symmetry is observed through the plane containing the cross section in Fig. 4.1 (a). This figure clearly emphasizes the need for investigating the influence of system inclination angle as each orientation experiences a unique three-dimensional solid-liquid interface.

It is common knowledge that base heated PCM systems are preferred relative to side heated systems. Therefore, the enhancement in natural convection from the heated disc is most beneficial when it is located below the PCM with $\alpha = 0^\circ$ as perceived by the completion of melting by $t = 90$ min and not for $\alpha = 90^\circ$. On the other hand, heat transfer from the HP, and also rod, may be more beneficial when in a horizontal orientation by a resulting thinner thermal boundary layer. However, in Fig. 4.7 (b), it can be seen that after about $t = 60$ min for each non-vertical case, all the remaining solid PCM resides below the HP. Therefore, the HP is less effective as it cannot provide natural convection currents which aid further

melting. Further, in Fig. 4.7 (c), these regions are shown to be melted by the copper disc that is in a relatively lower position compared to the location of the solid PCM. Yet, for the horizontal orientation, neither the HP nor the copper disc can effectively melt the PCM and the remaining PCM melts in a conduction-dominated manner.

4.4.3 Liquid fraction histories

While temperature profile histories and photographs aid the explanation of the physical phenomena that occurs during phase change, they cannot provide detailed information as to the actual amount of PCM which has melted or solidified until complete phase change occurs. Hence the need to determine the liquid fraction histories is of the utmost importance to investigate PCM systems, since it can be related to the stored latent energy. By monitoring the change in air pressure and temperature and assuming it acts as an ideal gas, the liquid fraction can ultimately be calculated in a similar manner as [25]. Again, the sequential perturbation method [39] is utilized to quantify the uncertainty in liquid fraction, which was less than approximately ± 0.15 for all cases in this experiment.

The effects of system inclination angle and heat transfer through the copper disc during solidification and melting for the HP-PCM configuration with $\Delta T = 17^\circ\text{C}$ are presented in Fig. 4.8. As expected, system inclination angle during solidification is insignificant with an average variation in liquid fraction of less than $\Delta f_l = 0.03$. Heat transfer through the copper disc decreased the average time for 95 % complete solidification (for each α) from $t_s = 112$ min with an acrylic disc to $t_s = 82$ min with a copper disc. However, during melting, natural convection may significantly change the melting rates depending on the respective locations of the heated base and solid PCM. With heat transfer through a copper disc (open symbols), the liquid fraction with $\alpha = 90^\circ$ reached a liquid fraction that was approximately $\Delta f_l = 0.09$ higher than with $\alpha = 0^\circ$ until all the solid PCM remained below the horizontal HP. Also note that for $\alpha = 30^\circ$ and $\alpha = 60^\circ$, the liquid fraction histories lie between the two extreme cases with $\alpha = 0^\circ$ and $\alpha = 90^\circ$. Therefore, the cases with $\alpha = 30^\circ$ and $\alpha = 60^\circ$ will not be further presented for brevity.

When the copper disc was replaced with an acrylic disc to minimize heat transfer, the liquid fraction with $\alpha = 90^\circ$ was higher than $\alpha = 0^\circ$ by a value of $\Delta f_l = 0.20$ (filled symbols) as seen in Fig. 4.8.

Therefore, the underlying principle here is that as the HP length increases, the effect of heat transfer through the medium securing the HP, such as a plate or tube, becomes insignificant. Therefore, when a HP is embedded in a PCM without any additional enhancer, such as foils or foam, it may be beneficial in a horizontal rather than vertical configuration.

By comparing the HP-PCM cases with the same inclination angle in Fig. 4.8, the copper disc achieves a liquid fraction that is higher than an acrylic disc by approximately $\Delta f_l = 0.35$ with $\alpha = 0^\circ$ and only $\Delta f_l = 0.12$ with $\alpha = 90^\circ$ at the time corresponding to $f_l = 0.80$. Hence, the effect of heat transfer through the copper disc during melting is very significant for the vertical case and has a lower impact on the overall melting rate for the horizontal case.

In Fig. 4.9, the liquid fraction histories during solidification for the HP-Foil-PCM, HP-Foam-PCM, HP-PCM, Rod-PCM, Foam-PCM and non-enhanced PCM cases with vertical and horizontal orientations are presented. The effect of driving temperature between the HTF and PCM is investigated with the triangle, square and circle symbols representing values of 8 °C, 17 °C and 25 °C, respectively. The solid and open symbols for each driving temperature represent the vertical ($\alpha = 0^\circ$) and horizontal ($\alpha = 90^\circ$) orientations, respectively.

A quick observation of Fig. 4.9 reveals that nearly all cases have a similar overall shape where the solidification rate decreases with time. The decreasing solidification rate for all configurations is the result of the constantly increasing distance between the heat transfer surfaces (disc and HP or rod) and the solid-liquid interface which renders the overall (95 %) solidification rate meaningless. For the most part, the effect of orientation is negligible during solidification except for the HP-Foil-PCM case with $\Delta T = 17$ °C and $\Delta T = 25$ °C. For all other configurations and driving temperatures, the convergence is explained by the conduction-dominated nature of solidification. However, the non-converged liquid fraction histories for these two HP-Foil-PCM cases may be attributed to the performance of the HP, mainly its heat transfer throughput and orientation.

The rate of heat transfer through the HP is identified since it only appears for the HP-Foil-PCM configuration with the two fastest solidification times of all cases studied. Yet, the same configuration

with $\Delta T = 8\text{ }^{\circ}\text{C}$ (triangles) exhibits converged solidification liquid fraction histories with a lower solidification rate.

The second attribute affecting the non-converged liquid fraction is the specific orientation of the HP and its resulting operation. During solidification with $\alpha = 0^{\circ}$, the HP evaporator is situated above its condenser causing the capillary forces within the wick to act in opposition to gravity. At higher heat transfer rates, the pumping requirement of the internal wick increases which may ultimately reach its capillary limit. This argument is justifiable since solidification is conduction dominated and the horizontal orientation has an appreciably higher performance of $\Delta f_l = 0.09$ ($\Delta f_l = 0.06$) with $\Delta T = 25\text{ }^{\circ}\text{C}$ ($\Delta T = 17\text{ }^{\circ}\text{C}$). While the capillary forces in the horizontal HP with $\alpha = 90^{\circ}$ do not oppose gravity, they do not act against it either, which would result in less flow resistance for the return of the working fluid to the HP evaporator, and therefore higher performance compared to $\alpha = 0^{\circ}$.

The liquid fraction histories during melting are shown in Fig. 4.10 for each configuration with $\Delta T = 17\text{ }^{\circ}\text{C}$. Unlike solidification, most cases do not have a converged liquid fraction since the system orientation affects the natural convection currents during melting. The HP-Foil-PCM and HP-Foam-PCM configurations show a similar trend during melting where a slightly higher liquid fraction of $\Delta f_l = 0.03$ and $\Delta f_l = 0.05$, respectively, is observed with $\alpha = 0^{\circ}$ compared to $\alpha = 90^{\circ}$. Since natural convection is greatly suppressed for these two configurations, this difference is most likely attributed to gravity assisting the return of the internal working fluid of the HP with $\alpha = 0^{\circ}$ as the HP evaporator is situated below its condenser.

A similar overall profile is observed in Fig. 4.10 for the liquid fraction history for the HP-PCM and Rod-PCM configurations during melting. At each driving temperature, the horizontal case has a higher liquid fraction history by approximately $\Delta f_l = 0.09$ until a liquid fraction of about $f_l = 0.8$ where it suddenly decreases and is surpassed by the vertical case. Once the liquid fraction reaches this critical value, all the remaining solid PCM resides below the HP or rod when $\alpha = 90^{\circ}$, as seen in Fig. 4.7 (b). As previously stated, the effect of natural convection no longer aids the melting process after $f_l = 0.80$ since the higher temperature PCM rises further away from the solid PCM.

The Foam-PCM configuration has a similar liquid fraction history during solidification (melting) for each orientation as seen in Fig. 4.9 (e) (Fig. 4.10 (e)). The rate of phase change monotonically decreases with time. Note that for all cases except the Foam-PCM case with $\alpha = 0^\circ$, the system is first solidified and subsequently melted in the same orientation angle. However, for this specific case, the lack of air pressure change observed by the pressure transducer during melting was circumvented by solidifying the system with $\alpha = 90^\circ$ prior to melting with $\alpha = 0^\circ$. This approach allowed for a small air gap to form at the top of the horizontal tube with $\alpha = 90^\circ$ as the PCM solidified which provided a pathway for the liquid PCM to occupy as the overall PCM volume expands during melting with $\alpha = 0^\circ$. Therefore, this case is not entirely consistent with all other configurations, yet, its results indicate that the orientation has little effect since it is mainly conduction-dominated. Note that a slightly higher liquid fraction is expected for $\alpha = 0^\circ$ since heating from below is beneficial to side wall heating for $\alpha = 90^\circ$, however, the difference would be insignificant relative to all other configurations.

The liquid fraction histories for the non-enhanced PCM configuration can be seen in Fig. 4.10 (f). Throughout the entire domain for $\alpha = 0^\circ$, buoyancy induced natural convection circulates liquid PCM between the heated disc and the cooler solid PCM, causing a favorable heat transfer gradient. Side wall heating, on the other hand, for $\alpha = 90^\circ$ is not as effective since conduction-dominated melting follows the natural convection-dominated regime due to an unfavorable buoyancy induced temperature gradient. This configuration demonstrates the improvement in performance, which can be achieved by a proper design that effectively utilizes natural convection by heating the PCM from below.

4.4.4 Performance comparison for each heat transfer enhancement technique

The liquid fraction histories for each configuration are presented with $\alpha = 0^\circ$ and $\alpha = 90^\circ$ in Fig. 4.11 with $\Delta T = 17^\circ\text{C}$. For the conditions considered here, examination of Fig. 4.11 reveals that the degree of enhancement can be separated into three main regions: (i) non-enhanced, (ii) single enhancement and (iii) combined enhancement. The inherent need for a heat transfer enhancement technique in PCM systems can be seen for the non-enhanced PCM configuration, particularly for solidification. When a HP, rod or foam is implemented to increase heat transfer rates, phase change occurs faster with the highest

performance for the HP-PCM configuration. When the HP was combined with the foils or foam, the degree of enhancement can be further increased by a considerable amount.

While these same conclusions were obtained for the vertical orientation in [26], the Foam-PCM and non-enhanced PCM configurations as well as the effect of system orientation are also considered here. The liquid fraction histories for the Foam-PCM configuration are shown to be similar to the Rod-PCM configuration in Fig. 4.11. Therefore, the contribution of foam on the enhancement in melting rates is not nearly as significant as reported by others which may be attributed to the larger length scale than many which have been studied previously. Its degree of enhancement during melting is also improved for the $\alpha = 0^\circ$ case relative to the $\alpha = 90^\circ$ case since heating from below is considerably effective for melting PCM. It is interesting to note that a nearly converged liquid fraction history is obtained for the HP-PCM, Rod-PCM, and Foam-PCM cases with $\alpha = 90^\circ$ with an average variation of about $\Delta f_l = 0.05$ during melting.

In general, the effect of heat transfer through the copper disc is more significant for the HP-Foam-PCM configuration relative to the HP-Foil-PCM configuration with $\alpha = 0^\circ$. This is attributed to the orientation of the foils being parallel to the disc resulting in highly two-dimensional (r, θ) heat transfer, while the foam is more accommodating to three-dimensional heat transfer from both the base and HP. During the initial 5 min of operation, especially for $\Delta T = 25^\circ\text{C}$ in Fig. 4.10 at $\alpha = 0^\circ$ (filled circles), the HP-Foam-PCM configuration has a higher liquid fraction than the HP-Foil-PCM configuration with the same driving temperature and orientation. This may be attributed to either superior operation of the HP in the vertical orientation as discussed previously, or that natural convection within the foam is somewhat significant at the onset of melting which decreases shortly due to the high flow resistance within the foam.

4.4.5 Average melting rates

As previously mentioned, the solidification rates do not merit comparison between distinct cases since the liquid fraction histories are non-linear, as observed in Fig. 4.9. On the other hand, the liquid fraction histories during melting with $\alpha = 0^\circ$, and melting rates for the HP-Foil-PCM, HP-Foam-PCM and non-enhanced PCM configurations with $\alpha = 90^\circ$ are fairly linear up to $f_l = 0.95$. These melting rates are

calculated with Eq. (4) and the results are summarized in Table 4.2. It may be seen that the melting rate for the HP-Foil-PCM cases are 8.5 and 9.5 times that of the non-enhanced PCM cases with $\alpha = 0^\circ$ and $\alpha = 90^\circ$, respectively.

4.4.6 Effectiveness at 95 % complete phase change

In the previous studies regarding the HP-Foil-PCM configurations [25,26], the base case was the Rod-PCM configuration. However, in this work, the base case is the non-enhanced PCM configuration which has longer overall melting and solidification times. Using the non-enhanced PCM configuration rather than the Rod-PCM configuration as the base case increases the uncertainty in effectiveness since the time duration of the HP-Foil-PCM configuration is only a small fraction compared to the non-enhanced PCM configuration. Therefore, rather than displaying the effectiveness as a function of time, the effectiveness (ε_m and ε_s) will only be presented at the time of 95 % complete phase change (t_m and t_s), and is presented in Table 4.2 and Fig. 4.12 (circle symbols).

The highest effectiveness is achieved for the HP-Foil-PCM configuration with a value of 5.7 and 11.9 (5.3 and 9.4) with $\alpha = 0^\circ$ ($\alpha = 90^\circ$) during melting and solidification, respectively. Therefore, the combination of the HP and foils are approximately 70 %, 370 %, 450 % and 670 % (45 %, 150 %, 180 % and 220 %) more effective during melting (solidification) for each orientation than the HP-Foam-PCM, HP-PCM, Rod-PCM and Foam-PCM configurations, respectively.

The effectiveness during melting is seen to be considerably larger than during solidification and can be understood by examining Eqs. (2) and (3) along with Fig. 4.11. The liquid fraction for the non-enhanced PCM configuration during melting is much lower than during solidification since it is initially conduction-dominated and the liquid PCM has a lower thermal conductivity. For example, the liquid fraction for the HP-Foil-PCM and non-enhanced PCM configurations with $\alpha = 0^\circ$ during solidification (melting) is approximately 0.05 and 0.80 (0.95 and 0.08) at $t = 13$ min ($t = 16$ min), respectively. Hence, the solidification and melting effectiveness is 5.7 and 11.9, respectively, for the HP-Foil-PCM configuration with $\alpha = 0^\circ$ and $\Delta T = 17$ °C. Overall, for the range of conditions studied here, an increase (decrease) in driving temperature increases (decreases) the effectiveness as expected.

4.4.7 Time ratio for complete phase change

An additional figure of merit to compare distinct cases is the ratio of times for each case to reach 95 % phase change (t_m , t_s) relative to that of the non-enhanced PCM case defined in Eqs. (5) and (6). In Fig. 4.12, the square markers denote the time ratio during melting $(t/t_{bc})_m$ and solidification $(t/t_{bc})_s$ with $\Delta T = 17$ °C for each case. The figure shows that $(t/t_{bc})_m$ and $(t/t_{bc})_s$ are approximately 0.11 and 0.03 for the HP-Foil-PCM case regardless of orientation. Therefore, the complete melting and solidification times for the HP-Foil-PCM configuration are approximately 11 % and 3 % of the total time for the non-enhanced PCM (HP-PCM) configuration, respectively, regardless of orientation. The values for each configuration may be seen in Table 4.2.

4.5. Conclusions

Experiments were conducted to investigate the effect of system inclination angle for a cylindrical PCM system with heat transfer through both an underlying copper disc and a HP or rod, while the HP was further enhanced with aluminum foam or foils. Experimental results for the liquid fraction, temperature distribution and photographs are presented to analyze both melting and solidification. A total of 6 configurations and 28 case studies were investigated with varying orientation and driving temperatures. During solidification, orientation was insignificant, with the exception of the HP-Foil-PCM configuration, due to conduction-dominated heat transfer. The orientation of the HP-Foil-PCM configuration was dependent on the internal operation of the HP in which a capillary limit was most likely being approached. This variation is due to the HP evaporator being positioned above its condenser during solidification with $\alpha = 0^\circ$, which increases with an increase in the heat transfer throughput.

During melting for the HP-PCM, Rod-PCM and non-enhanced PCM configurations, varying natural convection currents with orientation significantly change the melting rates. A notable finding for the HP-PCM and Rod-PCM configurations is that the liquid fraction in a horizontal case was increased by $\Delta f_l = 0.09$ ($\Delta f_l = 0.20$) relative to a vertical case with (without) heat transfer through the copper disc until the remaining solid PCM resided below the horizontal HP or rod.

For the HP-Foil-PCM and HP-Foam-PCM configurations, the average variation in liquid fraction between the vertical and horizontal orientations is $\Delta f_l = 0.03$ and $\Delta f_l = 0.05$ ($\Delta f_l = 0.07$ and $\Delta f_l = 0.01$) during melting (solidification), respectively. This variation is mostly attributed to the operation of the HP, which is preferred to be vertical to allow for gravity to assist in the return of the internal HP working fluid to the HP evaporator. However, when the complete melting and solidification times of each configuration are considered, the improvement in performance of the HP-Foil-PCM and HP-Foam-PCM significantly outweigh the slight variation due to orientation which makes these combinations promising heat transfer enhancement methods for use in LHTES systems. In this study, the HP-Foil-PCM configuration with porosity 0.945 and driving temperature of 17 °C was capable of increasing the melting rates by about 9 times and reducing the total solidification and melting times to about 3 % and 11 % percent that of the non-enhanced PCM configuration regardless of orientation.

Nomenclature

c_p	specific heat (J/kg·K)
f_l	liquid fraction
Δf_l	difference in liquid fraction
h_{sl}	latent heat of fusion (kJ/kg)
k	thermal conductivity (W/m·K)
L	length (mm)
m	mass (g)
r	radial coordinate (mm)
r_m	melting rate (g/min)
T	temperature (°C)
ΔT	driving temperature: the temperature difference between the heat transfer fluid and the phase change material (°C)
t	time (min)
t_m	time for 95 % complete melting (min)
t_s	time for 95 % complete solidification (min)
z	axial coordinate (mm)

Greek symbols

α	inclination angle measured from vertical (°)
φ	porosity
ε_m	melting effectiveness at $f_l = 0.95$

ε_s	solidification effectiveness at $f_l = 0.05$
θ	polar coordinate angle (°)
ρ	density (kg/m ³)
μ	dynamic viscosity (Pa·s)

Subscripts

l	liquid
m	melting
s	solidification, solid
bc	base case
pcm	phase change material

Acronyms

HP	heat pipe
HTF	heat transfer fluid
LHTES	latent heat thermal energy storage
PCM	phase change material

References

- [1] C.W. Robak, T.L. Bergman, A. Faghri, Economic evaluation of latent heat thermal energy storage using embedded thermosyphons for concentrating solar power applications, *Sol. Energy*. 85 (2011) 2461–2473.
- [2] F. Agyenim, N. Hewitt, P. Eames, M. Smyth, A review of materials, heat transfer and phase change problem formulation for latent heat thermal energy storage systems (LHTESS), *Renew. Sustain. Energy Rev.* 14 (2010) 615–628.
- [3] A. A. Al-Abidi, S. Mat, K. Sopian, M.Y. Sulaiman, A.T. Mohammad, Numerical study of PCM solidification in a triplex tube heat exchanger with internal and external fins, *Int. J. Heat Mass Transf.* 61 (2013) 684–695.
- [4] N. Sharifi, T.L. Bergman, A. Faghri, Enhancement of PCM melting in enclosures with horizontally-finned internal surfaces, *Int. J. Heat Mass Transf.* 54 (2011) 4182–4192.
- [5] M. Sugawara, Y. Komatsu, Y. Takahashi, H. Beer, Freezing enhancement around a horizontal tube using copper foil disks, *Heat Mass Transf.* 47 (2011) 1691–1698.
- [6] C. Alkan, A. Sari, A. Karaipekli, Preparation, thermal properties and thermal reliability of microencapsulated n-eicosane as novel phase change material for thermal energy storage, *Energy Convers. Manag.* 52 (2011) 687–692.

- [7] N. Calvet, X. Py, R. Olivès, J.-P. Bédécarrats, J.-P. Dumas, F. Jay, Enhanced performances of macro-encapsulated phase change materials (PCMs) by intensification of the internal effective thermal conductivity, *Energy*. 55 (2013) 956–964.
- [8] C.J. Ho, J.Y. Gao, Preparation and thermophysical properties of nanoparticle-in-paraffin emulsion as phase change material, *Int. Commun. Heat Mass Transf.* 36 (2009) 467–470.
- [9] Y. Tian, C.Y. Zhao, Thermal and exergetic analysis of metal foam-enhanced cascaded thermal energy storage (MF-CTES), *Int. J. Heat Mass Transf.* 58 (2013) 86–96.
- [10] C.W. Robak, T.L. Bergman, A. Faghri, Enhancement of latent heat energy storage using embedded heat pipes, *Int. J. Heat Mass Transf.* 54 (2011) 3476–3484.
- [11] N. Sharifi, S. Wang, T.L. Bergman, A. Faghri, Heat pipe-assisted melting of a phase change material, *Int. J. Heat Mass Transf.* 55 (2012) 3458–3469.
- [12] A. Faghri, Thermal Energy Storage Heat Exchanger, US Patent #4976308, 1990.
- [13] A. Faghri, Micro Heat Pipe Energy Storage System, US Patent #5000252, 1991.
- [14] A. Faghri, Heat Pipe Science and Technology, Taylor & Francis Group, Washington, D.C., 1995.
- [15] X. Gui, D. Tang, S. Liang, X. Yuan, Influence of radial thickness of phase change material on thermal performance of heat pipe receiver under microgravity, *Heat Transf. Eng.* 34 (2013) 608–616.
- [16] H. Shabgard, T.L. Bergman, N. Sharifi, A. Faghri, High temperature latent heat thermal energy storage using heat pipes, *Int. J. Heat Mass Transf.* 53 (2010) 2979–2988.
- [17] H. Shabgard, C.W. Robak, T.L. Bergman, A. Faghri, Heat transfer and exergy analysis of cascaded latent heat storage with gravity-assisted heat pipes for concentrating solar power applications, *Sol. Energy*. 86 (2012) 816–830.
- [18] Z. Liu, Z. Wang, C. Ma, An experimental study on the heat transfer characteristics of a heat pipe heat exchanger with latent heat storage. Part II: Simultaneous charging/discharging modes, *Energy Convers. Manag.* 47 (2006) 967–991.
- [19] C.Y. Zhao, W. Lu, Y. Tian, Heat transfer enhancement for thermal energy storage using metal foams embedded within phase change materials (PCMs), *Sol. Energy*. 84 (2010) 1402–1412.
- [20] K. Lafdi, O. Mesalhy, S. Shaikh, The effect of surface energy on the heat transfer enhancement of paraffin wax/carbon foam composites, *Carbon N. Y.* 45 (2007) 2188–2194.
- [21] O. Mesalhy, K. Lafdi, A. Elgafy, Carbon foam matrices saturated with PCM for thermal protection purposes, 44 (2006) 2080–2088.
- [22] Z.G. Qu, W.Q. Li, J.L. Wang, W.Q. Tao, Passive thermal management using metal foam saturated with phase change material in a heat sink, *Int. Commun. Heat Mass Transf.* 39 (2012) 1546–1549.

- [23] S.-T. Hong, D.R. Herling, Open-cell aluminum foams filled with phase change materials as compact heat sinks, *Scr. Mater.* 55 (2006) 887–890.
- [24] W.Q. Li, Z.G. Qu, Y.L. He, W.Q. Tao, Experimental and numerical studies on melting phase change heat transfer in open-cell metallic foams filled with paraffin, *Appl. Therm. Eng.* 37 (2012) 1–9.
- [25] N. Sharifi, T. Bergman, A. Faghri, M.J. Allen, Melting and solidification enhancement using heat pipe with foils, *Int. J. Heat Mass Transf.* (2014) Submitted.
- [26] M.J. Allen, A. Faghri, T.L. Bergman, N. Sharifi, Robust heat transfer enhancement during melting and solidification of a pcm using a combined heat pipe-metal foam or foil configuration, *J. Heat Transfer.* (2014) Submitted.
- [27] C.E. Andraka, K.S. Rawlinson, N.P. Siegel, Technical feasibility of storage on large dish Stirling systems, 2012.
- [28] H. Shabgard, A. Faghri, T.L. Bergman, C.E. Andraka, Numerical simulation of heat pipe-assisted latent heat thermal energy storage unit for dish-stirling systems, *J. Sol. Energy Eng.* 136 (2014) 021025–1–12.
- [29] W.-B. Ye, D.-S. Zhu, N. Wang, Effect of the inclination angles on thermal energy storage in a quadrantal cavity, *J. Therm. Anal. Calorim.* 110 (2012) 1487–1492.
- [30] B. Kamkari, H. Shokouhmand, F. Bruno, Experimental investigation of the effect of inclination angle on convection-driven melting of phase change material in a rectangular enclosure, *Int. J. Heat Mass Transf.* 72 (2014) 186–200.
- [31] N. Sharifi, C.W. Robak, T.L. Bergman, A. Faghri, Three-dimensional PCM melting in a vertical cylindrical enclosure including the effects of tilting, *Int. J. Heat Mass Transf.* 65 (2013) 798–806.
- [32] A. Hasan, Phase change material energy storage system employing palmitic acid, *Sol. Energy.* 52 (1994) 1994.
- [33] K. Sasaguchi, A. Ishihara, H. Zhang, Numerical study on utilization of melting of phase change material for cooling of a heated surface at a constant rate, *Numer. Heat Transf. Part* 29 (1996) 19–31.
- [34] B.W. Webb, R. Viskanta, Natural-convection dominated melting heat transfer in an inclined rectangular enclosure, *Int. J. Heat Mass Transf.* 29 (1986) 183–192.
- [35] K. Nithyanandam, R. Pitchumani, Computational studies on a latent thermal energy storage system with integral heat pipes for concentrating solar power, *Appl. Energy.* 103 (2013) 400–415.
- [36] K. Nithyanandam, R. Pitchumani, Analysis and optimization of a latent thermal energy storage system with embedded heat pipes, *Int. J. Heat Mass Transf.* 54 (2011) 4596–4610.

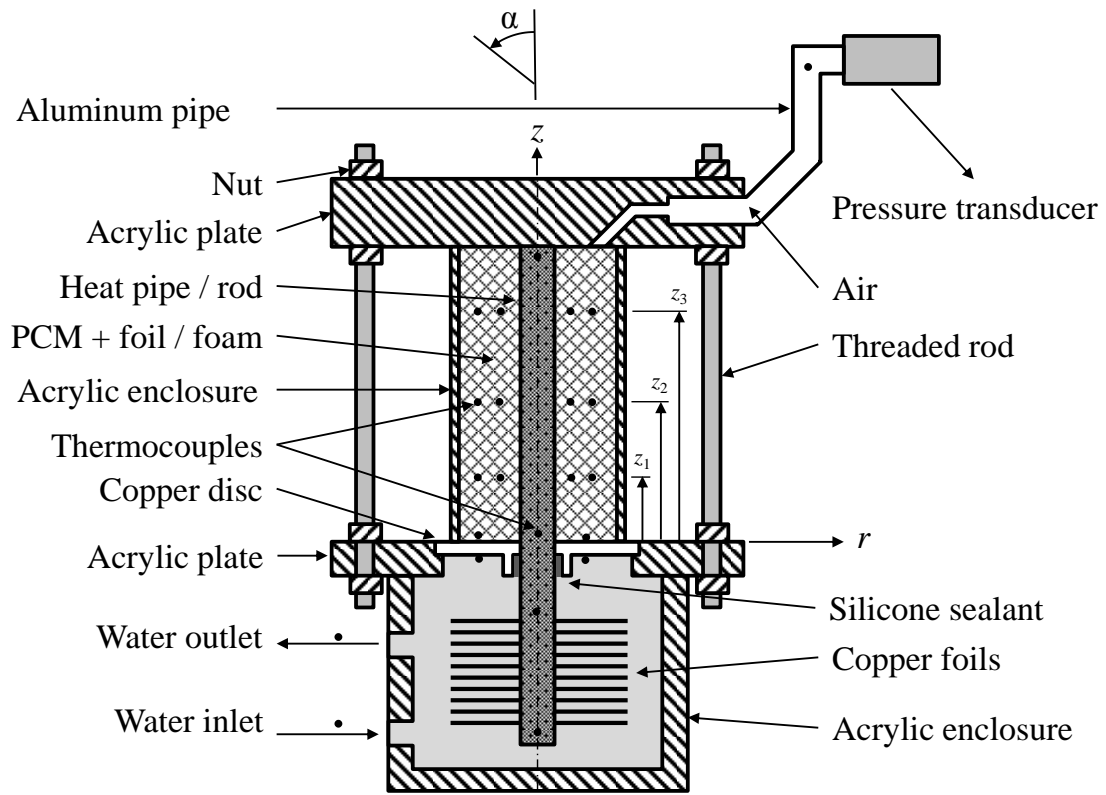
- [37] K. Nithyanandam, R. Pitchumani, Thermal energy storage with heat transfer augmentation using thermosyphons, *Int. J. Heat Mass Transf.* 67 (2013) 281–294.
- [38] Omega, *Epoxies and Thermal Conductive Pastes*, (2013).
- [39] R.S. Figliola, D.E. Beasley, *Theory and Design for Mechanical Measurements*, fourth ed., Wiley, Hoboken, 2006.

Table 4.1. Thermophysical properties of n-octadecane at $T = 301.5$ K [10].

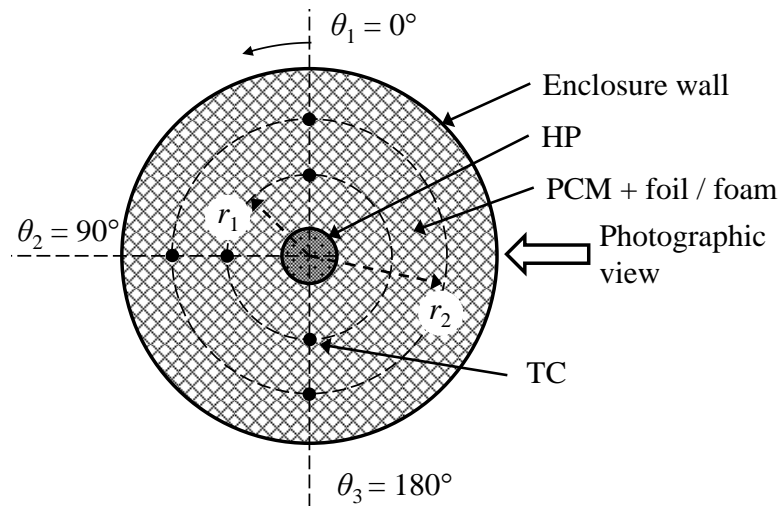
Parameter	Value
Melting point, T_m [K]	301
Latent heat of fusion, h_{sl} [kJ/kg]	243.5
Liquid thermal conductivity, k_l [W/m·K]	0.148
Solid thermal conductivity, k_s [W/m·K]	0.358
Liquid density, ρ_l [kg/m ³]	770
Solid density, ρ_s [kg/m ³]	800
Liquid specific heat, $c_{p,l}$ [J/kg·K]	2160
Solid specific heat, $c_{p,s}$ [J/kg·K]	1912
Dynamic viscosity, μ [Pa·s]	3.09×10^{-3}

Table 4.2. Time, effectiveness and melting rates for 95 % complete phase change (min).

Configuration	ΔT	t_s (min)		ε_s		t_m (min)		ε_m		r_m (g/min)	
		$\alpha = 0^\circ$	$\alpha = 90^\circ$	$\alpha = 0^\circ$	$\alpha = 90^\circ$	$\alpha = 0^\circ$	$\alpha = 90^\circ$	$\alpha = 0^\circ$	$\alpha = 90^\circ$	$\alpha = 0^\circ$	$\alpha = 90^\circ$
HP-Foil-PCM	8 °C	21	23	-	-	30	34	-	-	2.00	1.76
HP-Foil-PCM	17 °C	13	11	5.7	5.3	16	18	11.9	9.4	3.75	3.33
HP-Foil-PCM	25 °C	13	9	-	-	12	14	-	-	5.00	4.29
HP-Foam-PCM	17 °C	26	28	3.7	3.8	34	38	7.2	5.4	1.76	1.58
HP-Foam-PCM	25 °C	22	20	-	-	22	24	-	-	2.73	2.50
HP-PCM	8 °C	164	168	-	-	204	244	-	-	0.29	-
HP-PCM	17 °C	84	72	2.3	2.1	78	106	2.2	2.3	0.77	-
HP-PCM	25 °C	72	70	-	-	56	74	-	-	1.07	-
Rod-PCM	17 °C	102	98	1.9	2.0	96	118	2.0	1.9	0.63	-
Foam-PCM	17 °C	112	112	1.7	1.7	106	104	1.3	1.5	0.57	-
Non-enhanced	17 °C	398	428	1.0	1.0	136	172	1.0	1.0	0.44	0.35

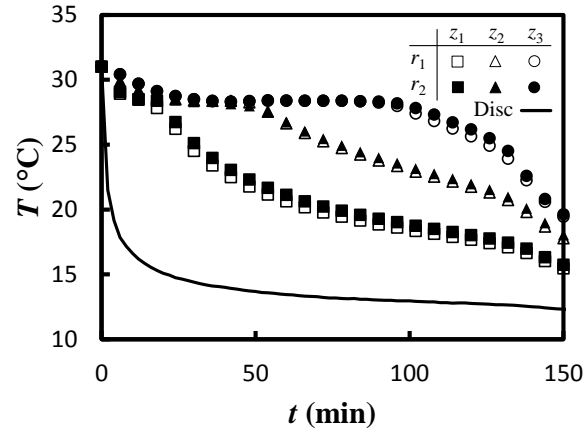


(a) central cross section parallel to the right side view (plane of symmetry)

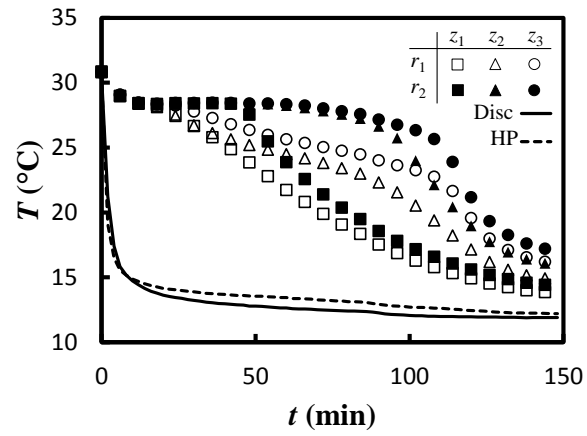


(b) top view

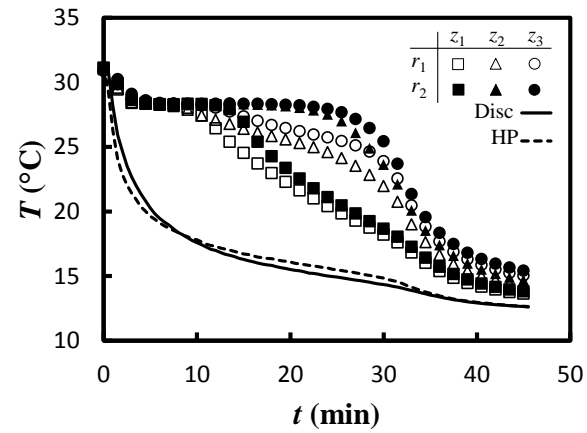
Fig. 4.1. Schematic of the experimental apparatus (a) central cross section parallel to the right side view (plane of symmetry) and (b) top view.



(a) Foam-PCM

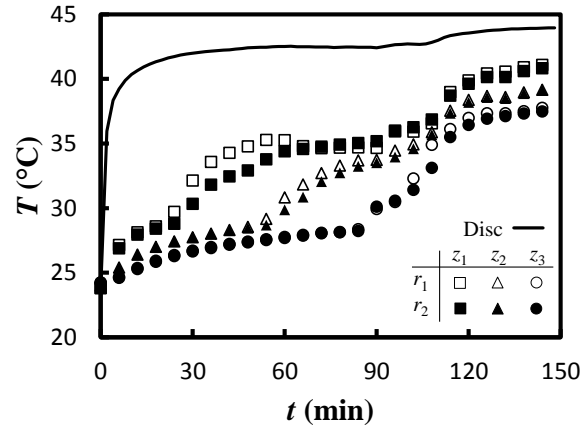


(b) HP-PCM

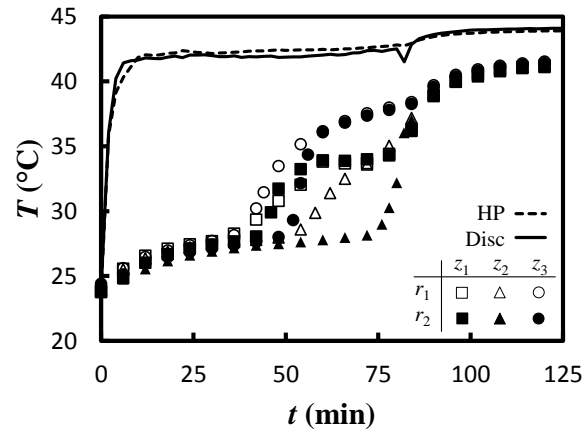


(c) HP-Foam-PCM

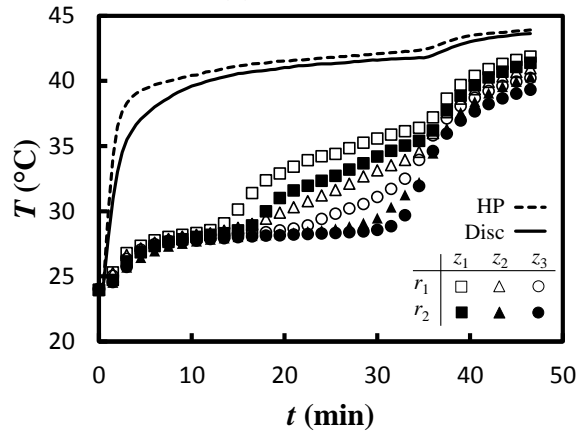
Fig. 4.2. Temperature distribution during solidification with $\alpha = 0^\circ$ and $\Delta T = 17^\circ \text{C}$ ($r_1 = 9 \text{ mm}$, $r_2 = 15 \text{ mm}$, $z_1 = 15 \text{ mm}$, $z_2 = 30 \text{ mm}$, $z_3 = 45 \text{ mm}$) for the (a) Foam-PCM, (b) HP-PCM and (c) HP-Foam-PCM configurations.



(a) Foam-PCM



(b) HP-PCM



(c) HP-Foam-PCM

Fig. 4.3. Temperature distribution during melting with $\alpha = 0^\circ$ and $\Delta T = 17^\circ\text{C}$ ($r_1 = 9\text{ mm}$, $r_2 = 15\text{ mm}$, $z_1 = 15\text{ mm}$, $z_2 = 30\text{ mm}$, $z_3 = 45\text{ mm}$) for the (a) Foam-PCM, (b) HP-PCM and (c) HP-Foam-PCM configurations.

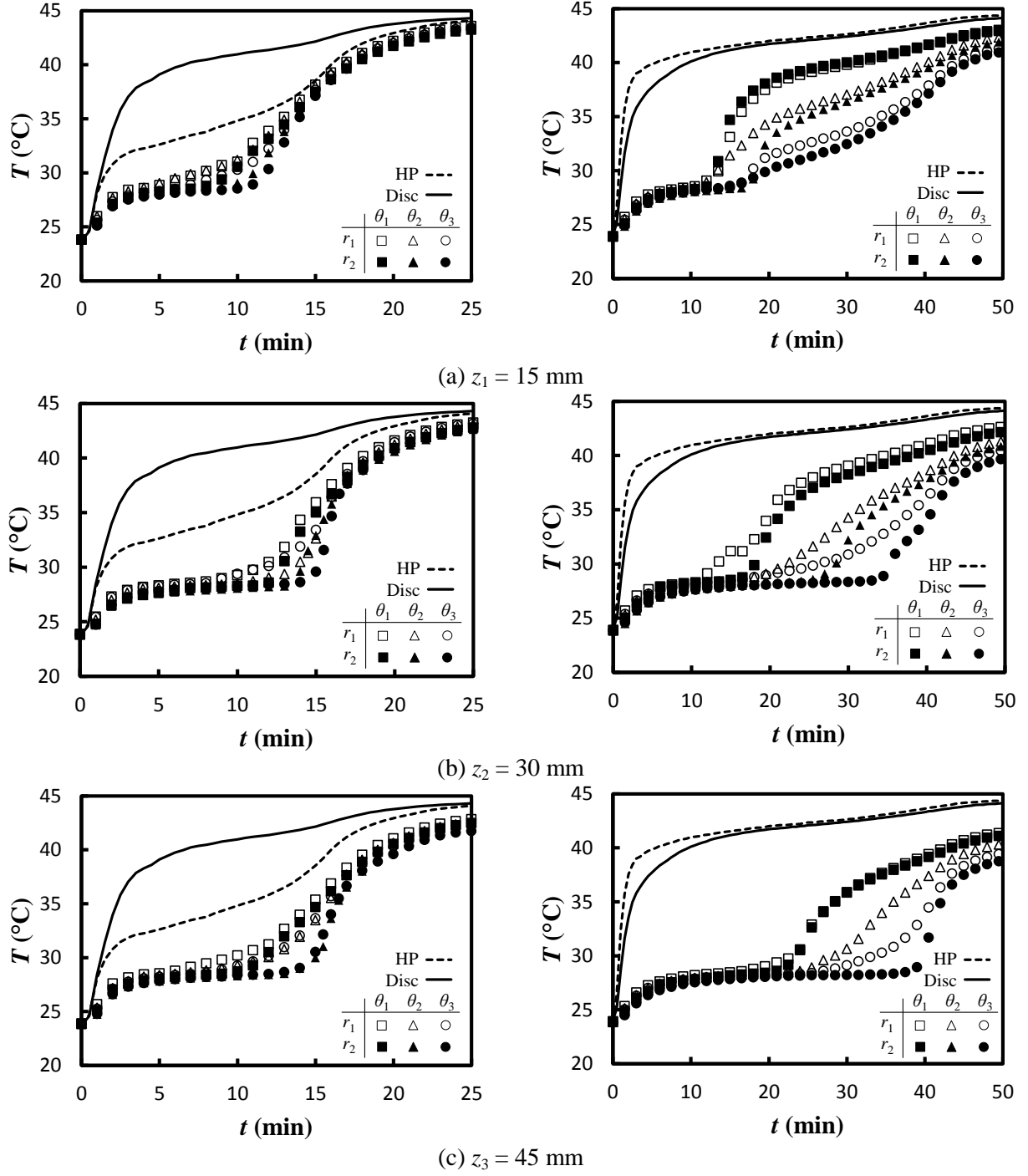
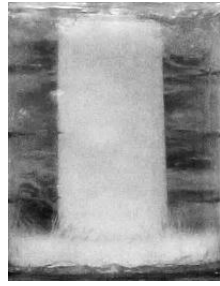
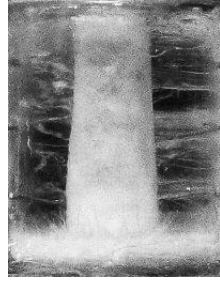
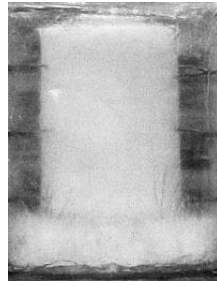


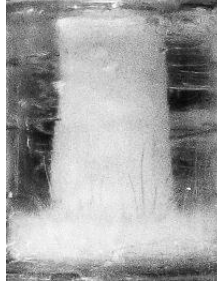
Fig. 4.4. Temperature distribution during melting for the HP-Foil-PCM (left) and HP-Foam-PCM (right) configurations with $\Delta T = 17$ °C and $\alpha = 90^\circ$ ($r_1 = 9$ mm, $r_2 = 15$ mm, $\theta_1 = 0^\circ$, $\theta_2 = 90^\circ$, $\theta_3 = 180^\circ$) for (a) $z_1 = 15$ mm (b) $z_2 = 30$ mm and (c) $z_3 = 45$ mm.



(a) HP-PCM



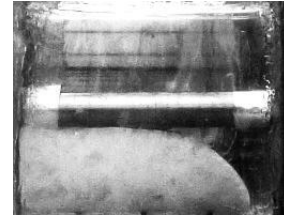
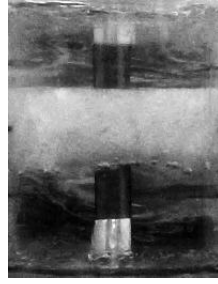
(b) Rod-PCM



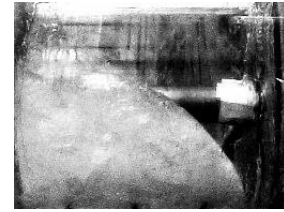
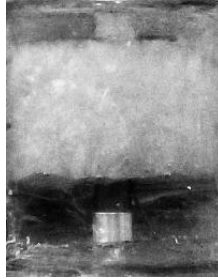
(c) non-enhanced PCM



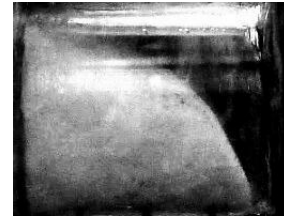
Fig. 4.5. Photographs during solidification with $\alpha = 0^\circ$ and $\Delta T = 17^\circ\text{C}$ for the (a) HP-PCM, (b) Rod-PCM, and (c) non-enhanced PCM configurations at $t = 15$ min (left) and $t = 30$ min (right).



(a) HP-PCM



(b) Rod-PCM



(c) non-enhanced PCM

Fig. 4.6. Photographs during melting at $t = 60$ min with $\alpha = 0^\circ$ (left), $\alpha = 90^\circ$ (right) and $\Delta T = 17^\circ\text{C}$ for the (a) HP-PCM, (b) Rod-PCM and (c) non-enhanced PCM configurations.

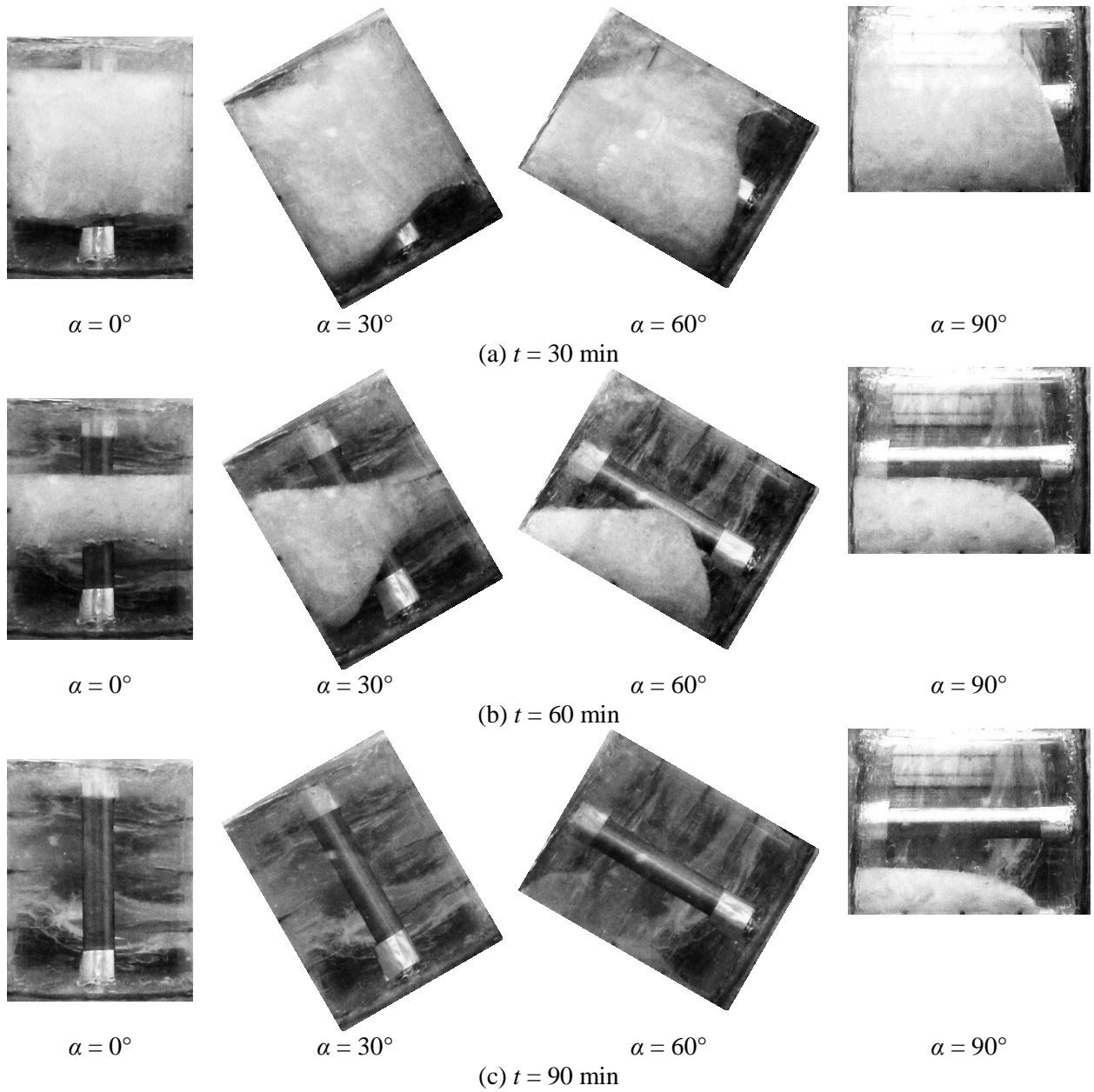


Fig. 4.7. Photographs progression during melting with $\alpha = 0^\circ$ (left), $\alpha = 0^\circ$ (left-middle), $\alpha = 0^\circ$ (right-middle), $\alpha = 90^\circ$ (right) and $\Delta T = 17^\circ \text{C}$ for the HP-PCM configuration at (a) $t = 30$ min (b) $t = 60$ min and (c) $t = 90$ min.

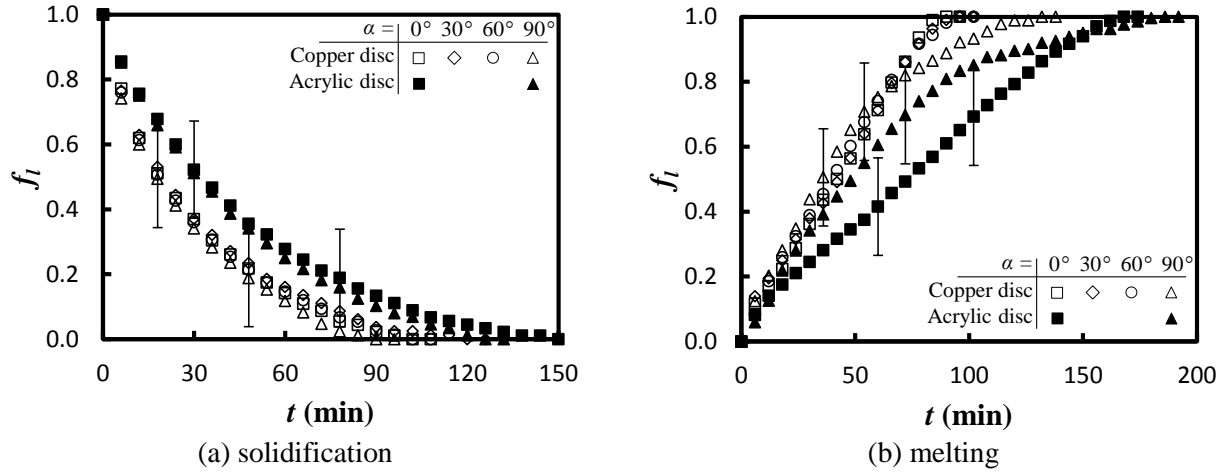
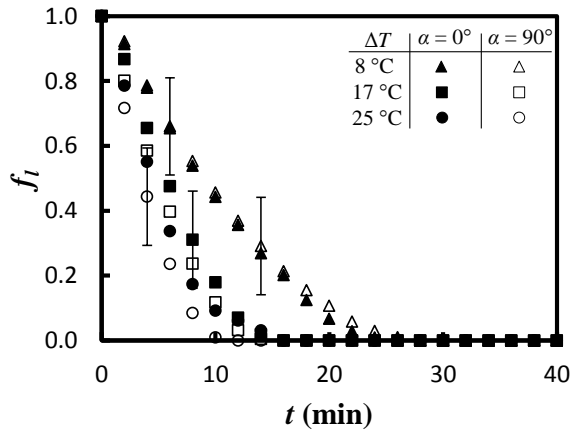
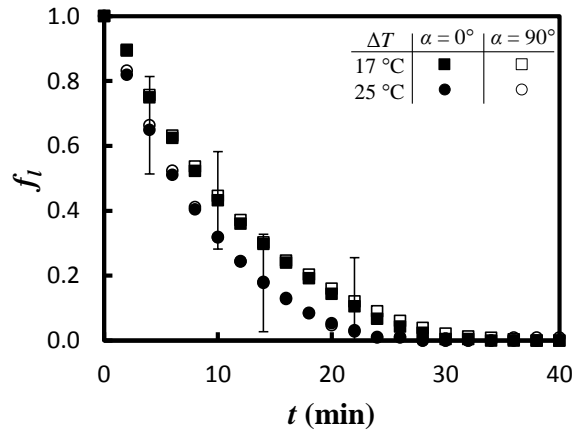


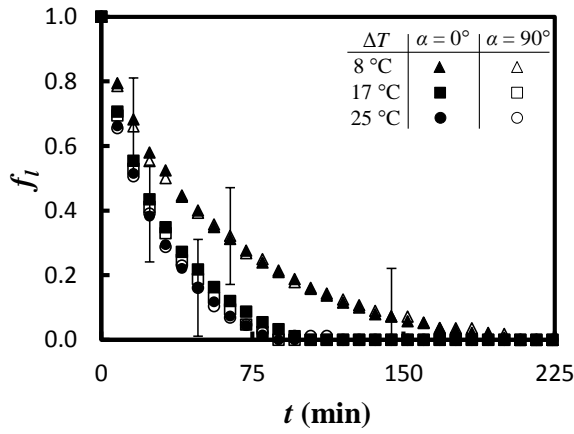
Fig. 4.8. Liquid fraction histories for the HP-PCM cases with $\Delta T = 17^\circ\text{C}$ using a copper disc (open symbols) and an acrylic disc (solid symbols) during (a) solidification and (b) melting.



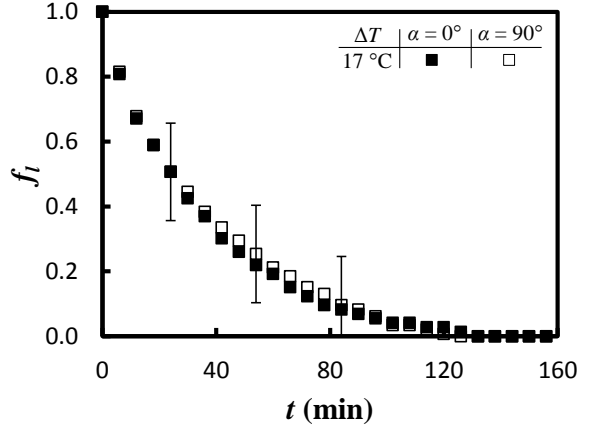
(a) HP-Foil-PCM



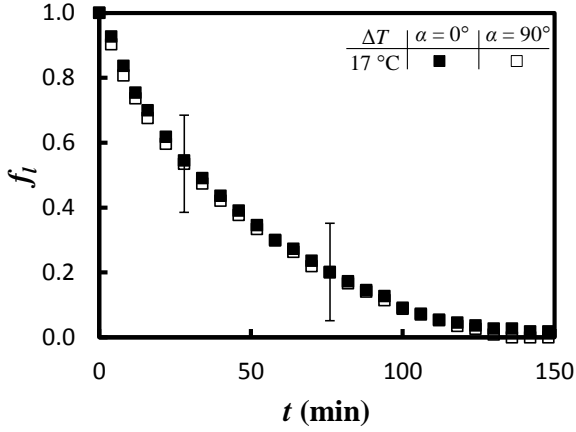
(b) HP-Foam-PCM



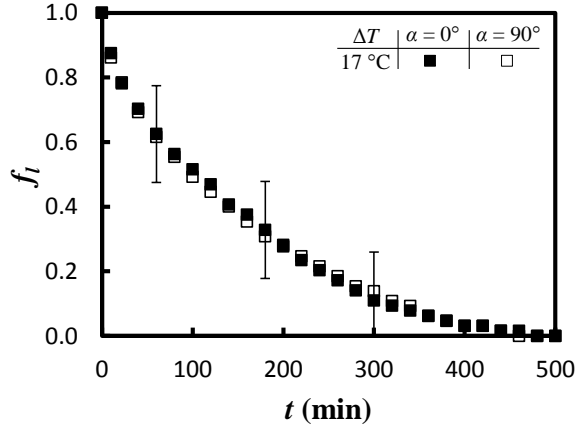
(c) HP-PCM



(d) Rod-PCM



(e) Foam-PCM



(f) non-enhanced PCM

Fig. 4.9. Liquid fraction histories during solidification with varying ΔT and orientation for the (a) HP-Foil-PCM, (b) HP-Foam-PCM, (c) HP-PCM, (d) Rod-PCM, (e) Foam-PCM and (f) non-enhanced PCM configurations.

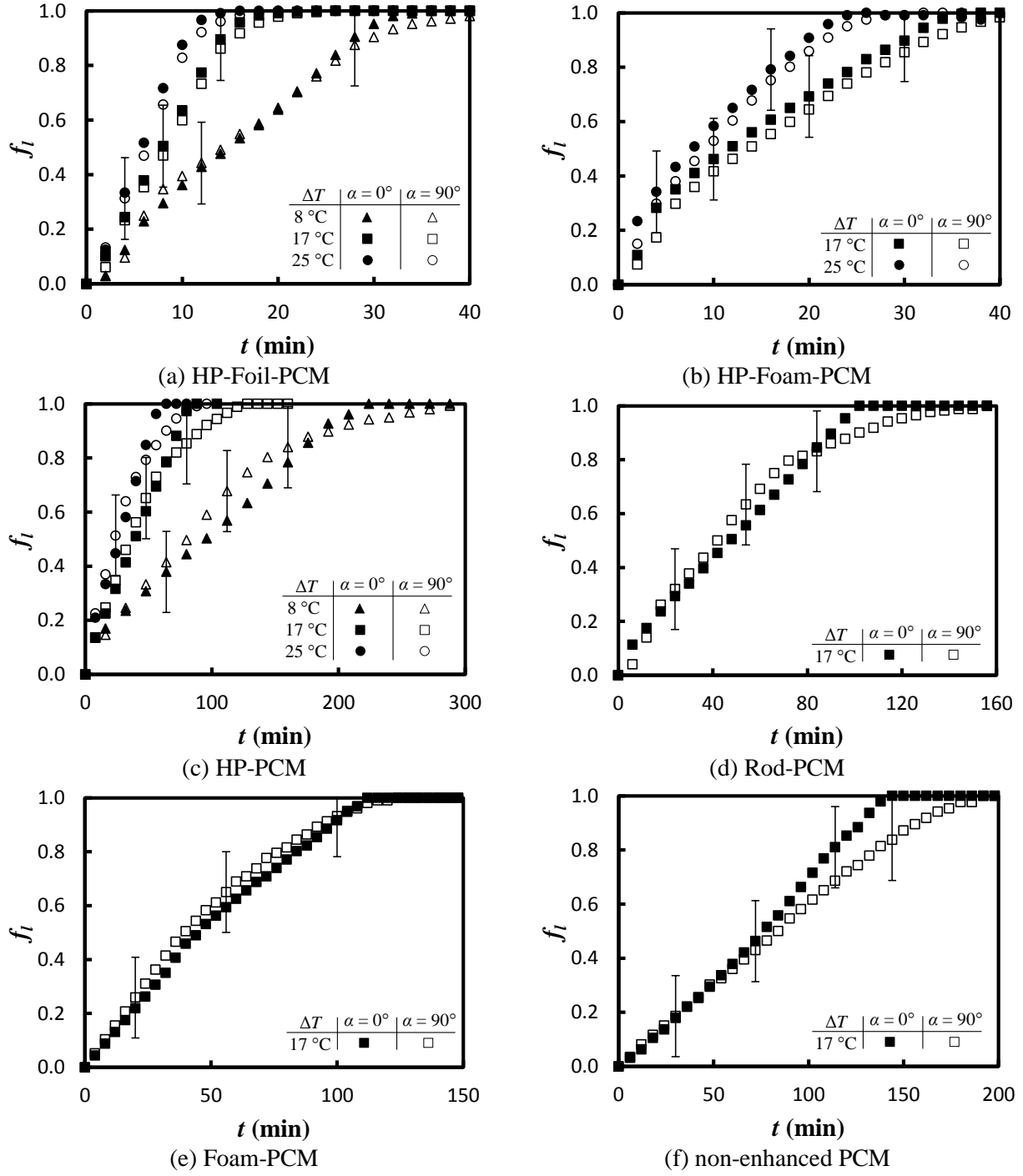


Fig. 4.10. Liquid fraction histories during melting with varying ΔT and orientation for the (a) HP-Foil-PCM, (b) HP-Foam-PCM, (c) HP-PCM, (d) Rod-PCM, (e) Foam-PCM and (f) non-enhanced PCM configurations.

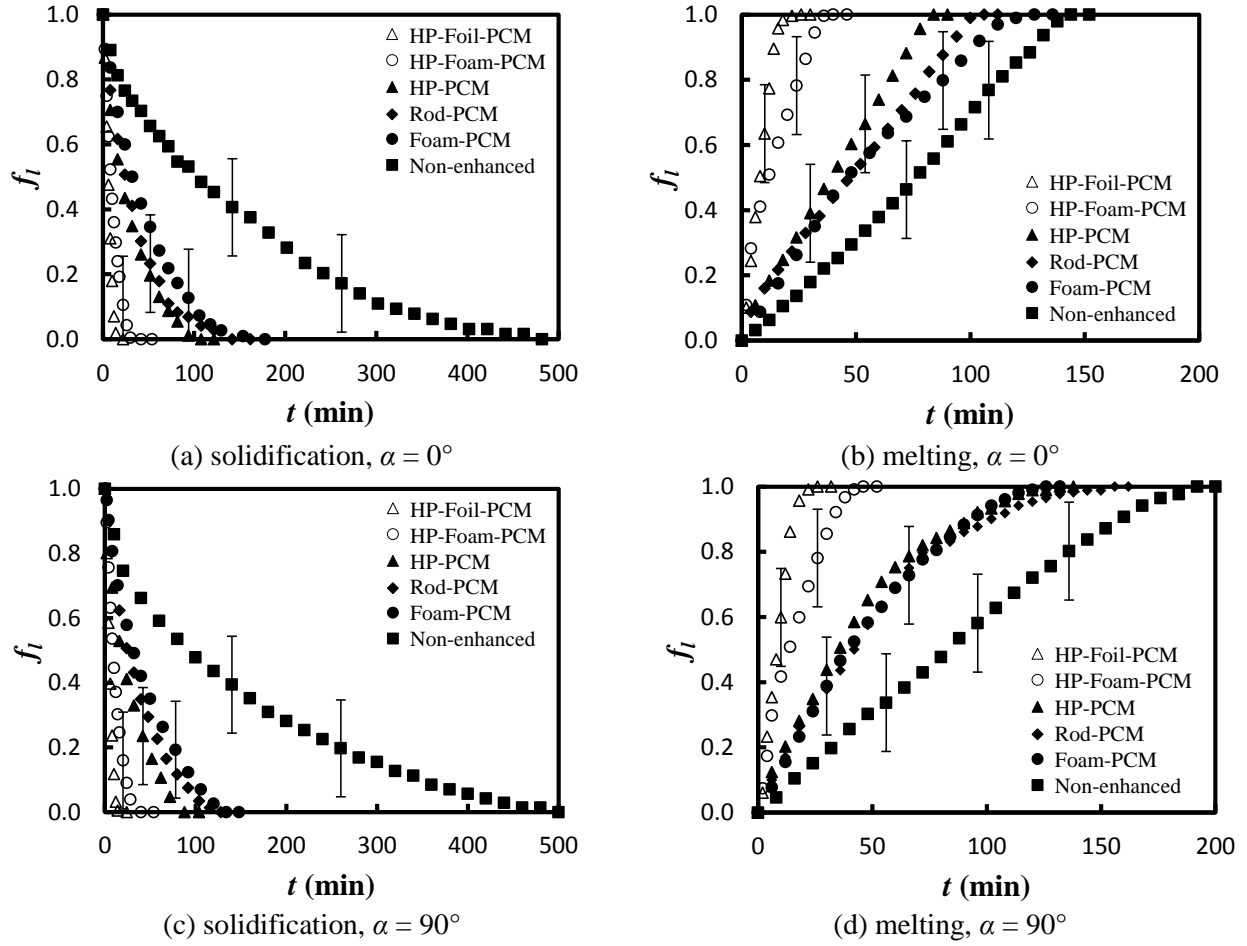


Fig. 4.11. Liquid fraction histories for each configuration with $\Delta T = 17^\circ\text{C}$ (a) solidification, $\alpha = 0^\circ$, (b) melting, $\alpha = 0^\circ$, (c) solidification, $\alpha = 90^\circ$ and (d) melting, $\alpha = 90^\circ$.

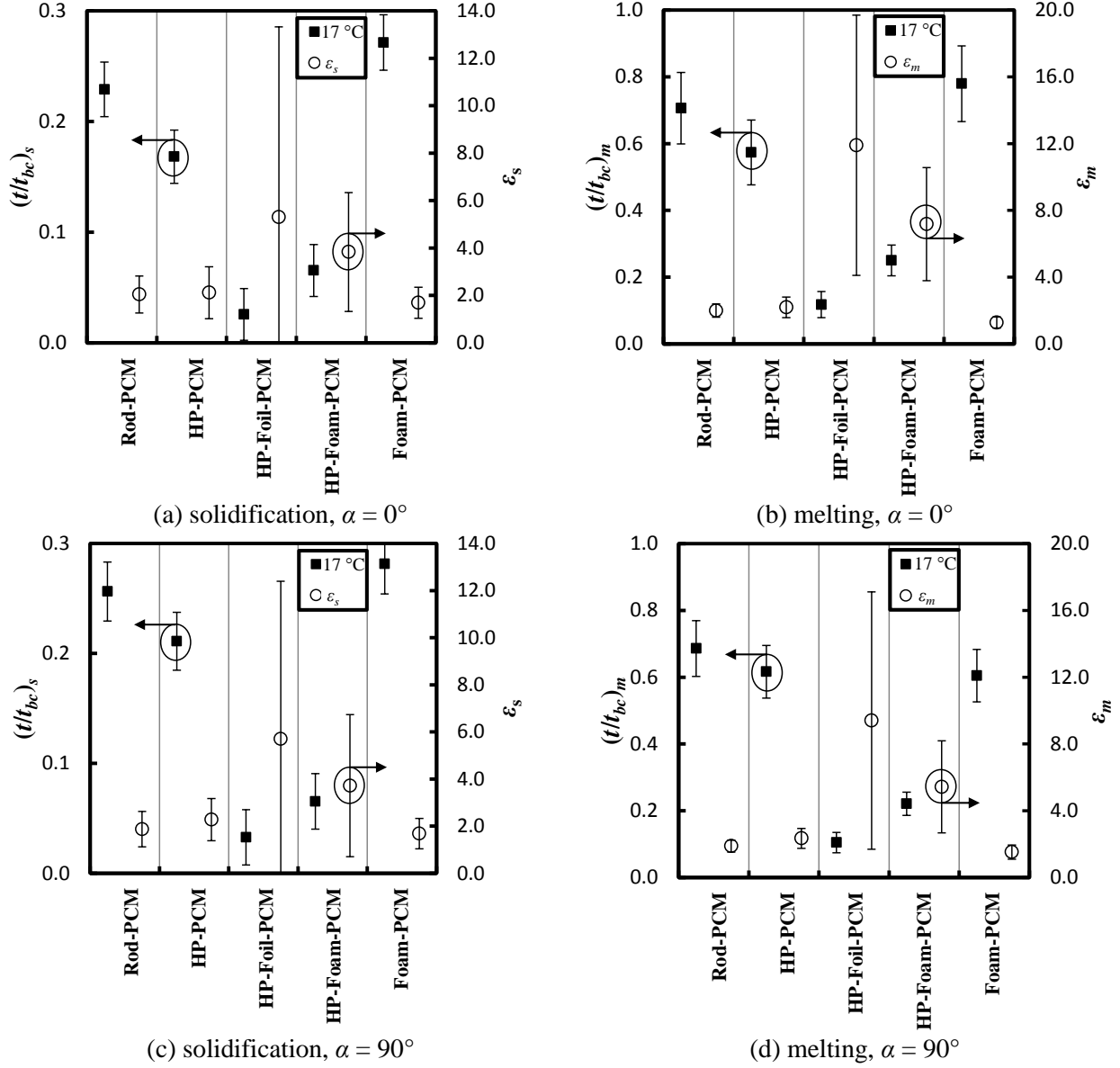


Fig. 4.12. Time ratio and effectiveness for each configuration at 95 % complete phase change with respect to the non-enhanced PCM case with $\Delta T = 17^\circ\text{C}$ (a) solidification, $\alpha = 0^\circ$, (b) melting, $\alpha = 0^\circ$, (c) solidification, $\alpha = 90^\circ$ and (d) melting, $\alpha = 90^\circ$.